New approaches for the synthesis of high-performance polyolefins reactor nanocomposites and blends

Ana Elisa Ferreira Santos Melo

THÈSE EN COTUTELLE PRÉSENTÉE

POUR OBTENIR LE GRADE DE

DOCTEUR DE

L'UNIVERSITÉ DE BORDEAUX

ET DE L'UNIVERSIDADE DE LISBOA

ÉCOLE DOCTORALE SCIENCES CHIMIQUES UBX

ÉCOLE DOCTORALE DE L' UNIVERSIDADE DE LISBOA

SPÉCIALITÉ POLYMÈRES

Par Ana Elisa FERREIRA SANTOS MELO

NEW APPROACHES FOR THE SYNTHESIS OF HIGH-PERFORMANCE POLYOLEFINS REACTOR NANOCOMPOSITES AND BLENDS

Sous la direction de Henri CRAMAIL, de M. Rosário RIBEIRO et de João LOURENÇO

Soutenue le 3 Mars 2016

Membres du jury :

M. BORDADO, João Professor Instituto Superior Técnico	Président
M. BOISSON, Christophe Rechercher Laboratory Chemistry, Catalysis, Polymers and Processes	Rapporteur
Mme GARCÍA, M. Luisa Rechercher Instituto de Ciencia e Tecnología de Polímeros	Rapporteur
M. PERUCH, Frédéric Rechercher LCPO, Université de Bordeaux	Examinateur

Acknowledgments

I am deeply indebted to many people who have contributed to the success of this work and have helped me to complete my thesis. I would like to thank:

First and foremost, Professor Maria do Rosário Ribeiro, my daily supervisor for giving me the opportunity to do this PhD in a so interesting research topic. Her guidance, enriched discussion, constant positive attitude and patience during this project are highly appreciated. Especially for believing me and in this work and for bringing me to this finish line.

My supervisor Professor João Paulo Lourenço for all the stimulating discussions and for all the trips between Faro and Lisbon. I would also like to thank all his support in the synthesis of the SBA-15. Thank you for receiving me. I am very grateful for his encouragement and valuable advice during my work and his assistance in the writing stage.

My supervisor Professor Henri Cramail for giving me the opportunity to join his research group, for his stimulating advice and all his support during my PhD. His insightful suggestions and corrections on the manuscript of this thesis are gratefully acknowledged.

Doctor Maria Luisa Cerrada for the invaluable help during my stay in Instituto de Ciência y Tecnologia de Polímeros (CSIC) in Madrid and for all her guidance in the characterization of the materials and for all the fruitful discussion.

Collaborations with many people and groups were crucial in the completion of my work. I would like therefore to thank Doctor Ernesto Pérez for all the help during my stays in CSIC, Professor Vicente Lorenzo for the indentation experiments, Professor Gilles Sèbe for providing the cellulose nanowhiskers and for the shared knowledge regarding this material and Professor Raul Quijada and Professor Enrique Vallés for the characterization of some samples.

Also this project would not be possible without funding from Fundação para a Ciência e a Tecnologia and Programa de Acções Universitárias Integradas Luso-Francesas.

Adapting to a new research group would not be possible without the great environment I found in the laboratory group. It was a great pleasure to work with all of you. I specially thank Doctor Artur Bento and Doctor João Campos for the intensive support in this, that and the other.

I would also like to thank my friends for being there for me. You know who you are!

My heartfelt thanks to my mother and sister who have encouraged me through all my life. I have been very fortunate to have their constant love and support. Also I express my best thanks to Naïr and António Alua for their support.

Lastly, I would like to extend my deepest thanks and best gratitude to Pedro Alua for his tremendous patience, support and kindness throughout this journey especially in the writing stage of the thesis.

Titre : Nouvelles approches pour la synthèse de polyoléfines de haute performance

Résumé

Malgré les propriétés remarquables de polyéthylène de masse molaire très élevée (UHMWPE), une généralisation de son application est limitée en raison des difficultés rencontrées lors de sa mise en forme, liées au taux d'enchevêtrement important des chaînes.

Le but de ce travail est de développer des nanocomposites et des mélanges à base de polyéthylène, par polymérisation *in situ*. A cet effet, des catalyseurs métallocènes et des post-métallocènes ont été immobilisés par différentes méthodes sur la silice mésoporeuse SBA-15. Le système poreux de ce support, avec des canaux bien définis à l'échelle nanométrique, peut entraîner des effets de confinement des chaînes macromoléculaires et/ou permettre un mélange intime des polymères.

Le comportement de la polymérisation de l'éthylène par catalyses homogène et supporté, ainsi que les méthodes d'immobilisation utilisées et leur effet sur l'activité de polymérisation et des masses molaires, ont été évalués.

Une caractérisation complète des nanocomposites et des mélanges comprenant différents aspects des matériaux (morphologie, cristallinité et homogénéité) a été réalisée. Les propriétés thermiques et mécaniques des matériaux finaux ont été également évaluées.

D'une manière générale, les nanocomposites à base de polyéthylène et les mélanges en réacteur ont montré des propriétés mécaniques améliorées, en termes de module d'élasticité, résistance mécanique, ténacité et résistance au fluage, par comparaison avec les polyéthylènes communs. En traitant la poudre d'UHMWPE par moulage, par compression à haute pression et au-dessous de sa température de fusion, une augmentation remarquable des paramètres mécaniques a été obtenue.

Les résultats préliminaires sur la préparation de nanocomposites en utilisant des nanocristaux de cellulose ont montré que cette approche est faisable et qu'elle présente un potentiel de développement.

Mots clés : polyéthylène, catalyseurs à site unique, SBA-15, nanocomposite, mélanges en réacteur

Title : New approaches for the synthesis of high-performance polyolefins reactor nanocomposites and blends

Abstract

Despite the remarkable properties of ultra-high molecular weight polyethylene, its application is limited by the difficulties encountered in conventional melt processing due the high degree of entanglement of the chains.

The aim of this work is to develop polyethylene based nanocomposites and in-reactor blends, by *in situ* polymerization. For this purpose metallocenes and post-metallocene catalysts were immobilized by different methods on mesoporous silica SBA-15. The porous system of this support, with well-defined channels at the nanometric scale, may cause confinement effects of macromolecular chains and/or potentiate intimate mixing of polymer blends.

Ethylene polymerization behavior of the homogeneous and the supported systems along with the immobilization methodologies used and their effect on the polymerization activity and polymer molar masses were evaluated.

A complete characterization of the nanocomposites and blends comprising different aspects of the materials properties (morphology, crystallinity and homogeneity) was carried out. The thermal and mechanical properties of the final materials were also evaluated.

In a general way the polyethylene based nanocomposites and in-reactor blends showed improved mechanical properties, in terms of elastic modulus, mechanical strength, toughness and creep resistance, when compared with neat polyethylenes. By processing the UHMWPE powders by compression molding, at high pressure and below its melting temperature a remarkable increase of the mechanical parameters was obtained.

Preliminary results on the preparation of nanocomposites using cellulose nanowhiskers have shown that this approach is feasible and show potential for further development.

Keywords : polyethylene, single-site catalysts, SBA-15, nanocomposite, in-reactor blends

---

Laboratoire de Chimie des Polymères Organiques recherche

[LCPO, UMR 5629 ENSCBP, 16 av. Pey-Berland, Bât A F-33607 Pessac cedex]

Résume Substantiel

Actuellement, les nanocomposites et les mélanges de polyoléfines haute performance, transformables par moulage par injection, extrusion de films et extrusion soufflage, sont des matériaux très recherchés du point de vue industriel. Parmi ce type de matériaux, on peut citer le polyéthylène de masse molaire très élevée (UHMWPE) et le polyéthylène haute densité (HDPE). Malgré les propriétés physiques et mécaniques remarquables de l'UHMWPE, ce dernier souffre d'un inconvénient majeur: une mauvaise processabilité et une incapacité à être porté à l'état fondu. Les efforts se concentrent maintenant vers des approches synthétiques alternatives pour atteindre des nanocomposites et des mélanges de polyoléfines haute performance, processables à l'état fondu.

Les silices mésoporeuses ayant des propriétés nanométriques présentent des caractéristiques uniques pour la synthèse de polyoléfines *in situ*. Leur structure constituée de canaux bien définis à l'échelle nanométrique peut entraîner des effets de confinement des chaînes macromoléculaires et/ou permettre un mélange intime des polymères produits sur des catalyseurs monosites co-supportés.

La capacité des catalyseurs supportés sur silice mésoporeuse, telle la SBA-15, pour produire des nanofibres polymères pourrait être une solution permettant d'avoir un système catalytique capable de promouvoir le mélange intime des polymères à l'échelle nanomètrique. Alors que l'emploi de catalyseurs multi-sites classiques mal définis nécessite une optimisation complexe des procédés, la combinaison de catalyseurs mono-sites supportés sur silice paraît plus robuste et doit permettre un réglage fin des masses molaires du mélange ainsi obtenu.

Le présent travail vise l'exploitation de ces géométries confinées pour la synthèse de nanocomposites et de mélanges de polyéthylènes présentant des hautes performances, qui combinent à la fois les avantages de la silice mésoporeuse et des catalyseurs de polymérisation mono-sites métallocène ou post-métallocène.

Le travail à effectuer comprendra: (i) la synthèse et la caractérisation des supports de catalyseur; (ii) la préparation de plusieurs catalyseurs métallocènes et post-métallocènes appropriés pouvant être co-supportés, (iii) la synthèse, par polymérisation en milieu confiné, de nanocomposites et de mélanges de polyéthylène haute performance; (iv) la caractérisation des nanocomposites et des mélanges, qui comprend l'étude de la morphologie, de la cristallinité et l'évaluation des propriétés thermiques et mécaniques. De cette façon, les nouveaux matériaux haute performance, comprenant des nanocomposites et des mélanges en réacteur de PE, sont censés être obtenus.

Cette thèse est divisée en 7 chapitres. Une analyse de la littérature est présentée dans une section du chapitre 1. Les caractéristiques de l'UHMWPE et les contraintes imposées par l'enchevêtrement dans la mise en œuvre des polymères sont d'abord discutés. Dans une seconde partie, les principaux systèmes catalytiques qui peuvent être utilisés pour la polymérisation de l'éthylène sont décrits: catalyseurs métallocènes et post-métallocènes. Ensuite, les avantages de l'immobilisation des systèmes catalytiques sur une silice de type SBA-15 sont discutés. En plus de permettre l'hétérogénéisation des systèmes catalytiques, la silice mésoporeuse peut jouer un second rôle en tant que charge, donc, dans la section suivante, les nanocomposites sont discutés. La dernière partie de l'étude de la littérature est consacrée aux mélanges de polyéthylène et à la façon dont ces mélanges combinent les

propriétés exceptionnelles de l'UHMWPE ou des polyéthylènes de haute masse molaire, et une bonne processabilité du HDPE.

Le chapitre 2 est dédié aux nanocomposites UHMWPE / SBA-15 synthétisés par polymérisation *in situ* avec le complexe bis [*N*-(3-*tert*-butylsalicylidene)-2,3,4,5,6-pentafluoroanilinate] titane (IV) dichlorure comme catalyseur (catalyseur FI), en association avec le co-catalyseur méthylaluminoxane (MAO). La justification du choix des substituants du complexe de métal de bis-phénoxy utilisé pour préparer UHMWPE et pour le SBA-15 utilisé comme support pour l'immobilisation des catalyseurs est expliquée de façon appropriée. Ce catalyseur, connu pour être très actif et présenté un caractère vivant, donne lieu à des activités de polymérisation très élevées en phase homogène. Toutefois, la dépendance des masses molaires sur le temps de polymérisation montre des écarts par rapport au caractère vivant attendu et même parfois une activité faible. En ce qui concerne l'influence de la variation du rapport Al/Ti, les résultats ont montré que ce paramètre ne semble pas influencer les masses molaires des polyéthylènes obtenus. Différentes méthodes ont été évaluées afin de supporter le catalyseur sur la SBA-15 et, comme prévu, il a donné lieu à une diminution importante de l'activité de polymérisation. Cette diminution est plus évidente lorsque le catalyseur est immobilisé après un prétraitement de la SBA-15 avec du MAO (méthode SBA-MAO), probablement due à la formation de liaisons avec des espèces Si-O-Al $(Me)_2$. En TGA, la décomposition dans des conditions oxydantes semble également être influencée par la méthode utilisée pour l'immobilisation du catalyseur. Cependant, aucune tendance spécifique n'a pas pu être identifiée dans un environnement inerte. Les thermogrammes DSC obtenus pour les différents échantillons préparés avec le catalyseur FI ont montré que la cristallinité est plus élevée lorsque les échantillons sont testés sous la forme de poudre plutôt que sous la forme de films obtenus par moulage par compression à 230 °C. Les températures de transition estimées par DSC semblent plutôt indépendantes de la présence de SBA-15 et du procédé de support du catalyseur FI. D'autre part, la présence de particules de SBA-15 dans la matrice polymère semble diminuer légèrement la cristallinité et également empêcher la cristallisation de l'UHMWPE. Il convient également de remarquer que le procédé de pré-activation (méthode PA) semble favoriser la formation de chaînes polymères à l'intérieur des canaux de la SBA-15.

En ce qui concerne le comportement mécanique de ces matériaux composites, il a pu être observé que la présence de SBA-15 donne lieu à des matériaux plus rigides avec un module d'élasticité, une résistance mécanique, une ténacité et une résistance au fluage plus élevés. La quantité de support et les masse molaires sont les principaux facteurs qui déclenchent le processus de déformation.

Lors du traitement des matériaux UHMWPE naissants à l'état solide, par moulage par compression à haute pression et au-dessous de sa température de fusion, des films d'UHMWPE de très haute cristallinité sont formés. Ces films T120 montrent une amélioration impressionnante de paramètres mécaniques (environ 300 % en module d'indentation, E_{it}, et 100% de la dureté, H_{it}) relativement à des échantillons comprimés moulés au-dessus de la température de fusion (films de T230).

Dans le chapitre 3, un système catalytique comprenant un catalyseur hafnocène (bis- (*n*-butylcyclopentadiényl) hafnium-dichloro) et méthylaluminoxane comme co-catalyseur a été utilisé pour la synthèse d'un ensemble de polyéthylènes synthétisés dans conditions de polymérisation homogènes et de différents nanocomposites par polymérisation *in situ* avec des particules mésoporeuses de SBA-15 comme support. L'utilisation du complexe Hf, avec

des caractéristiques différentes, en termes d'activité catalytique de polymérisation et de masses molaires des polyéthylène, en comparaison au catalyseur de FI, permet une meilleure compréhension de ce procédé de polymérisation *in situ* pour atteindre les objectifs de la thèse.

Contrairement au catalyseur FI, ce complexe hafnocène permet une immobilisation directe à la surface de la SBA-15 et, par conséquent, cette méthode a également été utilisée dans ce cas. L'activité de polymérisation dépend de la méthode d'immobilisation et du temps d'immobilisation. Dans des conditions optimisées, ce catalyseur montre des activités relativement élevées en comparaison avec le système homogène. De plus, on observe une augmentation notable de la masse molaire des polyéthylènes en utilisant le catalyseur hafnocène supporté, mettant en évidence la capacité de la SBA-15 à réduire les réactions de transfert de chaîne dans ces conditions de polymérisation confinées.

L'analyse par TGA de la décomposition thermique des polymères préparés avec ce catalyseur présente une structure complexe qui dépend de plusieurs facteurs, notamment l'ambiance (oxydant or inerte), la procédure d'immobilisation et la présence de SBA-15. En ce qui concerne les températures de cristallisation et de transition obtenues à partir des courbes de fusion DSC, aucune tendance spécifique n'a pas pu être observée. Cependant, l'effet du rapport Al/Hf et le procédé d'immobilisation est évidente dans des cas particuliers. La présence de SBA-15 semble empêcher la cristallisation du polyéthylène, et aucun effet nucléant n'a pu être observé. Comme dans le cas précédent, des preuves de la présence de chaînes de polyéthylène à l'intérieur des canaux de la SBA-15 ont été démontées.

Le comportement mécanique des matériaux préparés avec ce catalyseur est également similaire à celui des échantillons obtenus avec le catalyseur FI précédent. À savoir l'introduction de la SBA-15 dans la matrice de polymère augmente la rigidité des matériaux finaux par rapport aux polyéthylènes.

L'étude des systèmes précédant a été la base pour la prochaine étape impliquant l'immobilisation dans le même support de deux catalyseurs de polymérisation différents. Le chapitre 4 est consacré à ces mélanges en réacteur, les mélanges à base de PE préparés par polymérisation *in situ* de deux types de catalyseur à un seul site co-suportés sur la SBA-15 mésoporeuse. Un catalyseur FI ou un hafnocène est responsable de la composante de la masse de polyéthylène molaire plus élevée (UHMWPE lorsque le catalyseur FI est utilisé ou le polyéthylène haute masse molaire lorsque le hafnocène est utilisé) et est associé à un zirconocène qui produit HDPE.

Pour les mélanges FI et les mélanges Hf, donnent des activités moyennes de polymérisation de l'ordre de celles des catalyseurs individuels et peuvent être rationalisées en fonction de la proportion relative de Ti ou Hf par rapport au Zr. La décomposition thermique sous atmosphère inerte et rapport Al/Mt constant des deux ensembles de mélanges est un peu différente. Pour FI, l'augmentation de la proportion Ti:Zr donne lieu à une augmentation de la température de décomposition, alors que le comportement inverse est observé pour les mélanges Hf. L'augmentation de la masse molaire obtenue avec l'augmentation de la proportion de Ti est probablement la raison de la tendance qui a été observée. Pour les deux ensembles de mélanges, une seule fusion et un pic de cristallisation sont observés dans les thermogrammes DSC, indiquant que les chaînes individuelles synthétisées par les deux catalyseurs présents dans les mélanges ont leurs transitions thermiques à identiques

intervalle de température. Encore une fois, aucun effet nucléant n'a été observé en raison de la présence de SBA-15.

L'évaluation du comportement mécanique des mélanges FI a montré un effet de renfort dû à l'addition d'une quantité mineure du composant UHMWPE à la matrice HDPE, mais aucun effet de renfort ne peut être vu par addition d'une petite quantité du composant HDPE à la matrice UHMWPE. Dans le cas des mélanges Hf, cette tendance n'a pas été observée, ce qui est probablement liée à la plus petite différence entre les masses molaires des deux composants, en comparaison avec les mélanges FI.

Une autre tendance intéressante est que l'augmentation du module et E_{it} de H_{it}, en raison de la présence des particules de SBA-15, est plus important lorsque la matrice de polyéthylène est obtenue en utilisant un hafnocène supporté au lieu d'un catalyseur zirconocène supporté. Par conséquence, l'effet de renfort des particules de SBA-15 est plus sensible pour des matrices polymères avec des cristallinités inférieures.

Les préoccupations environnementales ont motivé le développement de nouveaux matériaux qui sont éco-compatibles et biodégradables. Dans ce contexte, les nanocomposites de cellulose ont été préparés. Le chapitre 5 se concentre sur une étude préliminaire d'une nouvelle approche pour la synthèse de nanocomposites en utilisant des nanocristaux de cellulose. La modification de surface est un moyen de surmonter les limites des nanocristaux de cellulose comme une mauvaise interaction avec une matrice hydrophobe, et il peut également améliorer la résistance thermique, et également faciliter la dispersion de ces CNW dans des liquides apolaires. Par conséquent, dans ce travail des nanocristaux de cellulose ont été modifiées avec le méthylaluminoxane, comme un moyen de promouvoir l'immobilisation d'un catalyseur de zirconocène à la surface des CNW.

L'activité de polymérisation de Cp_2ZrCl_2 en présence de nanocristaux de cellulose a été explorée et même avec CNW non séché, il a été possible d'effectuer la polymérisation d'éthylène, sans perte significative d'activité. L'immobilisation du catalyseur à la surface de CNW antérieurement enrobée avec le cocatalyseur MAO a été possible. Pour les nanocomposites synthétisés dans cette thèse, aucun effet de renfort n'a été observé en présence des CNW. Les propriétés des nanocomposites polymères renforcés avec des nanocristaux de cellulose sont principalement régies par la possibilité d'interactions entre particules solides par liaison hydrogène, qui sont exacerbés par l'effet nanométrique résultant de leurs dimensions. Le défi consiste donc à promouvoir la dispersion homogène des nanoparticules cellulosiques et éviter une agglomération au cours du traitement, ce qui nécessite des interactions charge/matrice favorables et, en même temps, de favoriser les interactions charge/charge pour permettre la formation bénéfique d'un réseau de percolation des nanoparticules. Ces deux exigences sont contradictoires et donc d'autres travaux sont encore nécessaires.

Le chapitre 6 est consacré aux conclusions les plus importantes et, la section finale de la thèse, chapitre 7, décrit les procédures expérimentales utilisées pour préparer et caractériser toutes les matières utilisées dans ce travail.

Globalement, cette étude a montré que l'approche synthétique utilisée ici, impliquant la polymérisation *in situ* associée à l'immobilisation ou la co-immobilisation des catalyseurs choisis pour cibler une masse molaire spécifique en utilisant un support de silice mésoporeuse, est un moyen efficace pour produire des nanocomposites et mélanges en réacteur de polyéthylène haute performance. Ces matériaux présentent généralement un

module d'élasticité, une résistance mécanique, une ténacité et une résistance au fluage plus élevés que ceux trouvés pour le polyéthylène seul. La cristallinité et les masses molaires des échantillons de polymère, ainsi que la teneur en SBA-15, sont des paramètres essentiels pour contrôler le comportement mécanique. En outre, les matériaux à base d'UHMWPE avec un nombre réduit d'enchevêtrements peuvent être obtenus en utilisant un catalyseur à base de titane phénoxy-imine. Par un traitement postérieur de ces poudres par moulage par compression à haute pression et en dessous de sa température de fusion, des films d'UHMWPE de très haute cristallinité peuvent être formés. Une augmentation impressionnante des paramètres mécaniques (environ 300% pour le module d'indentation, E_{it}, et 100% pour la dureté, H_{it}) est obtenue de cette façon.

Table of contents

List of Figures

List of Tables

Abbreviations

CNW Cellulose Nanowhiskers

D Dispersity

DSC Differential Scanning Calorimetry

E_{it} Indentation modulus

f_c^C Crystallinity for crystallization

f_c^m Crystallinity for first melting

HDPE High Density Polyethylene

H_{it} Indentation hardness

MAO Methylaluminoxane

MWD Molecular Weight Distribution

PE Polyethylene

TEM Transmission Electron Microscopy

TGA Thermogravimetric Analysis

T_C Crystallization temperature

T_m Melting temperature

TMA Trimethylaluminum

UHMWPE Ultra-High Molecular Weight Polyethylene

XRD X-ray Diffraction

1. Introduction

Nowadays high-performance polyolefin nanocomposites and blends, processable by injection molding, film extrusion, and blow molding, are very desirable materials from the industrial point of view. Examples of this type of materials may include ultra-high molecular weight polyethylene (UHMWPE) and high density polyethylene (HDPE). Despite the remarkable physical and mechanical properties of UHMWPE it suffers a major drawback: the poor processability and the inherent inability to melt processing. Efforts are now focused towards alternative synthetic approaches to attain melt-processable high performance polyolefin nanocomposites and blends.

Mesoporous silicas present unique features for the synthesis of polymers with nanoscaled properties, by *in situ* polymerization of olefins. Their framework of well-defined channels at the nanometric scale may cause confinement effects on macromolecular chains and/or potentiate intimate mixing of polymer blends, produced via cosupported single-site catalysts.

The ability of the catalysts supported on mesoporous silica such as SBA-15 to produce polymer nanofibers could be an important feature to achieve a catalytic system able to promote intimate mixing of polymers at the nanometer scale. While conventional multi-site catalysts were rather ill defined and required tedious process optimization, silica-supported multiple single-site catalyst may be very robust and enable molecular fine tuning of molar masses.

The present work aims at the exploitation of these confined geometries for the synthesis of high performance polyethylene nanocomposites and polyethylene blends exhibiting intimate mixing, that will combine the advantages of both mesoporous silicas and single-site metallocene or post-metallocene polymerization catalysts.

The work to be performed will comprise: (i) synthesis and characterization of the catalyst carriers; (ii) preparation of adequate multiple single-site olefin polymerization catalysts by cosupporting metallocene and post-metallocene catalysts; (iii) synthesis, through space confined polymerization, of high performance polyethylene nanocomposites and polyethylene blends; (iv) characterization of the nanoscaled reactor polymer nanocomposites and blends including study of morphology, crystallinity and evaluation of thermal and mechanical properties. This way novel high performance materials comprising PE based nanocomposites and in-reactor PE blends are expected to be obtained.

This thesis is divided in 7 chapters. The literature survey is presented in the next section of this Chapter. It starts by describing the characteristics of UHMWPE and the constraints imposed by entanglement in the polymer processing. In a second part, the main catalytic systems that can be used for ethylene polymerization are described: metallocene and post-metallocene catalysts. Then the advantages of the immobilization of theses catalytic systems on SBA-15 are discussed. Besides enabling the heterogenization of the catalytic systems, the mesoporous silica may play a second role as filler so, in the next section, nanocomposites will be discussed. The last section of the literature survey is dedicated to the polyethylene blends and how these blends intent to combine the outstanding properties of UHMWPE or high molar mass polyethylene and the good processability of HDPE.

Chapter 2 deals with UHMWPE/SBA-15 nanocomposites synthesized by *in situ* polymerization with a bis [*N*-(3-*tert*-butylsalicylidene)-2,3,4,5,6-pentafluoroanilinate] titanium (IV) dichloride complex as catalyst (FI catalyst) in association with a methylaluminoxane (MAO) cocatalyst. The rationale for the selection of the substituents of the bis-phenoxy metal complex used to prepare UHMWPE and for the SBA-15 used as support for the immobilization of the catalysts is appropriately explained. Then, the ethylene polymerization behavior of the homogeneous and the supported systems along with the immobilization methodologies used and their effect on the polymerization activity and polymer molar masses is evaluated and discussed. Finally the thermal characteristics and mechanical behavior of the produced nanocomposites are investigated and their performance discussed.

In Chapter 3, a catalytic system comprising a hafnocene catalyst (bis-(*n*-butylcyclopentadienyl)-dichloro-hafnium) and methylaluminoxane as cocatalyst has been used for the synthesis of a set of polyethylenes synthesized under homogenous polymerization conditions and of different nanocomposites by *in situ* polymerization with mesoporous SBA-15 particles as support. The effect of the distinct immobilization approaches on polymerization behavior is first discussed. Then, the thermal stability, melting and crystallization transitions and mechanical behavior have been evaluated for the different materials.

Chapter 4 is dedicated to in-reactor PE based blends prepared by *in situ* polymerization of two types of single-site catalyst cosupported on mesoporous SBA-15. A FI catalyst or a hafnocene is responsible for the highest polyethylene molar mass component (UHMWPE when the FI catalyst is used or high molar mass polyethylene when the hafnocene is used) and is combined with a zirconocene that produces HDPE. The blend's synthetic aspects and characterization are discussed.

Environmental concerns have motivated the development of novel materials that are eco-friendly and biodegradable. In this context, cellulose nanocomposites came into existence. Chapter 5 focuses on a preliminary study of a new approach for the synthesis of nanocomposites using cellulose nanowhiskers. Surface modification is a way to overcome limitations of cellulose nanocrystals like poor interaction with hydrophobic matrix, it may also improve thermal resistance, and facilitate dispersion of CNW in apolar liquids. Therefore, in this work cellulose nanowhiskers are modified with methylaluminoxane in a way to promote the immobilization of a zirconocene catalyst in the CNW surface.

Chapter 6 highlights of the most important conclusions and the final section of the thesis, Chapter 7, describes the experimental procedures used to prepare and characterize all the materials used in this work.

1.1 Literature survey

1.1.1 Ultra-high molecular weight polyethylene (UHMWPE)

UHMWPE is a very attractive polymer with remarkable physical and mechanical properties. Most impressive are its chemical inertness, lubricity, impact resistance, and abrasion resistance [1-3]. These characteristics have been exploited since the 1950s in a wide range of applications, including pickers for textile machinery, lining for coal chutes and dump trucks, runners for bottling production lines, as well as bumpers and siding for ships and harbors.

Moreover, because of its biocompatibility, high strength and stiffness, low fatigue, and wear characteristics it is widely used in medical device applications [4, 5]. For the past 45 years, UHMWPE has been used in orthopedics as a bearing material in artificial joints. Each year, about 2 million joint replacement procedures are performed around the world, and the majority of these joint replacements incorporate UHMWPE [6].

UHMWPE comes from a family of polymers with a misleading simple chemical composition, consisting of only hydrogen and carbon. However, the simplicity inherent in its chemical composition hides a more complex hierarchy of organizational structures at the molecular and supramolecular length scales. At a molecular level, the carbon backbone of polyethylene can twist, rotate, and fold into ordered crystalline regions. At a supramolecular level, the UHMWPE consists of powder that must be consolidated at elevated temperatures and pressures to form a bulk material. Further layers of complexity are introduced by chemical changes that arise in UHMWPE due to radiation sterilization and processing.

One can visualize the molecular chain of UHMWPE as a tangled string of spaghetti over a kilometer long. Because the chain is not static, but imbued with internal (thermal) energy, the molecular chain can become mobile at elevated temperatures. When cooled below the melt temperature, the molecular chain of polyethylene has the tendency to rotate about the C-C bonds and create chain folds. This chain folding, in turn, enables the molecule to form local ordered, sheetlike regions known as crystalline lamellae. These lamellae are embedded within amorphous (disordered) regions and may communicate with surrounding lamellae by tie molecules [3]. All of these morphological features of UHMWPE are shown schematically in Figure 1.1.

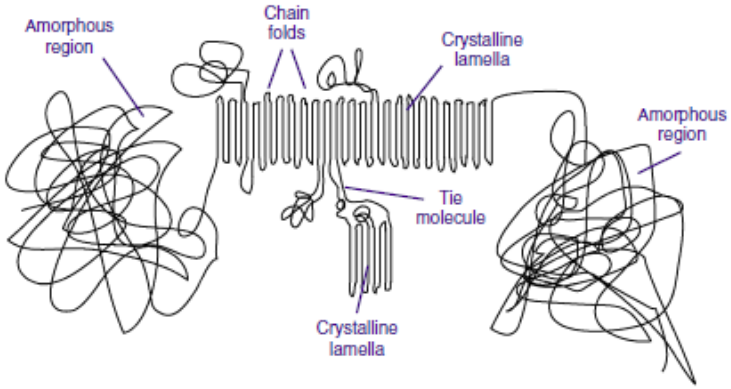

Figure 1.1: Morphological features of UHMWPE. Reprinted from Ref. [3]

When processing UHMWPE, the entanglement of the polymer chains plays an important role. It is well known that the entanglement of ultra-high molecular weight polyethylene chains accounts for high melt viscosity reflected by very low melt flow, slow chain mobility, and slow crystallization rates. As a result, UHMW polyolefins are difficult to process by conventional melt techniques like extrusion and injection molding. Instead, typically UHMWPE is processed by less broadly used batch methods such as ram-extrusion [7, 8], compression molding [9, 10], or sintering of nascent powders [11, 12] to produce sheets, plates, and rods, which require subsequent machining. These processes are of long duration (namely several hours) and consist in applying elevated temperatures (above the melting point) and pressures to consolidate the powders into a bulk material [8]. A direct consequence is the high energetic cost and the risks of thermal degradation of the polymer [13]. In addition, the extremely high pressure requirements during conventional melt processing, result in a high degree of entanglements that leads to grain boundaries or fusion defects during sintering and compression molding [7, 14]. These defects occur because the long relaxation times associated with melt-state UHMWPE hinder diffusion of chains from one melt-state UHMWPE particle to another [7, 14].

Several approaches have been proposed along years to overcome this actual problem during the manufacture of final UHMWPE based products. Nevertheless, it should be kept in mind that entanglements might be desirable in the final objects to trigger some of its extraordinary and specific properties. Smith and Lemstra [15-18] proposed in the 1980s the dissolution of the polymer in a suitable solvent in a ratio of 5% v/v (polymer in the solvent) to reduce the viscosity and, accordingly, the entanglements between the macrochains and, then, the obtainment of a viscous solution able to be drawn/spun into fibers. Rastogi *et al.* described, on one hand, the results concerning chain mobility during annealing [19] in a temperature range close to but below the melting point of UHMWPE solution-crystallized. On the other hand, they also reported [20] almost simultaneously a solid state sintering process from UHMWPE solution-crystallized films via hexagonal phase at high temperature and high pressure, which took advantage from the high chain mobility of the hexagonal crystal. Later on, a hot isostatic pressing was proposed and a well-consolidated UHMWPE material [21] was obtained at sufficient temperatures, heat soaking time and processing pressure. Temperature required was, however, too high employing this

methodology. More recently, other method was developed from polymer powders through a sintering process based on high velocity compaction [10, 22]. In contrast to ram-extrusion or hot-compaction, the powder was heated at a temperature just below the melting point. Particle sintering was attained thanks to the high energy impacts that promoted a very close contact of the powder grains and generated a temperature increase slightly above the polymer melting point. Moreover, this approach allows achieving specimens with optimized properties in a few minutes in comparison with the several hours required for conventional compression-molding of isotropic bulk parts.

A more advanced approach to achieve disentanglement of the polyethylene chains, thus enabling extended chain formation during crystallization, is via direct polymerization using a single-site catalytic system in the reactor [23]. It should be noted that, due to the nature of the crystalline phase, entanglements can only be found in the amorphous phase: by increasing the crystallization rate of the growing chain, it is then possible to decrease the occurrence of entanglements.

Examples in open literature based on this concept include special polymerization techniques or conditions that result in formation of single chain crystals (e.g., polymerization with decreased number of active sites or single-site catalysts [24-27] /or the use of decreased polymerization temperature [28-30]).

Reduction of entanglements leads to enhanced chain mobility, toughness, drawability, and fatigue resistance as well as decreased oxygen permeability and reduced pressure requirement for conventional melt processing [25].

Special processing technology such as gel spinning was developed to produce ultra-strong disentangled extended-chain polyethylene fibers, exhibiting a tensile modulus equivalent to the theoretical value [15].

Early attempts made to reduce entanglements by the use of controlled polymerization conditions were carried out, in 1987, by Smith *et al.* [28]. These authors reported the synthesis of a UHMWPE with a reduced number of entanglements by using a VCl_4 catalyst supported on a glass slide and lowering the polymerization temperature to -40°C. They have related this finding to the rapid crystallization of the growing chains when polymerization takes place at very low temperatures, thus inhibiting the formation of entanglements between neighboring chains. However, due to the poor catalytic activity of VCl_4 system at these low temperatures, this synthetic route was no longer pursued.

In 2011, Rastogi group [24] observed that the entanglement density tended to decrease with increasing polymerization time and this was explained by the favored crystallization rate over the polymerization rate. Several effects may contribute to this: (a) suppression of the nucleation barrier due to crystallization of chains synthesized at the earlier stages, (b) decrease in catalyst activity related to increased diffusion restrictions of ethylene to the active center, (c) and decrease in the temperature difference between the catalyst and its surroundings due to exothermic polymerization.

According to these authors the two above mentioned aspects, favoring crystallization rate over chain growth rate and keeping sufficient distance between growing chains, are the key points for the synthesis of disentangled UHMWPE. In principle, any catalyst able to produce UHMWPE would also be able, in suitable conditions, to produce a polymer with a reduced

number of entanglements [31]. Particularly, controlled polymerization using single-site catalytic systems, such as metallocene and post-metallocene catalysts, provides one elegant route to reduce the number of entanglements.

1.2 Catalytic systems

The first catalysts for olefin polymerization, generally known as Phillips catalysts, were developed in the 1950s by Phillips Petroleum using chromium oxides supported on either silica or alumina [32]. These catalysts produced polyethylene with moderate molecular weights, in the range of 10−20 $kgmol^{-1}$. In 1953, Karl Ziegler discovered that polyethylene with molar masses exceeding 20 $kgmol^{-1}$ could be prepared in larger quantities using a catalytic system combining $TiCl_3$ and Et_2AlCl [33]. This system showed high ethylene polymerization activity even under mild conditions. The catalytic system was further developed by Natta who used crystalline α-$TiCl_3$ in combination with $Al(C_2H_5)_3$. In this way, the synthesis of HDPE and, for the first time, isotactic polypropylene was successfully achieved [34-36].

1.2.1 Metallocene catalysts

A major breakthrough in olefin polymerization was the discovery of highly active metallocenic systems comprising a metallocene complex as catalyst and methylaluminoxane (MAO) as cocatalyst. In contrast to Ziegler-Natta systems, metallocene catalysts are soluble in hydrocarbons, and show only one type of active site. A precise control over the molecular architecture of the catalyst may also be attained enabling the production of a wide range of polyolefin products with tuned properties. The use of bis-(cyclopentadienyl) titanium (or zirconium) dichloride give rise to polyolefins with a narrow molar mass distribution lower than 2. Metallocenes have gained increased importance with the substitution of the η^5- cyclopentadienyl unit(s) by larger aromatic ligands, such as fluorenyl or indenyl, and furthermore by bridging these ligands with silylene or alkylene moieties [37]. These modifications allow the synthesis of chiral catalysts capable of adjusting the stereochemistry of polymerized substituted olefins, such as propylene or hexene.

Metallocenes are known since the early years of Ziegler-Natta catalysts but they only become relevant with the discovery of methylaluminoxane, by Sinn and Kaminsky in 1980 [38]. This discovery and its further application made possible to enhance the activity by a factor of 10 000 or more. MAO is an oligomeric compound in which aluminum and oxygen atoms are arranged alternately and free valences are saturated by methyl substituents. MAO plays a crucial role in olefin polymerization and motivated an intense research effort along the years. However, even today the exact structure is unknown, since equilibria between the oligomers and complexation of the oligomers with each other and with unreacted trimethylaluminum may occur [39]. According to Sinn [40] and Barron [41], it consists mainly of units of the basic structure $[Al_4O_3Me_6]$. These units join together forming clusters and cages. A probable association and cage like structure of four $[Al_4O_3Me_6]$ units are shown in Figure 1.2.

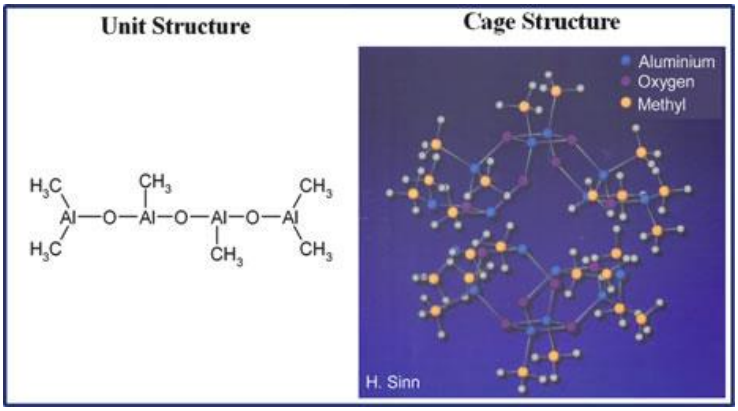

Figure 1.2 a): Unit structure of MAO, b): MAO cage formed by four linear unit structures. Reprinted from [42].

With metallocene/MAO based systems, various types of polyolefins can be produced with very high productivities [43]. Similar to the Ziegler catalysts, the aluminum compound acts as a methylating agent and enables the formation of a cationic active species with a coordinative vacancy, by abstraction of one of the leaving groups. Sequential coordination insertion of monomer in this active site allows chain polymer to growth (Figure 1.3).

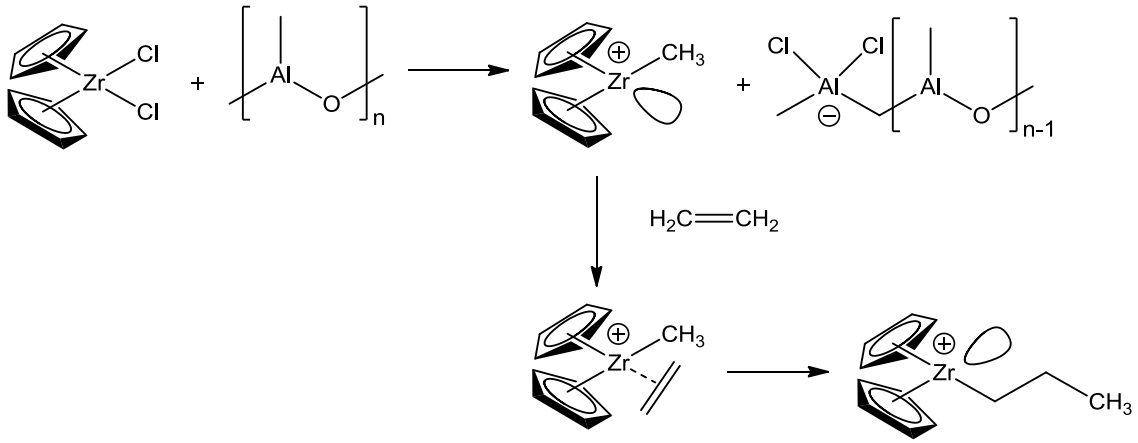

Figure 1.3: Activation and polymerization of olefins.

This is the most probable route to the active catalyst, but it is in fact a rather simplistic view. In reality, the role of MAO is not yet fully understood and following many investigations, several species have been identified and structures proposed at differing aluminum/metal ratios [44-46]. One function of MAO is the alkylation of the metallocene complex, when dichloride complexes are used. The other is the formation of an ion-pair. The bulky MAO cluster takes a chlorine-atom or a methyl-group from the metallocene together with an electron, originating a cationic metallocene which is stabilized by ion-pair interactions with an anionic MAO species $[Cl\text{-}MAO]^-$. Jordan [47] and Bochmann [48]

showed that the activity of metallocene catalysts depends on the formation of these coordinative unsaturated cationic species.

The first addition of monomer occurs at the free coordination site (vacant site). Then the polymerization is initiated by the insertion of the monomer between the cationic metal center and the alkyl group. This illustration, however, is highly simplified since a cage of MAO is additionally formed around the active site during the activation process [49].

The polyolefin industries use MAO in a large scale, since extremely high Al/Metal ratios are needed to attain high activities. In 2010, over 5 million tons of polyolefins, especially different kinds of polyethylene, were produced in commercial processes using MAO as cocatalyst [38]. Currently, companies such as Albermale, Akzo, Chemtura, and Mitsui produce hundreds of tons of MAO by reaction of water or ice with trimethylaluminum and in some cases add other aluminum alkyls to increase their solubility.

Amongst the group 4 metallocenes, the majority of the experimental and theoretical work on polymerization catalysts has focused on zirconocenes. Despite its lower activity hafnocenes have attained increasing interest since they have been shown to produce higher molar masses polymers than the corresponding zirconocene analogues [50]. As a result of the 4f lanthanide contraction of Hf, zirconocenes and hafnocenes are isostructural with practically the same atomic radii [51]. Considering the dichloride precursor forms, the main structural difference between the two metallocenes is the M–Cl distance, which is about 0.02 Å shorter in hafnocenes [52]. Moreover, hafnium complexes usually possess stronger M–C bonds [53]. Hence, the bonds between the metal and the leaving groups (Cl, Me), *i.e.* the bonds that are broken during the activation step, are stronger in hafnocenes. The stronger M–Cl and M–C bonds in hafnocenes explain the lower polymerization activity but higher molecular weight of the polymer in comparison to zirconocenes [54, 55].

1.2.2 Post-metallocene catalyst

The most recent advances in the catalytic polymerization of olefins have emerged from the development of “non-metallocene” single-site catalysts (known as post-metallocenes) and those based on diimine complexes of nickel and palladium and phenoxy-imine complexes of zirconium and nickel have received particular attention.

Discovery of highly active α-diimine nickel catalysts, which produce branched polyethylene without using comonomers via a “chain-walking” mechanism [56], resulted in a very intensive research on post-metallocenes in recent years [57]. Interestingly, post-metallocene complexes bearing late transition metals (Ni, Pd) are able to synthesize functional polyolefins due to their higher resistance against polar groups, compared to complexes of early transition metals (Ti, Zr, Hf) [58, 59].

Furthermore, the development by Fujita and co-workers of group IV transition metal complexes having bis(phenoxy-imine) ligands, known as FI catalysts, has been reported [60-65]. FI catalysts, when activated, exhibit unprecedented catalytic activities for the polymerization of ethylene. In fact, prior to the discovery of FI catalyst, metallocene catalysts were the most active catalysts for ethylene polymerization, but now many FI catalysts display substantially higher activities than metallocene catalysts.

FI catalysts are different from metallocene catalysts both structurally and electronically [61] (Figure 1.4). Structurally, FI catalysts are octahedral complexes while metallocene catalysts are tetrahedral ones, which results in a significantly different positional relationship between the central metal and the substituent in the ligand ([O-, N] or Cp ligand). Electronically, FI catalysts incorporate O- and N-based ligands while metallocene catalysts contain C- and H-based (Cp-based) ones, leading to considerably different electronic properties referring to the central metal and the metal–ligand bonding [66, 67].

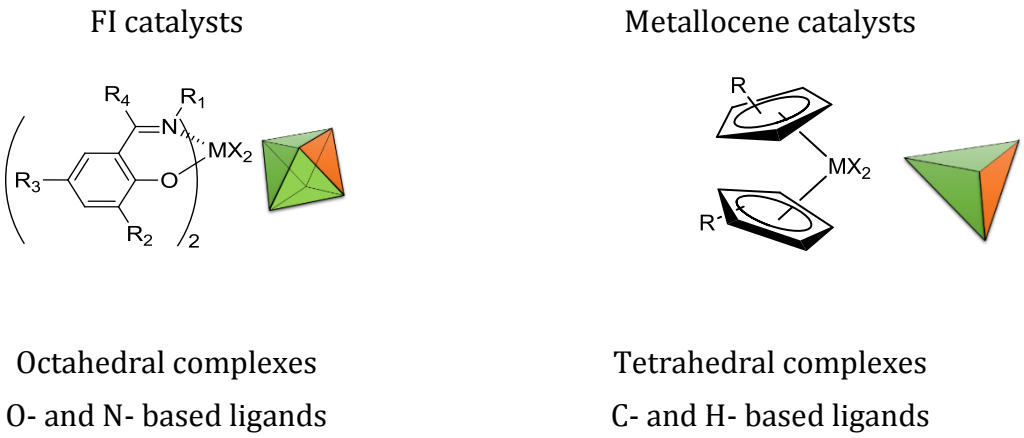

Figure 1.4: General structures of FI catalysts and metallocene catalysts. Reprinted from [61]

Further studies aimed at developing higher performance FI catalysts resulted in the discovery of a new family of fluorinated Ti-FI catalysts for living olefin polymerization. These catalysts are able to produce polyethylenes having extremely high molar masses, M_w > 2 million, and narrow MWDs due to their "living polymerization" character. The living polymerization is characterized by an efficient initiation and by chain termination/transfer rates that are negligible in comparison to the rate of propagation. There are seven generally accepted criteria for a living polymerization: (1) polymerization proceeds to complete monomer conversion, and chain growth continues upon further monomer addition; (2) number average molecular weight (M_n) of the polymer increases linearly as a function of conversion; (3) the number of active sites remains constant during the polymerization; (4) molecular weight can be precisely controlled through stoichiometry; (5) polymers display narrow molecular weight distributions, described quantitatively by the ratio of the weight average molecular weight to the number average molecular weight ($M_w/M_n \sim 1$); (6) block copolymers can be prepared by sequential monomer addition; and (7) end functionalized polymers can be synthesized [68].

In 2001, Fujita and co-workers reported that bis [*N*-(3-*tert*-butylsalicylidene)-2,3,4,5,6-pentafluoroanilinato] titanium (IV) dichloride (Figure 1.5) in association with MAO polymerizes ethylene at 25°C, and produces linear PE with high molecular weight and narrow molecular weight distribution (after 1 min of polymerization M_n = 412000 g/mol, M_w/M_n = 1.13) [69]. Furthermore, polymerizations at 25, 50 and 75°C exhibited a linear

increase in M_n with reaction time. The living behavior of this system was also demonstrated through the synthesis of PE and poly(E-co-P) containing di- and tri-block copolymers.

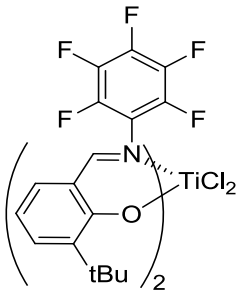

Figure 1.5: bis [N-(3-tert-butylsalicylidene)-2,3,4,5,6-pentafluoroanilinato] titanium (IV) dichloride.

Later on, in 2004, as a result of NMR experiments Makio and Fujita [70] demonstrated that the MAO activated form of the previous described catalyst was a cationic methyl-containing species (Figure 1.6).

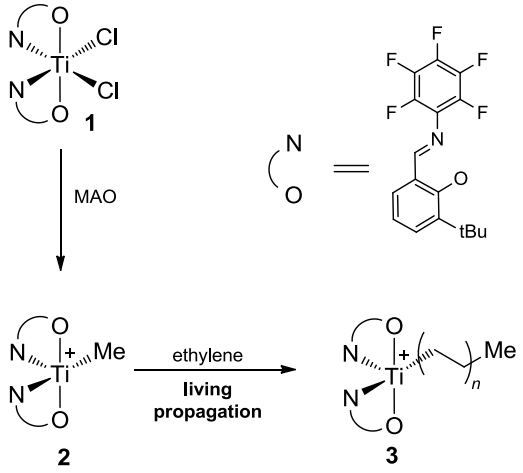

Figure 1.6: Activation and polymerization of bis [N-(3-tert-butylsalicylidene)-2,3,4,5,6-pentafluoroanilinato] titanium (IV) dichloride.

Ti-FI complexes incorporating fluorine atom(s) ortho to the imine-nitrogen ligands have been demonstrated to promote an unprecedented living polymerization of ethylene [71, 72]. This living character was explained by an attractive interaction between the fluorine atom in the ligand and a β-hydrogen atom on the growing polymer chain (Figure 1.7) that induces the suppression of chain termination processes (*i.e.* β-hydride elimination at the growing polymer chain and polymeryl transfer to the cocatalyst, or to $AlMe_3$ present in the MAO), thus enabling consecutive enchainment without termination.

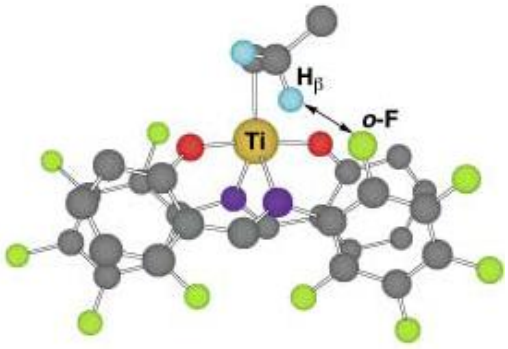

Figure 1.7: Structure of an active species derived from the complex presented in Figure 1.5 calculated by DFT. tBu groups are omitted for clarity. Reprinted from [71]

This attractive interaction provides a conceptually new strategy for the achievement of highly controlled living olefin and gives rise to monodisperse polyethylene [71].

1.3 Heterogeneous catalytic systems

In the last 20-30 years, intensive research on well-defined single-site catalysts for olefin polymerization has resulted in an ever-increasing number of novel homogeneous catalysts. However, despite the numerous advantages of these catalysts their application in commercial gas and slurry-phase processes for polyolefin production has fall off behind initial expectations. The use of large amounts of solvents, the lack of ability to control polymer morphology, and undesirable phenomenon of reactor fouling are the main disadvantages that the homogeneous catalysts face, in order to be applied in industrial processes [73, 74]. Among these, reactor fouling is one of the main problems that affect process operability. It consists in the formation of polymer deposits on the surface of a reactor, and on its internal parts such as: gas-distribution plates, heat exchangers, impeller blades and thermocouples or additional process hardware such as recycling lines and compressors. These polymer deposits build up over a period of time, contributing to a decrease in the ability to control the process (heat-transfer, catalyst efficiency, product throughput and split-control in cascaded processes), and hence the ability to produce the desired polymer resin to specification. This can be unmanageable to a point where the reactor needs to be shut down, cleaned, and restarted. Fouling is also detrimental to all parts of a polymerization process, including the reactor and its associated hardware (pumps, motor and gearboxes, etc.), which may need to be changed or maintained. The cleaning, maintenance and restart process can take several days, and is extremely costly and time-consuming.

Immobilization of these catalysts onto supports can provide a promising way to overcome these drawbacks. For industrial applications, supported catalysts are more appropriate because they have enhanced thermal stability and improved adaptability to various commercial processes such as slurry and gas phase processes. With the heterogenization of the catalyst, polymer of uniform particles with narrow size distribution and high bulk

density is produced and problems with the reactor fouling are prevented allowing continuous operation [75, 76].

1.3.1 Immobilization of single-site catalysts

A single-site olefin polymerization catalyst is a well-defined molecular entity which is intolerant to virtually everything, and its performance is critically dependent on the precise ligand environment of the transition metal center. It therefore became evident, that the immobilization of such catalyst is a complicated task. Apart from the requirements for the support, which must be inert in polymerization conditions, harmless to the polymer end-user and suitable for morphology control (which involves delicate issues of shape replication, fragmentation and heat/mass transfer properties, etc.), the main difficulty is how to introduce a strong, non-labile binding between the support and the active species without deteriorating the performance of the latter.

When considering the heterogenization of a catalyst, despite some basic problems of general relevance such as catalyst productivity and selectivity issues another factor to take into consideration is the competition between the operating reaction processes. In fact, the immobilization of a single-site catalyst affects the kinetics of all reactions occurring at the catalyst, which includes (poly/) insertion, chain transfer, and isomerization processes. It is very unlikely that such an effect would be proportional for all such processes, and therefore it is expected that some microstructural features of the polymer produced (e.g., long and/or short branches, terminal unsaturations, average molecular mass and molecular mass distribution, regiodefects, etc.) will change upon catalyst immobilization.

The catalyst selectivity is also a factor to take into consideration since the proximity to a surface inevitably represents a perturbation to the catalyst active site, not only in terms of accessibility but also of symmetry. This way the stereoselectivity of some catalysts can be altered by the immobilization, since this may change the relative monomer insertion frequency.

Regarding the catalyst productivity for an efficient catalytic action, it is mandatory that the monomer has an easy access to the active sites. So, introduction of a strong link between the catalyst and support, without limiting the accessibility of the active sites, can be extremely complicated. Many different supports and immobilization methods have been investigated, but it is frequently observed that after immobilization the catalyst activity is considerably reduced leading to a productivity one or more orders of magnitude lower than that of the same catalysts in solution [73, 74, 77]. Exceptions to this trend occur when immobilization results in stabilization of the active species, preventing the deactivation that often occurs in homogeneous polymerization. In fact, one advantage of immobilized catalysts is that intermolecular catalyst deactivation processes which may be highly detrimental in solution are usually frozen on surfaces; therefore, if a good productivity can be achieved it tends to be maintained for a longer reaction time.

1.3.2 Mesoporous silica as supports

Inorganic oxides like silica, alumina or aluminosilicates are by far the most frequently used supports for the immobilization of metallocenes and other single-site catalysts, although alternatives such as magnesium chloride, clays and polymeric supports have also received considerable attention. These low cost materials can be obtained with varied morphologies and particle sizes, show relatively high surface areas (several hundred m^2/g) and are stable and inert in polymerization conditions. Their surface chemistry is simple but versatile enough to allow the heterogenization of the catalytic system using several methods.

Ordered mesoporous silicas such as MCM-41 and SBA-15 emerged in the 1990s and exhibit a hexagonal arrangement of uniformly sized cylindrical pores, with a narrow pore size distribution and large surface area [78, 79]. They are used as supports for a wide variety of catalysts and, in recent years, proved to be well suited for the immobilization of several organometallic complexes. Compared to MCM-41, SBA-15 possesses pores of larger diameter, typically, around 3 nm for MCM-41 and 7 nm for SBA-15. Moreover, these pores may act as polymerization nanoreactors, and may influence the pattern of monomer insertion and the polymer morphology [80, 81]. These structured silicas present unique features for the synthesis of polymers with nanoscaled properties by *in situ* polymerization of olefins. In fact, their framework of well-defined channels and cavities at nanometric dimension may cause confinement effects on macromolecular chains and/or potentiate intimate mixing of polymer blends, produced via supported single-site catalysts. Research papers published in recent years have demonstrated the ability of these mesoporous silicas to produce nanometer scaled PE through space confined polymerization [82-88] as well as to affect the entanglement of molar masses in the case of UHMWPE [23, 89]. Kageyama *et al.* [90], using titanocene supported on mesoporous silica fiber, have produced polyethylene nanofibers and first demonstrated the potential of using nanochannels for the control of chain structure and polymer morphology. In Figure 1.8 we can visualize how the polymer chains formed at the activated titanocene sites within the individual mesopores, are extruded into the solvent phase and assembled to form extended-chain crystalline fibers.

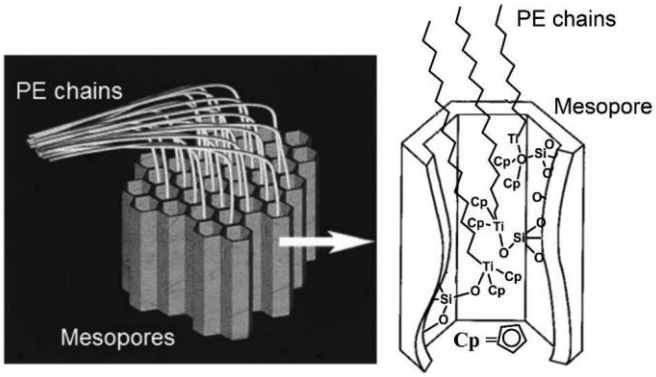

Figure 1.8: Conceptual scheme for the growth of crystalline fibers of polyethylene by mesoporous silica-assisted extrusion polymerization. Reprinted from [90]

To support this extrusion polymerization mechanism, the authors evaporated a reaction mixture consisting of catalyst-mesoporous silica MAO and toluene, to dryness and exposed the residue to ethylene. The SEM images of the polymerization mixture indicated the formation of PE only on the circular cross-sections of the silica fibers where the pore exits are opened.

Other reports have also shown the possibility of preparing polyethylene nanofibers using metallocene and other single-site catalysts supported on MCM-41 and similar mesoporous carriers [91-93]. Dong *et al.* obtained fibrous morphology in PE produced by *in situ* polymerization with Cp_2ZrCl_2 supported in MCM-41, where the MCM-41 nanochannels serve as template to suppress the kinetically favored chain folding process and obtain PE extended-chains. In this paper, the nanofibers and floccules were the major morphological units of the materials obtained. These nanofibers, with a diameter of 80-100 nm, aggregated uniformly to form fiber aggregates and bundles. With the extension of polymerization time, the number of the PE floccules increased, which could be used to control the proportion of nanofibers and floccules in the samples and changed the PE properties since the melting point of the PE with nanofibers was higher than that of common polyethylene [91].

This research group also reported the production of PE nanofibers with Cp_2ZrCl_2 fixed on MCM-41 and SBA-15 where the later support, due to its higher pore diameters, leads to larger nanofibers [80].

A similar result was obtained by Ye *et al.* when investigating in detail the fibrous morphology of nascent PE using SEM, and suggested that the microfibers had diameters of between 1 and 30 μm that in turn consisted of extended-chain nanofibrils with diameters of approximately 60 nm. Furthermore, the nanofibrils were parallel-packed into individual microfibers [92].

Guo *et al.* also produced PE with a fibrous morphology using nickel diimine catalyst immobilized on SBA-15 [81]. After supporting an iron(II)-bisimine pyridine catalyst in SBA-15, Xu *et al.* obtained polyethylene with higher molecular weight and fibrous morphology [94].

There are two main methods for catalyst immobilization on a support: physical impregnation and chemical tethering. Simple impregnation of the support with the catalyst and/or cocatalyst avoids the often complicated synthetic procedures involved in chemical tethering of the catalyst, but care should be taken to avoid catalyst leaching from the support that could lead to fouling problems. When using inorganic oxides supports, impregnation techniques are one of the most important preparation routes used for supported olefin polymerization catalysts (Figure 1.9).

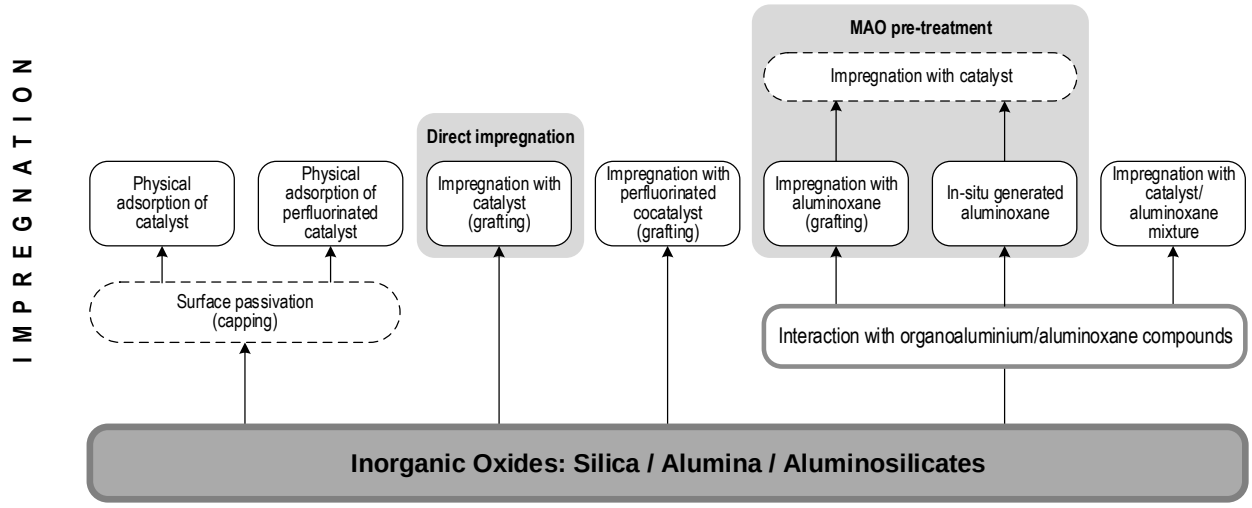

Figure 1.9. Main routes used for the preparation of supported olefin polymerization catalysts using inorganic oxides as supports. Adapted from [83]

Although numerous individual synthetic strategies have been employed to produce a catalyst from a combination of MAO, silica, and a catalyst complex, they fall into three main routes: a) the direct impregnation technique, where the catalyst contacts directly with the support; b) the MAO pre-treatment technique where the MAO or a alkylaluminum source is first contacted with the silica and the catalyst complex is introduced in a subsequent step; and c) the activation of the catalyst with MAO prior to impregnation of the silica, one of the simplest and most effective methods [95].

The MAO pre-treatment technique is one of the earliest and most frequently used and commercially available means to facilitate the immobilization of single-site polymerization catalysts. Impregnation of silica with MAO, optionally together with a catalyst, results in at least partial tethering of the cocatalyst via reaction with surface Si–OH groups. Silica and MAO are indeed the most commonly employed and commercially successful support material and cocatalyst, respectively, in polyolefin catalyst immobilization. Welborn [96] and Takahash [97] were among the first to disclose the contacting of silica with a toluene solution of MAO. In both cases, isolation and treatment of the silica-supported MAO with a dichloride or dialkylmetallocene yielded supported single-site catalysts that were effective in the homopolymerization and copolymerization of ethylene in a stirred-bed, gas-phase process. Similar procedures have been reported for a range of catalysts [73].

The combination of a solution of the catalyst with MAO, prior to contact with a silica support, has become a frequently utilized and successful technique for producing a supported, single-site polymerization catalyst. Some authors refer that because catalyst is activated in solution, this procedure may increase the number of active sites and lead to highly active catalysts. The process has several advantages, particularly from an industrial viewpoint. For example, it reduces the amounts of solvent used and byproducts produced and also involves a limited number of steps, particularly the time- and energy-intensive steps such as drying. All of these benefits typically result in a lowering of manufacturing costs. In addition, precontacting allows MAO to solubilize a poorly soluble catalyst prior to

impregnation, and can also allow a more effective activation of the metal center to be carried out in a homogeneous solution rather than in a heterogeneous phase, where problems with diffusion or side reactions may occur. An early and highly successful example of the above procedure was disclosed by Burkhardt and coworkers at Exxon [98].

Several review papers are available in literature providing a comprehensive discussion on supports and treatments applied to them, on the method and conditions of immobilization of the catalyst and how this affect the polymerization behavior of the supported system [73, 74, 99].

In the case of the FI catalysts, to the best of our knowledge, there is no reference to the direct immobilization of this catalyst on silica. Nevertheless, regarding the $MgCl_2$ supports Fujita and coworkers have found that bis(phenoxy-imine) complexes can be effectively immobilized and activated using these supports treated with $R_mAl\text{-}(OR)_n$ producing narrow molecular weight distribution polyethylenes with very high activities, comparable to those found for MAO activator systems. It was suggested that the effectiveness of the $MgCl_2$-based activator was related to the presence in the bis (phenoxy-imine) complex of O and N heteroatoms capable of electronic interaction with the support. Therefore $MgCl_2$ may work as an activator for the bis(phenoxy-imine)Ti complexes since these complexes possess O and N heteroatoms in the ligands, which are capable of electronically interacting with $MgCl_2$ [100, 101]. Well-defined polymer particle morphology could also be obtained using these systems [102].

In the case of the silica, several authors used the MAO pre-treatment technique to immobilize FI catalysts. Ethylene polymerization with dried SiO_2 first treated with MAO and then with a titanium complex resulted in polymers with higher molar mass, higher melting temperature and better morphology than those obtained with the corresponding homogeneous catalyst [103]. The anchoring of a nickel catalyst to MAO-treated silica produced a thermally stable nickel-heterogenized catalyst able to polymerize ethylene with higher productivity and resulting in PE with increased molar mass, in comparison to its homogeneous counterpart [104]. A zirconium FI complex was immobilized in SBA-15/MAO and produced nanofibrous polyethylene [105], another zirconium complex on MCM-41/MAO provided a supported catalytic system that produced extended-chain polyethylene nanofibrils with diameters of about 10 - 100 nm [106].

Ronca *et al.* [89] also explored the effect of the heterogenization of the catalytic system in the disentangled state of the UHMWPE. To achieve the conditions leading to “single-chain forming single-crystal”, the catalyst was supported on nanoparticles of high-surface area and the polymerization performed at room temperature. Figure 1.10 depicts differences in entanglements formation arising from the different density of the active catalytic sites during polymerization. For example, due to a higher density of the catalytic sites combined with a higher polymerization temperature, a larger number of entanglements is developed when using heterogeneous Ziegler-Natta catalysts (A) compared to homogeneous catalyst in low concentration(B), and a catalyst supported on high-surface area nanoparticles (C). For (B) and (C) crystallization rate is further enhanced by reducing the polymerization temperature below 30°C.

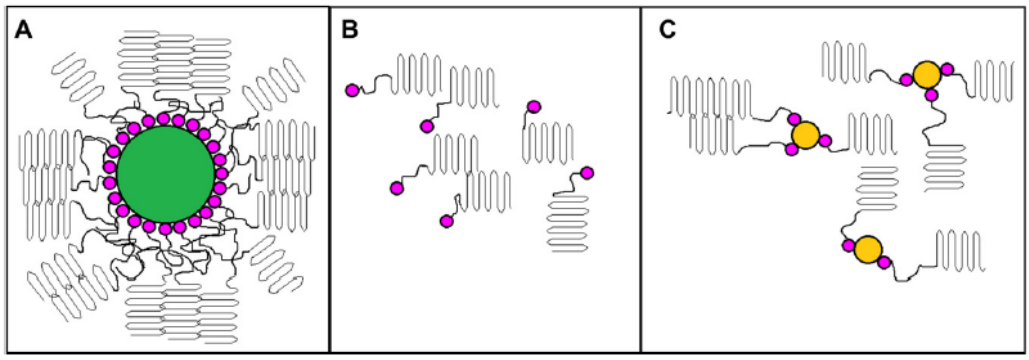

Figure 1.10: Entanglements formation during polymerization with A) heterogeneous Ziegler-Natta catalyst; B) single-site catalyst; C) single-site catalyst supported on nanoparticles. Reprinted from [89]

Besides enabling the heterogenization of the catalytic system, the mesoporous silica may play a second role as filler allowing the production of intercalated nanocomposites.

1.4 Polyolefin nanocomposites

Inorganic–polymer nanocomposites refer to polymer composites composed by inorganic building blocks and a polymer matrix. These building blocks may include: layered silicates (e.g. montmorillonite, hectorite, and saponite), metal nanoparticles (e.g. Au, Ag), oxides (e.g. SiO_2, TiO_2, and Al_2O_3), semiconductors (e.g. PbS, CdS) and so on.

Since nanocomposites aim to combine the characteristic properties of polyolefins with those of an inorganic material, they are of great interest because of their high potential as materials with novel properties. In general, inorganic materials possess better mechanical and thermal properties than the polymer matrix, e.g., modulus, strength, hardness, thermal stability, low thermal expansion, etc. Therefore, most of the inorganic nanofillers have a potential to improve the mechanical and thermal properties of the nanocomposites as compared with those of the matrix polymers. Chemical structure and amount of the fillers are just a part of factors that determines the properties of the composites. The other important factors include morphological factors such as shape, size, and state of dispersion of the fillers. Interface between the filler and the matrix polymer is also crucial for composite properties. The small size of the nanofillers yields a very large interfacial area, which may give rise to a significant amount of interphase material with properties different from the bulk. This fact opens the possibility to have synergistic phenomena that produce effects greater than the sum of the individual components. Provided that a good dispersion is achieved even low nanoparticle contents are already sufficient to obtain new or modified material characteristics. By the addition of reinforcing fillers, the physical as well as the dynamic-mechanical properties change: the material gets stronger and elasticity is reduced. Different types and amounts of fillers allow tailoring the properties of the material. The major challenge to overcome is the high surface energy of the nanofillers that favors the agglomeration into larger particles. The consequence is poor nanoparticle dispersion within the nanocomposite that usually leads to degradation of the properties and, for this reason, the preparation process becomes critical [94, 107].

1.4.1 Nature of the filler

The properties of the nanocomposites are not only influenced by microstructure of the polyolefins but also by the nature of the nanofillers, which includes their size, shape, concentration, and interactions with the polymer matrix. Moreover, the lack of compatibility between inorganic particles and polymer matrix limits the applications of nanoparticles in composites. As a result of incompatibility, the homogeneous dispersion of nanoparticle in polymer matrices is a challenge since they are known to be very prone to form aggregates. The ability to keep nanoparticles isolated and uniformly dispersed is crucial in creating composites that retain the fluidity of the host polymer while incorporating a high fraction of inorganic particles with their associated properties. In this system, competition between particle–particle, particle–matrix, and matrix–matrix associations have to be balanced. Therefore, sometimes it is necessary to modify the nanoparticles to overcome their tendency to aggregate and improve their dispersion in polymer matrices [108]. Two ways are generally used to modify the surface of inorganic particles: modification of the surface by chemical treatment and by the grafting of functional polymeric molecules to the hydroxyl groups existing on the particles. Surface modification of inorganic particles is a popular technique because it produces a good integration and an improved interface between inorganic filler and the polymer matrix.

Regarding the type of fillers, several studies have been made with different reinforcement agents: carbon nanotubes [109, 110], carbon fibers [111], or UHMWPE fibers, leading in the latter case to self-reinforced UHMWPE composites [112]. Nevertheless, up to now the main fillers used are porous inorganic oxides, particularly silica. Among the numerous inorganic-organic nanocomposites, polymer composites reinforced with nanosilica are the most commonly reported in the literature, having attracted substantial academic and industrial interest and being employed in a variety of applications. As referred before, silica nanoparticles present several advantages, such as the ease of preparation at a relatively low cost, possibility of performing surface modifications with different functional groups and acceptable biocompatibility. The addition of relatively small amounts (<3 wt.%) of inorganic particles, such as silica, titania, or calcium carbonate having dimensions in the nanometer scale was proven to increase both rigidity and toughness of several thermoplastics [113, 114]. As an example, an improvement in tensile modulus and impact strength was observed for high-density polyethylene (HDPE)/silica nanocomposite [115].

1.4.2 Preparation process of nanocomposites

The properties of the nanocomposites are not only influenced by the nature of the filler but also by the microstructure of the polyolefins and the preparation method.

Polymer nanocomposites can be prepared following various synthetic routes, according to the way that each phase is introduced. The organic polymer matrix can be introduced as a precursor (monomer or oligomer), as a preformed linear polymer (in molten, solution, or emulsion states), or as a polymer network, physically or chemically cross-linked. The nanofiller, in turn, can be introduced as pre-existing nanoparticles or in the form of precursors.

For the preparation of typical polymer/silica nanocomposites three general methods are generally used according to the starting materials and processing techniques: blending, sol–gel processes, and *in situ* polymerization (Figure 1.11) [107].

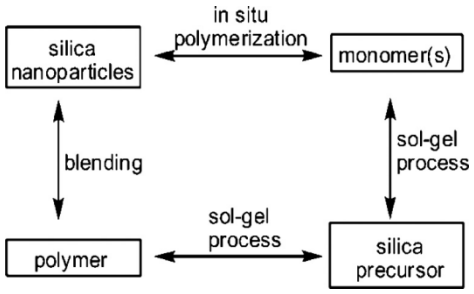

Figure 1.11: Scheme showing the three general approaches to prepare polymer/silica nanocomposites. Reprinted from Ref. [107]

Blending involves simple mixing of the polymer matrix and the silica fillers, and agglomeration of nanoparticles is a usual drawback. The sol-gel method process begins with a mixture of both silica and polymer monomers, followed by the polymerization of the monomers. The *in situ* polymerization is based on direct mixing of monomers with silica particles followed by a polymerization process favoring this way the dispersion of the filler within the polymer matrix. Compared with other methods, the method of *in situ* polymerization has the advantage of better compatibility of the systems, and the composites show good dispersion and mechanical properties.

Although PE nanocomposites are mostly produced by the conventional method of physical blending, as referred before one of the crucial drawbacks of UHMWPE is its extremely high melt viscosity, which hinders the use of these traditional processing techniques [116]. Due to its very high molecular weight and entanglement density, the mobility of the UHMWPE chains is limited and the complete melting of the polymer during its processing is hardly achieved, leading to a heterogeneous final product with fusion defects and/or grain-boundaries. Furthermore, it is difficult to effectively disperse nanofillers throughout the polymeric matrix by using conventional methods, which leads to poor mechanical and thermal properties of the nanocomposites. An alternative method for the fabrication of homogenously dispersed nanocomposites is the *in situ* polymerization approach. Good dispersions of the fillers and more effective filler/polymer interactions can be obtained with this method [109, 117].

By using *in situ* polymerization, Kaminsky *et al.* [117] produced UHMWPE/multiwalled carbon nanotube (MWCNT) nanocomposites using a metallocene as the polymerization catalyst, Sánchez *et al*. [110] reported the production of UHMWPE/MWCNT nanocomposite using a $TpTiCl_2(Et)$ system and Park and Choi [118] prepared UHMWPE/MWCNT nanocomposites by using half-titanocene catalytic system.

In another paper UHMWPE/fumed silica nanocomposites were prepared via *in situ* polymerization to investigate the effect of fumed silica on thermal and mechanical properties of the nanocomposites [119]. Scanning electron microscope images showed the

homogenous dispersion of nanoparticles throughout the UHMWPE matrix while no nanoparticle cluster has been formed. Addition of fumed silica to the matrix resulted in a slight increase in melting temperature while it also significantly improved the thermal stability of nanocomposites. Besides, via tensile testing, it was confirmed that addition of nanoparticles caused considerable improvement in the mechanical properties of UHMWPE/fumed silica nanocomposites compared to pure PE such as Young's modulus, yield stress, and tensile strength of samples while the elongation at break declined by addition of more nanoparticles.

HDPE/MCM-41 nanocomposites with a wide range of filler contents up to 28% were also obtained by *in situ* ethylene polymerization. They revealed improved mechanical performance and easier degradability at the end of their life cycle [82].

More recently, attempts to improve dispersion and interfacial adhesion of micro or nanosized mesoporous MCM-41 particles within a HDPE matrix by *in situ* polymerization were reported. The applied methodologies involved either the functionalization of PE chains by copolymerization with a polar monomer or the modification of MCM-41 surface by several modifying agents, before polymerization [120, 121].

Recently, Ronca *et al.* reported on the formation of UHMWPE nanocomposites prepared by *in situ* polymerization using FI catalysts supported on TiO_2, ZrO_2, hydroxyapatite, and CNT. The resulting nanocomposites exhibited improved nanofiller dispersion and reduced number of entanglements [23, 89]. The authors demonstrated that the fillers can be homogeneously distributed in the disentangled nascent ultra-high molecular weight polymer. The synthesized polymers, having high abrasion and wear resistance, can be drawn in a broad temperature processing window, exceeding 20°, below the equilibrium melting point of the linear polyethylene. The also shown that the modulus and tensile strength of the uniaxially drawn tapes is influenced by the presence of fillers and it is dependent on the filler-polymer interaction.

1.5 UHMWPE/HDPE Blends

The widespread uses of UHMWPE led to the urgent development of methods aiming to improve its performance, which is essential to fulfill the continuous market needs of this material with tailored mechanical and/or thermal properties. Among these methods, the blending of UHMWPE with other polymers, mineral particles, or the addition of reinforcement agents into the polymeric matrix [122-125] have proved to be interesting strategies to attain these goals.

HDPE, a low price polymer, has good flow properties and is widely used in commodity markets, as it can be transformed by traditional processes of extrusion, blow molding, injection molding, and rotational molding.

HDPE and UHMWPE have good compatibility since they have the same chemical composition. Moreover, UHMW polyethylenes may serve as ''tie molecules'' linking together polyethylene crystallites via cocrystallization [85, 126]. In this context, the mix between HDPE and UHMWPE is very interesting since it has the potential to combine the outstanding properties of UHMWPE and the good processability of HDPE under

conventional techniques. But due to the viscosity mismatching, it is hard to get the homogeneous HDPE/UHMWPE blend [127, 128].

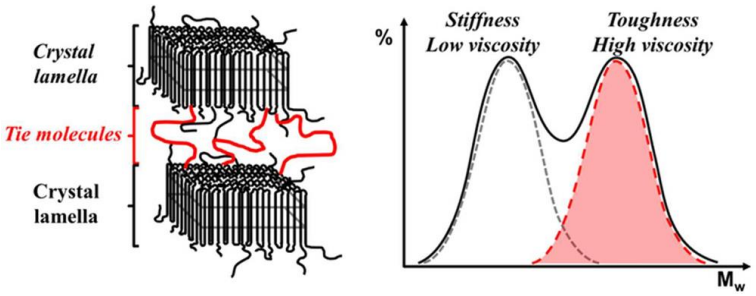

Figure 1.12: Polyethylene (HDPE/UHMWPE reactor blends) with bimodal MWDs containing short-chain-branched UHMWPE as tie molecules linking together polyethylene crystal lamellae. Reprinted from [126]

Different strategies have been reported for the preparation of UHMWPE blends and, in most of them, the blending is achieved by post-polymerization mixing such as melt mixing in an extruder or hot pressing. However due to entanglement density of UHMWPE, the tolerable amount of UHMWPE was restricted to a few percent in conventional melt processing.

Zuo *et al.* prepared blends of UHMWPE and HDPE by direct blending in a twin screw extruder and using a two-step processing and concluded that the addition of UHMWPE into HDPE could improve the mechanical properties of the final films [129]. The tensile strength and tear strength increased by 50% and 21%, respectively, when compared with those of pure HDPE film. DSC results show that the blends had a single melting endotherm peak, suggesting that co-crystallization may occur between UHMWPE and HDPE and are due to the better dispersion gained by the special screws structure in the twin screw extruder.

The presence of a filler was also considered by Suwanprateeb [130] that investigated HDPE/UHMWPE blends filled with calcium carbonate, produced by twin-screw extrusion followed by compression molding. The addition of UHMWPE helped to increase the strain at break and impact resistance of composites moderately without decreasing modulus or strength. The degree of toughening was found to increase with increasing UHMWPE content, but to decrease as the filler volume fraction was increased.

Various blend ratios of HDPE and UHMWPE were prepared via melt mixing by Lim *et al.* with the objective of determining their suitability as biomaterials [131]. A 50:50 (w/w) blend yielded optimum properties in terms of the processability and mechanical properties. In particular, the tensile strength and Young's modulus of the blend were between the values for neat HDPE and neat UHMWPE, but the strain at break increased 200% in comparison with that of both neat resins. The synergetic effect observed in the blends for properties such as the energy to break and tensile strain showed that the presence of UHMWPE improved the toughness properties. SEM fractography showed a similar trend, with extensive plastic deformation detected for the blends in comparison with neat HDPE.

The effect of the ultra-high molar mass component on the crystallization of bimodal polyethylene was investigated by Song *et al.* [132]. The authors introduced, by melt blending, a small amount of UHWMPE in HDPE and studied both the isothermal crystallization kinetics and crystal morphology of HDPE/UHMWPE composites by differential scanning calorimetry and polarized optical microscopy, respectively. DSC results showed that the presence of UHMWPE gives rise to an increase of the initial crystallization temperature of HDPE and the crystallization kinetics revealed an accelerating effect on the isothermal crystallization rate. The morphological development during crystallization demonstrated that the nucleation rate of HDPE is increased by the presence of UHMWPE which is in accordance with the kinetic results. During self-nucleation and annealing process, the UHMWPE chains act as nucleating centers in HDPE matrix, which help to form thicker lamellar crystal. Rheological measurement results proved that HDPE/UHWMPE blend is as easy to process as neat HDPE. Moreover, at lower shear rate, the blend shows higher melt viscosity, which makes it more sag-resistant.

In another study, Lucas *et al.* [133] obtained blends of HDPE with UHMWPE, with a molar mass of 4×10^6 g/mol, by melt mixing in a twin screw extruder at concentrations ranging from 10 to 30% by weight. The addition of UHMWPE to HDPE improved its abrasion resistance to abrasive paper and the mechanical properties, including the Izod impact strength, tensile strength at break, and also the strength and elongation at yielding. These improvements were explained by the good compatibility between the two polymers, as suggested by the SEM micrographs. Figure 1.13 displays the dispersed UHMWPE particles in the HDPE matrix. In fact, it was observed that the sample fractures occurred through the central region of some of the UHMWPE particles, breaking them in half, and not around the interface between HDPE and UHMWPE, indicating a very resistant interface. An increase in the impact strength of the blend samples was also observed in comparison to the pure HDPE.

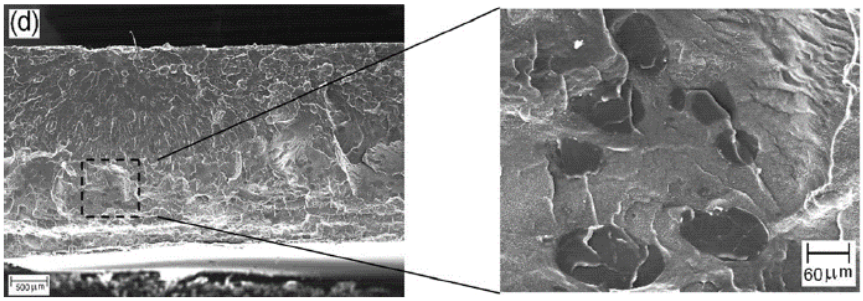

Figure 1.13: SEM micrograph image of the fractured surface of HDPE + 30 wt. %UHMWPE blend. Reprinted from [133].

These results are similar to those found previously by Boscoletto *et al.* [134] that prepared HDPE/UHMWPE blends containing up to 20 wt. % UHMWPE using two different processing apparatus, a single screw extruder and an internal mixer. According to these authors, the increase in the impact strength can be attributed to the greater capacity of UHMWPE to absorb impact energy, which is associated with the good interface of the two polymers in

the blend samples. Based on rheological and impact properties studies, they reported a dissolution of UHMWPE up to 2.6% wt. of the original amount, thus explaining the good interface observed by SEM and the increase in impact strength of those samples. Lucas *el al.* also agree that this dissolution may also be responsible for the good interface that has been verified and, therefore, for the good impact resistance and other mechanical properties of the blend samples. As was observed by Boscoletto *et al.*, in samples fractured under impact at room temperature, the presence of concentric rings can be detected, confirming the model proposed by the authors (presented in Figure 1.13b) that the fracture of these particles occurs from the outside, with a significant contribution by UHMWPE in absorbing energy and resisting crack propagation.

Lim *et al.* [131] related the resistance to the crack propagation to the high tenacity, of UHMWPE particles that can counteract the force applied at the time of the application of impact energy, thereby slowing the spread of cracks.

Aiming to evaluate the use of UHMWPE as additive for the elimination of distortions in PE processing, Aguilar *et al.* observed that the melt blending of PE and UHMWPE gives rise to heterogeneous complex systems of regularly dispersed particles of UHMWPE material embedded in a matrix of PE. They concluded that the addition of UHMWPE to the PE by melt blending strongly affects the rheological behavior of the melt in the linear viscoelastic regime since enhanced storage modulus and viscosity values at low frequencies are observed in the blends, when compared with the properties of the bare PE [135]. According to the thermal analysis, in such systems there is some degree of interaction at the interface between the UHMWPE particles and the matrix. In the conditions of the mixing method used, the morphological and thermal observations indicate that the UHMWPE concentration needed to obtain a homogeneous particle distribution should be lower than 7 wt. % at least. Dumoulin *et al.* also found that a small fraction of UHMWPE can effectively be incorporated in a PE matrix under similar blending conditions [136].

In a more recent study, Shen *et al.* [137] demonstrated that high temperature melting at 280 °C (HTM) of HDPE/UHMWPE blends was very effective in increasing chain entanglements through phase interfaces by using properly selected melting temperatures and durations. The UHMWPE dispersed particles were swelled partially first by HTM, and then the swollen parts could be dissolved in the HDPE matrix by a subsequent shear. These two steps generated a better integration of HDPE with UHMWPE than that obtained by a conventional process. Based on accelerating diffusion of polymer chains at high temperature, the HTM enhanced chains diffusion across the phase interface, and consequently the integration of HDPE with UHMWPE components was improved.

Work on HDPE reinforced with UHMWPE fibers produced via hot pressing has also revealed an improvement in the creep and wear properties of the composite [138]. The materials studied have tensile strength and Young's modulus more than one order of magnitude above bulk PE. The wear resistance of the PE/PE composites was found to increase continuously with the fiber content. Composites with V_{Fiber}>30% reached almost the wear performance of UHMWPE.

Diop *et al.* [128] demonstrated the usefulness of solid-state shear pulverization (SSSP) in the preparation of UHMWPE/HDPE blends containing up to 50 wt.% UHMWPE . Injection-molded sample bars made from SSSP blends with 30-50 wt. % UHMWPE exhibit very high

values of impact strength, about 4 times higher than neat HDPE). For a blend prepared with 5 wt. % UHMWPE via SSSP, the authors didn't observe discernible agglomerates of UHMWPE in thin films of the blends (as was the case with a blend of similar composition prepared via solution blending). Additionally, as a result of the effective mixing achieved for both SSSP and solution-blended samples (each containing 5 wt.% UHMWPE), non-isothermal crystallization data showed that blend components participated in cocrystallization. On the contrary, for a blend prepared by melt mixing and containing 5 wt. % UHMWPE, easily visible UHMWPE agglomerates and no indication of co-crystallization were observed as a result of the poor dispersion of UHMWPE in the HDPE matrix.

In all the above described research works, the incomplete melting of UHMWPE greatly affect the final blend properties. In view of improving both sustainability and performance of polyethylene commodities, it is an important challenge to explore new routes toward melt-processable UHMWPE or UHMWPE/HDPE blends with a high UHMWPE content without requiring special processing and without sacrificing economic and ecological benefits typical of polyethylene materials. To meet these goals, robust and highly active multisite catalysts and reactor blend technology are in great demand.

Traditionally, PE with bimodal molar mass distributions is obtained by means of multi-reactor technology. Typically, cascades of reactors operate at different polymerization conditions with variations of temperature, pressure, and hydrogen partial pressure [95, 139-142]. Although cascade reactor technology is widely used in polyolefins industry, an alternative strategy would be the use of two different single-site catalysts ("dual-site catalysts") simultaneously producing UHMWPE and PE and thus enabling the formation of polyolefin reactor blends in one step in a single reactor [73, 143] (Figure 1.14).

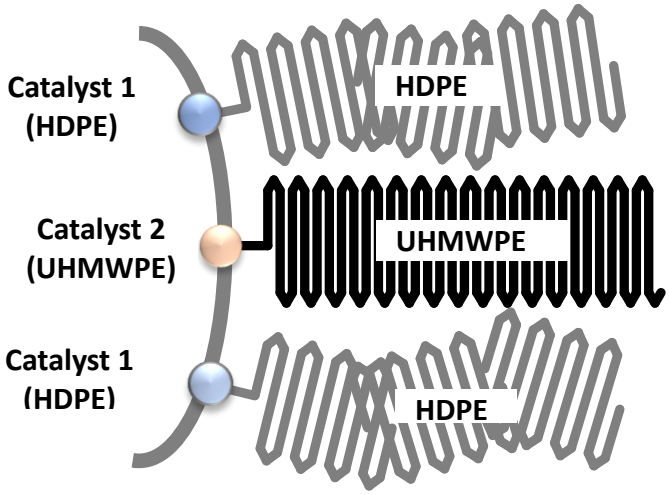

Figure 1.14: Synthesis of blends of two different single-site catalysts.

The close proximity of both sites enables highly efficient mixing on a mesoscopic scale, which cannot be achieved by melt compounding. For instance, Mota *et al.* reported on blends produced by the use of early and late transition metal complexes and this way obtained reactor blends of linear and branched PE [144]. In another approach, Liu *et al.*

prepared bimodal polyethylene in homogeneous phase using a FI-type catalyst in combination with $ZnEt_2$ as chain transfer agent [145]. Yet, homogeneous catalyst systems are known to account for severe reactor fouling, owing to the formation of dustlike fine polyolefin particles. Hence, the group of Rastogi immobilized several catalysts on $MgCl_2$/ $AlEt_n(OEt)_{3-n}$, thus producing polyethylenes with bimodal MWD exhibiting flow-induced orientation phenomena [146]. Intimate mixing of the two fractions was apparent from the polymer melting and rheological behavior. The presence of a high-molecular weight fraction led to orientation of long-chain molecules when shear was applied to the polymer melt, resulting in shear-induced crystallization and the formation of a shish-kebab polyethylene crystalline morphology [146].

The formation of polyolefin reactor blends, prepared by combining either Ziegler-Natta catalysts with single-site catalysts or by blending together different single-site catalysts, has attracted considerable attention in academia and industry [147-151].

Recently, Mülhaupt group has developed silica-supported dual-site catalysts based upon binary blends of chromium and/or iron post-metallocene catalysts for tailoring polyethylene reactor blends with bimodal and ultra-broad MWD, in which the amount of UHMWPE is varied over a very wide range without affecting the average molar masses of the individual PE fractions produced on different catalytic sites [85, 152, 153].

Working with a different catalytic system, Kurek *et al.* [85] reported the synthesis of melt processable polyethylene reactor blends with tailor-made MWDs, by using a ternary blend of two chromium (III) and one iron (II) post-metallocenes complexes supported on mesoporous silica. The authors studied the preferred cosupporting sequence of this ternary blend and concluded that cosupporting these post-metallocenes catalysts on MAO pretreated mesoporous silica did not hinder the single-site nature of the blend components. Therefore, this method represents a very versatile synthetic route to produce multiple single-site catalysts with excellent control of polyethylene MWDs by varying the mixing ratios of the catalytic sites. Considering that the average molecular weight of the PE fractions is unaffected by their mixing ratio, it is possible to vary the dispersities exclusively via the content of an individual catalyst blend components. This allows creating virtually any shape of MWD curves including symmetric as well as asymmetric MWDs. In addition, the average molecular weights of the individual PE fractions can be tuned by varying the architectures of the blend components. Ultra-broad MWDs are readily tailored with dispersities varying between 10 and 420.

Silica nanofoams (NF) with an interconnected pore system and average pore sizes of 20 nm are very effective supports for the heterogenization of single-site metallocene and post-metallocene catalysts. Highly active single- and dual-site catalysts supported on NF has been shown to enable the tailoring of bimodal PE molar mass distribution in ethylene polymerization and also the control of both polyethylene morphology [152]. Producing dual-site catalysts by immobilizing blends of a chromium post-metallocene together with metallocene and post-metallocene complexes on MAO-tethered NF, represents a very versatile synthetic strategy toward designing bimodal PE, varying the UHMWPE content as a function of the different catalysts molar ratio.

Very recently, Kurek [153] described the simultaneous and sequential immobilization ("cosupporting") of Fe and Cr based post-metallocenes on a MAO-tethered silica support,

affording a versatile two-site catalyst family. The catalytic system contains catalytically active Cr single-sites, producing UHMWPE, and Fe single-sites, producing lower molecular weight PE. Hence, such cosupported two-site catalysts produce PE reactor blends with bimodal MWD containing variable amounts of UHMWPE. The Fe/Cr molar ratio controls the weight ratio of both PE fractions but does not affect their average MW. The sequential cosupporting of Fe/Cr is preferred to the simultaneous cosupporting Fe + Cr to achieve high content of UHMW. While UHMWPE formation impairs catalyst activities, most likely due to diffusion limitations, the MWD control with Fe/Cr two site catalysts is remarkably robust, enabling stable operation and facile MWD control. The linear correlation between Cr content of Fe/Cr catalyst permits an easy selection of MWD ranges. Moreover, cosupporting can be expanded from two-site catalysts to a great variety of multiple-single-site catalysts producing bi-, tri and multimodal polyethylene MWDs, which are readily tailored to match the demands of individual applications. The manufacturing of tailor-made polyolefins via cosupported multiple single-site catalysts represents a very versatile tool for polyolefin synthesis, which can be employed to achieve improved control of mechanical and rheological properties.

In spite of the obvious benefits of such mixed catalysts in olefin polymerization, it is rather difficult to control MWD over a wide range because different sites interact with each other or with alkyl activators. Frequently, complex mixtures are formed by multi-site catalysts, because polymer MW varies as a function of catalyst composition and polymerization process parameters. Hence, it is an important aim in polyolefin research to explore blends of single-site catalysts, which do not interact and form robust two-site catalyst systems. The ideal multi-site catalyst should enable MWD control by varying the blend ratio of low and UHMWPE as a function of the molar ratio of the different catalytic sites without affecting the MW of these PE fractions, produced on different contiguous sites [73, 143].

Nevertheless, this has now become a commercially viable option. For example, Univation Prodigy systems has developed for ethene/α-olefin copolymerization a combination of a metallocene and a McConville type catalyst, immobilized on silica, and used it to produce pipe-grade polyethylene comprising a low molecular weight fraction with low comonomer content and a high molecular weight fraction significantly richer in comonomer [154]. Another example of an industrial development involving co-immobilization has been the efforts of Mihan and coworkers at LyondellBasell, who have described ethene/1-hexene copolymerization with a combination of a Brookhart–Gibson iron catalyst and $(n\text{-}BuCp)_2HfCl_2$ immobilized on silica [155]. The very low copolymerization ability of iron catalysts makes them particularly attractive for this type of bimodal polyethylene.

It should be noted however, when discussing catalyst stability and deactivation, that controlling a co-immobilized catalyst is still difficult, as each catalyst invariably has a different response to process operation and impurities.

2. UHMWPE based nanocomposites prepared by *in situ* polymerization with a titanium phenoxy-imine (FI) catalyst: synthetic aspects and characterization

The first part of this chapter describes the synthesis of neat UHMWPE and UHMWPE based nanocomposites by *in situ* polymerization. It starts with a brief description regarding the selection of the bis-phenoxy metal complex to be used as catalyst and of the corresponding support for immobilization. Next, it presents the ethylene polymerization behavior of the homogeneous and the supported systems along with the immobilization methodologies used and their effect on the polymerization activity and polymer molar masses. Then, the thermal characteristics and mechanical behavior of the produced nanocomposites are investigated and their performance discussed. Finally, it is presented an approach to process UHMWPE in solid-state, by compression molding below its melting temperature. Differential scanning calorimetry and X-ray diffraction are used to access the crystallinity values exhibited by these films; while the mechanical parameters, elastic modulus and hardness, are assessed through indentation measurements.

2.1 Selection of the catalyst and of the support/filler

The development of the phenoxy-imine family of complexes has been associated with the latest advances in the catalytic polymerization of olefins. The high catalytic performance of these early and late metal catalysts toward olefin insertion, requires the presence of sterically demanding groups at the imine nitrogen (R_1) and *ortho* to the phenolic oxygen (R_2) [61, 156] (Figure 2.1).

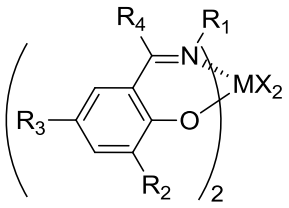

Figure 2.1: General structure of the phenoxy-imine complexes.

In the case of group IV metal complexes these bulky substituents are needed in order to attain catalytic active geometries, bearing cis-oriented X ligands, as well as to increase catalytic activity.

Typically, bulky R_1 substituents increase the molar masses of the polymer both for early and late metal complexes. This behavior is probably due to the fact that a 6-membered ring intermediate for β-H transfer to the coordinating monomer is sterically more demanding than a 4-membered ring intermediate for the propagation reaction (Figure 2.2). Therefore the chain transfer reaction is less favored than the propagation due to repulsive interactions with R_1.

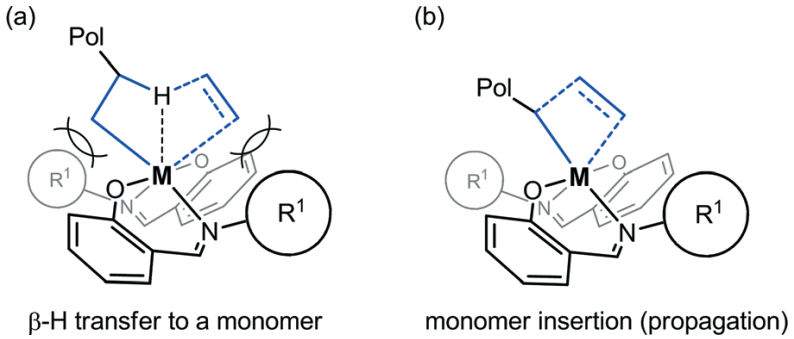

Figure 2.2: Structures of intermediates for (a) β-H transfer to a monomer (6-membered ring) and (b) monomer insertion (propagation) reaction (4-membered ring) in FI catalysts. Reprinted from [156]

On the other hand, electron withdrawing substituents generally increase the polymerization activity of phenoxy-imine complexes, which is not necessarily true for metallocene catalysts. The difference between phenoxy-imine and metallocene complexes might come from the fundamental difference in the bonding properties between the metal and the ligands. In the case of phenoxy-imine complexes these bonds involve O and N heteroatoms and in the case of metallocenes these are M-Cp´ bonds.

Finally, olefin polymerization catalysts have the latent coordination site at the electron deficient metal centre. Olefin monomers must compete against other potential coordinating species in the polymerization media, such counterions, neutral catalyst precursors, alkylaluminum species and β-agostic hydrogen. Bulky R2 substituents enhance dissociation of such coordinating species and shift the equilibrium to the olefin-coordinating species. Simultaneously, R2 substituents will protect the vulnerable phenolic oxygens from the Lewis acidic species, which may cause irreversible deactivation by ligand transfer to alkylaluminum species. Moreover, another role of the R2 substituents was suggested by theoretical calculations. It has been shown that large R2 substituents significantly destabilized the olefin π-complex, but the energy of the subsequent transition state for olefin insertion remained similar to that obtained with small R2 substituents. This behavior favors the olefin insertion in presence of large R2 substituents because the overall insertion barrier is lower [157].

Taking into consideration the features described above, the FI catalyst, bis [*N*-(3-*tert*-butylsalicylidene)-2,3,4,5,6-pentafluoroanilinato] titanium (IV) dichloride, was selected in this thesis to produce UHMWPE. This catalyst has a bulky an electron withdrawing substituent in R_1 and a bulky substituent in position R_2 as depicted in Figure 2.3.

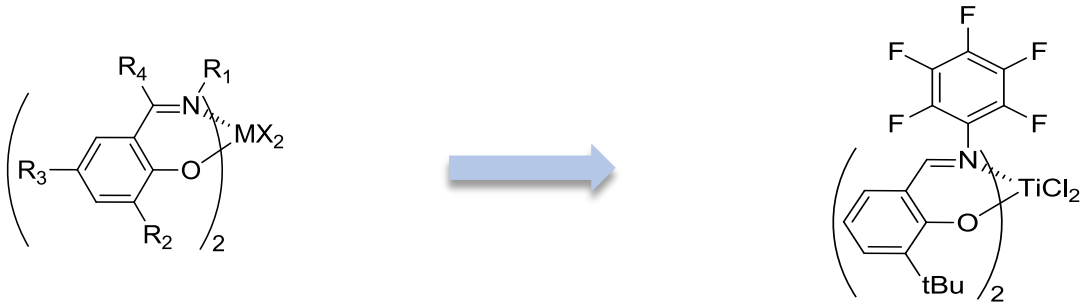

(a) **(b)**

Figure 2.3: (a) General structure of the phenoxy-imine complexes and (b) Structure of the bis [N-(3-tert-butylsalicylidene)-2,3,4,5,6-pentafluoroanilinato] titanium (IV) dichloride, FI catalyst used in this work.

In what regards the selection of the support, previous studies have described the immobilization of different catalysts on mesoporous materials like MCM-41 and SBA-15 [106, 158-161]. The results showed that textural properties of the ordered mesoporous supports influence the structure of the supported catalysts and, therefore their catalytic activity. In this sense, supports with narrower pore diameters presented lower catalytic activities suggesting the higher probability of inactive bimolecular species formation due to the proximity among the catalytic precursors within the pores [162]. Smaller pores also contribute to the formation of surface obstacles, which may hinder reactant diffusion [158, 163].

Due to these considerations, mesoporous silica SBA-15 was selected as a suitable catalyst support, since it has large pores, which can facilitate the access of the catalyst and enable the catalyst and cocatalyst (MAO molecules) to be anchored not only on the surface but also inside the porous structure, leading to polyethylene chains growing inside the channels [159, 164].

2.2 Characterization of SBA-15

SBA-15 is a mesoporous material showing periodically organized two-dimensional hexagonal structures, which are constituted by the arrays of uniform mesopores within a specific size interval. The powder XRD pattern of the as-synthesized SBA-15 (Figure 2.4) shows the expected highly ordered hexagonal structure identified by the three diffraction peaks that can be indexed as (100), (110) and (200) reflections associated with the *p6mm* hexagonal symmetry [165].

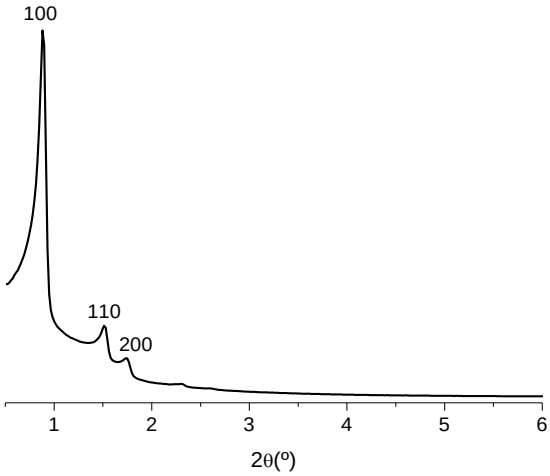

Figure 2.4: XRD pattern of as-synthesized SBA-15.

SEM and TEM micrographs of the SBA-15 synthesized are depicted in Figure 2.5a and 2.5b, respectively, where the particle morphology and the well-defined channel structure with the hexagonal arrangement are evidenced.

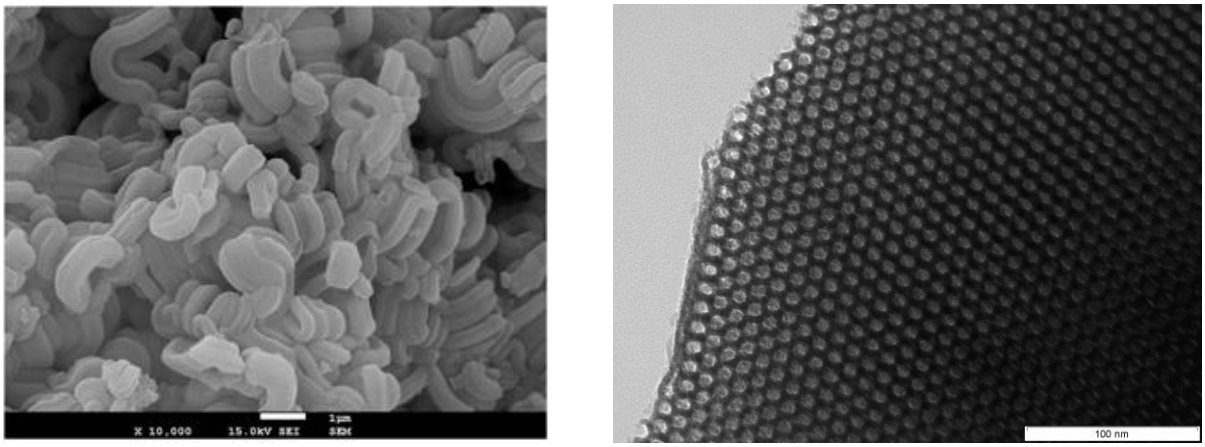

Figure 2.5: (a) SEM image (b) TEM micrographs of SBA-15.

Figure 2.6 displays the N_2 adsorption isotherm obtained for the sample of SBA-15 and Table 2.1 summarizes the textural parameters calculated from this experimental isotherm, which are similar to others reported for this type of supports [166].

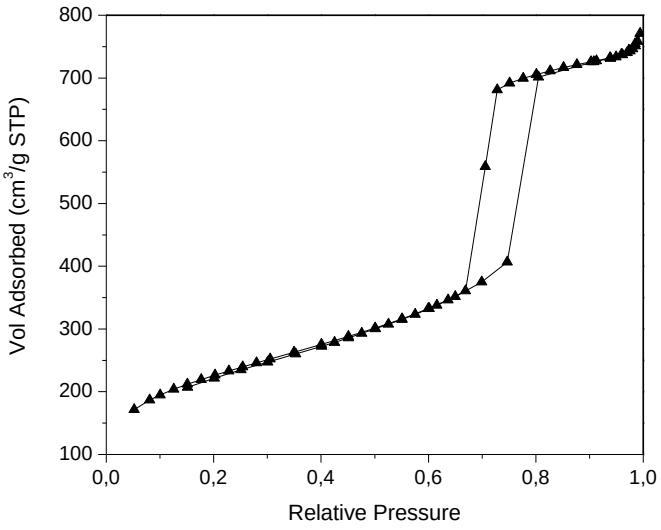

Figure 2.6: Nitrogen isotherm of SBA-15.

Furthermore, SBA-15 exhibits an N_2 adsorption-desorption type IV isotherm with an H1 hysteresis, characteristic of well-formed SBA-15 material [166] with the presence of a well-defined pore filling step with a narrow range of p/p_0 (capillary condensation), demonstrating the fine organization of cylindrical pores of uniform size.

Table 2.1: Parameters of the SBA-15 used as support

Sample	S_{BET} (m^2/g)	V_p (cm^3/g)	D_p (Å)
SBA-15	758	1.05	68

S_{BET}: specific surface area, V_p: specific pore volume (calculated at the top of the adsorption step), D_p: average pore diameter estimated by BJH (desorption)

2.3 Ethylene polymerization behavior of the homogeneous catalytic system

As stated before, FI catalysts combined with appropriate activators exhibit very high catalytic activity and particularly Ti-FI catalysts possessing fluorine atom(s) *ortho* to the imine-*N* can induce highly controlled living ethylene polymerizations [61, 167]. In these first experiments the FI catalyst was used as catalyst to produce neat UHMWPE under homogeneous conditions, as reported in former studies [72, 156].

The effect of experimental parameters, such as Al/Ti ratio and polymerization time, on the behavior of this complex under homogeneous conditions was first investigated. The obtained results are summarized in Table 2.2 and Figure 2.7.

Table 2.2: Polymerization conditions, activities, productivities, molar masses and dispersities for the polyethylenes attained under homogenous conditions.

Sample	Al/Ti	Reaction time (min)	Average activity (kgPE/molTi.h)	Productivity (kgPE/molTi)	M_w (10^6 g/mol)	D
FIHOM014	500	6.5	17660	2019	1.045	n.a
FIHOM003	1500	6.5	19730	2140	-	-
FIHOM004	1500	13	19150	4150	1.479	n.a.
FIHOM008	2500	6.5	20380	2210	1.172	1.3
FIHOM002	2500	13	19310	4180	1.359	1.5
FIHOM018	2500	26	14580	6308	2.033	1.6
FIHOM005	5000	6.5	21380	2316	1.197	1.4
FIHOM007	5000	26	15150	6565	1.881	n.a.
FIHOM016	16000	6.5	22470	2834	-	-

Figure 2.7 shows the kinetic profiles obtained for several Al/Ti ratios at distinct polymerization times. It may be seen that quite stable profiles are obtained for polymerizations carried out for 6.5 min or 13 min but the activity decay is much more pronounced at longer polymerization runs. Accordingly, the average activity and productivity (see Table 2.2) show almost a two-fold increase when the polymerization time increases from 6.5 to 13 min, but this linear dependence is lost at the highest polymerization time of 26 min. The behavior exhibited at short reaction times is in accordance with the reported living character, whereas it starts to deviate from purely living characteristics as polymerization times become longer [168].

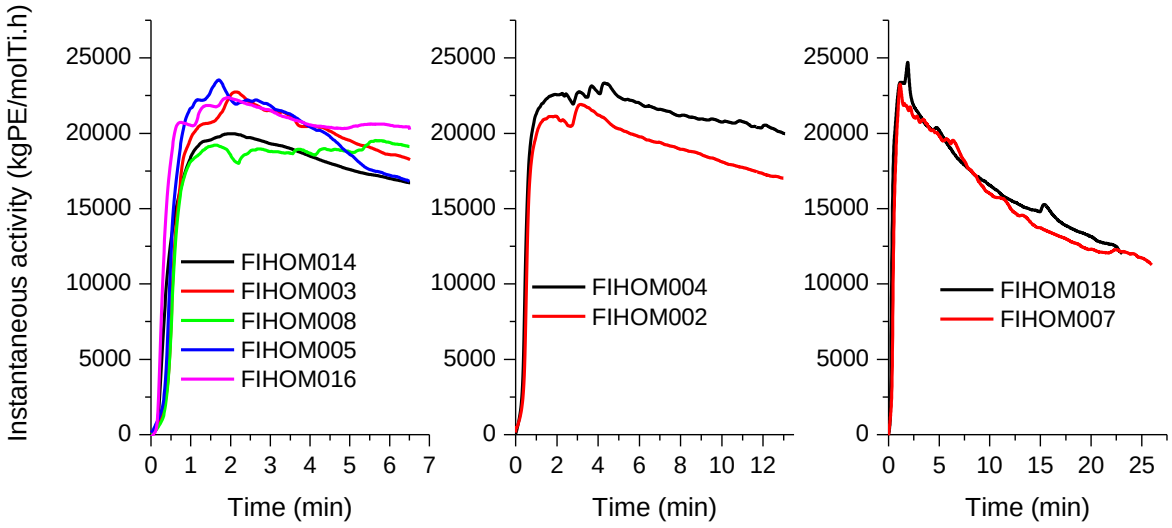

Figure 2.7: Kinetic profiles for different ethylene polymerizations performed at distinct Al/Ti ratios and polymerization times. Left plot 6.5 min, middle plot 13 min and right plot 26min.

The analysis of the polymer molar masses and dispersity (D) values, shown in Table 3.2, indicates that as expected the molar mass distributions are moving to higher Mw values as polymerization time increases. Nevertheless, the dependence of Mw with time it is not linear and that the catalytic system is already deviating from a living character at low polymerization time, showing a dispersity of 1.3, and this deviation is enlarged with time reaching a D of 1.6 after 26 min.

Heterogenization of the catalyst and mass transport limitations within the growing polymer particles enclosing the active sites or a gradual deactivation of the catalyst by the growing polymer after a certain polymerization time have been proposed to account for this deviation [169, 170]. Accordingly and due to these phenomena, the dependence of the activity on the Al/Ti ratio only exhibits an increasing trend for the runs at the shortest polymerization times. Although data on the effect of Al/Ti over polymerization is scarce for this type of catalyst, a similar dependence has been described by other authors [171, 172]. On the other hand, a stronger decay of activity seems to occur at the higher Al/Ti ratios and, therefore, the role that may play the increasing concentration of trimethylaluminum, invariably present in MAO, in deactivation of FI catalyst should not be neglected [70, 173].

Lemstra *et al.* reported that rising Al/Ti ratio results in an increase of the molar mass, arguing that the chain transfer to aluminum does not play a major role in their catalytic system [168]. In the present conditions, the values of M_w obtained for polymerizations at identical reaction time of 6.5 min, samples FIHOM014, FIHOM008 and FIHOM005, indicate that molar mass barely increases with the Al/Ti ratio. This behavior may be explained by two different effects acting simultaneously: on one hand, the increase of the Al/Ti would promote the activation and stabilization of the catalytic species but, on the other hand, a detrimental influence is also expected with the rise of Al/Ti ratio due to the easy

deactivation of the catalyst by the trimethylaluminum present in MAO. The balance of these two opposing effects will determine the catalytic behavior that, under the conditions used here, gives rise just to a slight increase in the polymer molar masses.

On the contrary, at constant Al/Ti ratio an increase in the polymerization time significantly increases the polymer molar mass, as clearly deduced from Table 2.2. Nevertheless, the catalyst starts deviating from the living character at short polymerization times, as a non-linear M_w dependence on time is observed.

2.4 Ethylene polymerization behavior of the supported catalytic systems

Two different immobilization methods have been used in this work to perform the synthesis of UHMWPE nanocomposites by *in situ* supported polymerization. Methylaluminoxane is needed in both approaches for the FI catalyst to be immobilized on the SBA-15. The direct impregnation of FI catalyst on SBA-15 was also attempted in an early stage but it was proved to be ineffective. In fact, to the best of our knowledge, there is no reported data in open literature regarding the direct immobilization of this catalyst on any type of silica. Steric reasons may account, most probably, for this feature.

The first approach used involves immobilization of the catalyst on SBA-15 formerly modified with MAO (SBA-MAO method), as displayed in Figure 2.8. This is one of the most widely used techniques to support catalysts and comprises the treatment of the silica surface with MAO before incorporation of catalyst to form the catalytic complex with the surface-anchored MAO [99]. Other authors have used the same methodology to immobilize FI catalysts on silica. Cui *et al*. carried out ethylene polymerization with dried SiO_2 firstly treated with MAO and then with a titanium complex that turned out in polymers with a higher molar mass, a higher melting temperature and a better morphology than the ones obtained with the corresponding homogeneous catalyst [103]. Carlini *et al.* anchored a nickel catalyst to MAO-treated silica and obtained a thermally stable nickel-heterogenized catalyst able to polymerize ethylene with higher productivity in comparison with its homogeneous counterpart [104]. The same procedure was applied to mesoporous silicas: a zirconium FI complex was immobilized on SBA-15/MAO and nanofibrous polyethylene was produced [161]. Another zirconium FI complex supported on MCM-41/MAO leaded to extended-chain polyethylene nanofibrils with diameters of about 10 - 100 nm [106].

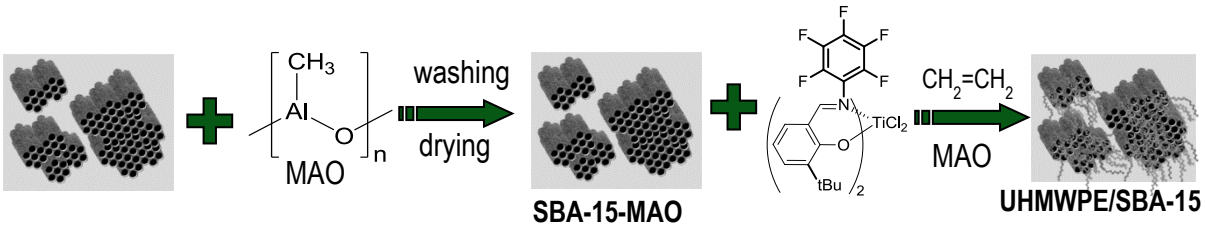

Figure 2.8: Impregnation of catalyst on SBA-15 previously modified with MAO.

The second method implies the pre-activation of catalyst with MAO prior to its contact with SBA-15 (PA method). This route was applied before to metallocene catalysts and it was reported that the number of active sites was increased, leading to highly active catalysts. This method has also the benefit of simplifying the experimental set-up for immobilization (see Figure 2.9).

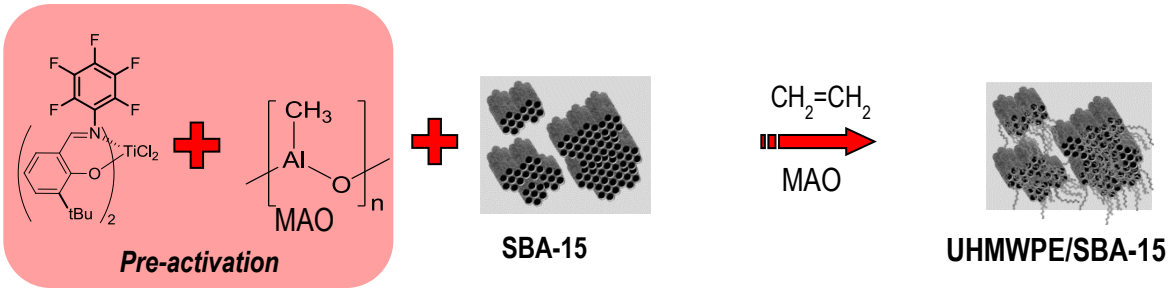

Figure 2.9: Impregnation on SBA-15 support of pre-activated catalyst with MAO.

Both treatments were performed in a way that the final Al/Ti ratio is the same after the immobilization of the catalyst.

EDX maps of Al and Si were recorded in order to evaluate the MAO distribution on the surface of SBA-15 after modification (as described in the experimental part). Figure 2.10 indicates a homogeneous distribution of MAO on SBA-15 (homogeneous distribution of Al).

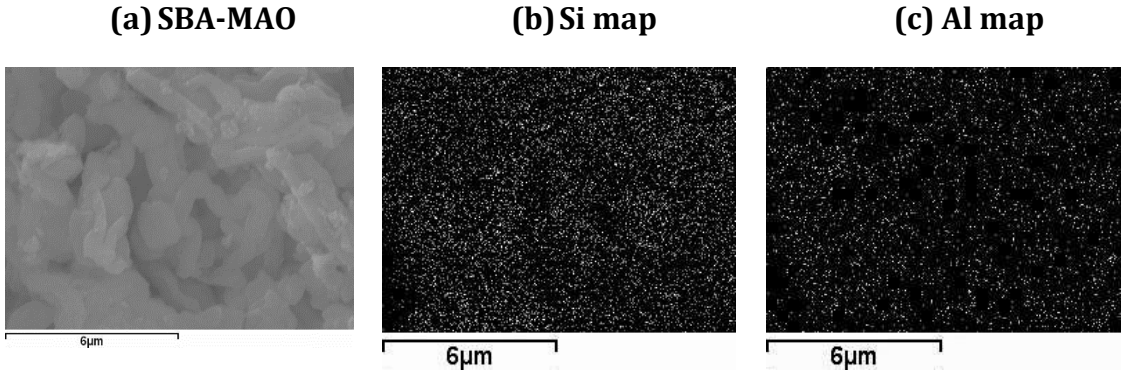

Figure 2.10: (a) SEM (b) Si-EDX (c) Al-EDX of a sample of SBA-15 modified with MAO.

The influence of these two routes on activity and polymer properties will be discussed now. Results listed in Table 2.3 indicate a significant decrease of the activity upon FI immobilization on SBA-MAO, as compared with those values shown in Table 2.2 for neat polyethylenes achieved under homogeneous conditions.

Table 2.3: Polymerization conditions, activities, productivities, molar masses and dispersities obtained for the polymeric materials attained with the supported catalyst.

Sample	Method	FI catalyst loaded in the support (10^{-6} mol/g)	Impregnation time (min)	Al/Ti	Reaction time (min)	Average activity (kgPE/molTi.h)	Productivity (kgPE/molTi)	M_w (10^6 g/mol)	D
FISBA005	SBA-MAO	19	4	2500	12	3320	663	-	-
FISBA007	SBA-MAO	19	4	2500	12	3160	632	0.541	2.2
FISBA004	SBA-MAO	19	60	5000	153	380	960	-	-
FISBA003	SBA-MAO	19	180	2500	146	220	696	0.339	2.6
FISBA001	SBA-MAO	19	1140	2500	60	140	663	-	-.
FISBA016	PA	8	90	1250	9	8120	1305	4.144	3.0
FISBA017	PA	8	90	2500	15	5460	1364	0.838	2.5

This is a common feature when catalysts are supported and it is generally attributed to catalyst deactivation pathways during immobilization. For the FI catalyst type, this aspect may be even more pronounced in the present conditions since MAO has been used to immobilize the FI catalyst. It is well known from literature that titanium FI-catalysts are very sensitive toward TMA, which is always present in the cocatalyst MAO [70, 173]. The proposed deactivation pathway is depicted in Figure 2.11 [61]. In the presence of TMA, one of the ligands is abstracted from the cationic Ti species **2** with the consequent formation of the species **3**. The resulting Al and Ti species are barely active for olefin polymerization. In fact, in the case of ethylene polymerization promoted by the homogeneous FI catalyst it was observed a decrease of the activity of ca. 30% (from 20380 to 13870 kgPE/molTi.h) when using a pre-activated FI catalyst (which was contacted during 15 min with MAO prior to polymerization) while maintaining the rest of experimental conditions identical to those used for the neat polyethylene FIHOM008.

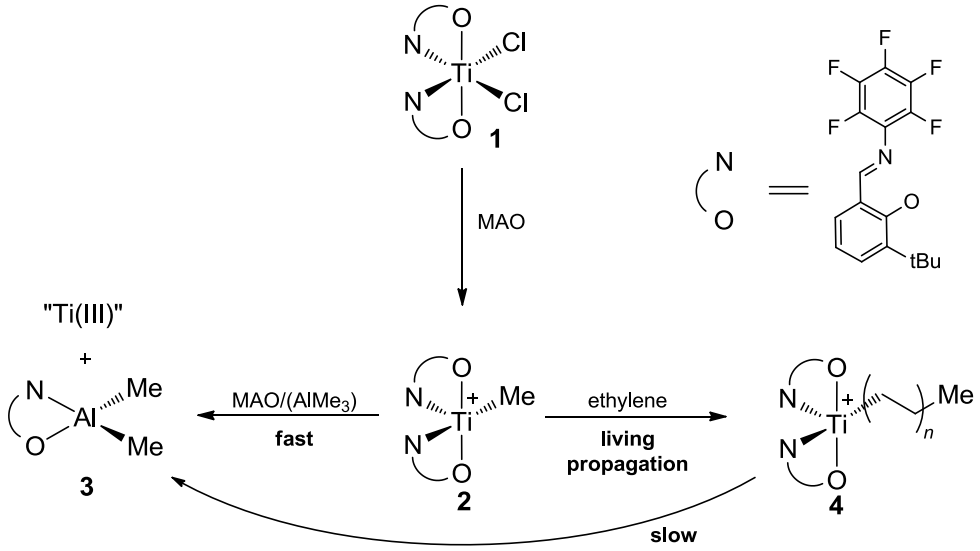

Figure 2.11: Proposed pathways for the reaction of the FI catalyst with MAO. Reprinted from [61].

The pre-treatment of the SBA-15 with MAO is expected to generate surface-bonded Si-O-Al(Me)$_2$ species [174] that may be involved in ligand transfer reactions and enhance them relatively to those occurring with free TMA. Therefore, higher catalyst deactivation may be expected for the supported catalysts.

In relation to this reasoning, the polymerization activity is significantly reduced by increasing the time of contact between the FI catalyst and the SBA-MAO support (from 4 min to 19h), as observed when comparing the samples FISABA005, FISBA007 and FISBA004, FISBA003 and FISBA001 (Figure 2.12). It is also worthwhile to notice that a significant decrease of the molar masses and a broadening of the molar mass distribution are revealed when applying the SBA-MAO method for the immobilization of FI catalyst and especially at very high impregnation times (see samples FIHOM002, FIHOM018, FISBA007 and FISBA003). This observation corroborates our assumption related to the significant enhancement under these conditions of the deactivation pathways inhibiting living propagation.

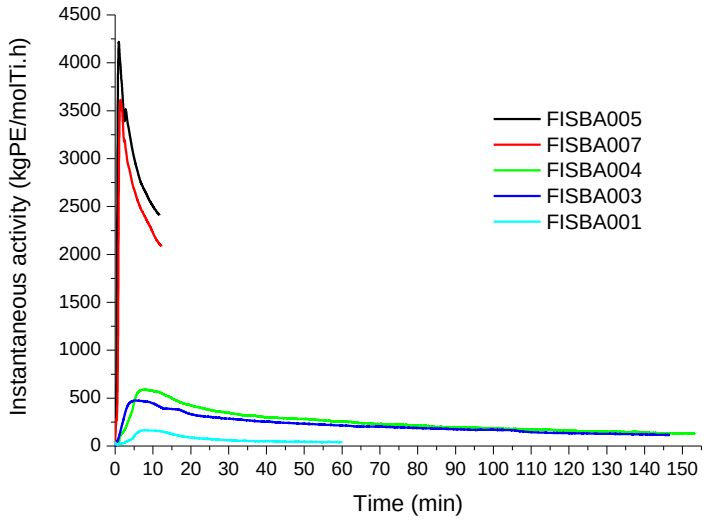

Figure 2.12: Kinetic profiles for ethylene polymerizations with the SBA-MAO method using different immobilization times.

In the PA approach, the FI catalyst is pre-activated by the addition of MAO in an Al/Ti ratio of 150 for 15 min, and then the FI-MAO system is contacted with the SBA-15 support. During pre-activation, the orange catalyst turned brownish, which may indicate that certain amount of the catalyst could be decomposed, a fact that might contribute to the decrease in the polymerization activity observed.

This is in agreement with the already mentioned decomposition of titanium FI catalyst by the presence of TMA [70]. An interesting feature is that by using the PA method the time necessary for immobilization significantly increases in relation to the previous method. Despite the longer impregnation time that is expected to promote the detrimental effect of TMA over FI catalyst, higher activities are surprisingly obtained. In this case, a fraction of the catalyst is deactivated during the catalyst pre-activation by action of free TMA, but the support has not been previously pre-treated with MAO and, accordingly, a lower amount of surface-bonded Si-O-Al(Me)$_2$ species are expected. Therefore, the deactivation pathways that may involve these surface-bonded species are reduced. Consequently, at similar experimental conditions, the polymer molar mass obtained with the PA method is considerably higher than that achieved using SBA-MAO route. A very interesting feature, although not clearly understood, is that at a particular set of experimental conditions the PA method leads to an extremely high value for the polymer molar mass (M_w= 4.144·10^6 g/mol), which is a much higher value than those obtained with the homogenous FI catalyst.

As a general trend the nanocomposites, independently of the immobilization method used for its synthesis, show a broadening of the molar mass distribution when compared to the values obtained for the neat polyethylene samples. In particular the sample with the highest molar mass is the one that also presents the larger molar mass distribution.

In order to determine if significant diffusional aspects may be operating under the experimental conditions used, the normalized kinetic profiles of representative homogeneous and supported catalytic systems are shown in Figure 2.13.

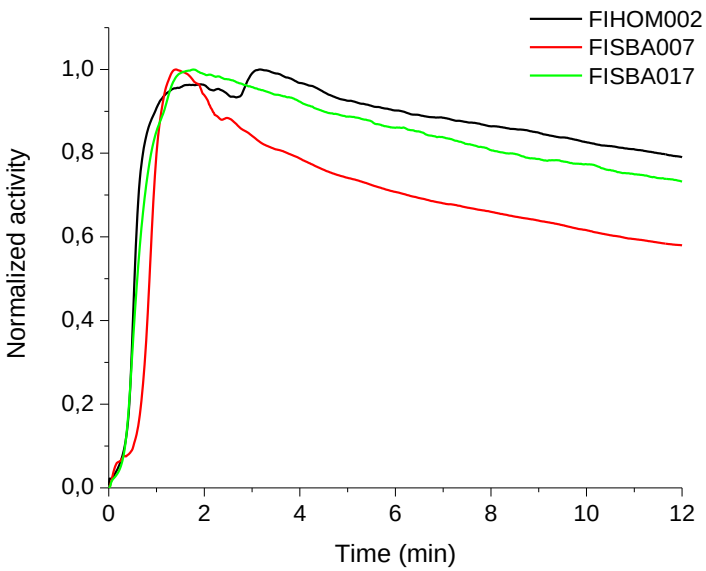

Figure 2.13: Normalized kinetic profiles for ethylene polymerizations.

It can be seen that all the curves exhibit a fast increase of the initial activity as well as short and similar induction periods, characteristic of the catalytic systems without significant diffusional constraints. It is worthwhile to notice that the homogeneous and the PA systems show analogous deactivation trends, while a slightly higher deactivation rate is observed for the SBA-MAO method. This may be related to the presence of higher amounts of the surface-bonded Si-O-Al(Me)$_2$ species, as already mentioned.

Figure 2.14 shows the morphology found by SEM in powder samples, obtained directly from the reactor, for a neat polyethylene and two composites synthesized under two distinct immobilization approaches. The formation of fibrils in the nanocomposites is well evident, while in the neat polyethylene these elongated fibrils are hardly observed. Moreover, it seems that the latter are more numerous and narrower in FISBA017 than in FISBA007.

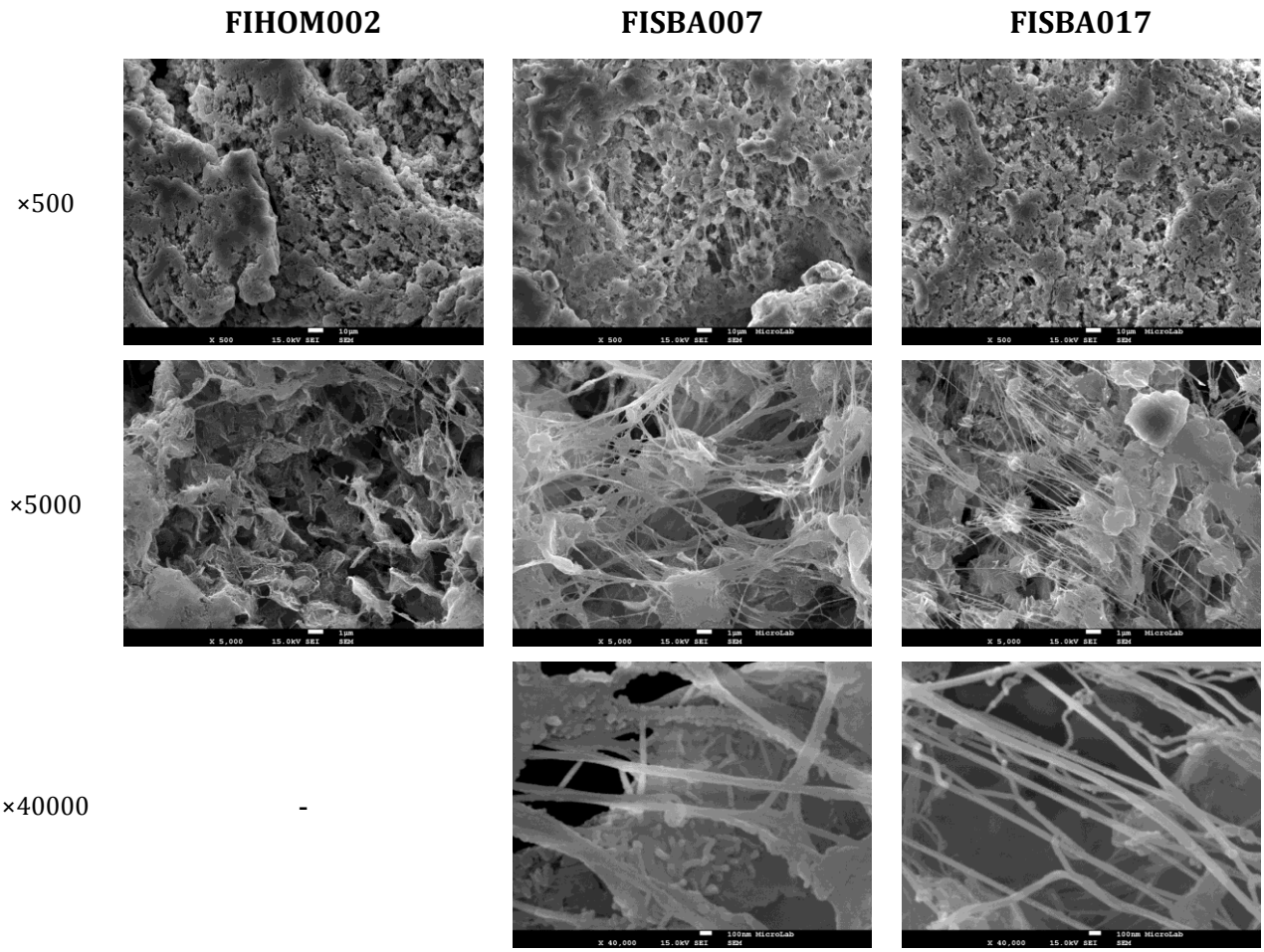

Figure 2.14: SEM micrographs for the FIHOM002 neat polyethylene and FISBA007 and FISBA017 nanocomposites at different magnifications.

2.5 Characterization of UHMWPE based materials

2.5.1 Identification of SBA-15 in the synthesized materials

SBA-15 used as catalyst support for the synthesis of polyethylene was not removed at the end of polymerization stage. As the polymerization is expected to occur both in the external surface and within the mesoporous, the resulting materials can be considered nanocomposites comprising a polymeric matrix and the mesoporous SBA-15 particles as filler.

XRD profiles do not provide information concerning the spatial distribution of the mesoporous material within the polymer matrix but it allows to assess the presence of SBA-15 in the final nanocomposite.

Figure 2.15 shows the X-ray pattern of SBA-15, a neat polyethylene and a nanocomposite at the low angle region. The polyethylene (sample FIHOM014) does not show any diffraction peak at that low angle region ($2\theta < 5°$). The presence of diffraction peaks in this region for

the nanocomposites samples clearly indicates that SBA-15 retains its structural integrity during the polymerization process.

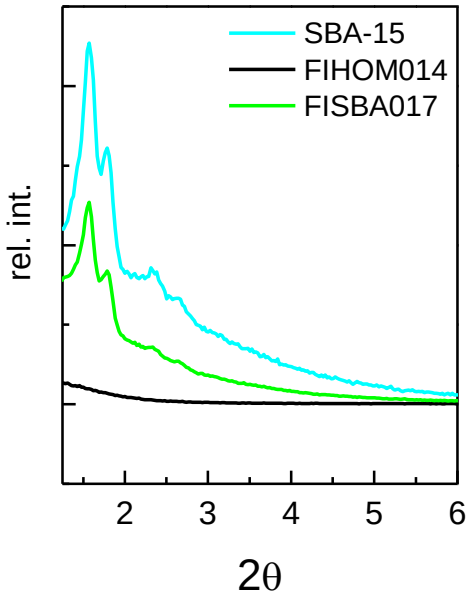

Figure 2.15: Diffraction patterns at room temperature for the SBA-15, a neat polyethylene and polyethylene-based hybrid material.

This is corroborated by the TEM micrograph of FISBA017 sample at high magnification presented in Figure 2.16, where the regular pore structure of SBA-15 is clearly seen.

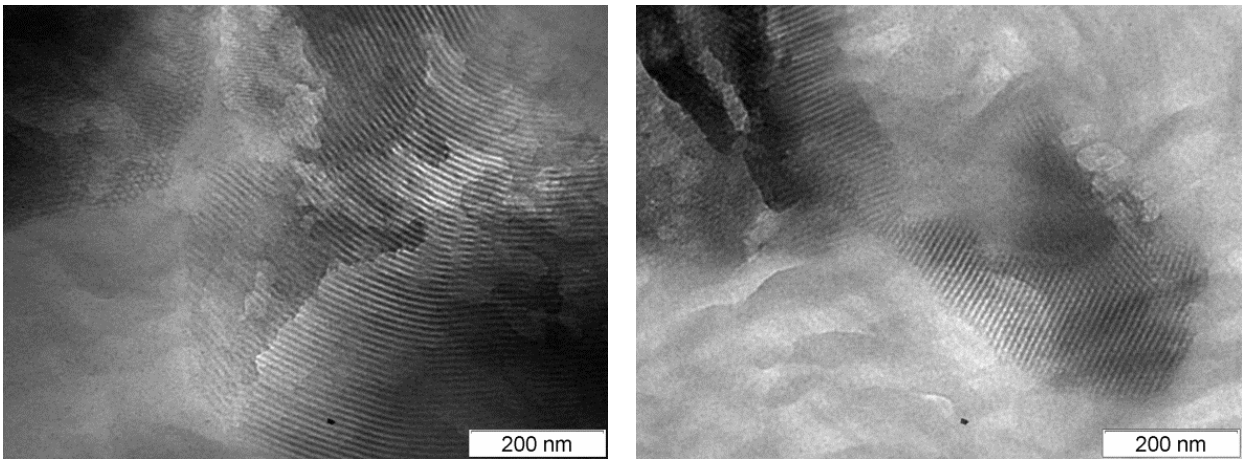

Figure 2.16: TEM micrograph of the FISBA017 sample.

2.5.2 Thermal behavior

2.5.2.1 Thermogravimetric analysis

Once different UHMWPE based materials, either neat polyethylenes or those incorporating SBA-15, have been synthesized through different methodologies, knowledge of some of their physical characteristics is required. The choice of the specimens to be characterized has been mainly made depending on the amount of UHMWPE based material produced and the amount required for a given experiment.

Thermogravimetric analysis allows learning about the thermal stability exhibited by specimens, the distinct decomposition processes involved depending on the atmosphere used and, the determination of the SBA-15 amount in the nanocomposites. It has been observed that the content estimated at a given specimen is rather independent of the environment used, mainly in those nanocomposites prepared by the approach where FI catalyst has been pre-activated with MAO before the further impregnation on SBA-15 surface, labeled as PA. Average values obtained from inert and oxidative conditions are listed in Table 2.4.

Figure 2.17 shows the thermogravimetric curves under inert and oxidant environments for some of the different polymeric materials. Under inert conditions, a single primary stage of decomposition is observed in the temperature range from 200 to 650 °C for the neat UHMWPE and the different composites, as represented in the upper plots on the left and right, respectively. Thermal decomposition of polyethylene has been reported to occur under these conditions through a random scission mechanism that turns out in the rupture of original polymeric chain into fragments of varying length. The mechanism describes a random generation of free radicals along the polymer backbone, followed by the scission of the chain that results in the formation of a molecule with an unsaturated end and another with a terminal free radical. Subsequent hydrogen chain transfer reactions transform the radical fragments into straight chain dienes, alkenes and alkanes [175].

However, four different degradation processes are noticeable at identical temperature interval when air is the environment used, as depicted in the bottom plots of Figure 2.17. It is well known that the initial reaction of the polyethylene thermal oxidation is the formation of alkyl radicals from polymeric chains followed by the reaction of alkyl radicals with oxygen to form hydroperoxides, which can decompose to alkoxyl radicals. Then, the alkoxyl radicals abstract hydrogen from the chain and other alkyl radical forms. Finally, various carbonyl species are generated.

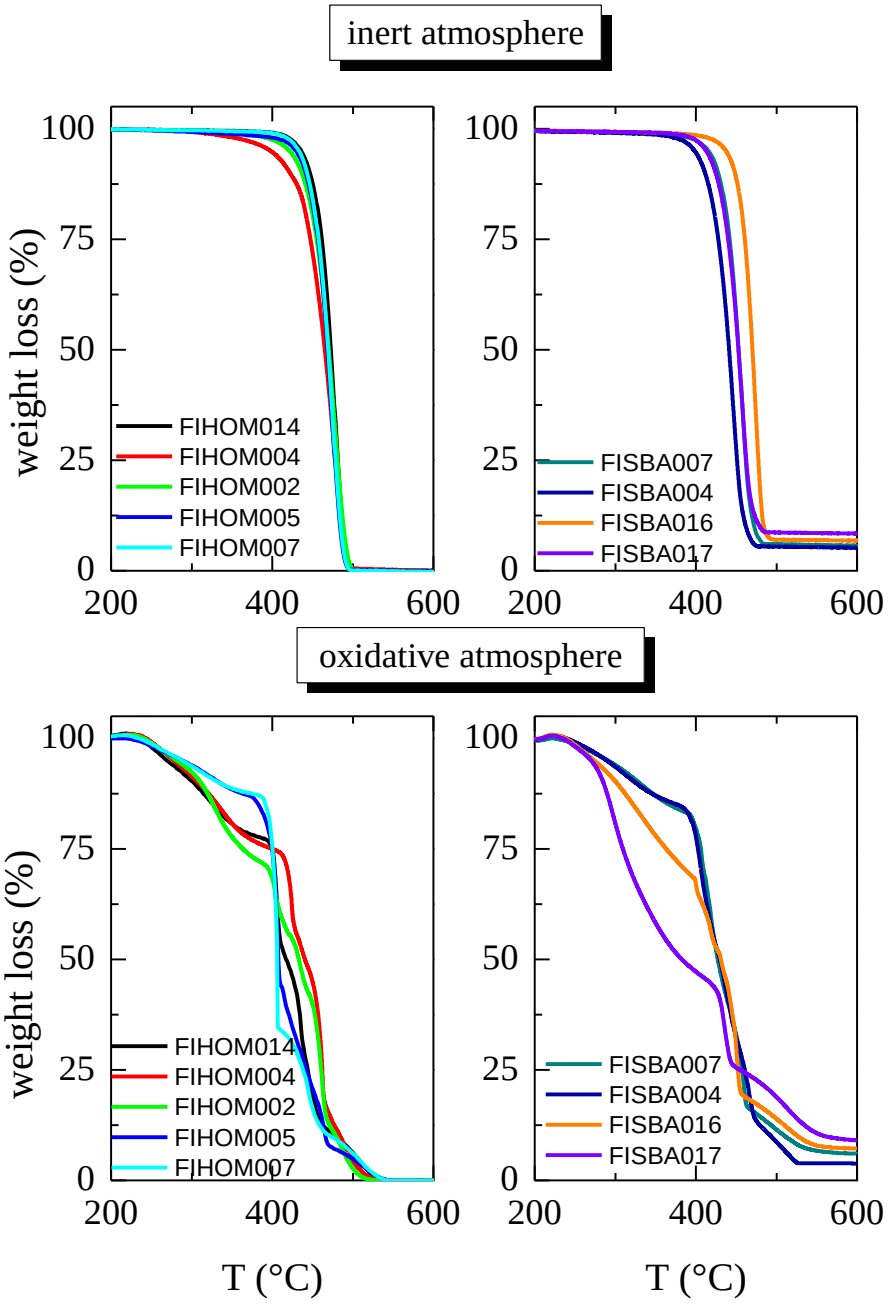

Figure 2.17: TGA curves of neat UHMWPE (left) and its nanocomposites (right) under inert (top) and oxidative atmosphere (bottom).

Table 2.4: Average SBA-15 wt. % content, characteristic decomposition temperatures under nitrogen and air atmospheres for neat UHMWPE and nanocomposites (the temperatures of 5%, T5%, and 50%, T50%) and the SBA-15 wt. % content at a specific environment.

Sample	Average SBA-15 wt.% content	Inert atmosphere			Oxidative atmosphere		
		$T_{5\%}$	$T_{50\%}$	SBA-15 wt.% content	$T_{5\%}$	$T_{50\%}$	SBA-15 wt.% content
FIHOM014	0	435	473	0	269	417	0
FIHOM004	0	398	465	0	278	440	0
FIHOM002	0	421	470	0	282	433	0
FIHOM005	0	429	468	0	288	408	0
FISBA007	5.8	415	453	5.6	290	427	6.0
FISBA004	4.5	398	441	5.2	289	429	3.8
FISBA016	6.9	437	470	6.8	273	431	7.0
FISBA017	8.5	413	441	8.4	270	383	8.6

Molar mass seems not to affect much the temperature at which decomposition reaches a 50 % loss of weight in the neat UHMWPE under inert conditions (see $T_{50\%}$ in Table 2.4). Different trend is observed under oxidative atmosphere and a shift to higher temperatures is seen as molar mass is increased.

It is clearly noticeable in Figure 2.17 that presence of SBA-15 alters the thermal stability in the nanocomposites when compared with that presented by neat UHMWPE under inert conditions. The temperature at which the mass loss is a 50 wt. % is shifted to lower values in the hybrids (with the exception of FISBA016 that presents a M_w above 4 millions) in comparison with those found in the pristine polyethylene although decomposition process starts at similar temperatures.

Moreover, it seems that the synthetic approach is important for the decomposition characteristics exhibited under oxidative conditions. In fact, the 5 % weight loss occurs at temperatures slightly higher than in the neat polyethylenes while $T_{50\%}$ remains rather analogous in those prepared with the SBA-MAO method. On the contrary, $T_{5\%}$ is shifted to lower temperatures in both of UHMWPE composites synthesized by PA methodology and $T_{50\%}$ is significantly reduced in the FISBA017 hybrid. This effect is not observed in FISBA016 probably because of its huge M_w. These features point out a catalytic outcome of the presence of small amounts of SBA-15 in these PA samples. In fact, MCM-41, which is other mesostructured silica particle, is frequently used as degradation catalyst. An important shift to lower temperatures of the main degradation process under inert conditions has been reported with increasing MCM-41 composition in nanocomposites

prepared by *in situ* polymerization of MCM-41 and ethylene, the former also acting as catalyst carrier and as nanofiller [84]. The catalytic degradation mechanism implies an initial cracking of large hydrocarbon molecules into small C3–C5 olefins in the catalytically active sites, followed by oligomerization, cyclization and hydrogen transfer reactions that result in the formation of aromatics, light paraffins and olefins.

2.5.2.2 Differential scanning calorimetry

The DSC results are summarized in Table 2.5 and Figure 2.18. Table 2.5 reports information on the first melting process of samples obtained either from the reaction powder or the corresponding processed films. As a general trend, independently of being synthesized under homogeneous or supported conditions, there is a significant difference in crystallinity and melting temperature between both types of specimens: reactor powders and films. Crystallinity and melting temperature, this last one directly related to the size of crystalline entities, are considerable larger in the as-powder samples, because disentangled chains are able to crystallize during polymerization giving rise to rather chain-extended crystals with a very small proportion of amorphous regions. On the contrary, chains after melting, because of their large length and the high mobility degree that they possess at those high temperatures, are able to establish a great number of entanglements between them and crystal formation will be hindered during crystallization along the cooling process applied for films manufacture. Then, a significant reduction is observed in crystallinity and melting temperature of the crystallites generated during film processing.

Table 2.5: DSC calorimetric data of neat UHMWPE and nanocomposites.

Sample	**SBA-15 wt.%^{TGA}**	***Powder***		***Film***			
		f_c^m	**T_m (°C)**	**f_c^m**	**T_m (°C)**	**f_c^C**	**T_C (°C)**
FIHOM014	0	0.82	140.5	0.51	130.0	0.55	116.5
FIHOM004	0	0.82	140.0	0.52	131.5	0.54	118.0
FIHOM002	0	0.83	140.5	0.53	131.0	0.54	118.0
FIHOM005	0	0.82	140.5	0.51	131.5	0.56	117.5
FIHOM007	0	0.81	141.0	0.48	131.5	0.51	118.0
FISBA007	5.8	0.78	141.0	0.49	130.0	0.49	117.5
FISBA004	4.5	0.82	142.0	0.57	133.0	0.56	118.5
FISBA016	6.9	0.78	140.5	0.49	132.5	0.47	118.0
FISBA017	8.5	0.77	139.5	0.49	132.5	0.46	118.5

Moreover, results point out that the different homogeneous UHMWPE samples exhibit crystallinity values slightly higher than those in the supported specimens that incorporate SBA-15 (with the exception of FISBA004 that shows an analogous value in the as-powder

sample and the highest one in the film). This feature is a general trend since this lower crystallinity is evident in the as-powder sample as well as during first melting of films and their further crystallization. In addition, the presence of SBA-15 particles slightly inhibits UHMWPE crystallization. Nevertheless, transition temperatures (melting and crystallization temperatures) are rather independent of specimen types and of the SBA-15 presence.

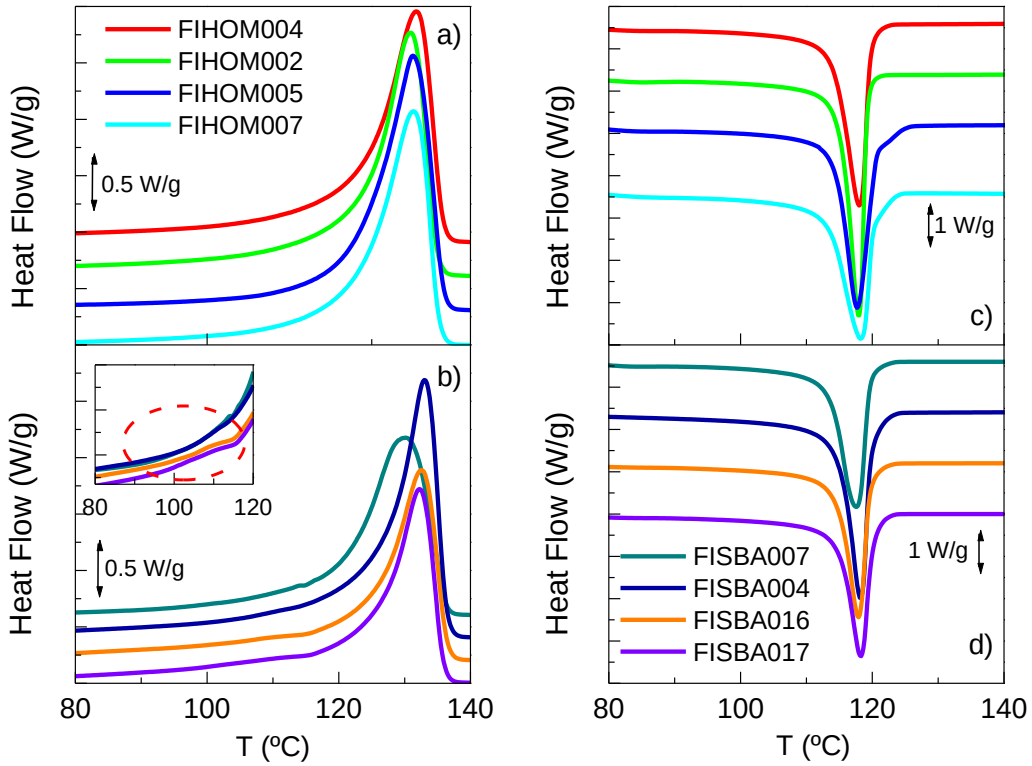

Figure 2.18: DSC curves of the first melting (a and b) and subsequent crystallization processes (c and d) of as films neat UHMWPE and nanocomposites. Melting region of the small crystallites in the inset

Figure 2.18b shows that there are some differences in the thermal behavior of the nanocomposites, at temperature ranging from 80 to 110 °C, depending on the synthetic approach used. At that interval, a small shoulder is observed in the specimens prepared by PA method while its presence is rather less evident in those SBA-MAO samples. That small endothermic peak is attributed to those UHMWPE crystallites that are developed inside the SBA-15 channels, similarly to evidences found in nanocomposites with MCM-41 [84]. Channel confinement prevents a further growth of the crystallites and, accordingly, these crystalline entities generated within SBA-15 particles are of much smaller size than those that can grow at its surface and in the UHMWPE bulk. Then, melting temperature is much lower. Therefore, this feature seems to point out that there are none or a very small amount of crystallites within SBA-15 channels in samples synthesized by SBA-MAO approach. This may also be in relation to the earlier decomposition of samples obtained by PA method (where UHMWPE crystallites are developed inside the SBA-15 channels) compared to SBA-MAO and neat polyethylene samples.

2.5.3 Mechanical properties

2.5.3.1 Stress-strain

Left plot of Figure 2.19 depicts the stress-strain behavior at room temperature for two neat polyethylenes, FIHOM004 and FIHOM002, and their comparison with two nanocomposites, FISBA004 and FISBA016, representative of the two immobilization methodologies used. Table 2.6 lists the different parameters obtained for the several samples at the two temperatures analyzed.

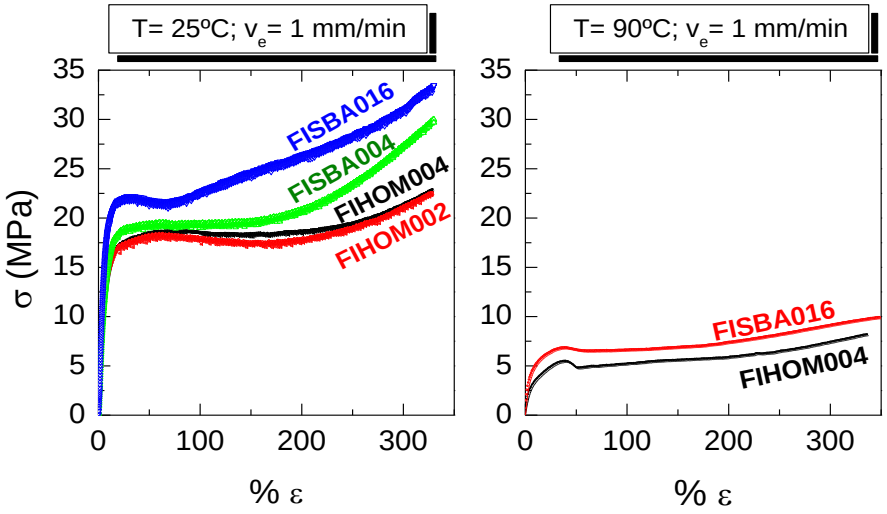

Figure 2.19: Stress-strain curves for different neat polyethylenes and composites: at 25 °C (left) and 90 °C (right).

The stress-strain curves for all these specimens are characteristic for ductile polymers. Results demonstrate that there are practically no differences between the two neat polyethylenes neither in their mechanical parameters values nor in the whole deformation process, including cold drawing and strain hardening. These features are related to the similar molar mass of both UHMWPEs and, consequently, to analogous characteristics of their macromolecule entanglements, involving subsequently, similar tensile strength and toughness.

Table 2.6: Mechanical parameters of different samples, analyzed at 25 °C and at 90 °C: Young's modulus, E; average value. $E^{average}$; yield deformation, ε_Y; yield stress, σ_Y; final stress, σ_{end}.

Sample	SBA-15 wt.%	$E^{average}$ (MPa)	ε_Y (%)	σ_Y (MPa)	σ_{end} (MPa)
T = 25 °C at 1 mm/min					
FIHOM002	0.0	227	50	18.2	21.6
FIHOM004	0.0	230	50	18.4	22.8
FISBA004	4.5	262	48	19.9	31.3
FISBA016	6.9	326	35	20.7	33.5
T = 90 °C at 1 mm/min					
FIHOM004	0.0	60	42	5.5	8.1
FISBA016	6.9	107	38	6.7	9.8

However, the incorporation of SBA-15 particles leads to stiffer materials with higher mechanical strength and toughness compared with those found in the neat polyethylenes. Thus, the Young`s modulus, the σ_{end} and the value of the area under stress-strain curve are higher in FISBA004 and FISBA016 than in the neat polyethylenes FIHOM002 and FIHOM004. All these features are clearly deduced from the left plot of Figure 2.19. The best response is exhibited along the whole stress-strain curve for the FISBA016 nanocomposite. Therefore, it shows the higher mechanical parameters (E, σ_Y, σ_{end}), these features being associated with its superior SBA-15 content and much higher molar mass (M_w in FISBA004 has not been determined but it is assumed to be similar to that found in the other SBA-MAO composites). On the other hand, it should be mentioned that only four strips have been stretched at a given sample because of the lack of material. Nevertheless, a good reproducibility of stress-strain response at a specific temperature was found, both in the shape of deformation process and in the mechanical magnitudes derived from these experiments (Figure 2.20).

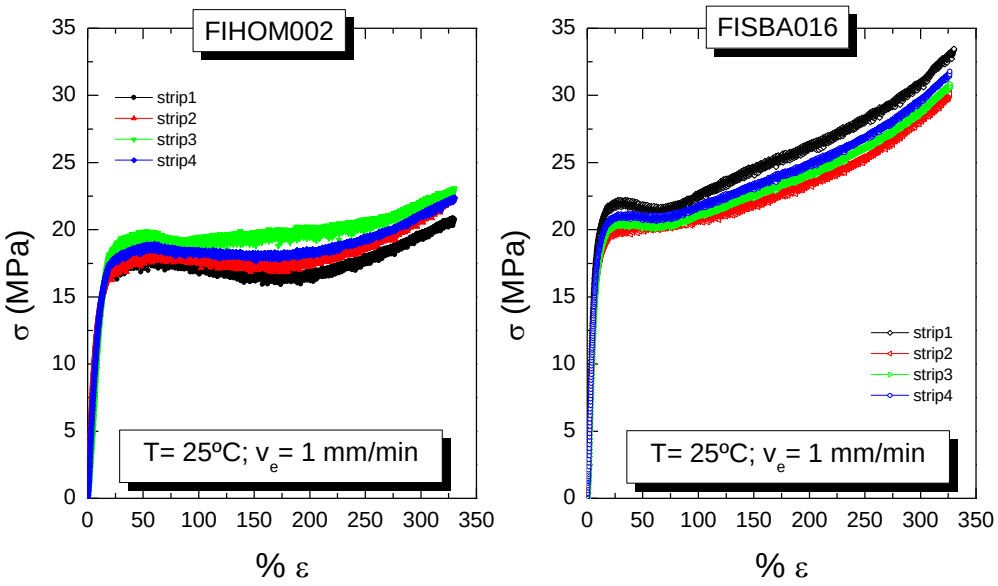

Figure 2.20: Stress-strain curves for different strips of a neat polyethylene (left) and a nanocomposite (right).

On the other hand, these two nanocomposites (FISBA004 and FISBA016) were prepared using two different methodologies. A straightforward correlation between the mechanical responses and the preparation approach cannot be undoubtedly established because, first of all, the final SBA-15 content is not identical in both of them. Secondly, feasible differences that might exist at microscopic level after synthesis would disappear during film processing from the molten state. And finally, analogous polymer-filler interactions are expected to be developed within these nanocomposites. Then, it seems that the most important factors that trigger deformation process in these nanocomposites are either the SBA-15 amount or further molar mass variations. The synthetic methodology may also play an indirect role as it might be responsible for obtaining materials with lower (those by SBA-MAO method) or higher (those by PA approach) molar masses or with bigger or smaller proportion of PE chains within the SBA-15 channels. Consequently, the FISBA016 hybrid exhibits the highest mechanical parameters (Young´s modulus, yield stress and tensile strength -as deduced from stress at the end of the experiment) compared with those shown by the pristine polyethylene and by the FISBA004 nanocomposite, which incorporates less SBA-15 amount Moreover, deformation process undergoes some changes from neat polyethylene to FISBA016 hybrid. Three stages are observed in the two neat polyethylenes and in the FISBA004: the initial elastic zone, a uniform region of cold-drawing and, finally, the strain hardening, which is more pronounced in the FISBA004 nanocomposite because of SBA-15 incorporation. Cold-drawing stage is very narrow in the FISBA016 and, then, strain hardening starts at much lower strains because of its high rigidity and extremely high M_w. This superior stiffness and chain length will impose higher constraints for disentangling UHMWPE macrochains in the FISBA016 and, then, tensile strength increases compared with that found in the FISBA004 nanocomposite.

The effect of temperature is clearly deduced from the right plot in Figure 2.19 and results listed in Table 2.6. All the mechanical parameters (Young´s modulus, yield stress and tensile

strength) are significantly reduced with respect to those obtained for a given specimen at 25 °C. Incorporation of SBA-15 particles in the nanocomposite leads again to a stiffer material with high toughness. Differences in the mechanical parameters between the neat polyethylene and the nanocomposite are now more noticeable at this high temperature.

2.5.3.2 Indentation experiments

Indentation has been used as a fast and reliable mechanical test for the evaluation of the hardness, modulus and creep variations upon incorporation of the filler [176], in a way to get information on the rigidity and resistance of the materials to plastic deformation. The indentation results are depicted in Figure 2.21 for loading-maintenance-unloading experiments performed in some of the neat polyethylenes (left plot) and nanocomposites (right representation) under study. Significant variations are observed depending on the pristine polyethylenes molar mass and SBA-15 presence in the nanocomposites, both on the shape of curves and on the indentation depth reached. The FIHOM007 is the neat polyethylene with the highest M_w and, consequently, higher amount of entanglements; and the indenter cannot penetrate too much in its surface. The other two neat polyethylenes, FIHOM004 and FIHOM002, exhibit a rather analogous M_w and indenter depth reached at identical load is larger, because both are softer than FIHOM007. Therefore, it seems that higher molar mass hinders indenter penetration under neat polyethylenes surface. Hardness is in agreement with this penetration hindrance and values are very similar for FIHOM004 and FIHOM002 and lower than that found in FIHOM007.

Right plot in Figure 2.21 proves the great influence that incorporation of SBA-15 particles exerts on these loading-maintenance-unloading processes. It is clearly seen that indenter can go more deeply into the material and, accordingly, depth attained is significantly enlarged in the neat polyethylene FIHOM002 compared with those achieved in the composites. Thus, SBA-15 acts as reinforcing agent and stiffer component and its content is in FISBA017 higher than in FISBA016. Nevertheless, M_w is just the opposite: in FISBA016 higher than in FISBA017. Results seem to indicate that for this mechanical measurement at composite surface the SBA-15 content is more crucial than a larger amount of entanglements. Consequently, depth reached at a given load is reduced in the FISBA017 nanocomposite, which contains the highest SBA-15 composition, and hardness value is enlarged.

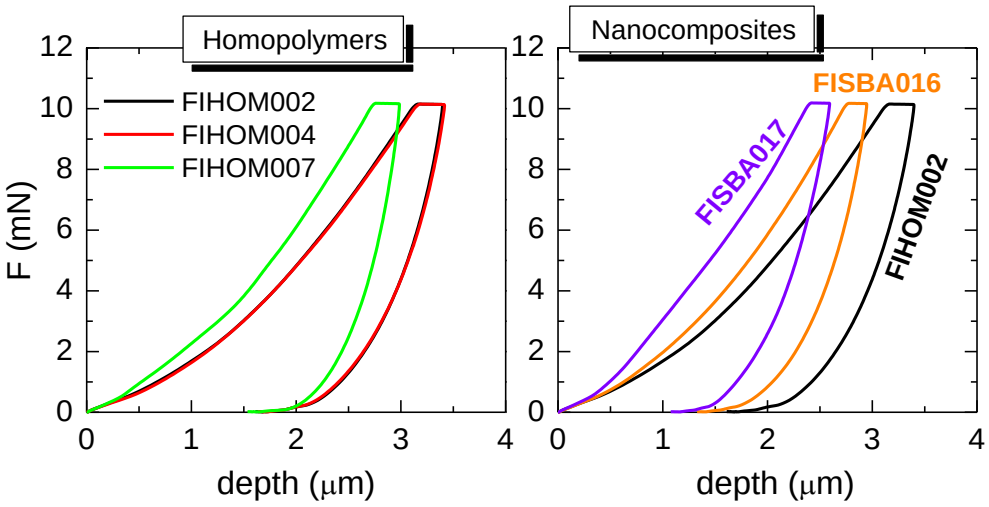

Figure 2.21: Indentation curves of load-maintenance-unload vs. depth for some neat polyethylenes (left) and composites (right).

Additional information can be deduced from the depth vs. indentation time representation, as displayed in Figure 2.22. The loading-maintenance-unloading processes are clearly observed as well as their dependence on molar mass and SBA-15 content. Thus, deformability is reduced and, accordingly, depth is decreased along loading stage if molar mass is increased in the pristine polyethylenes (upper plot) and if SBA-15 is incorporated. The maintenance at a constant load for 5 seconds allows learning on creep response of these materials. An increment of penetration depth is seen for all the specimens during this maximum load at 10 mN, L^{max}, *i.e.*, during the maintenance period (Figure 2.22). This depth is dependent again on molar mass and presence of SBA-15 in the ultimate material. Accordingly, polyethylenes prepared in homogenous conditions become more compliant as molar mass is lowered and their creep resistance is lower compared with that exhibited by the hybrids.

Figure 2.22 also displays that the unloading process is mainly dominated by the viscoelastic recovery of the different materials. Once experiment is over, a permanent deformation (plus a small amount of delayed elastic recovery) is attained in all the specimens since they are not completely elastic. The softening process involves a very small rise of the amount in the plastic deformation in the samples with lowest molar masses. Moreover, a decrease in this viscous and non-reversible contribution is observed as SBA-15 content is raised.

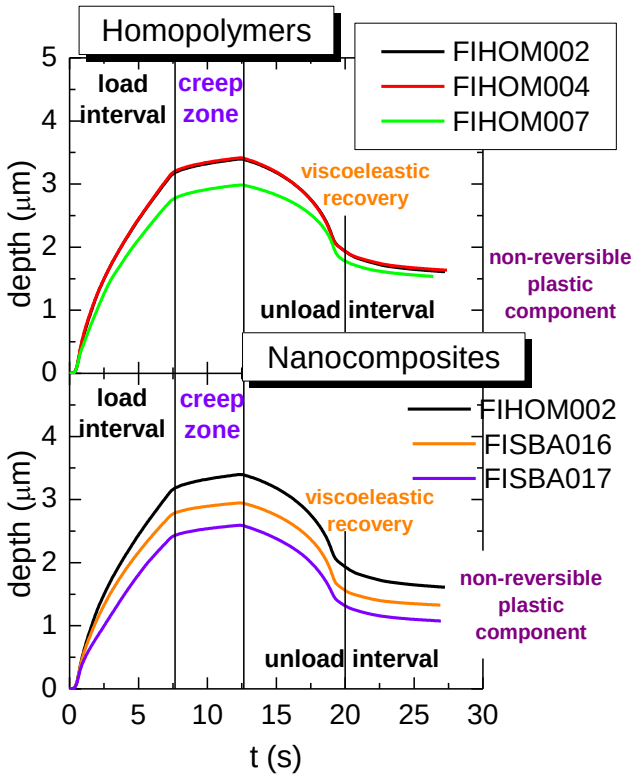

Figure 2.22: Indenter depth dependence on experimental time for some neat polyethylenes (top curves) and composites (bottom curves).

FISBA007

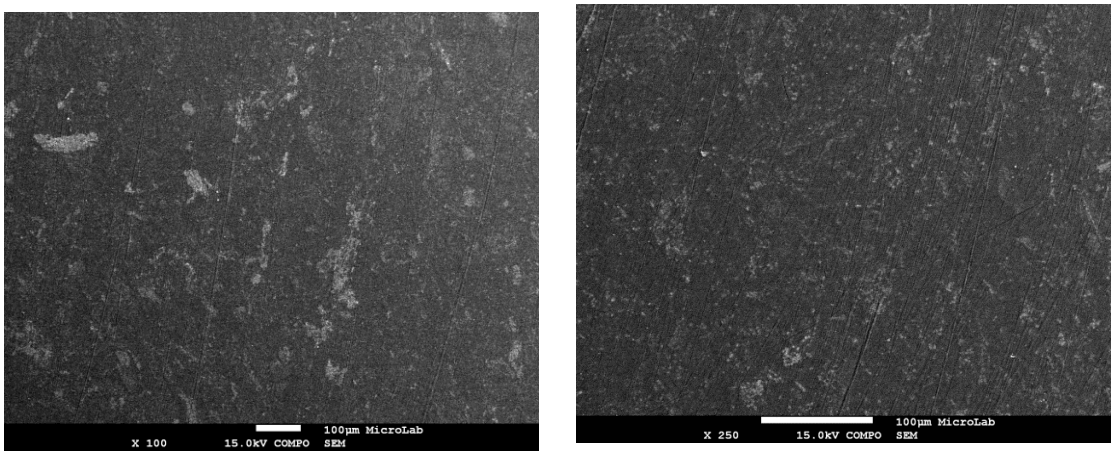

FISBA016

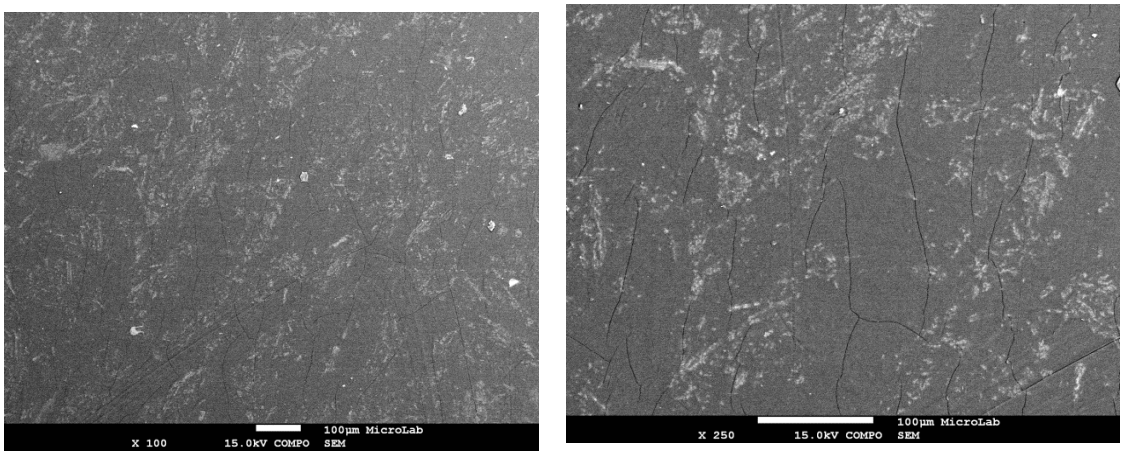

FISBA017

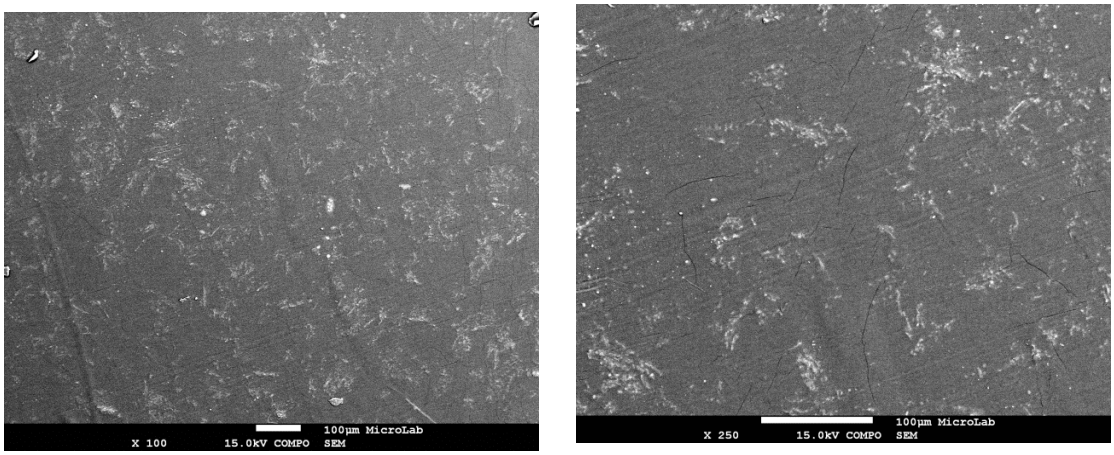

Figure 2.23: SEM of the nanocomposites

Properties of nanocomposites are usually highly dependent on the minor component content and also on its distribution [177]. Figure 2.23 shows the SEM images of the

UHMWPE/SBA-15 materials and it allows learning about particle distribution and size of the agglomerates of the SBA-15 within the polyethylene matrix. From the micrographs it is clear that SBA-15 is not uniformly dispersed within the UHMWPE matrix. Thus, the resulting nanocomposite turns out heterogeneous.

The maximum SBA-15 content tested in the present work is 8.5 wt. % due to the known tendency of silica to agglomerate. Nanofiller loadings higher than 10 wt. % are frequently not considered because agglomeration starts to play a significant role and mechanical enhancement levels-off or even decreases. A 10% E increase was found upon addition of 5.0 wt.% raw MWCNTs to UHMWPE [177], ascribed to the poor nanofiller-matrix interface, the presence of voids and the nanotube waviness that limits the efficiency of the reinforcement.

The optimization of the properties in polymeric nanocomposites depends also on the interaction between the matrix and the filler. The dispersion state of the filler and the nature of the interface/interphase with the host matrix are the main two factors accounting for the interaction between filler and matrix, and in turn, compromising the performance of the nanocomposite.

Figure 2.24 shows the micrographs of two nanocomposites, FISBA007 and FISBA017, representative of each immobilization method used. No significant changes on the overall morphology can be detected.

FISBA007

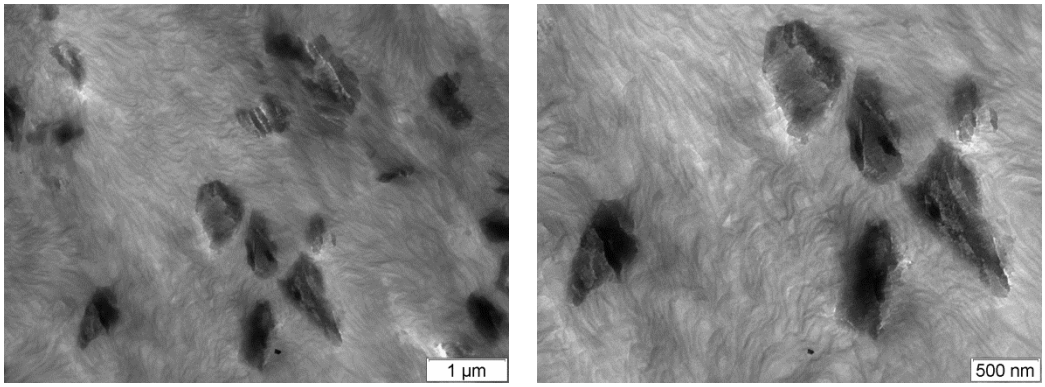

FISBA017

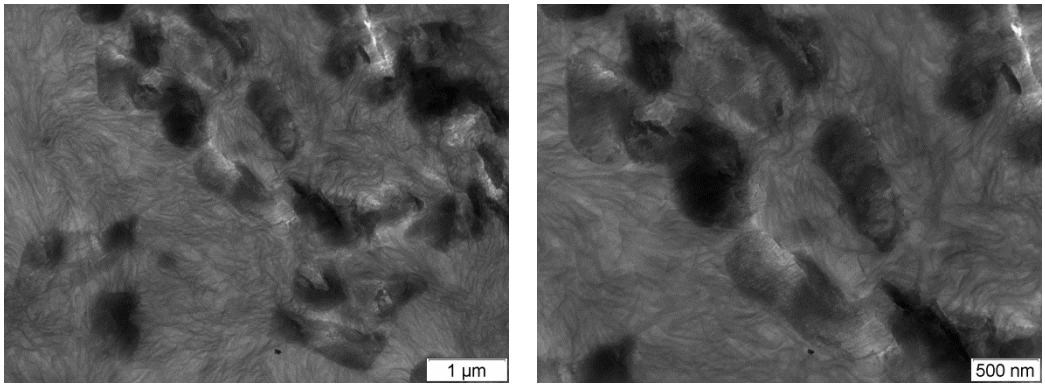

Figure 2.24: TEM micrographs for FISBA007 and FISBA017 nanocomposites, obtained by SBA-MAO and PA approaches respectively.

2.6 Disentangled UHMWPE films: Influence of SBA-15 particles in phase transitions and mechanical behavior

When processing UHMWPE, the entanglement of the polymer chains plays an important role and accounts for the high melt viscosity reflected by very low melt flow, slow chain mobility, and slow crystallization rates. Thus these polymers are difficult to process and the current technology used presents several drawbacks such as: high energetic cost and risks of thermal degradation of the polymer [178]. Moreover, the resulting molten material might contain numerous flaws, including either incomplete fused particle boundaries or fusion defects.

As already referred, in the previous chapter, a more advanced approach to produce disentangled crystals in UHMWPE is via direct polymerization using a single-site catalytic system in the reactor [23]. At low polymerization temperatures and low catalyst concentration, individual growing chains will form their own folded chain crystals. Consequently, the UHMWPE obtained will have a reduced number of entanglements with an initial melt viscosity lower than that corresponding to its entangled state. Those nascent powders having a reduced number of entanglements were processed in solid-state below its melting temperature [26], leading to UHMWPE products, such as fibers and tapes. This route avoids any use of solvent during processing, allows milder temperature conditions during the process, reducing the polymer degradation, and also gives better mechanical properties.

In this section some of the previously synthesized samples are processed by compression molding at the regular temperature of 230 °C, but also at 120 °C and, subsequently, some of their properties are evaluated. The melting temperature and crystallinity of nascent powders, of non-entangled films processed at 120 °C and of films molded at regular temperatures (230 °C) for 5 min is estimated by differential scanning calorimetry. Actual incorporation of SBA-15 particles and crystalline structure is determined by X-ray diffraction at room temperature and weight content of mesoporous particles is analyzed by termogravimetric analysis. Mechanical response is characterized by indentation depth sensing measurements. Parameters, as important as elastic modulus and hardness are obtained as well as information on creep and plastic (non-recoverable) properties.

Three distinct UHMWPE based materials are under study: one prepared under homogenous conditions (FIHOM016) and two nanocomposites. For the hydrides, the materials were prepared with different approaches for immobilizing the catalyst. The sample labelled as FISBA007 was prepared with the SBA-MAO approach whereas, the one labelled as FISBA014 was prepared by the PA protocol. This last sample was obtained under the same polymerization conditions that the FISBA017 specimen, so they are replicas.

Figure 2.25 shows the calorimetric heating curves for the different specimens as nascent powders from the reactor, compressed films at T=120 °C and 2950 bar (T120) and compressed films at T=230 °C and 10 bar (T230). It is noticeable the significant difference observed in melting temperature and in the melting enthalpy involved in the process, independently of the SBA-15 presence or not, between either those powdered or the T120 samples and those ones processed at 230 °C. The former samples exhibit their maximum of the melting endotherm at around 140 °C while T_m in those specimens from the films

prepared at 230 °C is located at about 130 °C (see Table 2.7). Crystallinity values change from around 0.75-0.80 in the former specimens to around 0.50 in the T230 samples processed at 230 °C.

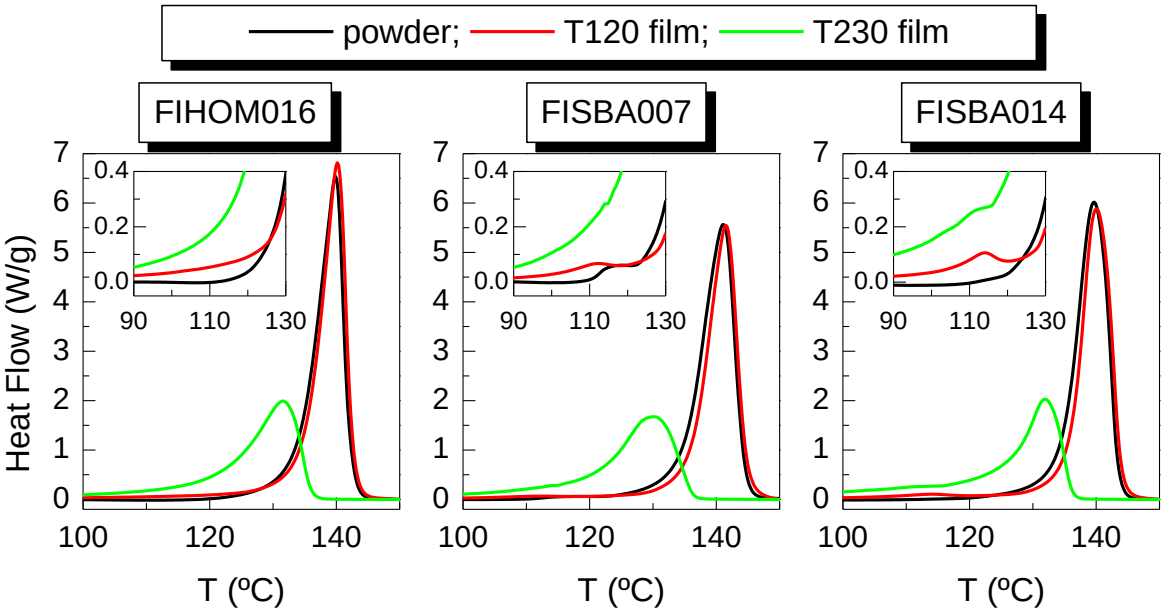

Figure 2.25: Normalized DSC curves for the actual polyethylene amount for the first melting process: pristine UHMWPE (FIHOM016) and its nanocomposites: FISBA007 and FISBA014. Melting region of the small crystallites in the inset.

Table 2.7: Average SBA-15 wt. % content estimated from TGA and DSC calorimetric data for the neat UHMWPE and its nanocomposites.

Sample	SBA-15 wt.%^{TGA}	f_c^m	T_m (°C)	f_c^C	T_c (°C)
FIHOM016*p*	0	0.75	140.0	0.45	118.5
FIHOM016T120	0	0.80	140.0	0.45	119.0
FIHOM016T230	0	0.51	131.5	0.52	118.0
FISBA007*p*	5.8	0.78	141.0	0.46	118.5
FISBA007T120	5.8	0.73	141.5	0.44	119.5
FISBA007T230	5.8	0.49	130.0	0.49	117.5
FI SBA014*p*	6.4	0.78	139.5	0.44	119.0
FI SBA014T120	6.4	0.77	140.0	0.43	120.0
FISBA014T230	6.4	0.50	132.0	0.50	119.0

These features can be ascribed to the disentangled chains existing in the powders from the reactors where crystallization is competing with polymerization at those experimental conditions used. The T120 specimens show similar characteristics in terms of high enthalpy values and, consequently, crystallinity and melting temperatures to those found in the powders from the reactor. This means that macrochains have not been entangled during the processing conditions probably because temperature is close but lower to the melting process. The crystallinity values attained are analogous to the ones described by Rastogi *et al.* [26] for nascent disentangled powders synthesized with identical catalyst. The parameters used (temperature, pressure and time) are enough to sintering the initial particles and lead to a films but not for developing entanglements. Then, rather chain-extended crystals with a very small proportion of amorphous regions are formed and crystallinity is high as well as melting point of the crystallites. On the contrary, chains after being at 230 °C for several minutes, because of their large length and the higher mobility degree that they possess at those high temperatures, are able to establish a great number of entanglements between them and crystal formation is hindered during processing. Then, a significant reduction is observed in crystallinity and melting temperature of the crystallites generated during the T230 film processing in comparison with those obtained from the powder and T120 specimens.

Contrary to the features found in specimens whose sintering was also performed at 120 °C by high velocity compaction [10], the T120 samples here examined present a unique primary endotherm instead of two melting overlapped peaks.

The primary endothermic processes, independently of initial state of the samples, are in FIHOM0016 and FISBA014 narrower than those exhibited by the hybrid FISBA007, which has been synthesized using the SBA-MAO immobilization methodology. This effect is more evident in the T230 specimen and it seems to indicate that crystallite size distribution is broader in FISBA007 and its T_m is shifted to slightly lower temperatures.

As in all the DSC measurements performed so far, insets in Figure 2.25 show different trends in the calorimetric curves within the interval between 90 and 120 °C, for the neat polyethylene and those materials that contain mesoporous SBA-15 particles. Then, the former one, FIHOM016 sample, does not present any significant feature while a small shoulder is exhibited in the FISBA007 and FISBA014 hybrids, this being more evident for the one prepared by the PA approach. This small endothermic peak is attributed to those UHMWPE crystallites that are within the SBA-15 channels, similarly to evidences found in nanocomposites with MCM-41 [84]. Channel confinement hinders a further growth of the crystallites and, consequently, they are of much smaller size than those that can grow at its surface and in the UHMWPE bulk. Then, their melting temperature is much lower than the one corresponding to the primary melting process.

Figure 2.26 displays a very interesting characteristic. The cooling curves are dependent on the initial history applied at a given material. It is supposed that once the melting process takes place, the final state should be identical. Nevertheless, because of the high molar masses of the sample under study, this assumption is not accomplished.

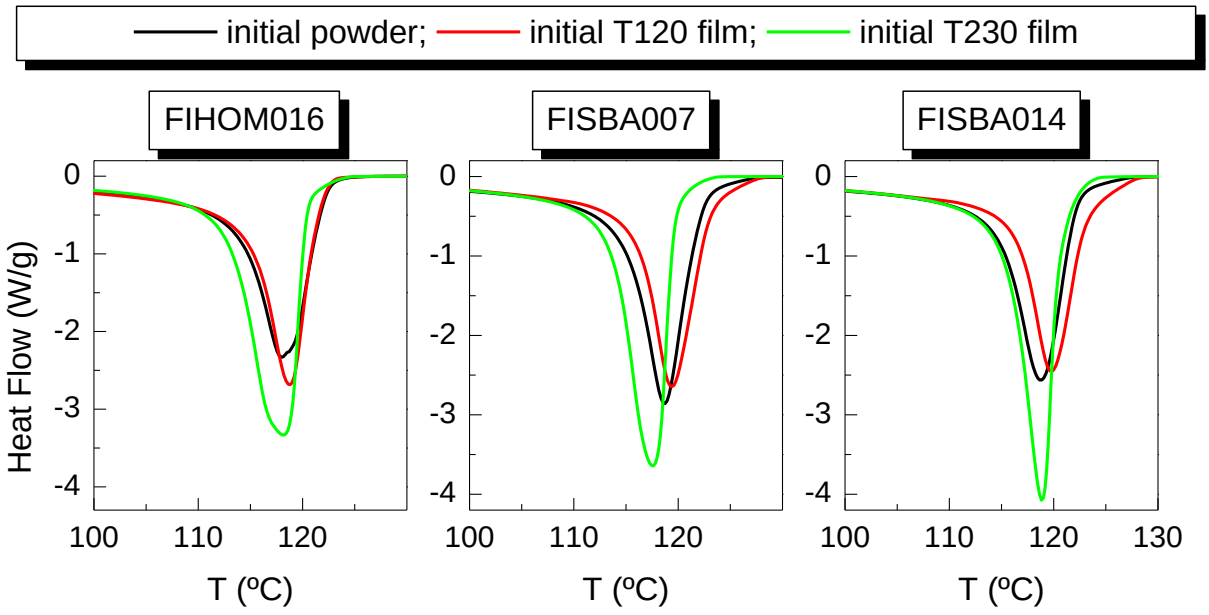

Figure 2.26: Normalized cooling DSC curves for the actual polyethylene amount immediately after the first melting process: pristine UHMWPE (FIHOM016) and its nanocomposites: FISBA007 and FISBA014.

There are rather similarities for those samples coming from the powders and the T120 films while those exotherms achieved after melting the sample taken from the 230 films show higher enthalpies involved, narrower temperature range and T_c at slightly lower temperatures. The presence of entanglements in the molten states of those samples that have been created along compression molding at 230 °C for some minutes slightly delays crystallization. This process takes place in a narrower temperature interval probably because the length of the chains between entanglements in the network is already homogeneous contrary to what occurs in those initially disentangled samples.

Figure 2.27 shows the X-ray profiles for the T120 films whose mechanical response by indentation is further analyzed. As in the nanocomposites analyzed in the previous sections, at low angles, the presence of SBA-15 is found in the FISBA007 and FISBA014 hybrids. As referred in section 2.2, SBA-15 shows a highly ordered hexagonal structure identified by the three main diffraction peaks that can be indexed as (100), (110) and (200) reflections associated with the *p6mm* hexagonal symmetry [165]. It should be commented that the present X-ray profiles are acquired from 1 ° in 2θ scale and, consequently, the (110) and (200) diffractions are the only ones observed in this angular range.

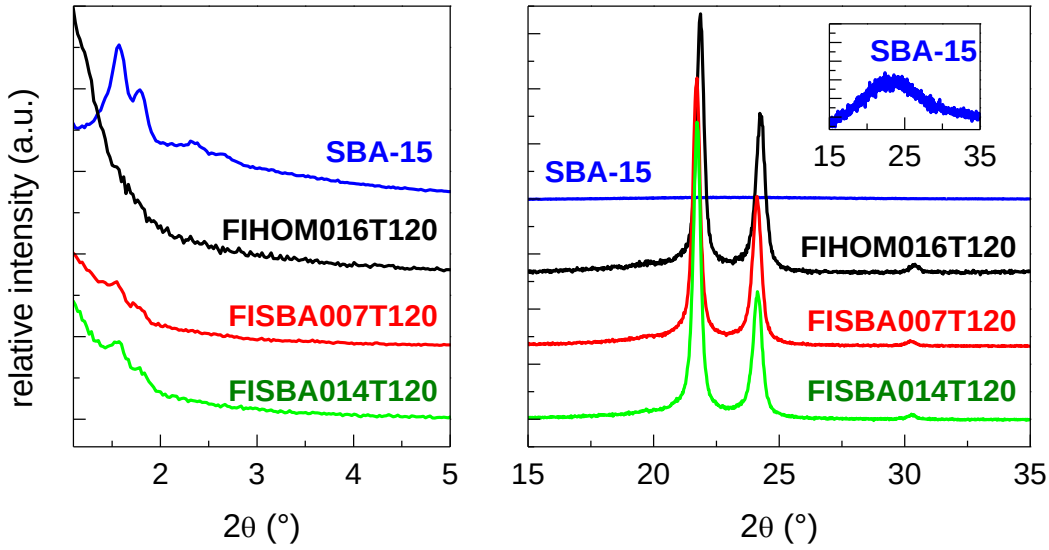

Figure 2.27: X-ray diffraction patterns at room temperature for the UHMWPE based materials, FIHOM016, FISBA007 and FISBA014, as well as pristine mesoporous SBA-15 particles.

Intensity of the characteristic SBA-15 diffractions is considerably reduced in the FISBA007 and FISBA014 nanocomposites since SBA-15 content incorporated is quite low in these hybrids. Nevertheless, their location has not been changed although they seem to be slightly distorted probably because of the presence of UHMWPE within the channels.

The right plot represents those diffractions that correspond to the crystalline structure of polyethylene. In spite of the high pressure applied the only polymorph that is developed is the orthorhombic lattice, characterized by its main (110) and (200) reflections. There is no

evidence of the hexagonal lattice [20] probably because the temperature used has been even inferior to the main melting point although a significant pressure has been applied.

The crystallinity exhibited by these samples is extremely high and, consequently, their amorphous halo is not practically noticeable. Values are 0.85, 0.79 and 0.82 for the FIHOM016, FISBA007 and FISBA014, respectively. These values are in a very good agreement with those estimated from DSC measurements for the T120 samples. Crystallinity determination for the FIHOM016, which does not contained SBA-15 particles since it has been synthesized under homogeneous conditions, consists of performing the decomposition of the X-ray profile into the different crystalline diffractions and an amorphous contribution. On the other hand, as seen in the Figure 2.28, SBA-15 presents its amorphous halo at identical angular range. Therefore, it is first required in the FISBA007 and FISBA014 specimens to subtract the contribution of the SBA-15 amorphous halo before proceeding to the deconvolution of the polyethylene profile (as depicted in Figure 2.28).

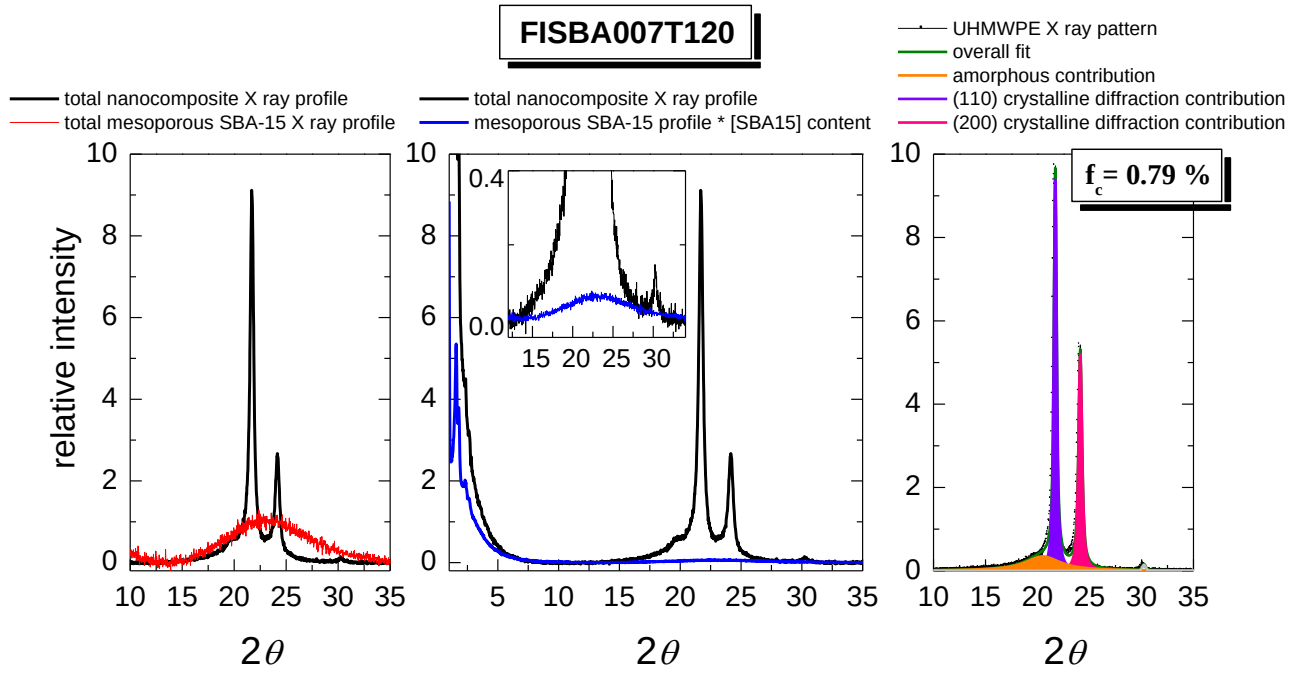

Figure 2.28: Determination of UHMWPE crystallinity in the FISBA007T120 film. Total FISBA007T120 and SBA-15 profiles, normalized at same area (left picture); total FISBA007T120 profile and normalized SBA-15 pattern at its actual content (5.8 wt.%) (middle representation); and, decomposition of exclusively UHMWPE profile into the amorphous and the two main (110) and (200) crystalline diffractions (right plot).

Excellent properties are attributed to UHMWPE (as fatigue, abrasion, impact and wear resistances, among others) that come from its entanglement density and, consequently, the formation of a physical entanglement network. The interest in processing UHMWPE in a disentangled state is mainly related to reach freedom in the design and capability for tuning

shape and thickness in the resulting manufacture objects, to preserve its thermal integrity avoiding the exposure at high temperatures for long times, and, obviously, to save money during its production by reducing the high energetic cost involved until now. Nevertheless, the evaluation of disentangled films behavior can be important not only as initial state of the final completely entangled state but by itself if there is any significant property. It is true that an appropriate approach that leads to steady films whose response does not evolve on time is required. Thermal transitions as well as crystallinity (estimated from DSC and X-ray diffraction) are identical in these T120 solid state films obtained at 120 °C and at 2.95 kbar maintained at room temperature for, at least, six months. Its high crystallinity values allow assuming a good mechanical performance.

There is not much work in literature concerning physical properties of disentangled specimens. The sintering of UHMWPE nascent powders by high velocity compaction [179] leads to partial melting and subsequent recrystallization processes with an average overall crystallinity of 0.55 depending on the number of hits applied during the manufacture at 115 °C. The highest Young´s modulus reported by these authors is 1.3 GPa. Rastogi *et al.* [26] described a combined protocol involving compression-molding at 129 °C followed by rolling in a calander at 130 °C and a stretching process at 139 °C. The tensile modulus in those tapes is rather large since they are disentangled drawn tapes with draw ratio as high as 180 and crystallinity values of 0.95.

Figure 2.29 displays the indentation results found in FISBA007 films processed either at 120 °C or 230 °C for loading-maintenance-unloading experiments. On the left plot, force is represented as function of depth while, on the right plot, dependence of depth on time is depicted. Differences in the mechanical response of both films at a given material are really significant. Along loading step, the indenter is only able to reach a depth of around 1.7 μm at the end of the loading stage in the FISBA007T120 while it goes deeper inside, up to 2.7 μm, in the FISBA007T230. This considerable variation is related to changes in the rigidity of both films, which is directly dependent on the distinct crystallinity values and the absence or presence of entanglements. But difference are not only concerning to stiffness but to creep response found during the second part of the experiment when material is kept at constant force. Change in FISBA007T230 is 30 % higher than FISBA007T120. Moreover, important differences are also observed in the unloaded interval, mainly for the instantaneous viscoelastic recovery, which is also much superior in the former film probably because of the presence of an entanglement network.

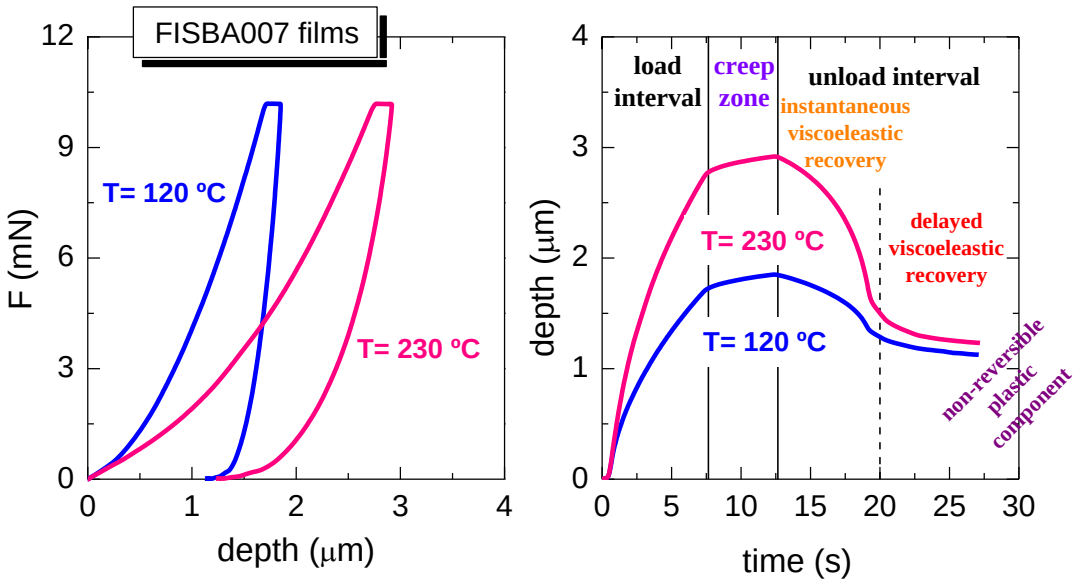

Figure 2.29: Indentation curves of load-maintenance-unload vs. depth (left plot) and depth vs. time (right plot) for FISBA007 films processed at 120 and 230 ºC.

Figure 2.30 shows the results for the three different UHMWPE films processed at 120 °C: the pristine polyethylene, FIHOM016T120, and the two ones that incorporate an analogous amount of SBA-15 particles, FISBA007T120 and FISBA014T120. Differences found between them are much less than those found between T120 and T230 films in FISBA007; In fact, the T120 film shows an impressive increase of E_{it} (from 890 to 2860 MPa) and of H_{it} (from 61 to 125 MPa) when compared to the T230 film, which is attributed to the strong increase in crystallinity (from 0.49 to 0.73). On the other hand when comparison is made among T120 films it should be considered that differences in crystallinity values are significantly less important (0.80, 0.73 and 0.77 for FIHOM016T120, FISBA007T120 and FISBA014T120, respectively) and that SBA-15 content is not too high. Nevertheless, indentation modulus increases from FIHOM016T120 < FISBA007T120 < FISBA014T120, as seen from the values reported in Table 2.8. Incorporation on SBA-15 during polymerization has a great influence in the resulting mechanical response. Then, FISBA007T120 that has a considerably lower crystallinity than the homogenous FIHOM016T120 exhibits a significantly higher indentation modulus and hardness. Then, SBA-15 acts as reinforcing agent and stiffer component. The modulus value is further enlarged in the FISBA014T120 because of its slightly higher crystallinity and SBA-15 content compared with the FISBA007T120 film. It should be also kept in mind that the approach for immobilizing the catalyst has been also different between these two samples and these differences found (or part of them) might be also related to some morphological aspects derived from the two protocols.

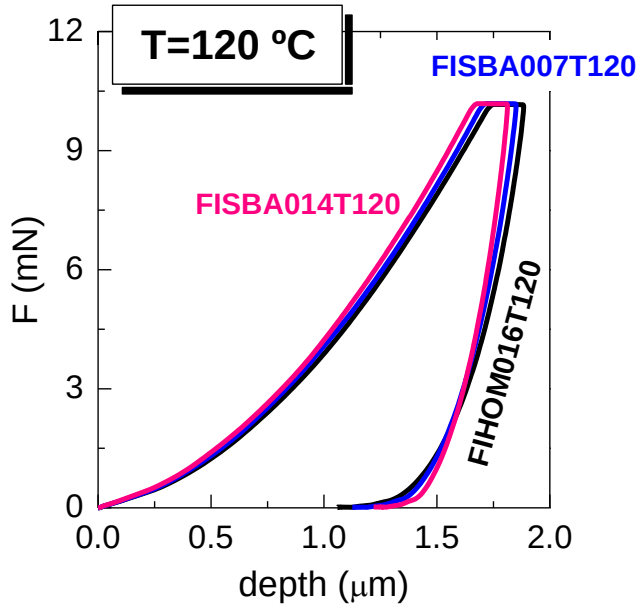

Figure 2.30: Indentation curves of load-maintenance-unload vs. depth for the different films processed at 120 °C: FIHOM016T120; FISBA007T120 and FISBA014T120.

Table 2.8: SBA-15 wt. % content estimated from TGA, crystallinity degree determined for X-ray diffraction and mechanical parameters (indentation modulus, E_{it}, and hardness, H_{it}) deduced from indentation measurements.

Sample	**SBA-15 wt.%^{TGA}**	**f_c^{XRD}**	**E_{it} (GPa)**	**H_{it} (MPa)**
FIHOM016T120	0	0.85	2.25	124.9
FISBA007T120	5.8	0.79	2.86	142.4
FISBA014T120	6.4	0.82	3.33	137.4

Dependence of depth on time shows that deformability of the homogeneous FIHOM016T120 is superior to that presented by those samples that contain SBA-15 particles, as noticeably deduced from Figure 2.31.

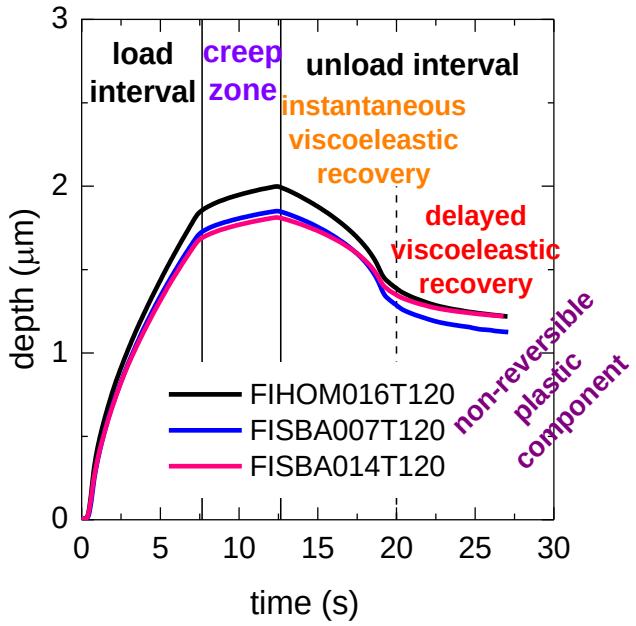

Figure 2.31: Variation of depth on time (right plot) for the different films processed at 120°C.

Subsequently, variation in depth at constant force is higher in the FIHOM016T120. A reduction of around 13 % is deduced from dimensional variability in FISBA007T120 and almost a 20% is exhibited by FISBA014T120 (as depicted in Figure 2.32). This feature might be ascribed to the presence of SBA-15, both acting as stiff components, minimizing the undesirable creep impact.

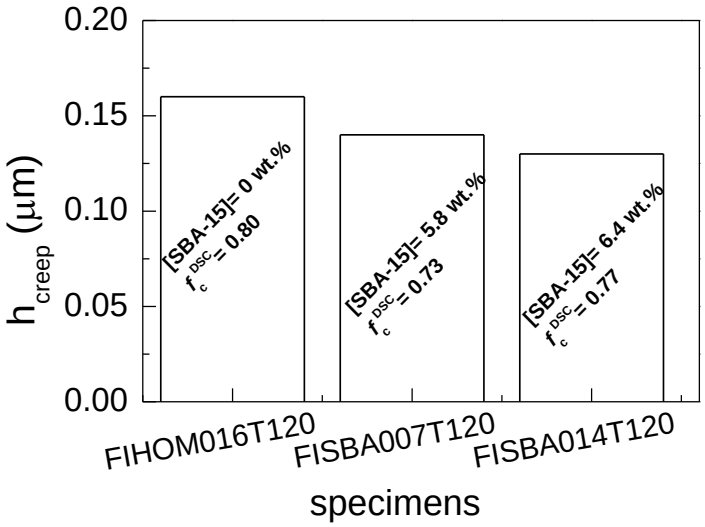

Figure 2.32: Indentation creep depth for the distinct T120 films under study.

There are also differences in the instantaneous viscoelastic recovery, this being more important in the softest material, *i.e.*, in the FIHOM016T120 film. Finally, FISBA007T120 film is that hybrid showing the lowest non-reversible plastic component.

2.7 Conclusions

Different UHMWPE have been synthesized under homogeneous conditions using a FI catalyst with living character. Moreover, this catalyst has been immobilized by two different approaches onto SBA-15 particles giving rise to UHMWPE based composites.

Very high activities in ethylene polymerization are obtained for the homogeneous FI catalyst, as expected from literature data. Moreover, although the average activity and productivity display almost a linear increase at low times, this linearity is lost at highest times Dependence of molar masses on polymerization time shows deviations from the expected living character even at low times in the neat polyethylenes.. On the other hand, an increase in Al/Ti ratio seems not to affect significantly molar masses in the neat UHMWPE. This behavior might be explained by the balance of two opposite effects acting simultaneously: promotion of the activation and stabilization of catalytic species and a detrimental deactivation of the catalyst by the presence of trimethylaluminum, TMA.

An important decrease of the activity is observed upon immobilization of the FI catalyst by the SBA-MAO methodology. This reduction is more considerable than that undergone when FI catalyst is supported by the pre-activated approach in spite of the shorter impregnation time required by the former method. It is suggested that the deactivation pathways that may involve Si-O-Al$(Me)_2$ surface-bonded species are lowered using the latest methodology.

Decomposition characteristics exhibited under oxidative conditions seem to be affected by the synthetic approach used during preparation of UHMWPE/SBA-15 materials. Nevertheless, none specific trend is seen under inert environment.

Very high crystallinity values are exhibited by the distinct UHMWPE samples in the form of as-powder from the reactor, either pristine polyethylenes or composites, in comparison with those estimated from films. Moreover, crystallinity from the first melting process is in the neat polyethylenes generally higher than that in the hybrid materials independently of the approach used for their preparation. It is also seen during cooling process that presence of SBA-15 particles slightly inhibits crystallization of the UHMWPE. Nevertheless, transition temperatures (melting and crystallization temperatures) are rather independent of the SBA-15 presence and of the method for supporting the FI catalyst. On the other hand, composite specimens prepared by PA show a weak but noticeable shoulder on heating from 80 to 110 °C, which is attributed to the melting of those UHMWPE crystallites developed inside the SBA-15 channels.

The incorporation of SBA-15 particles leads to stiffer materials, as deduced from stress-strain and indentation measurements, with higher elastic modulus, mechanical strength and toughness compared with those magnitudes found in the neat polyethylenes. Moreover, it seems that the most important factor that triggers deformation process is, in these nanocomposites, the SBA-15 amount followed by molar mass variations. Neat

polyethylenes become more compliant as molar mass is diminished and their creep resistance is lower compared with that exhibited by the hybrids.

Distinct UHMWPE based materials (one neat polyethylene and two nanocomposites) were processed by compression molding under different conditions, T120 (2950 bar and 120 °C) and T230 (10 bar and 230 °C) and the effect on their properties evaluated.

The T120 specimens show similar characteristics in terms of high crystallinity and melting temperatures to those found in the powders from the reactor meaning that macrochains have not been entangled during the processing conditions probably because temperature is close but lower to the melting process. On the other hand, chains after being at 230 °C for several minutes are able to establish a great number of entanglements between them and crystal formation is hindered during processing and a significant reduction is observed in crystallinity and melting temperature of the crystallites generated during the T230 film processing. Accordingly the T120 samples are considerably stiffer, which is directly related with its higher crystallinity values and absence of entanglements.

In summary, the catalytic system used here allowed the synthesis of nascent UHMWPE based materials with a reduced number of entanglements, that may be processed in solid-state by compression molding below its melting temperature and high pressure, originating disentangled UHMWPE films of very high crystallinity and showing strongly improved mechanical parameters (indentation modulus, E_{it}, and hardness, H_{it}) relatively to common compressed molded samples above melting temperature.

3. Polyethylene based nanocomposites prepared by *in situ* polymerization with an hafnocene catalyst: synthetic aspects and characterization

This chapter describes the *in situ* polymerization of ethylene catalyzed by a hafnocene complex combined with MAO under either homogeneous or supported conditions. Once again mesoporous SBA-15 particles have been chosen as catalytic support since MCM-41 and SBA-15 have been proved to be excellent candidates to perform synthesis with metallocene catalytic systems in heterogeneous media. Accordingly, neat polyethylenes and nanocomposites based on polyethylene and SBA-15 were obtained and additionally characterized. Moreover, the mechanical response and its correlation with the conditions used during synthesis used have been evaluated. Three different immobilization techniques have been examined to prepare the catalytic heterogeneous systems and, consequently, the resulting nanocomposites. The effect of those distinct approaches on polymerization activity and on properties of the materials synthetized has been also studied.

3.1 Ethylene polymerization behavior of the homogeneous catalytic system

The catalytic performance is sensitive to the experimental conditions of polymerization, being influenced by factors such as temperature, solvent type, monomer concentration and catalyst/cocatalyst ratio. Along with the reaction conditions, the polymerization activity is also strongly affected by the molecular structure of the metallocene catalyst. The ligand structure plays a primary role, and the stabilities of the cationic catalyst intermediates, generally increase with the electron-donating ability of methyl substituents thereby lowering the activation energies for chain propagation. For this study, a hafnocene complex, known to attain higher polyethylene molar masses than zirconocene, and possessing two *n*-butyl substitutes in the cyclopentadienyl ligand has been selected.

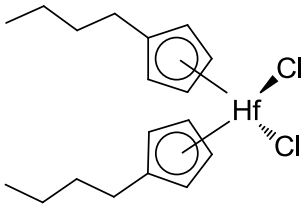

Figure 3.1: Chemical structure of the metallocene catalyst used: bis-(n-butylcyclopentadienyl)-dichloro-hafnium.

The effect of Al/Hf ratio in the ethylene homogeneous polymerization was studied and the results obtained are shown in Table 3.1 and Figure 3.2. For Al/Hf of 500 and 1000 no change in the polymerization activity could be observed. Nevertheless, a further increase in MAO amount to values to 2500 and 5000 originated an enhancement in the polymerization activity. It should be mentioned that, as expected, the activities attained exhibit values much

lower than those commonly found when the catalytic system is based on a zirconocene catalyst [180].

Table 3.1: Polymerization conditions, activities, molar masses and dispersities for the pristine polyethylenes obtained under homogeneous conditions. Polymerization time: 18 min

Sample	Al/Hf	Average activity (kgPE/molHf.h)	M_w (g/mol)	D
HfHOM004	500	1060	479500	1.6
HfHOM021	1000	1060	488300	1.6
HfHOM002	2500	1780	505410	1.9
HfHOM006	5000	1930	540700	1.5

In these polymerization conditions, it was observed just a slight increase in the polyethylene average molar masses with respect to the Al/Hf ratio at the interval evaluated. The average values are around 500000 g/mol, which are significantly higher than the regular molar masses achieved when zirconocene catalysts are used [180, 181]. As mentioned before, the stronger M–Cl and M–C bonds in hafnocenes explain the lower polymerization activity and the higher PE molar masses obtained with these systems when compared to zirconocenes [54, 55]. It is noticeable, however, that the polyethylene prepared with the Al/Hf of 5000 presents the highest molar mass. So it seems that chain transfer to aluminum does not play a major role in this catalytic system, similarly to that observed in the previous Chapter for the FI titanium complex bearing fluoride bis(phenoxy-imine) ligands. On the other hand, the dispersities observed are close to those found for other single-site systems.

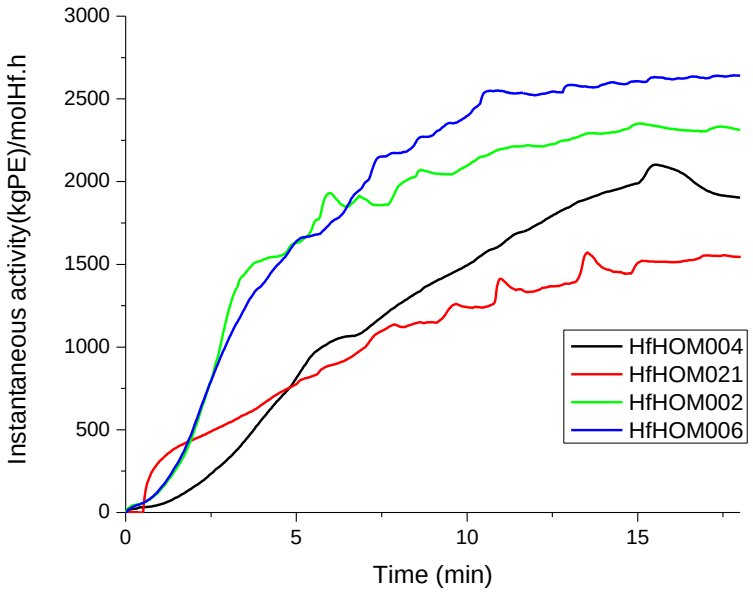

Figure 3.2: Kinetic profiles for different ethylene polymerizations performed at distinct Al/Hf ratios.

Figure 3.2 shows the kinetic profiles for the consumption of ethylene obtained at the different Al/Hf ratios studied. It may be seen that these profiles follow a build-up type, characterized by an induction period of very low activities followed by a slow rising of polymerization rate and then reaching a maximum or a plateau of activity.

3.2 Ethylene polymerization behavior of the supported catalytic systems

The approach used for supporting the metallocene catalyst and the methylaluminoxane (MAO) cocatalyst is a key variable on the catalytic behavior. Moreover, nanocomposites can be prepared by *in situ* polymerization using mesoporous silica particles (like MCM-41 or SBA-15) since polymeric chains can grow within mesoporous channels giving rise to intercalated polyethylene chains [82, 84, 120].

Three different methods have been used in this study to immobilize the hafnium catalyst on the SBA-15 particles: direct immobilization; immobilization of the catalyst on the SBA-15 previously modified with MAO and preactivation of the catalyst with MAO prior to its contact with SBA-15.

The simplest methodology is the first one, where the catalyst contacts directly with the support (see Figure 3.3), but it is sometimes not successful depending on the catalyst used, as observed in the previous Chapter for the FI catalyst. The other two approaches have been already explained in Chapter 2 and basically, the SBA-MAO method consists in the immobilization of the catalyst on SBA-15 previously modified with MAO and the PA method is based in the impregnation of a catalyst/MAO mixture on SBA-15. The final Al/Hf ratio is the same after the immobilization of the catalyst in these last two procedures.

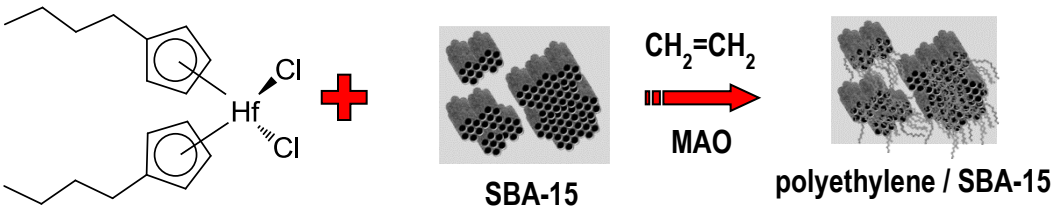

Figure 3.3: Direct impregnation of the catalyst on SBA-15 support.

The minimum time necessary for the complete immobilization of a specific amount of catalyst was first determined in the direct immobilization method. The initial time tested was 8 h based on our prior experience with zirconocene catalysts, where immobilization took 16 h [182]. Nevertheless, the complete amount of catalyst is immobilized after 3h. Moreover, a significant activity decrease with the increase of the impregnation time is observed after those initial 3 h (see Table 3.2).

Table 3.2: Correlation between impregnation time and activity for the direct impregnation approach Al/Zr=2500

Impregnation time (h)	**Average activity (kgPE/molHf.h)**
8	360
6	610
3	1050

The kinetic profiles obtained (see Figure 3.4) show that the induction times get higher and the polymerization rates are lowered when increasing the immobilization time. So, optimal immobilization times are crucial in order to reduce deactivation pathways and attain higher polymerization activities with these supported hafnocene catalysts.

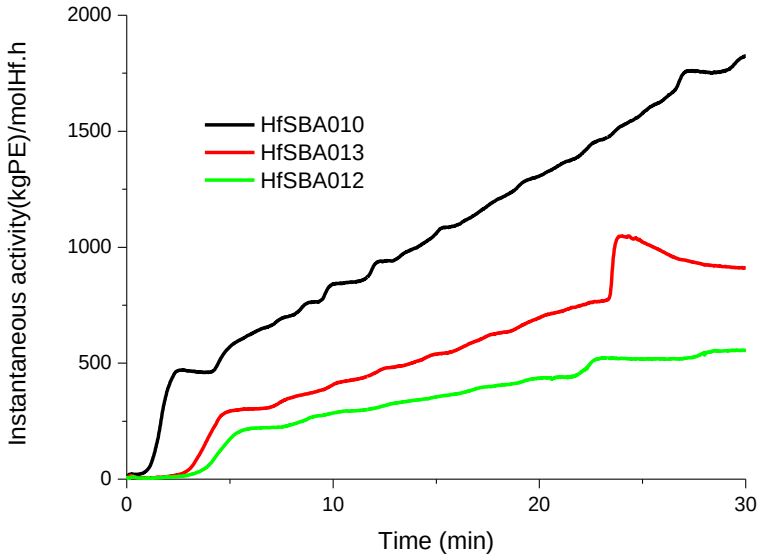

Figure 3.4: Kinetic profiles for different ethylene polymerizations for the direct impregnation approach performed at distinct immobilization times.

For the other two immobilization methods, the preliminary impregnation times tested were based on our previous experience of immobilization of the fluorinated titanium bisphenoxy-imine catalyst on an identical mesoporous SBA-15 support (see Chapter 2). These times were confirmed to be adequate and of sufficient duration for a complete immobilization. The results of the three methods are presented in Table 3.3.

Table 3.3: Minimum immobilization time required for the complete immobilization of 14 µmol of hafnocene in 100 mg of SBA-15.

Method	**Immobilization time (min)**
Direct Impregnation (Method DI)	180
Pretreatment of SBA-15 with MAO and impregnation of the hafnocene on pretreated support (Method SBA-MAO)	5
Impregnation of MAO pre-activated Hf catalyst on SBA-15 (Method PA)	90

Once the minimum immobilization time was checked and confirmed through these initial experiments for the three approaches, all the polymerization reactions were performed using supported catalysts prepared with those minimum immobilization times. The influence of the methodology used for the catalyst immobilization on the activity and on the

polymer molar mass is discussed below and the results obtained are listed in Table 3.4 and Figure 3.5. Values reported in Table 3.4 show that under optimized conditions the supported systems show quite high activity values compared with that observed under homogeneous conditions. Activity of supported heterogeneous systems is, in general, much lower than the one exhibited by the same catalyst under homogeneous conditions, due to the occurrence of diffusion constraints as well as to the deactivation of numerous active sites along the supporting protocol [183]. Particularly, a noticeable decrease in the activity upon the catalyst immobilization is usually observed in the case of zirconocenes (it may reach an order of magnitude) [93]. However this effect is not that strong in this current case with the hafnocene catalyst.

The reason to this behavior may be related to the ability of the surface hydroxyl groups of the support to anchor $AlMe_3$ present in MAO [174]. This leads to a decrease of the amount of free $AlMe_3$, when compared to a polymerization run of a homogeneous hafnocene complex, which may benefit polymerization activity. This way, usual deactivation pathways occurring in supported systems are somehow compensated and, in the overall the decrease on activity upon immobilization is significantly reduced. In fact it was reported by Severn and Chadwick [95] that the presence of $AlMe_3$ can depress activity via the formation of dormant alkyl-bridged species of type $[Cp_2Mt(\mu\text{-}R)(\mu\text{-}Me)AlMe_2]^+$, blocking monomer coordination to the transition metal [184, 185]. $AlMe_3$ has a particularly large rate depressing effect with hafnocenes, due to the high stability and therefore high proportion of the dormant species $[Cp_2Hf(\mu\text{-}R)(\mu\text{-}Me)AlMe_2]^+$.

For the direct impregnation method, the polymerization activity decreases for the highest Al/Hf ratio of 5000, which can also be related to the depressing effect of $AlMe_3$ on activity. For an Al/Hf ratio of 2500 similar activities are obtained for the direct impregnation and SBA-MAO method while PA method leads to a lower value.

Table 3.4: Polymerization conditions, activities and molar masses obtained for the nanocomposites synthesized with the supported catalyst (polymerization time: [a]18 min, [b]30 min).

Sample	Method	Hf load in the support (10^{-6} mol/g)	Impregnation time (min)	Al/Hf	Average activity (kgPE/molHf.h)	M_w (g/mol)	D
HfHOM002	-	-	-	2500	1780[a]	505410	1.9
HfSBA015	DI	14	180	500	530[b]	n.d.	n.d.
HfSBA010		14		2500	1050[b]	863340	n.a.
HfSBA011		14		5000	550[b]	n.d.	n.d.
HfSBA024	SBA-MAO	14	5	2500	1080[b]	n.d.	n.d.
HfSBA019	PA	9	90	2500	690[b]	n.d.	n.d.

Figure 3.5 displays the kinetic profile for ethylene polymerizations under homogeneous and supported catalyst at an Al/Hf ratio of 2500. It can be seen that the profiles corresponding to the heterogeneous polymerization have also a build-up type, as observed in the homogeneous polymerization reactions. Nevertheless, induction periods tend to be higher and polymerization rates lower when the catalyst is supported.

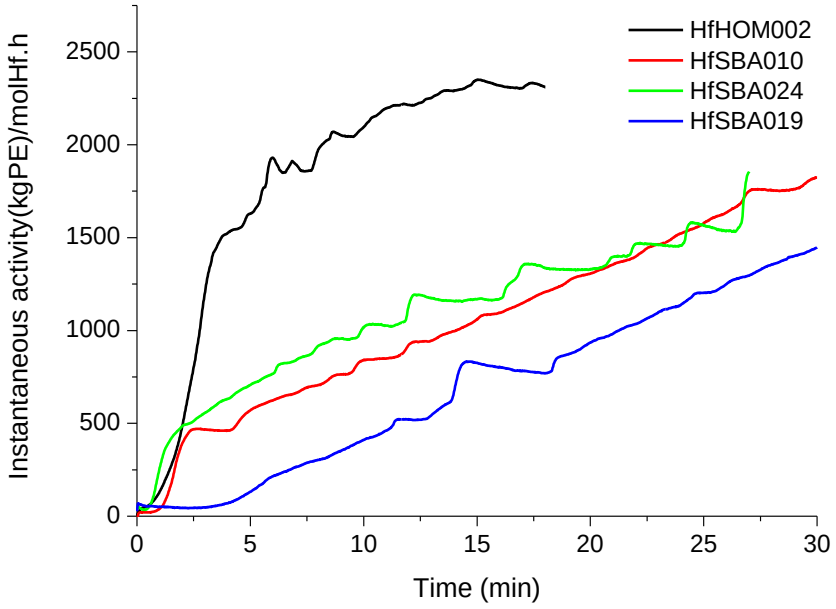

Figure 3.5: Kinetic profile for ethylene polymerizations.

In what concerns the molar mass, this parameter has been found to increase for the nanocomposite compared with its neat counterpart synthesized under homogenous conditions. This increase seems to indicate that the SBA-15 support is efficient in reducing chain transfer reactions during the polymerization. This effect was already reported in literature [186] and can be explained by a large steric hindrance of the active centers influenced by the channel walls, thus decreasing the occurrence of β-H elimination during the polymer growth and slowing down the chain transfer rate. This fact turns out in a major growth of the polymer and, consequently, in the higher molar masses of the macrochains synthesized under these confined polymerization conditions.

Figure 3.6 shows the morphology found by SEM in a neat polyethylene and three composites synthesized with the distinct immobilization approaches.

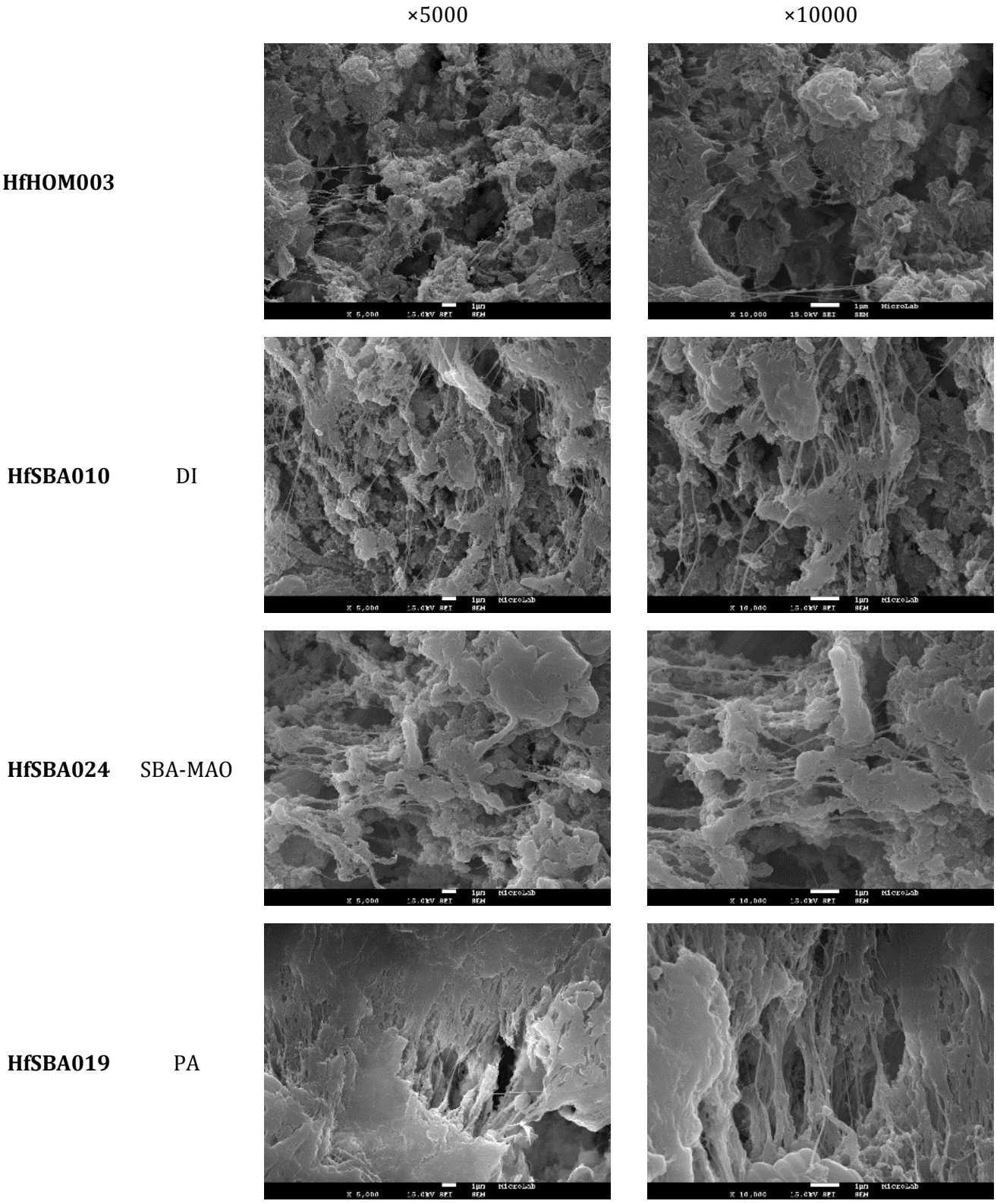

Figure 3.6: SEM micrographs for the HfHOM003 neat polyethylene and HfSBA010, HfSBA024 and HfSBA019 composites at different magnifications.

The formation of fibrils in the hybrids is well evident, while in the neat polyethylene these elongated fibrils are less noticeable. Moreover, it seems that these fibrils are very thin in HfSBA010 composite, and their thickness is increased in the HfSBA024 material and further enlarged in the HfSBA019 hybrid.

3.3 Characterization of the polyethylene based materials

3.3.1 Identification of SBA-15 in the synthesized materials

Figure 3.7 shows the X-ray pattern of SBA-15, some pristine polyethylene and some nanocomposites at the low angle region and it is possible to easily assess the presence of SBA-15 in the final nanocomposites synthesized with the hafnocene catalyst. As referred before, it can be seen that the SBA-15 profile displays a sharp peak that corresponds to the (100) planes and other weak peaks, which come from the (110), (200) and (210) reflections of these ordered two-dimensional hexagonal mesostructures [187].

The polyethylene does not show any diffraction at that low angle region ($2\theta < 5°$), as seen for the homogenous samples, HfHOM004 and HfHOM006. Then, it becomes very simple to conclude that the mesoporous structure remains unchanged and has not been destroyed in the hybrid materials during polymerization. This ordered structure is observed after the processing as films by compression molding, as deduced from the comparison of the profiles attained for the SBA-15 with those exhibited by the HfSBA011 and HfSBA015 samples. The intensity is, nevertheless, significantly reduced for the different diffractions since the SBA-15 amount is always minority in the resulting materials.

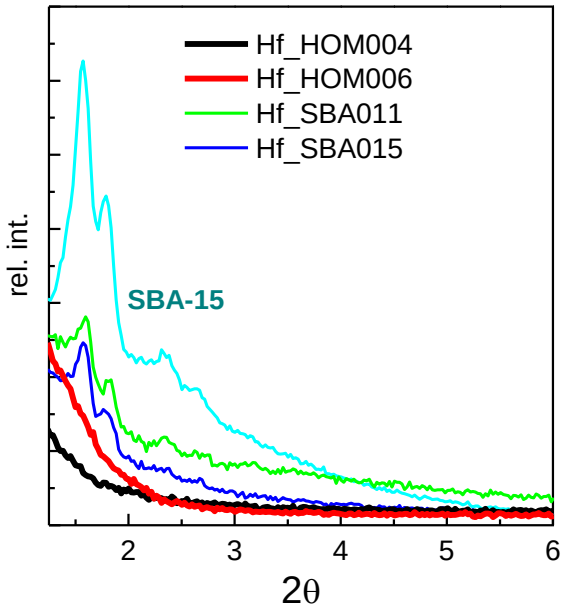

Figure 3.7: X-ray pattern of SBA-15, two homogenous polyethylene (samples HfHOM004 and HfHOM006) and two nanocomposites (samples HfSBA011 and HfSBA015).

3.3.2 Thermal behavior

3.3.2.1 Thermogravimetric analysis

Thermogravimetric analysis allows evaluating the thermal stability exhibited by the neat PE as well as the effect of SBA-15 incorporation in the degradability of the nanocomposites, being all of them synthesized at identical Al/Hf ratio. Moreover, the actual content of SBA-15 present in the nanocomposites is determined by this experimental technique.

Figure 3.8 depicts the thermogravimetric curves of the neat PE and of the nanocomposites under inert and oxidative atmospheres. As for the materials synthesized with the FI catalyst, decomposition process under inert conditions occurs in a single step while this mechanism is much more complex under oxidant environment and, thus, several processes are noticeable independently of the presence or absence of SBA-15 mesoporous particles. The complexity of this decomposition process is due to the presence of oxygen that promotes the formation of different intermediate species.

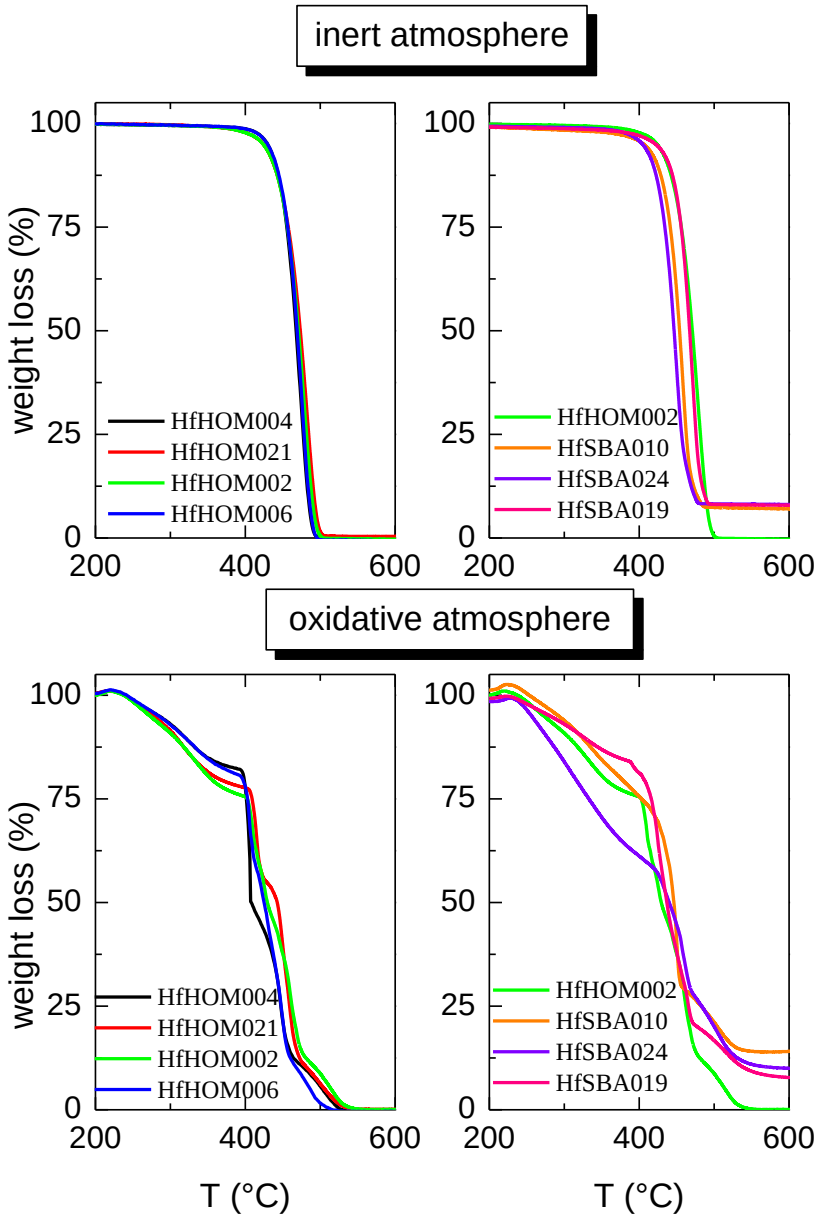

Figure 3.8: Thermogravimetric curves of neat polyethylene and nanocomposites under inert (top) and oxidative atmospheres (bottom).

Similar decomposition behavior is observed for the different polyethylenes obtained under homogeneous conditions independently of the Al/Hf ratio. Then, there are not great differences between the temperature of mass losses of 5 and 50 wt. %. Nevertheless, incorporation of SBA-15 to the nanocomposites leads to some changes depending on the approach used during the polymerization reactions. Under inert conditions, the sample HfSBA024 prepared by the SBA-MAO protocol is that presenting the lowest $T_{5\%}$ and $T_{50\%}$ temperatures, pointing out that degradation takes place easily. The HfSBA019 synthesized

by the PA method shows an analogous stability to that found in the pristine polyethylene HfHOM002.

The thermal decomposition under oxidative conditions shows two different trends as function of function of temperature, as deduced from Figure 3.8 and

Table 3.5. At the lowest values ($T_{5\%}$ temperature), the HfSBA024 exhibits the greatest weight loss. In fact, the HfSBA024 specimen has lost around 40 wt. % at 400 °C whereas that loss is in HfHOM002 and HfSBA010 samples of about 25 wt. % and only 15 wt. % for the HfSBA019 nanocomposite. It seems that if the mesoporous particles are previously contacted with MAO prior to hafnocene immobilization, the resulting polyethylene is more susceptible to degradation under oxidant conditions. Nevertheless, this trend varies as temperature is raised. Consequently, all the samples show rather analogous $T_{50\%}$ temperatures, independently of being prepared under homogenous or supported conditions and of the approach used to incorporate those mesoporous SBA-15 particles.

Thermogravimetric analysis allows determining the actual amount of SBA-15 incorporated into the PE into the PE matrix along in situ polymerization. Results of

Table 3.5 indicate that the SBA-15 weight content estimated through experiments performed under both inert and oxidant environments correlates rather well, turning out similar SBA-15 composition for the different experiments.

Table 3.5: Average SBA-15 wt.% content, characteristic decomposition temperatures under nitrogen and air atmospheres for neat PE and nanocomposites synthesized by three different approaches (the temperatures of a loss weight of 5%, $T_{5\%}$, and 50%, $T_{50\%}$) and the SBA-15 wt.% content at a specific environment.

Sample	Al/Hf	Average SBA-15 wt.% content	Inert atmosphere			Oxidative atmosphere		
			$T_{5\%}$	$T_{50\%}$	SBA-15 wt.% content	$T_{5\%}$	$T_{50\%}$	SBA-15 wt.% content
HfHOM004	500	0	429.5	468.0	0	284.5	407.0	0
HfHOM021	1000	0	423.5	473.5	0	276.5	442.5	0
HfHOM002	2500	0	423.5	471.0	0	272.5	429.5	0
HfHOM006	5000	0	429.5	469.0	0	284.0	425.0	0
HfSBA010	2500	7.6	406.0	454.0	7.9	292.5	446.0	7.4
HfSBA024	2500	8.9	404.5	446.5	9.7	256.5	440.0	8.0
HfSBA019	2500	8.0	421.5	467.5	7.7	281.0	436.5	8.3

3.3.2.2 Differential scanning calorimetry

The DSC results of these samples are listed in Table 3.6 and represented in Figure 3.9. Table 3.6 also details the values of crystallinity and melting temperature (T_m) for some of the samples corresponding to both the powder from the reactor and the films processed by

compression molding. Independently of the specimens being synthesized under homogeneous or supported conditions, the trend that can be observed is the same: there is an important variation, at a given sample, in crystallinity and melting temperature between the powder and the film. Thus, these two properties are considerable higher in the reactor powder, most probably because chains are much more disentangled in this state and rather chain-extended crystals with a small proportion of amorphous regions can be developed. Once chains are molten during compression molding process, they are able to be entangled one to another, which will constrain crystal formation during crystallization along the cooling process and a significant reduction of crystallinity and melting temperature of those crystallites is, accordingly, found. Moreover, it seems that specimens as powders that contain SBA-15 particles lead to slightly lower crystallinity but slightly higher T_m compared with those synthesized under homogeneous conditions. A similar decrease of crystallinity of UHMWPE samples upon incorporation of SBA-15 particles was also observed in the previous chapter, when using the FI catalyst.

Table 3.6: DSC calorimetric data of neat polyethylenes and nanocomposites.

Sample	Al/Hf	% SBA-15$_{TGA}$	*Powder*		*Film*			
			f_c^m	T_m (°C)	f_c^m	T_m (°C)	f_c^c	T_c (°C)
HfHOM004	500	0	n.d.	n.d.	0.50	130.0	0.53	117.0
HfHOM021	1000	0	0.73	136.0	0.55	130.0	0.58	117.5
HfHOM002	2500	0	0.74	136.0	0.50	130.0	0.53	117.0
HfHOM006	5000	0	n.d.	n.d.	0.53	126.5	0.57	116.0
HfSBA010	2500	7.6	0.69	137.0	0.49	129.0	0.48	117.5
HfSBA024	2500	8.9	0.67	137.5	0.50	129.5	0.45	117.0
HfSBA019	2500	8.0	0.65	138.5	0.54	130.5	0.49	117.5

It should be also commented that even higher crystallinity and melting temperatures have been found in as-powder samples synthesized by the bis(phenoxy-imine) titanium complex instead of the hafnocene used here (see Chapter 2). This might be ascribed to the longer chains (higher molar masses) attained during polymerization when using the former titanium complex. Crystallization seems to be then promoted in the synthetic experimental conditions used and, therefore, amorphous content is reduced and larger crystallites are formed.

Regarding the processed films, it can be observed that the different homogenous polyethylenes exhibit values of crystallinity quite similar and no clear tendency is seen as a function of the Al/Hf ratio used along polymerization. Nevertheless, the T_m at the highest Al/Hf proportion, 5000, shows a noticeable decrease down to 126.5 °C. It is interesting to mention it as, in a previous study regarding neat polyethylenes and nanocomposites based on polyethylene synthesized with zirconocene and hafnocene catalysts, a strong decrease in

T_m as Al/M_t is raised, has been also observed [188]. In the crystallization process however this trend is not that clear.

It is also noticeable in Figure 3.9 that the endothermic peak ascribed to the melting process is rather broad in these polyethylenes prepared with the homogeneous hafnocene, fact that seems to indicate that the distribution of crystallite sizes is also relatively wide. Interestingly the width of the overall melting process seems to decrease when using the Al/Hf ratio of 5000.

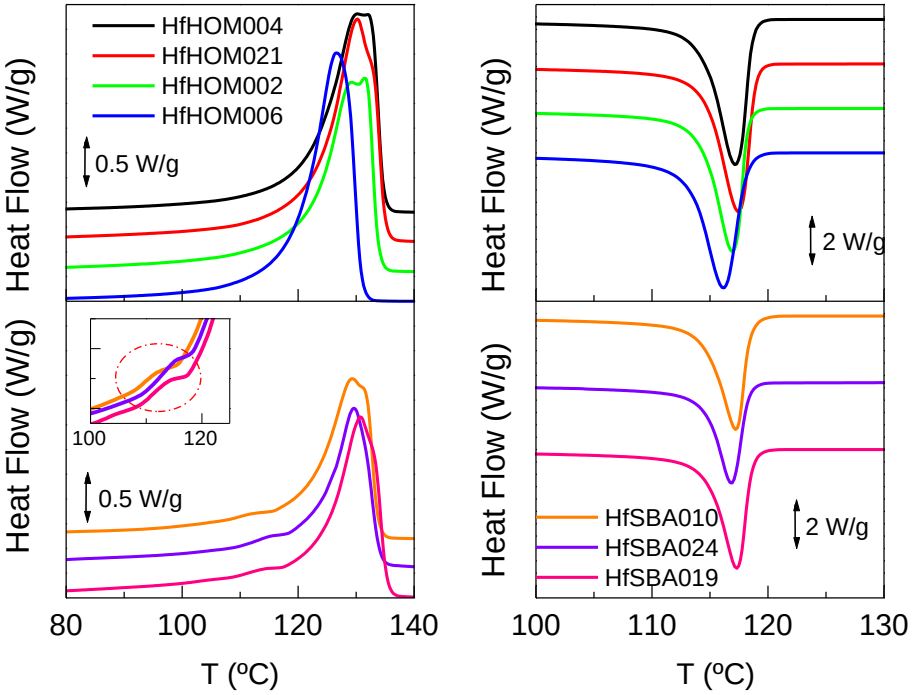

Figure 3.9: DSC curves of the first melting and subsequent crystallization processes of neat as films polyethylenes and the nanocomposites.

Incorporation of SBA-15 particles leads to distinct effects depending on the approach used to support the hafnocene catalyst prior polymerization when comparing the resulting composites with the homogenous HfHOM002 synthesized at identical Al/Hf ratio. DI and SBA-MAO method do not affect the crystallinity. Nevertheless, chains achieved from the PA methodology are able to crystallize in a slightly higher amount and the crystallites are somewhat larger than those formed from the other two approaches.

The insert in Figure 3.9 points out that an endothermic shoulder is seen for the three composites at temperatures ranging from approximately 105 to 120 °C. This feature is attributed to the presence of PE chains within SBA-15 channels, which are able to be ordered three-dimensionally although the sizes of these crystals are rather small, as a result of the confinement phenomenon, and, then, their melting takes place at temperatures well below the main endothermic process. Based on this, it may be assumed that these

nanocomposites consist in polyethylene chains incorporated within the SBA-15 channels in combination with other PE macrochains surrounding the mesoporous nanofiller. These observations are in agreement with what was described in the Chapter concerning nanocomposites prepared with FI catalyst and also in previous work reported by Cerrada *et al.* for nanocomposites with MCM-41 [84].

In addition, the presence of SBA-15 seems to inhibit polyethylene crystallization because crystallinity values achieved along crystallization process in the nanocomposites are decreased, relatively to those observed in the melting process, mainly in those synthesized by the SBA-MAO and PA approaches. This effect has been also described in other hybrids incorporating MCM-41 particles [120].

On the other hand, crystallization temperature remains practically constant and, then, a possible nucleant effect of the SBA-15 is not noticeable for these specimens. Ribeiro *et al.* reported results on nanocomposites based on HDPE and non-modified MCM-41, these mesoporous particles acting as a catalyst carrier. In that work, it was found that at the lowest MCM-41 contents, crystallization was maintained, practically at an identical temperature to the one observed in the neat HDPE, while T_c was shifted to higher temperatures at compositions greater than 6 wt.%.

3.3.3 Mechanical properties

3.3.3.1 Indentation experiments

Values of indentation modulus (E_{it}) and hardness (H_{it}) are reported in Table 3.7 for different samples under study. Looking, first, at the samples prepared under homogenous conditions, the HfHOM002 sample exhibits the lowest E_{it} and H_{it} values. This inferior surface rigidity can be related to its lower crystallinity. Although the differences are not too large, it seems that they are enough to reduce to some extent both mechanical parameters. As crystallinity increases in the other specimens, HfHOM006 and HfHOM021, respectively, their corresponding indentation modulus and hardness values are also, consequently, raised.

Table 3.7: Indentation parameters attained at 25 °C: indentation modulus (E_{it}) and hardness (H_{it}) for some pristine polyethylenes synthesized at different Al/Hf ratio, some nanocomposites prepared by three distinct catalytic immobilization approaches and two more additional ones by means of PA method at varying SBA-15 contents.

Sample	Synthetic Approach	Al/Hf	wt.% SBA	f_c^{DSC}	E_{it} (MPa)	H_{it} (MPa)
HfHOM021	-	1000	-	0.55	935	48
HfHOM002	-	2500	-	0.50	738	46
HfHOM006	-	5000	-	0.53	916	51
HfSBA010	DI	2500	7.6	0.49	856	56
HfSBA024	SBA-MAO	2500	8.9	0.50	897	58
HfSBA019	PA	2500	8.0	0.54	923	59
HfSBA027	PA	5000	6.7	0.55	827	55
HfSBA029	PA	5000	14.0	0.54	1264	76

The left plot in Figure 3.10 also shows the softer character of the pristine HfHOM002 with respect to that exhibited by HfHOM006 and HfHOM021, respectively. The complete loading-maintenance-unloading cycle is represented in that figure for the distinct specimens, and it is clearly noticed that the largest deformability is found for the softest HfHOM002 specimen. Consequently, indenter can penetrate deeper inside at a given force when compared with the other two pristine polyethylenes.

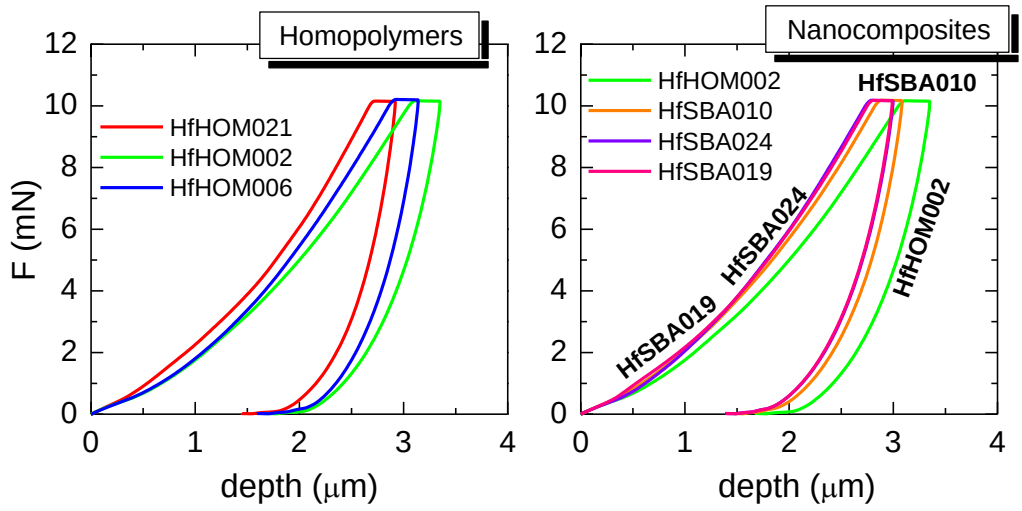

Figure 3.10: Indentation curves of load-maintenance-unload vs. depth for some neat polyethylenes (left) and composites (right).

Incorporation of inorganic mesoporous SBA-15 is expected to increase the final stiffness. This trend is accomplished when HfHOM002 is taken as reference, since it has been synthesized under an Al/Hf ratio identical to that used for the nanocomposites. Indenter is able to penetrate at the end of the loading stage in the neat polyethylene more than in the nanocomposites. The modulus and hardness values follow in these hybrids, as reported in Table 3.7, the order of HfSBA010 < HfSBA024 < HfSBA019. It should be commented that variations between them are not too large but it can be deduced that HfSBA010 sample, which has the lowest crystallinity and SBA-15 particle content, presents the smallest values of both mechanical parameters. Differences between the other two specimens can be understood in terms of crystallinity/SBA-15 content balance. Therefore, HfSBA024 incorporates the highest amount in inorganic particles but polyethylene crystallized less than in HfSBA019 that exhibits a smaller SBA-15 content. For these samples no significant changes for SBA-15 dispersion is observed in the TEM micrographs (Figure 3.11). It is worthwhile to notice that at higher magnifications we can see the SBA-15 ordered channel structure in the polyethylene matrix.

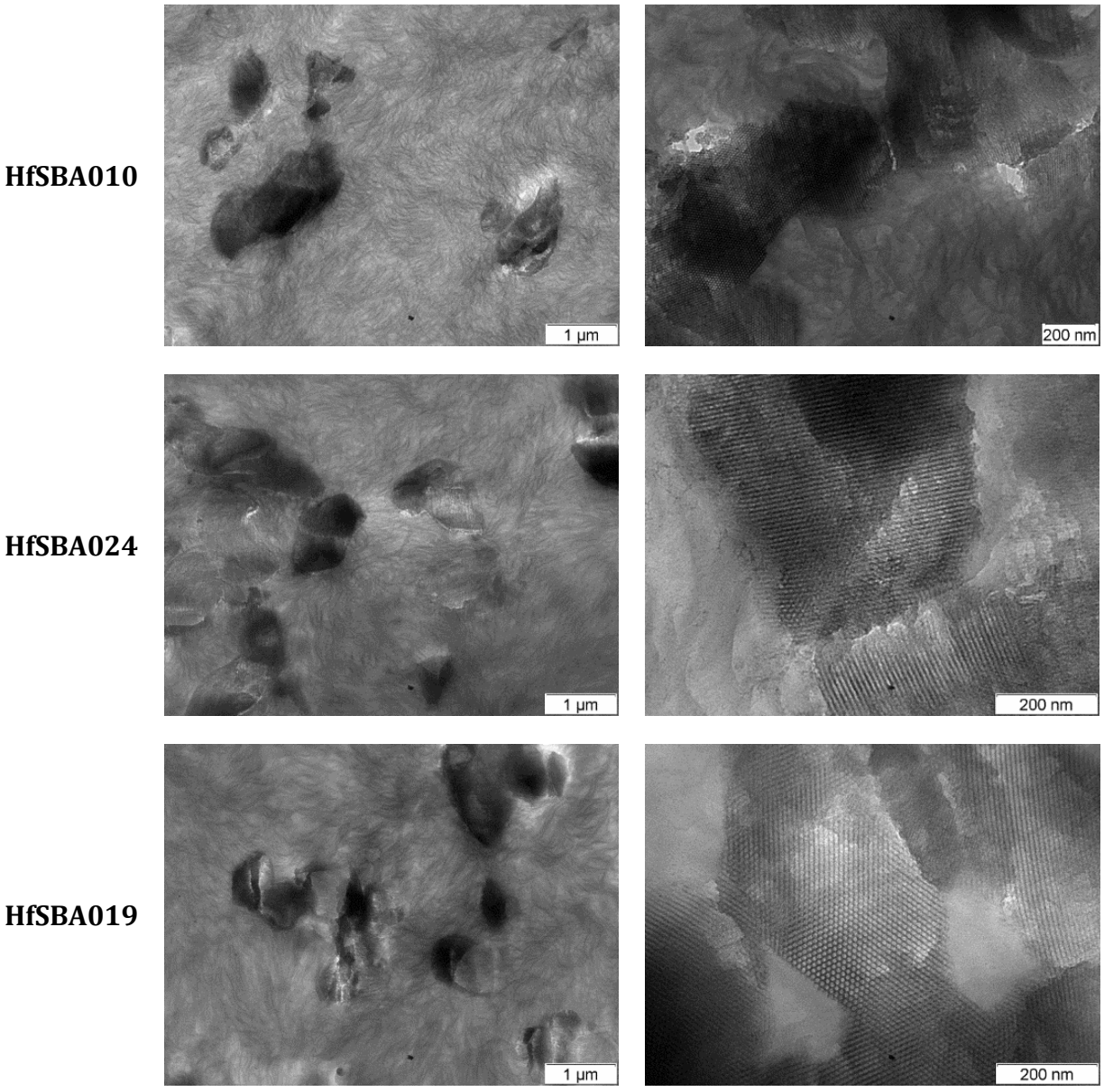

Figure 3.11: TEM micrographs of three nanocomposites obtained by the different immobilization methods: DI (sample HfSBA010), SBA-MAO (sample HfSBA024) and PA (sample HfSBA019).

The upper plot in Figure 3.12 represents the depth as a function of time along the whole loading-maintenance-unloading cycle for the different composites. It is noticeable that HfHOM002 is the material where the indenter can go through deeper because it is the softest one. Incorporation of SBA-15 leads to a hindrance for indenter to penetrate as much as in the neat polyethylene and, accordingly, deformability in the different nanocomposites is reduced along the load stage.

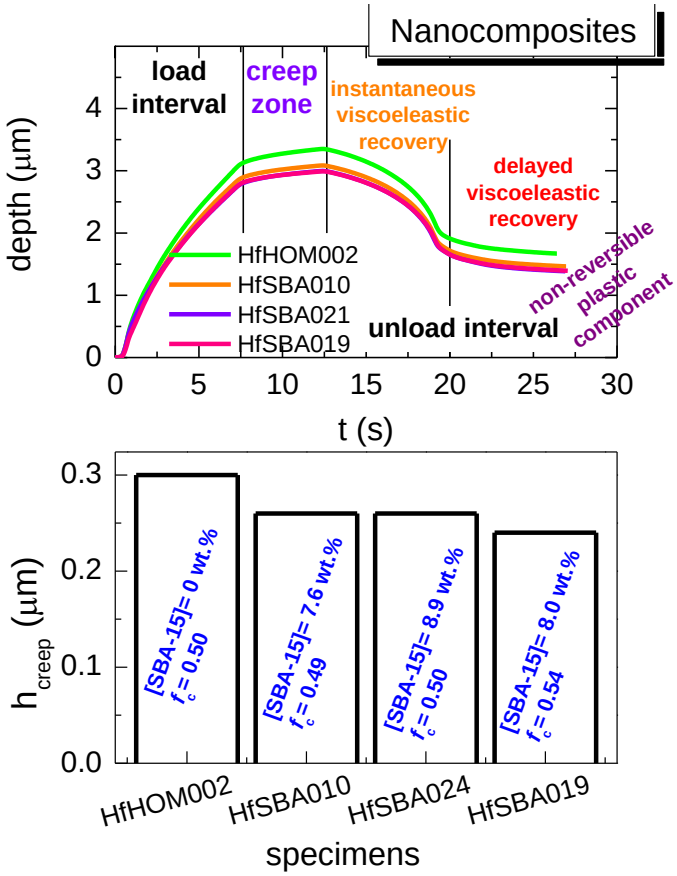

Figure 3.12: Indenter depth dependence on experimental time (top plot) and indentation creep depth (bottom plot) for neat polyethylene and its nanocomposites at Al/Hf = 2500.

The maintenance at a constant load for 5 second allows also learning on creep response of these materials. An increment of depth takes place for all the specimens at this maximum load of 10 mN, L^{max}, *i.e.*, during the maintenance period (see upper plot in Figure 3.12). Quantification of that increase, depicted in the bottom plot of Figure 3.12, indicates its dependence on absence or presence of SBA-15 in the ultimate material and on the crystallinity/SBA-15 content balance. Accordingly, neat polyethylene becomes more compliant, its creep resistance is lowered and, then, length variation along creep period is the highest compared with that exhibited by the hybrids, which show rather similar values one to another. Nevertheless, the lowest creep is observed, as expected from results in Table 3.7, in the HfSBA019 material, which is that with the highest indentation modulus and hardness, *i.e.*, the stiffest composite because of the appropriate combination of the rigid entities, in terms of PE crystallites and SBA-15 particles.

To get a deeper knowledge on the mechanical behavior of these materials synthesized using a hafnocene catalyst, two additional nanocomposites have been prepared by using the PA approach at different SBA-15 contents, taking into account that this methodology led to the nanocomposite showing the best response.

Table 3.7 also reports the corresponding results for these two new materials. All of the hybrids synthesized by the PA method exhibit rather similar values of crystallinity and, consequently, variation in the mechanical properties should be mainly associated with the different SBA-15 incorporation. It is noticeably deduced the dependence of E_{it} and H_{it} on mesoporous particle content, as seen in Figure 3.13 for both magnitudes. The values for the corresponding homogenous polyethylene HfHOM002 have been also represented for comparison. Improvement of overall rigidity and some related parameters, like indentation modulus and hardness, seems to be very smooth at low SBA-15 contents. Nevertheless, stiffness changes practically linearly upon mesoporous amount above an intermediate weight composition at around 7 wt. %. And, importantly, the trend is rather analogous for both mechanical magnitudes.

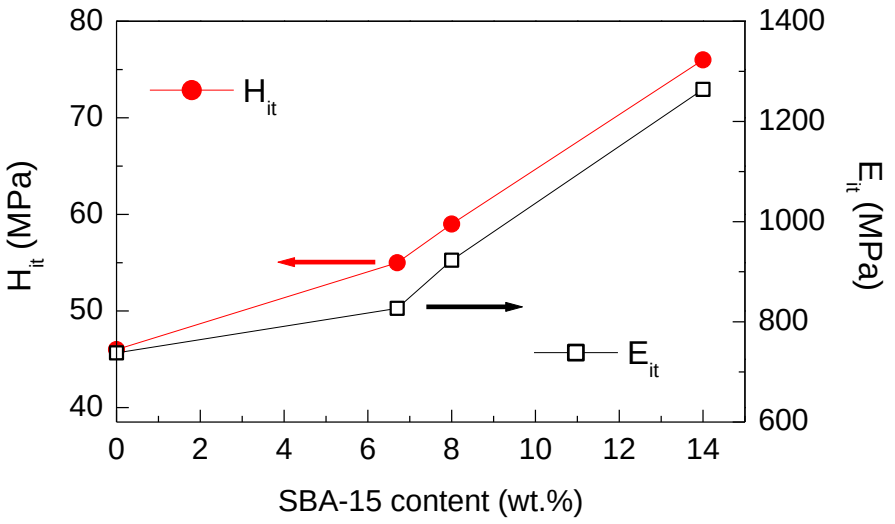

Figure 3.13: Values of indentation modulus and hardness depending on SBA-15 wt. % content for a set of nanocomposites synthesized by the PA approach.

3.3.3.2 Stress-strain experiments

Figure 3.14 depicts the stress-strain behavior at room temperature, 25 °C, with drawing rate of 1 mm/min for the nanocomposites obtained by the PA method and containing the highest and the lowest SBA-15 contents as well as for the HfHOM002 taken as reference. All the samples were stretched until a final strain of around 350%. The different average mechanical parameters obtained for the analyzed samples are reported in Table 3.8.

Table 3.8: Mechanical parameters of different samples, analyzed at 25°C and 90°C: Young's modulus, E; average value. $E^{average}$; yield deformation, ε_Y; yield stress, σ_Y; stress at break σ_B; load at break $load^{break}$.

Sample	% wt. SBA-15	f_c^{DSC}	$E^{average}$ (MPa)	ε_Y (%)	σ_Y (MPa)	σ_B (MPa)	$load^{break}$ (N)
25 °C							
HfHOM002	0	0.50	210	40	16.0	17.9	5.2
HfSBA027	6.7	0.55	304	35	19.5	28.2	7.7
HfSBA029	14.0	0.54	342	30	19.6	26.3	9.2
90 °C							
HfHOM002	0	0.50	64	46	5.5	7.6	1.9
HfSBA027	6.7	0.55	98	35	6.9	13.0	3.7

The results concerning Young´s modulus, E, in Table 3.8 can be compared with those of the indentation modulus E_{it} that can be found in Table 3.7. It can be seen that E values range from 200 to 350 MPa whereas E_{it} values are between 750 and 1275 MPa, yielding a ratio E_{it}/E close to 4. This discrepancy can be explained by considering the rather different deformation rates involved in both types of experiments. Whereas the deformation rate of the tensile tests for these experiments, that can be estimated as the ratio of the drawing rate to the calibrated length of the specimens, is $1.7x10^{-3}$ s^{-1}, that of the indentation tests, that is proportional to the ratio of the loading speed to the maximum load [189, 190], is $7.5x10^{-2}$ s^{-1}.

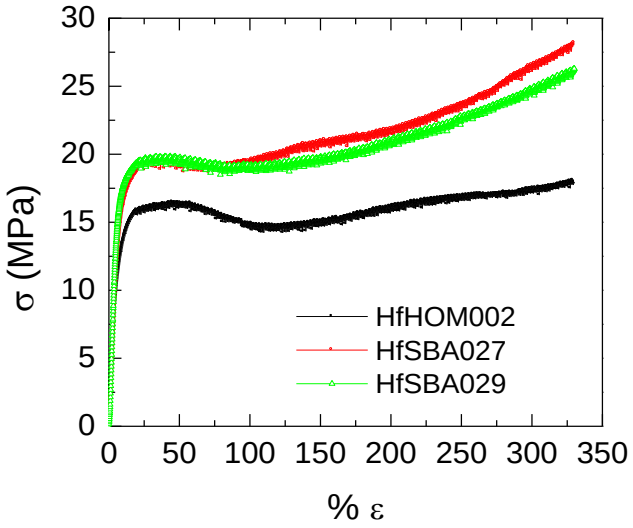

Figure 3.14: Stress-strain curves at room temperature and at a rate of 1 mm/min for the pristine HfHOM002 and the HfSBA027 and HfSBA029 nanocomposites.

This behavior parallels the one previously reported for amorphous and semicrystalline poly(L-lactic acid) [191]: it has been found that the ratio E_{it}/E for these polymers is close to 2, a fact that was justified as a manifestation of the viscoelastic and anelastic mechanical response of polymers. It is also worthwhile to note that independently of the type of measurements made the reinforcement effect observed upon introduction of SBA-15 in the HDPE matrix is similar. In both cases a significant increase on modulus of around 60 to 70% is observed when comparing the composite sample HfSBA029 containing 14% of SBA-15 with the HfHOM002 sample, corresponding to the pristine HDPE sample prepared in similar conditions.

The stress-strain curves observed for all these samples are characteristic for ductile polymers. The engineering stress-strain curves, depicted in Figure 3.14, show three distinct regions: initially, the stress rises on strain in a linear dependence and allows determining Young´s modulus; after this initial stage, an evident yield point is observed; and, finally, the stress starts again to increase with strain because of hardening associated with the beginning of stress-induced orientation. Then, deformation mechanism involves necking formation, which was also confirmed from the direct and *in situ* observation of the stretching process. It is also noticeable that the yield zone in the HfHOM002 is broader than in the nanocomposites, fact that can be attributed to the appearance of a second yielding point, as already reported in other polyethylenes, where the first yield point [192, 193] was related to a strain softening process and the second one to the necking formation. Other authors, as in the case of poly(ethylene naphtalate) [194], have ascribed the second yield point to the improvement of chain orientation by necking.

On the other hand, a rather good reproducibility of the stress-strain response has been found either in the shape of deformation process or in the mechanical magnitudes derived from these experiments for the different strips stretched at a given sample (Figure 3.15).

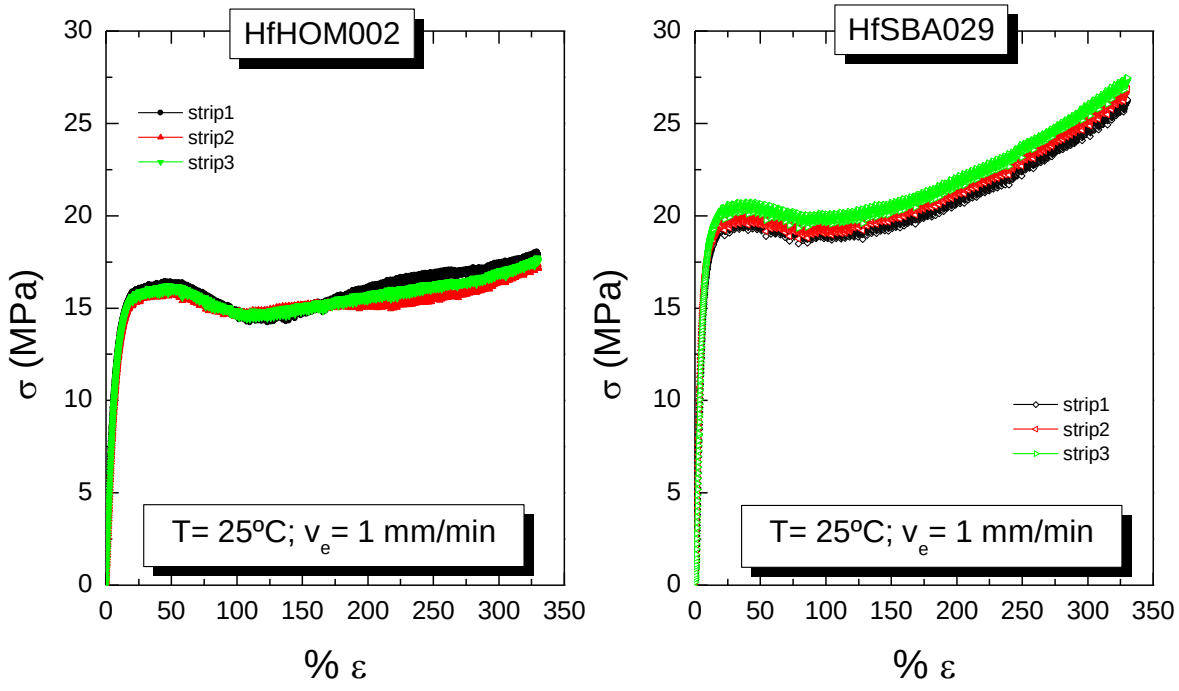

Figure 3.15: Stress-strain curves for different strips of a neat polyethylene (left) and a nanocomposite (right).

The incorporation of SBA-15 particles lead to stiffer materials with higher mechanical strength and toughness compared with the neat polyethylene although it does not alter how deformation takes place, as clearly noticed in Figure 3.14. Then, the Young`s modulus, the σ^{final} and the value of the area under stress-strain curve are higher in HfSBA027 and HfSBA029 than in neat polyethylene HfHOM002. Figure 3.14 also points out as significant feature the good deformability exhibited by HfSBA029, which contains a 14 wt. % in SBA-15 particles, since incorporation of inorganic nanoreinforcements commonly leads to an important reduction of strain at rupture and, consequently, reduction of impact strength [195, 196]. This maintenance of reaching high strain values could be related to the relatively high molar masses of these hafnocene catalyzed samples (see Table 3.1 for the neat polyethylene values; even higher values are expected for the nanocomposites as shown in Table 3.4).

Anyway, data from Table 3.8 points out that the highest elastic modulus is exhibited by PE from HfSBA029 because of its major content in SBA-15 particles. Nevertheless, differences in rigidity and breaking load are not really as large as that of the amount of mesoporous SBA-15 existing between both nanocomposites. This fact may be attributed to the low rate of stretching used. On one hand, it was selected to reduce probability of strips to break out because some defects (since there was not a lot of amount of each material to prepare many strips and to evaluate different rates). On the other hand, it was also chosen so low in order to assure that the different specimens are able to be stretched, achieving for all of them information from the stretching process.

Deformation has been also performed at much higher temperature, 90 °C, for the neat polyethylene HfHOM002 and the HfSBA027 hybrid, with a rate of 1 mm/min and until a final strain of around 350%. Stress-strain curves are represented in Figure 3.16 and results listed also in Table 3.8.

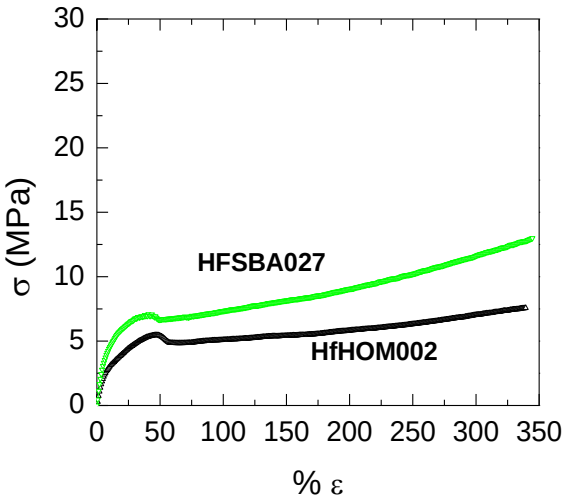

Figure 3.16: Stress-strain curves at 90 °C and at a rate of 1 mm/min for the pristine HfHOM002 and the HfSBA027 nanocomposite.

The alignment of the macrochains occurs also by necking formation at that high temperature and, thus, a noticeable yielding point is observed either in the neat polyethylene or in the nanocomposite. The latter one is much more rigid than pristine HfHOM002, as expected, and, then, Young´s modulus is significantly increased, as well as tensile strength (see Table 3.8). It is also important to remark that temperature allows reducing the stress required to reach identical strain than at room temperature in both samples. This feature reveals the great significance that temperature has on the ultimate mechanical performance of polymeric materials, in particular for these specimens obtained by using a hafnocene catalyst.

Properties in nanocomposites are usually extraordinary dependent on the minor component content and also on its distribution, since the ultimate optimization in these polymeric materials varies with the interactions between the matrix and the filler. The dispersion state of the filler and the nature of the interface/interphase with the polyethylene matrix are the two main factors accounting for the interaction between these two components, filler and matrix.

3.4 Conclusions

Using a hafnocene catalyst different polyethylenes were synthesized in homogeneous conditions varying the Al/Hf ratio. Additionally, a set of polyethylene/SBA-15 nanocomposites has been prepared taking advantage of the unique channel framework of SBA-15 particles, well suited for catalyst immobilization and intercalation polymerization.

In homogeneous conditions, the polymerization activity of the hafnocene complex depends on the Al/Hf ratio and the best activities are observed at the highest ratios. The average molar masses of the polyethylenes are around 500000 g/mol and tend to slightly increase with the Al/Hf ratio in the interval evaluated.

Three different methods have been used to immobilize the hafnocene catalyst precursor on the mesoporous silica SBA-15: direct immobilization; immobilization of the catalyst on the SBA-15 previously modified with MAO and preactivation of the catalyst with MAO prior to its contact with SBA-15. It was observed that the immobilization time has a strong influence on the kinetic profile and therefore on the polymerization activity. Under optimized conditions the supported systems show quite high activity values compared with those observed under homogeneous conditions, which was related to the ability of the surface hydroxyl groups of the support to anchor $AlMe_3$ present in MAO and this way to reduce the formation of dormant alkyl-bridged species of type $[Cp_2Hf(\mu\text{-}R)(\mu\text{-}Me)AlMe_2]^+$. A noticeable increase of polyethylene molar mass is observed when using the supported hafnocene catalyst. This points out the ability of SBA-15 to reduce chain transfer reactions under these confined polymerization conditions.

Similar thermal decomposition behavior is observed for the different samples prepared under homogenous conditions independently of the Al/Hf ratio. Incorporation of SBA-15 in the polyethylene matrix leads to some changes depending on the approach used during polymerization reactions. However, under oxidative conditions all specimens show rather analogous $T_{50\%}$ temperatures, independently of being prepared under homogenous or supported conditions and of the approach used to incorporate those mesoporous SBA-15 particles.

The crystallinity and the melting temperature of a given sample, are considerable larger for the reactor powders than for the films processed by compression molding. Most probably a more disentangled state and rather chain-extended crystals with a small proportion of amorphous regions can be developed under reactor polymerization conditions. Moreover, it seems that nanocomposites have slightly lower crystallinity but slightly higher T_m than neat polyethylenes synthesized under homogeneous conditions.

Regarding the processed films, the different homogenous polyethylenes exhibit values of crystallinity quite similar and no clear tendency with the Al/Hf ration is seen. On the other hand, a noticeable decrease of the Tm is observed for the highest Al/Hf ratio. In what concerns the nanocomposites, samples obtained by DI and SBA-MAO method have the same crystallinity that neat polyethylene, prepared at identical Al/Hf ratio, whereas the sample issued from PA methodology shows a slightly higher crystallinity. Not very significant changes were detected for T_m.

Furthermore, the presence of SBA-15 seems to inhibit polyethylene crystallization because crystallinity values of the nanocomposites are decreased, relatively to those observed in the

melting process, mainly in those synthesized by the SBA-MAO and PA approaches. A possible nucleant effect of the SBA is not noticeable for these specimens since crystallization temperature remains practically constant. The nanocomposites synthesized with the three different immobilization methods show an endothermic shoulder at temperatures ranging from approximately 105 to 120 °C. This feature is attributed to the presence of PE chains within SBA-15 channels, which crystals are rather small as a result of the confinement phenomenon.

For the neat polyethylene the indentation modulus and hardness are in direct correlation with the crystallinity. The incorporation of SBA-15 into the polyethylene matrix increases the final stiffness of the material. The differences on the indentation modulus and hardness values observed between the nanocomposites can be understood in terms of crystallinity/SBA-15 content balance. No significant changes for SBA-15 dispersion are observed in the TEM micrographs.

The stress-strain experiments show that the incorporation of SBA-15 particles into the polyethylene matrix, by *in situ* polymerization, lead to increased Young´s modulus, yield stress and tensile strength. Accordingly stiffer materials with higher mechanical strength and toughness compared with the neat polyethylene, while keeping a good deformability at high filler contents, are obtained.

4. In-reactor PE based blends prepared by *in situ* polymerization through dual catalyst immobilization on mesoporous SBA-15: synthetic aspects and characterization

This chapter covers the synthesis of in-reactor polyethylene based blends comprising two components: one with the lower molar mass, corresponding to a common HDPE and the other with a much higher molar mass. These in-reactor blends are produced by *in situ* polymerization in a single reactor, through dual catalysts immobilization. First, it is investigated the ethylene polymerization behavior, under different polymerization conditions, of the co-immobilized catalysts on mesoporous SBA-15. Then, studies on the thermal and mechanical characteristics of the produced in-reactor blends are presented and their performance are compared and discussed in a comprehensive way. Moreover, the effect of different filler contents on the properties exhibited by the resulting materials is investigated.

Two different catalysts are used for the production of the highest molar mass component of these blends. Accordingly, results are presented in two distinct sections, 4.2 and 4.3.

4.1 Definition of the dual-catalysts system and of the immobilization method

There are two main different strategies to obtain UHMWPE/HDPE blends: melt blending and blending in-reactor. However, melt blending of UHMWPE is rather difficult because commercial micrometer-sized UHMWPE pellets do not melt during the short residence time typical in melt extrusion. Moreover, efficient dispersion of immiscible polymers and of nanofillers in viscous polyolefin melts requires high shear forces and special preprocessing, both of which increase the energy demand and impair sustainability. Hence, the other approach, the so-called in-reactor blending, offers considerable cost and energy savings with respect to melt compounding. Intimate blending takes place during polymerization at much lower temperatures, thus enabling mixing of immiscible components at a nanometer scale without requiring high shear forces.

In this study the in-reactor blends are synthesized combining two different single-site catalysts, one for each targeted molar mass, co-immobilized on SBA-15. It is expected that the close proximity of different sites in a multi-site catalyst enable blending of different polyolefins on a nanometer-scale without requiring extensive shearing. In addition, the effect of those mesoporous SBA-15 particles as fillers in the blends will be analyzed.

The highest molar mass component is synthesized either by the phenoxy-imine or the hafnocene catalyst, used in Chapters 2 and 3) while the production of the lower molar mass component in the blend is always carried out with the metallocene Cp_2ZrCl_2 catalyst.

The pre-activation (PA) method, consisting in the contact of both catalysts with MAO before their further interaction with the SBA-15 particles, has been selected as immobilization approach. As referred in chapter X, the immobilization time is higher for PA method than for the SBA-MAO one. Thus, increasing probability of diffusion of the two catalysts within the support, and enabling ethylene polymerization inside their pores. Accordingly, a more intimate mixing of the blend components and a more disentangled state for UHMWPE may be expected. Moreover, results presented in Chapter 2 have shown that much higher molar

masses (up to several millions), can be attained when using the FI catalyst and the PA method. On the contrary, for the same catalytic system the SBA-MAO approach leads to a notorious decrease of M_w.

4.2 UHMWPE/HDPE blends prepared by *in situ* polymerization with a FI and a zirconocene catalyst

4.2.1 Ethylene polymerization behavior

A set of ethylene polymerization runs is conducted in order to obtain UHMWPE/HDPE blends with different compositions and molar masses, using the bis [*N*-(3-*tert*-butylsalicylidene)-2,3,4,5,6-pentafluoroanilinate] titanium (IV) dichloride to produce the UHMWPE component.

Two experimental parameters are studied: the Ti:Zr molar proportion between the two single-site catalysts and the Al/M_t ratio. Thus, first the Al/M_t ratio is fixed at 2500 and the Ti:Zr molar proportion varies between 20:80; 50:50 and 80:20; then the Ti:Zr molar proportion is fixed at 50:50 and the Al/M_t ratio is changed between 500, 1000 and 2500.

Additionally, in order to investigate the effect of different filler contents on the properties exhibited by the resulting materials, a second set of polymerization runs is carried out using the conditions just described but with a higher polymerization time. Thus, two sets of polyethylene blends containing around 10 and 5% of filler are produced. Due to the living character of the FI catalyst, by changing the polymerization time the effect of the different molar masses in the properties of the materials can be also studied.

The results obtained are summarized in Table 4.1 together with the results for the pristine polyethylenes and nanocomposites prepared with the two individual catalysts, in order to establish appropriate comparisons with the blends.

*Table 4.1: Polymerization conditions, activities, molar masses and dispersities for the materials obtained with the bis [*N*-(3-tert-butylsalicylidene)-2,3,4,5,6-pentafluoroanilinate] titanium (IV), FI catalyst, and the zirconocene. Cp_2ZrCl_2 both in homogeneous and supported conditions*

Sample	Ti (% molar)	Zr (% molar)	Al/M_t	Reaction time (min)	Average activity (kg/molM_t.h)	% inorg	M_w	D
ZrHOM010	0	100	2500	5	14030	0	187500	3.0
ZrHOM008	0	100	1000	4	10260	0	-	-
ZrSBA009	0	100	2500	26	2540	9.6	-	-
ZrSBA011[a)]	0	100	1300	20	1700	8.4	-	-
FIHOM002	100	0	2500	13	19310	0	1359000	1.5
FIHOM004	100	0	1500	13	19150	0	1479000	n.a.
FISBA016	100	0	1250	9	8122	6.9	4144000	3.0
FISBA017	100	0	2500	15	5460	8.5	838000	2.5
FIM004	20	80	2500	10	3640	6.4	-	
FIM001	50	50	2500	7	4880	8.5	1066000	1.7
FIM005	80	20	2500	9	4040	12.5	2015000	n.d.
FIM011	50	50	500	11	3170	11.1	-	-
FIM006	50	50	1000	10	3450	10.8	-	-
FIM008	20	80	2500	19	3660	4.6	939700	3.2
FIM013	50	50	2500	13	5430	4.3	1393000	1.6
FIM009	80	20	2500	17	4120	3.0	4920000	2.7
FIM012	50	50	500	21	3260	3.7	-	-
FIM010	50	50	1000	20	3500	3.6	1803000	4.1
FIM015 (H)	50	50	2500	4	8443	0	-	-

a) Data reported in a previous study [188]

As it was seen in Chapter 2, the FI catalyst used to produce the UHMWPE component in the blends, exhibits very high activities under homogeneous conditions. Nevertheless, the polymerization activity is considerably reduced upon immobilization of this catalyst on SBA-15. A reduction of activity is also observed upon immobilization of the zirconocene. It is worth mentioning that this diminishment in activity is higher for the zirconocene than for the FI catalyst.

As mentioned before, additional experiments have been performed to obtain two different filler contents. For that purpose identical experimental conditions were chosen and only the polymerization time was changed (as commented in the Experimental Section). These

experiments also enable to access the reproducibility of the polymerization reactions. Figure 4.1 shows the kinetic profiles of two sets of polymerizations: FIM011 versus FIM012 and FIM004 versus FIM008. The comparison of the profiles of the two samples at a specific set of experimental conditions (Ti:Zr molar proportion and Al/M_t ratio) indicates that polymerizations are quite reproducible; they have the same type of kinetic profile and only slight variations in the average activity. Table 4.1 clearly displays the similarity found in the activities when synthesizing the blends with different SBA-15 (~5 and ~10%) contents at a given experimental condition.

The activities values obtained during the preparation of the blends are in the range of the ones achieved for the individual supported catalysts used in the preparation of their respective ZrSBA009 or ZrSBA011 and FISBA016 or FISBA017 nanocomposites.

Table 4.1 shows that at a fixed Al/M_t ratio of 2500 and changing the Ti:Zr ratio from 20:80 to 80:20, the highest value of activity is obtained for the blend prepared with Ti:Zr of 50:50. This maximum on polymerization activity may be rationalized taking into account that on one hand the supported FI catalyst presents a higher activity than that reported for the supported zirconocene but, on the other hand it also deactivates in a sharper and faster way, as clearly deduced from the different instantaneous activity profiles represented in Figure 4.2. Accordingly, an optimal polymerization activity is observed for conditions where those two opposing effects are balanced.

Results on Table 4.1 also indicate that there is a trend of increasing activity for the blends prepared at a constant Ti:Zr molar proportion and increasing Al/M_t ratio.

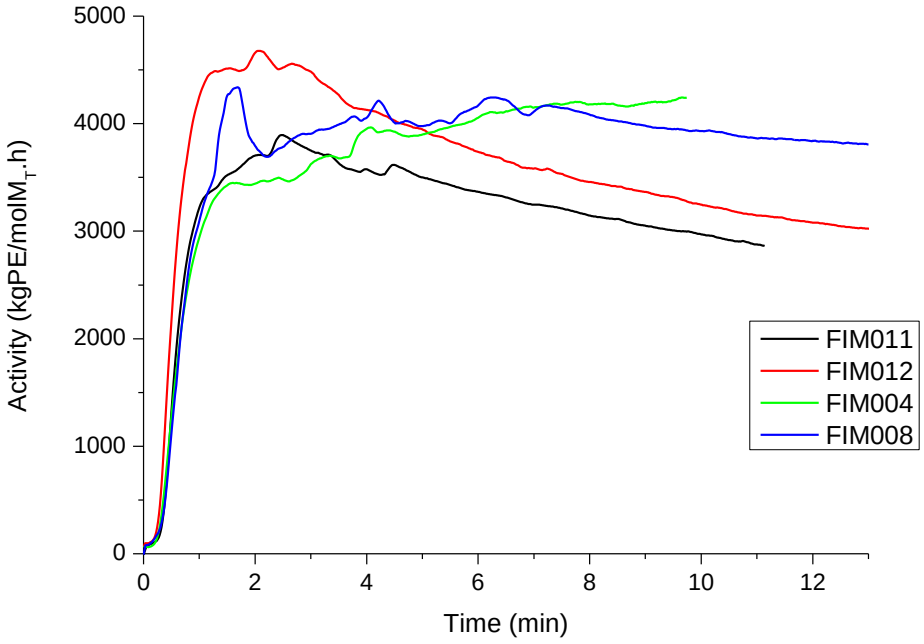

Figure 4.1: Kinetic profile for ethylene polymerizations. First set: FIM011 and FIM012; Second set: FIM004 and FIM008.

Figure 4.2 also points out that the immobilized zirconocene catalyst give rises to a more stable kinetic profile than the corresponding supported FI catalyst. This behavior is also clearly observed on the profiles obtained when FI and zirconocene are co-immobilized on SBA-15. Accordingly, the most stable profile is obtained for a Ti:Zr molar proportion of 20:80, followed by the one at a 50:50 proportion and then by the 80:20 proportion.

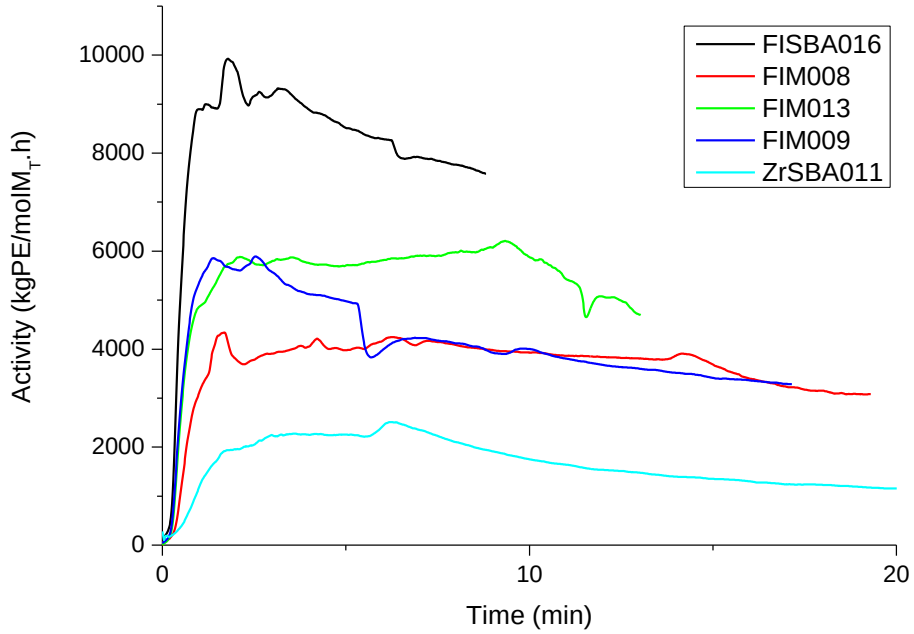

Figure 4.2: Kinetic profiles for ethylene polymerizations for the synthesis of two nanocomposites, FISBA016 and ZrSBA011 and three blends FIM008, FIM013 and FIM009.

As expected from literature, the molar masses of the polyethylenes obtained with the FI catalyst are much higher, (one order of magnitude) than the one obtained for the zirconocene catalyst (see Table 4.1). Accordingly, for each set of polymerization runs, the molar masses of the blends obtained at a fixed Al/M_t ratio, increase with the molar proportion of the FI catalyst in the supported catalytic system (see FIM008, FIM013 and FIM009 or FIM001and FIM005). On the other hand, when fixing the Ti:Zr proportion at 50:50, results seem to point out to a decrease of the molar mass of the blends at increasing Al/M_t ratios (compare FIM008, FIM013 and FIM009 or FIM001and FIM005). This trend may be probably related to the role of TMA (present in the MAO) on deactivation pathways that may lead to a loss of the polymerization control and that will reduce the polymer chain growth. In line with this, the molar masses of the blends obtained at the same Al/M_t proportion and Ti:Zr molar proportion but, at different polymerization times, tends to increase with time although not in a linear way.

4.2.2 Characterization of the blends

4.2.2.1 Thermal behavior

4.2.2.1.1 Thermogravimetric analysis

Once the different blends based on UHMWPE and HDPE have been synthesized, knowledge of some of their physical characteristics is required. Figure 4.3 shows the thermogravimetric curves under inert and oxidant environments for the blends prepared at the longest times. The curves corresponding to the neat FI and a hybrid with SBA-15 have been also included for comparison. Looking at the upper plot, as for all the materials characterized so far, a single primary stage of decomposition is observed under inert conditions in the temperature range from 200 to 600 °C for all the specimens. On the contrary, four different degradation processes are noticeable at identical temperature interval when air is the atmosphere used, as depicted in the bottom plot of Figure 4.3.

Under inert conditions and at a constant Al/metal ratio of 2500 (metal including Titanium and Zirconium that comes from both catalysts used) and varying the proportion of the catalyst supported in the mesoporous SBA-15, i.e., FIM008, FIM013 and FIM009 specimens, a displacement of the degradation process to higher temperatures is observed as the FI content in the support is increased. This feature might be ascribed to the differences found in the molecular masses between the distinct samples, in such a way, that the blend becomes more stable and, consequently, its decomposition starts at higher temperature, as molar mass rises.

In specimens prepared at 50:50 Ti:Zr molar proportion (samples FIM012, FIM010 and FIM013) also analyzed under inert conditions, an important effect is seen as Al/metal proportion is increased. Accordingly, FIM013 shifts its decomposition process to much lower temperatures than that corresponding to the FIM012 and FIM010 blends with a ratio of 500 and 1000, respectively. This fact could be associated with the higher acidity provided by a higher amount of aluminum [82] in the support that may promote degradation of the resulting material, FIM013 blend, reducing significantly its thermal stability.

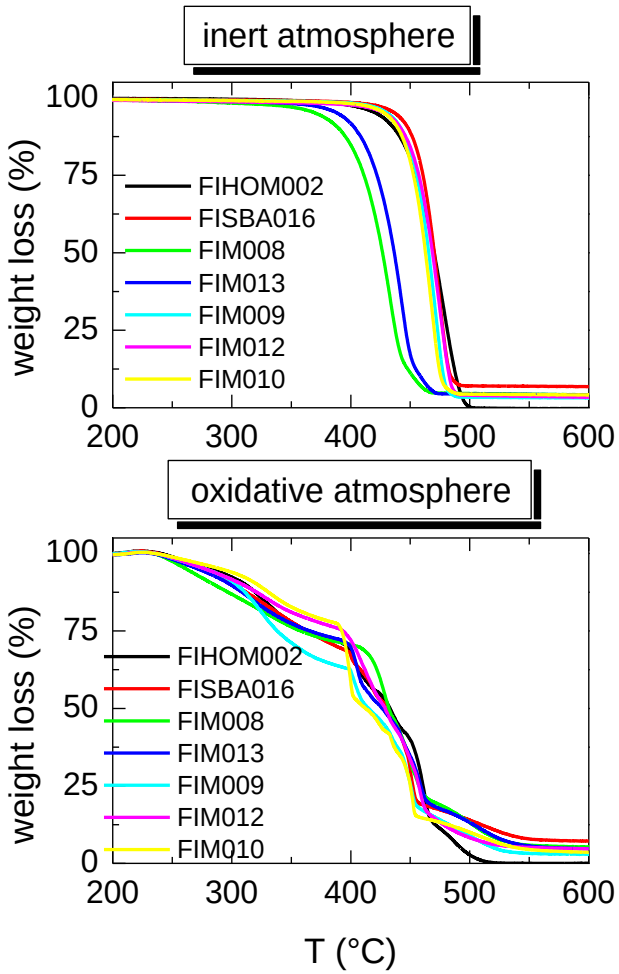

Figure 4.3: TGA curves of different UHMWPE/HDPE blends: at Al/metal = 2500 and several (20:80, 50:50 and 80:20) Ti:Zr molar proportions (specimens FIM008, FIM013 and FIM009, respectively) as well as at 50:50 Ti:Zr molar proportion and distinct (500, 1000 and 2500) Al/metal ratio (specimens FIM012, FIM010 and FIM013, respectively) under inert (top plots) and oxidant (lower plots) conditions. An UHMWPE and a hybrid both synthesized with FI catalyst have been incorporated.

The thermogravimetric curves obtained under oxidant atmosphere, depicted in the lower representation of Figure 4.3, show that the effect of the different variables is more important up to a temperature around 400 °C. Above that temperature, the differences between specimens are rather less significant and the thermal response of the distinct blends is quite analogous. At a constant Al/metal ratio of 2500 and varying the proportion on the catalyst supported in the mesoporous SBA-15, i.e., FIM008, FIM013 and FIM009 specimens, $T_{10\%}$ dependence (see Table 4.2) is similar to that found under inert conditions, i.e., a shift of the degradation process to higher temperatures is observed as FI content in the mesoporous SBA-15 is raised, this feature being ascribed to differences in molecular masses of the blends. This trend is modified at higher temperatures, and the lowest $T_{25\%}$ is now exhibited by FIM009, i.e., that containing the highest amount of FI on the support. This characteristic can be attributed to the great effect that PA immobilization approach has on

the oxidant decomposition of hybrids on SBA-15 synthesized with this FI catalyst at a ratio Al/Ti of 2500, as deduced from the results presented in Chapter 3.

Moreover, determination of the SBA-15 amount in the UHMWPE/HDPE blends is estimated from thermogravimetric analysis, TGA. Table 4.2 shows that the content at a given specimen is rather independent of the environment used, Average values obtained from inert and oxidative conditions are provided in Table 4.2.

Table 4.2: Average SBA-15 wt.% content, characteristic decomposition temperatures under nitrogen and air atmospheres for the UHMWPE/HDPE blends (the temperatures of 10%, $T_{10\%}$, and 25%, $T_{25\%}$) and the SBA-15 wt.% content at a specific environment.

Sample	Average SBA-15 wt.% content	Inert atmosphere			Oxidative atmosphere		
		$T_{10\%}$	$T_{25\%}$	SBA-15 wt.% content	$T_{10\%}$	$T_{25\%}$	SBA-15 wt.% content
FIHOM002	0	437	455	0	311	364	0
FISBA016	6.9	448	461	6.8	302	363	7.0
FIM008	4.6	391	412	4.1	285	358	5.2
FIM013	4.3	403	422	4.0	299	366	4.5
FIM009	3.0	442	455	3.1	304	338	2.9
FIM012	3.7	443	458	3.1	309	393	4.3
FIM010	3.6	441	452	4.1	322	392	3.2

Figure 4.4 displays the effect on the thermal stability of increasing the amount of the mesoporous SBA-15 in different blends. It is clearly seen under inert conditions as well as at constant Al/metal ratio and Ti:Zr molar proportion that the presence of a greater amount of SBA-15 leads to a significant displacement of the initiation of decomposition and its further progress. Therefore, SBA-15 particles seem to promote degradation. An analogous outcome is observed in oxidant atmosphere although the shift to inferior temperatures is minimized. It appears that there is a merge of the two initial decomposition stages under this aggressive condition in the blends containing higher SBA-15 content.

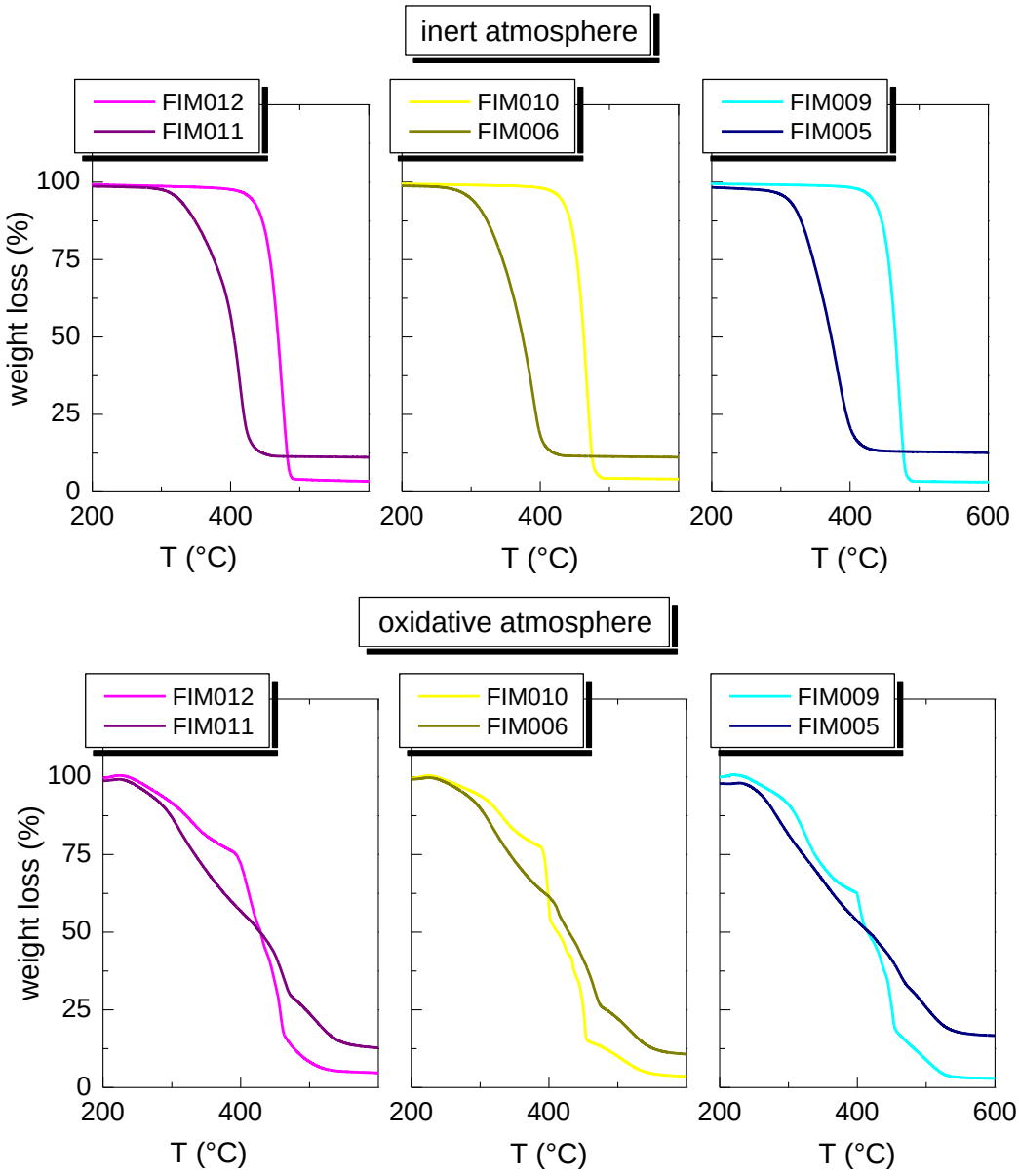

Figure 4.4: TGA curves of different UHMWPE/HDPE blends at constant Ti:Zr molar proportion and distinct (500, 1000 and 2500) Al/metal ratios varying the content in SBA-15 particles under inert (top plots) and oxidant (lower plots) conditions.

This catalytic influence of silica mesoporous materials in the degradation process of polyethylene has been already described in literature by Marcilla *et al.* [197] when studying the degradation of PE under N_2 in the presence and absence of mesoporous MCM-41 and by Campos *et al.* [198] in polyethylene based composites with MCM-41, both by thermogravimetric analysis. Aguado *et al.* [199] have also shown the efficiency of mesoporous aluminosilicate MCM-41 as a promoter towards degradation of polyolefins into liquid fuels. Nowadays, this may be attractive in what concerns the degradation of these polyolefins into basic petrochemicals feedstock or fuel for downstream processes after

their life service, making these self-reinforced polyolefinic materials economically and environmentally welcome [200].

4.2.2.1.2 Differential scanning calorimetry

Figure 4.5 shows that the melting and crystallization processes are exhibited as single peaks. This characteristic in blends indicates that both components undergo their phase transitions within identical temperature interval. This behavior could be expected taking into account that both present the same chemical structure and that blends have been prepared by *in situ* polymerization. Consequently, none conclusion on miscibility can be reached from DSC measurements.

Looking first at the upper left melting processes (Figure 4.5a) related to the blends synthesized at a constant Al/M_t ratio of 2500 and varying the proportion on the catalyst supported in the mesoporous SBA-15, *i.e.*, FIM008, FIM013 and FIM009 specimens as well as FIM015 (which does not contains SBA-15) used for comparative reasons, a displacement of the main endothermic process to slightly higher temperatures is observed as Ti:Zr varies from 20:80 to 80:20 proportion. Then, the order of T_m increase is: FIM008 < FIM013 < FIM009, these values being highest that the one exhibited by the FIM015 blend with a 50Ti:50Zr proportion without SBA-15.

In addition to the shift of T_m by the presence of mesoporous particles, the appearance of a small shoulder in the temperature interval ranging from 100 to 125 °C is noticeable in the blends with SBA-15. This secondary process is less intense in sample FIM009 since its SBA-15 content is the lowest one. As in the nanocomposites characterized in the previous chapters, this small endothermic peak is attributed to those polyethylene crystallites, either those coming from the UHMWPE or from the HDPE component, that are developed inside the SBA-15 channels, similarly to evidences found in nanocomposites with MCM-41[84]. Channel confinement prevents a further growth of the crystallites and, accordingly, these crystalline entities generated within SBA-15 particles are of much smaller size than those that can grow at its surface and in the UHMWPE and HDPE bulks.

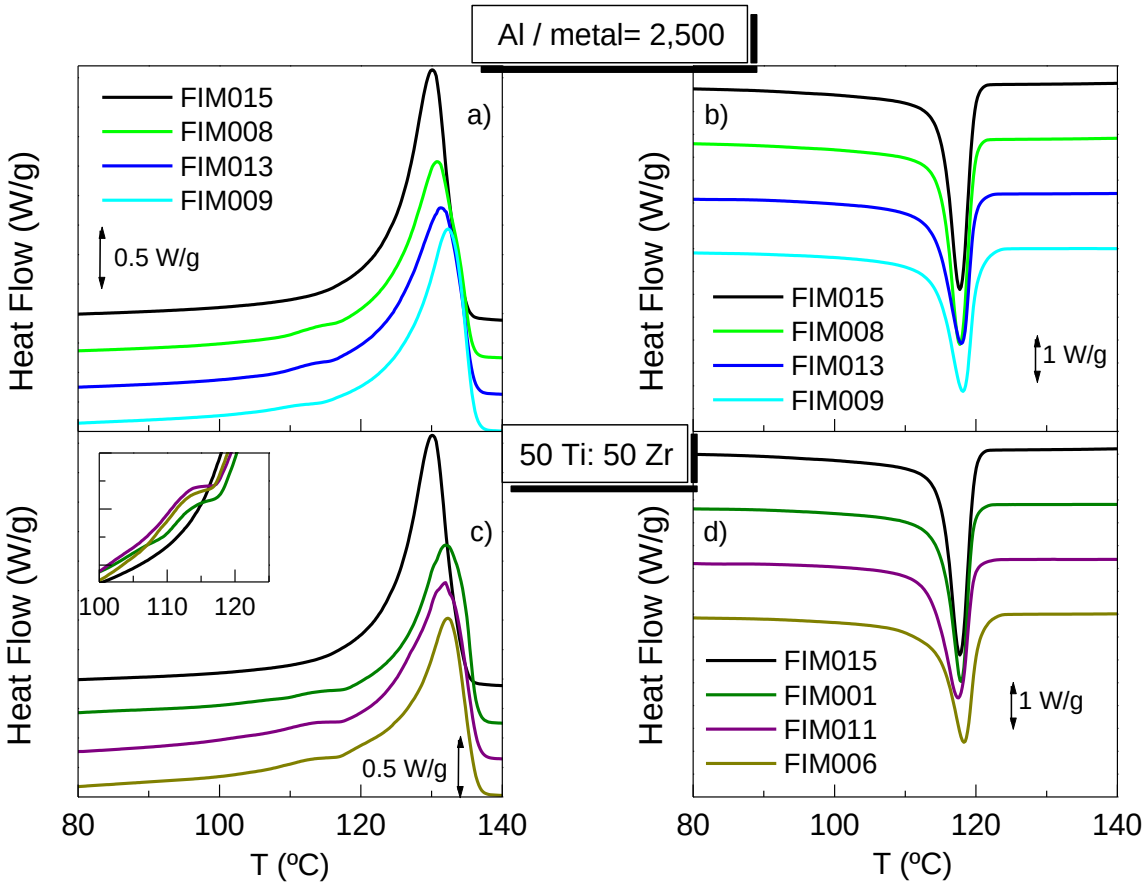

Figure 4.5: DSC curves of the first melting (left plots, a and c) and subsequent crystallization processes (right plots, b and d) of the blend without SBA-15 (FIM015) and on the top: blends with the lowest SBA-15 content at Al/M_t =2500 and different Ti:Zr molar proportion: FIM008 (20:80), FIM013 (50:50) and FIM009 (80:20). On the bottom: blends with highest SBA-15 content at 50:50 Ti:Zr molar proportion and distinct Al/M_t ratio: FIM001 (500), FIM011 (1000) and FIM006 (2500). Moreover, the melting region of the small crystallites is represented in inset of c plot.

Concerning their further crystallization, there is not significant variation in the location of T_c for these samples, as deduced from data reported in Table 4.3 and from Figure 4.5b.

Table 4.3: DSC calorimetric data of the materials prepared.

Sample	Ti (% molar)	Zr (% molar)	% inorg	M_w	*powder*		*film*			
					f_c^m	T_m (°C)	f_c^m	T_m (°C)	f_c^c	T_c (°C)
ZrHOM010	0	100	0	187.500	n.d.	n.d.	0.66	129.5	0.60	118.0
FIHOM002	100	0	0	1.359.000	0.83	140.5	0.53	131.0	0.54	118.0
FISBA016	100	-	6.9	4.144.000	0.78	140.5	0.49	132.5	0.47	118.0
Blends										
FIM004	20	80	6.4	-	0.68	136.8	0.52	130.5	0.52	118.5
FIM001	50	50	8.5	1.066.000	0.73	139.8	0.52	132.0	0.49	118.0
FIM005	80	20	12.5	2.015.000	0.77	140.9	0.55	132.0	0.43	117.5
FIM011	50	50	11.7	-	0.76	140.5	0.55	132.0	0.47	117.5
FIM006	50	50	10.8	-	0.75	140.1	0.54	132.5	0.47	118.5
FIM015 (H)	50	50	-	-	0.72	135.0	0.49	130.0	0.51	118.0
FIM008	20	80	4.6	939.700	0.74	138.3	0.48	130.5	0.48	118.5
FIM013	50	50	4.3	1.393.000	0.74	139.8	0.48	131.0	0.49	118.0
FIM009	80	20	3.0	4.920.000	0.78	140.4	0.48	132.5	0.47	118.0
FIM012	50	50	3.7	-	0.75	140.0	0.52	132.0	0.49	118.0
FIM010	50	50	3.6	1.803.000	0.70	140.2	0.49	132.0	0.49	118.0

A small T_m reduction in FIM13 is seen in comparison with the value of 132 °C found in FIM012 and FIM010 at constant Ti:Zr (50:50) as Al/M_t ratio is changed (FIM012, FIM010 and FIM013 blends). Although the difference is very small, only 1 °C from FIM013 to FIM012 and FIM010, it is interesting to indicate it because a noticeable decrease in T_m has also been observed as Al/M_t is raised in pristine polyethylenes and hybrids based on polyethylene synthesized with the Zr and Hf catalysts [188]. A similar behavior is pointed out in these blends in spite of the FI catalyst is also involved. A slight decrease in crystallinity is also found with increasing Al/M_t ratio. No variation has been observed in the subsequent crystallization process.

The bottom plots in Figure 4.5 (5.5*c* and 5.5*d*) represent the features found in the blends containing a higher amount in SBA-15 particles at the identical 50:50 Ti:Zr molar proportion and different Al/M_t ratios. Large amount of SBA-15 allows the formation of more crystallites of UHMWPE and HDPE within the SBA-15 channels and, then, the intensity of the shoulder appearing from 100 to 125 °C is increased compared with the one shown by the blends with SBA-15 content at around 4 wt.%. The T_m´s are similar for these three samples (FIM011, FIM006 and FIM001) and higher than the observed one in the blend without SBA-15 (FIM015 sample) similar to what is observed in the blends with less mesoporous particles. Nevertheless, crystallinity is now increased for the samples with the

highest SBA-15 content, as listed in Table 4.3. In spite of the higher SBA-15 content, there is not observed an evident nucleant effect during crystallization.

The phase transition temperatures do not show significant changes in the blends at constant 2500 Al/M_t as well as crystallinity values for the first melting process. Nevertheless, there is a considerable difference in the degree of crystallinity (FIM004 > FIM001 > FIM005) developed during crystallization and the variation might be related to the increasing content in SBA-15. It has been reported [120] for HDPE nanocomposites reinforced with MCM-41 that crystallization process is delayed for contents of MCM-41 around 10 wt.%. This was associated with the slower development of those crystallites belonging to chains within channels, *i.e.*, generated under great constraints. Then, confinement of the polymeric matrices (UHMWPE and HDPE, in this current case) makes that crystallization within the channels require much more time than that involved in the DSC experiment. If the blends are allowed to remain enough time at room temperature (hours), crystallization of all the polyethylenic chains ends, independently of their molecular masses, and the number of crystal entities increases up to attain finally a similar crystallinity than that achieved during first melting process.

Moreover, FIM005 is the blend containing a molar proportion of 80:20 in Ti:Zr and, then, the amount of UHMWPE chains is expected to be the highest one, fact that favor the diminution of the crystallization rate. On the contrary, FIM004 is the blend that is supposed to contain the most amount of HDPE and, accordingly, with the highest rate of crystallization. In fact, the molar masses that were achieved confirm this assumption (see Table 4.3).

4.2.2.2 Mechanical properties

The preliminary evaluation of the mechanical response of these UHMWPE/HDPE blends was carried out through Indentation measurements. Numerical results determined from these experiments, concerning the elastic modulus and hardness, E_{it} and $H_{it,}$ respectively, are detailed in Table 4.4 for the specimens with the high SBA-15 contents.

Table 4.4: Indentation parameters attained at 25 °C: indentation modulus (E_{it}) and hardness (H_{it}) for some pristine polyethylenes and nanocomposites as well as for the reactor blends prepared under different experimental conditions.

Sample	Ti (% molar)	Zr (% molar)	% inorg	M_w	H_{it} (MPa)	E_{it} (MPa)	f_c	T_m
ZrHOM010	0	100	0	187500	53	985	0.66	129.5
ZrSBA011[a)]	0	100	10.9	n.d.	65	950	0.63	132.0
FIHOM002	100	0	0	1359000	44	684	0.53	131.0
FISBA016	100	0	6.9	4144000	60	865	0.49	132.5
Blends								
FIM004	20	80	6.4	-	68	1093	0.52	130.4
FIM001	50	50	8.5	1066000	65	973	0.52	131.9
FIM005	80	20	12.5	2015000	63	831	0.55	131.9
FIM011	50	50	11.7	-	65	961	0.55	132.0
FIM006	50	50	10.8	-	70	1009	0.54	132.3
FIM015 (H)	50	50	-	-	55	893	0.49	130.1

[a)] Data reported in a previous study [188]

The pristine materials prepared from homogeneous zirconocene and FI catalysts, ZrHOM010 and FIHOM002, respectively, as well as their hybrids with SBA-15, ZrSBA011 and FISBA016, respectively, are examined before analyzing the UHMWPE/HDPE based blends prepared at different experimental conditions. Table 4.4 indicates that the samples synthesized using zirconocene catalyst either under homogeneous (ZrHOM010 specimen) or supported (ZrSBA011 composite) conditions exhibit higher E_{it} and H_{it} values than those materials prepared by the FI catalyst (FIHOM002 and FISBA016, respectively). This fact is correlated to the deformation mode applied during the experiment since crystallinity is a key parameter in rigidity. HDPE usually shows a degree of crystallinity higher than the one developed in UHMWPE because of the large length of its macrochains [201]. Differences are reduced if the respective nanocomposites are compared (ZrSBA011 and FISBA016 samples), *i.e.*, when rigid SBA-15 particles, playing the dual role of support and filler, are incorporated in the polymerization process and subsequently in the final polymer matrix. This behavior may be related to the fact that the reinforcement effect of SBA-15 is stronger and accordingly more noticeable when these particles are introduced on a less crystalline and softer UHMWPE matrix than when incorporated to an already more crystalline and harder HDPE polymer. Additional variations are also clearly observed from regular representations of indentation experiments. Figure 4.6a shows that the largest depth reached after applying identical load corresponds to the neat polyethylene synthesized using the FI catalyst. This feature indicates that sample FIHOM002 is the softest material and, then, indenter can penetrate deeper inside its surface. Moreover, its depth dependence on time, directly related to its deformability, is the greatest one, as depicted in Figure 4.6b,

when the response is compared with that exhibited by the ZrHOM010 pristine polyethylene and the FIM015 blend, which is a UHMWPE/HDPE reactor blend prepared with a 50:50 Ti:Zr molar proportion without adding SBA-15 particles.

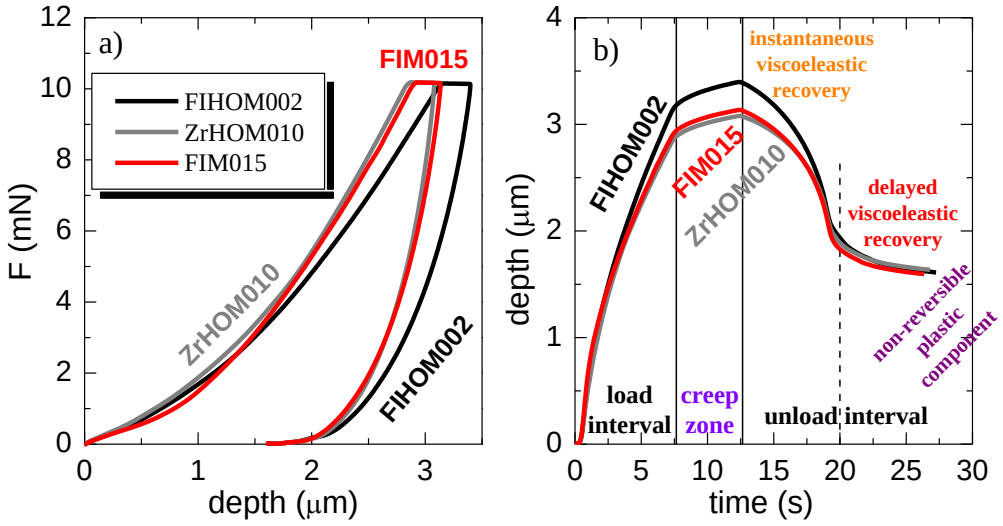

Figure 4.6: a) Indentation curves of load-maintenance-unload vs. depth for FIHOM002 and ZrHOM010 neat polyethylenes and the FIM015 blend; b) Indenter depth dependence on experimental time for some the two neat polyethylenes and their 50:50 Ti:Zr blend.

The effect of SBA-15 incorporation in a HDPE matrix was investigated in a previous study [188]. The ZrSBA011 sample containing around a 10 wt.% in SBA-15 exhibited E_{it} and H_{it} values of 950 MPa and 65 MPa, respectively. The elastic modulus, E_{it}, does not practically change when its value is compared to the one presented by the corresponding neat polyethylene but a significant increase in hardness is observed for the hybrid material. This fact seems to indicate that the presence of SBA-15 at those mesoporous particle contents, mainly affects the mechanical properties at the surface. Nevertheless, the mesoporous SBA-15 changes either bulk rigidity or superficial hardness in the softer materials, *i.e.*, those materials synthesized with the FI catalyst. Then, differences found in both parameters are considerable, and the E_{it} increases from 684 MPa in FIHOM002 specimen to 865 MPa in the FISBA016 sample and H_{it} from 44 to 60 MPa, respectively.

Figure 4.7 shows the effect of SBA-15 particles in a UHMWPE/HDPE blend obtained at identical synthetic conditions (FIM001 sample) to those used for polymerizing homogenous FIM015, *i.e.*, Al/M_t = 2500 and Ti:Zr= 50:50. It is noticeable the reinforcement role that SBA-15 particles exert on the resulting material. Then, on one hand, indenter depth after applying identical force is inferior in the FIM001 sample and, on the other hand, that FIM001 blend containing the mesoporous SBA-15 shows a higher rigidity and hardness, *i.e.*, greater E_{it} and H_{it} values (see Table 4.4). It has been reported that these mechanical parameters only undergo significant enhancements in HDPE synthesized with zirconocene

[84, 120] immobilized onto MCM-41 and HDPE prepared with Hafnium catalyst (as described in Chapter 3) supported on SBA-15 at filler contents above around 8 wt.%.

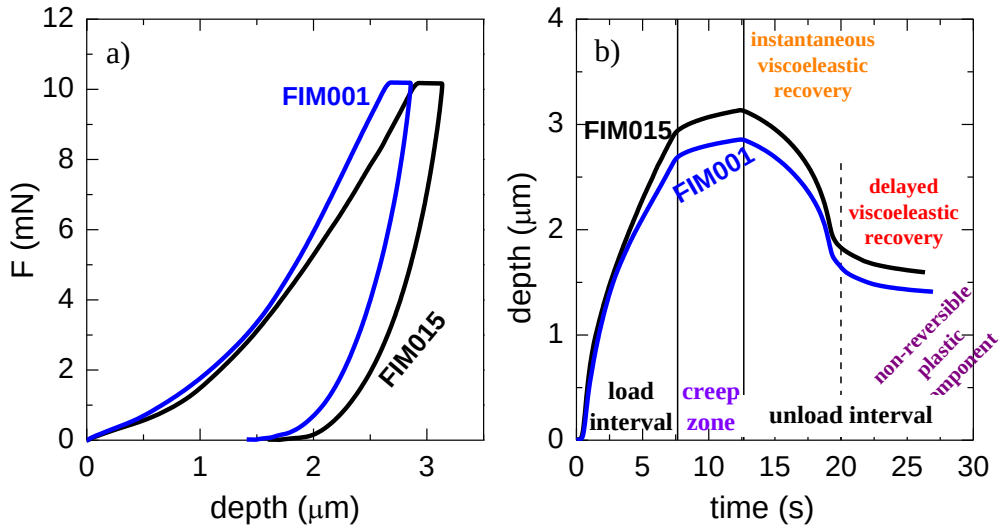

Figure 4.7: a) Indentation curves of load-maintenance-unload vs. depth for the neat FIM015 (Al/M_t= 2500) and the FIM001 (Al/M_t= 2500) blends, the latest one synthesized by supporting both catalysts (FI and zirconocene) on SBA-15 at and a 50:50 Ti/Zr ratio.

The UHMWPE/HDPE blends exhibit a behavior dependent on the Ti:Zr molar proportion used during polymerization. E_{it} and H_{it} values increase as Zr amount is raised in the Ti:Zr molar proportion (see Table 4.4). Figure 4.8 displays also the soft character and easy deformability of the FIHOM002 neat polyethylene in comparison with the FIM004 blend that contain a major amount of HDPE synthesized from the zirconocene catalyst. FIM001 and FIM05 blends are in between because of their different contents in UHMWPE and HDPE. Table 4.4 shows that the primary variable in these blends is their HDPE content, this parameter being even more important than the SBA-15 amount existing in the composite. Then, a reduction in rigidity and hardness values is observed as UHMWPE amount is supposed to be increased in the blend, *i.e.* as Ti:Zr molar proportion is raised.

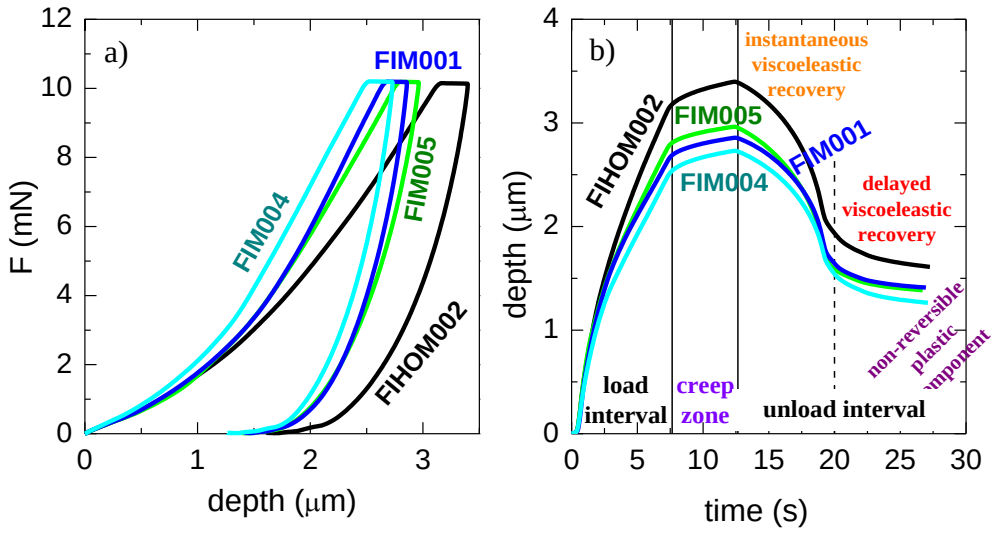

Figure 4.8: a) Indentation curves of load-maintenance-unload vs. depth for FIHOM002 and the blends synthesized at Al/M_t= 2500 and different Ti/Zr molar proportions: (80:20) FIM005; (50:50) FIM001; and, (20:80) FIM001 specimens, respectively. b) Indenter depth dependence on experimental time for some the FI neat polyethylenes and the several blends prepared from a ratio in Al/M_t= 2500.

From data presented in Table 4.4 on samples FIM004 e ZrSBA011, it also may be noticed the reinforcing effect of the addition of a minor amount of a UHMWPE component to a HDPE matrix. Despite the smaller SBA-15 content and the lower crystallinity of the blend (obtained from a Ti:Zr molar proportion of 20:80) when compared to the HDPE composite sample (synthesized from a 0:100 Ti:Zr molar proportion) an increase of the indentation modulus up to ~1100 MPa is observed for the blend.

On the other hand, when comparing the sample of UHMWPE (prepared with a Ti:Zr molar proportion of 100:0) with the blend FIM004 (prepared from a Ti:Zr molar proportion of 80:20), no increase of modulus is observed, despite the higher crystallinity and SBA-15 of the latter sample. Therefore, no reinforcement effect is observed upon addition of a small amount of a HDPE component to a UHMWPE matrix.

It is well known that size and dispersion state of the filler affects mechanical properties of polymeric composites. Figure 4.9 shows the TEM micrographs at several magnifications of FIM004 and FIM005 samples, containing respectively 6.4 and 12.5 % of SBA-15. For these samples changes on SBA-15 dispersion are not very drastic. Nevertheless, the highest content sample seems to present less well dispersed and bigger filler particles or aggregates. This can be another factor contributing to the lower performance of FIM005 sample. Interestingly, the SBA-15 channel like structure is clearly seen on the highest magnification pictures, confirming that the mesoporous structure is not lost after polymerization.

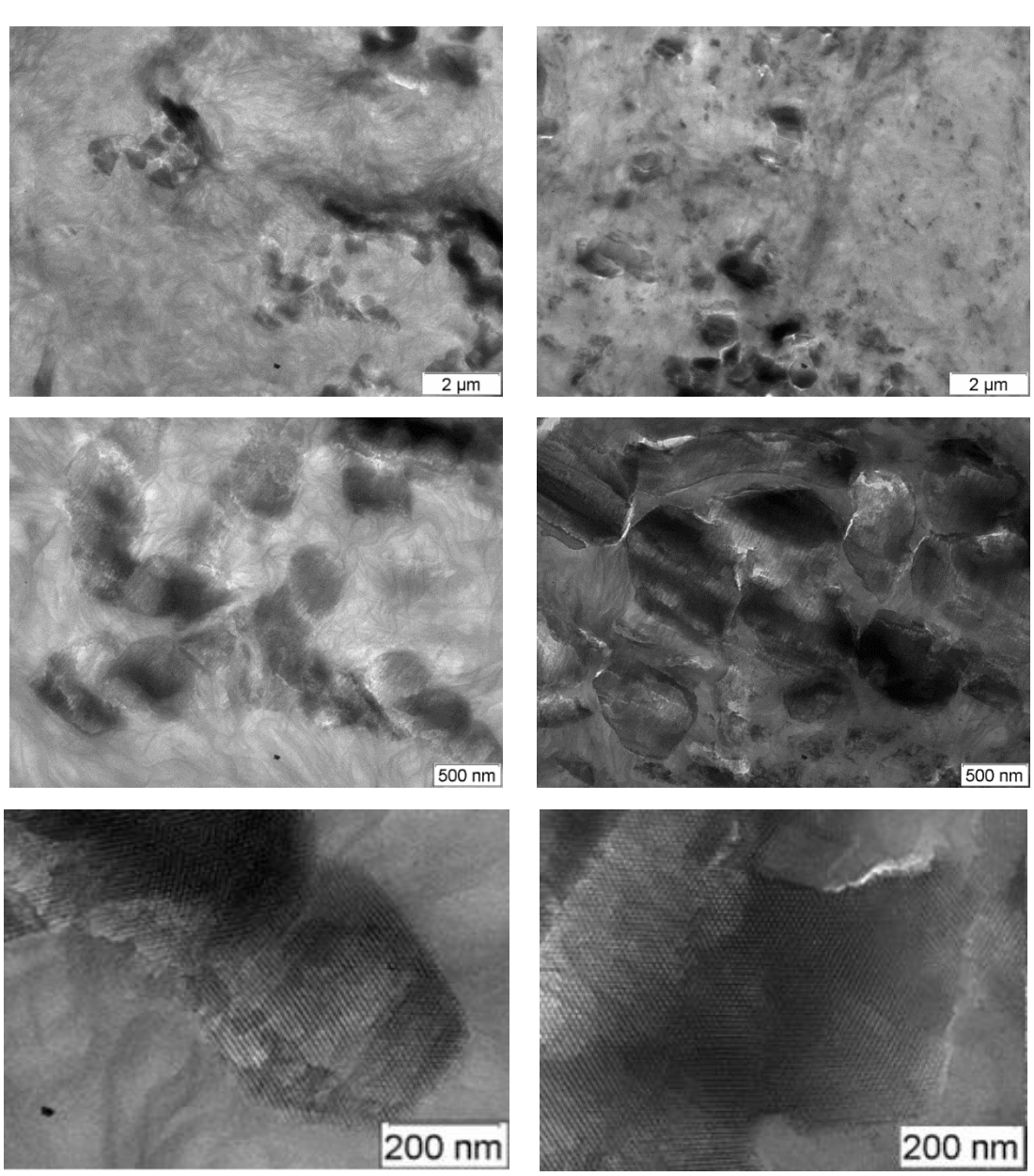

Figure 4.9: TEM micrographs at several magnifications of FIM004 and FIM005 samples.

Table 4.4 also shows that there is not a clear trend as the Al/M_t ratio is changed at constant 50:50 Ti:Zr molar proportion. Then, E_{it} and H_{it} values are rather analogous.

Creep characteristics can be deduced from the stage at constant force (F= 10 mN) in these indentation experiments. Creep resistance can be defined as a material's ability to resist any kind of distortion when it is under a load over a period of time, *i.e.*, it is related to its dimensional stability. An optimum performance and maximum lifetime require in engineering plastics a high creep resistance, *i.e.*, a low plastic deformation under load. Moreover, creep behavior is also one of the factors that limit the maximum application

temperature of a material. Creep is, then, a time dependent feature and the deformation that a material undergoes under stresses can be minimized if structural movements are constrained by, for instance, crosslinking and/or inclusions of stiff inorganic fillers. Three different parameters are, consequently, important in the UHMWPE/HDPE blends under study: overall crystallinity, average molar masses since entanglements might play a considerable role to avoid creep and SBA-15 content because of its rigidity. Figure 4.10 shows the variation in depth for the blends without and with SBA-15 at different Ti:Zr molar proportion and at constant Al/M_t ratio of 2500.

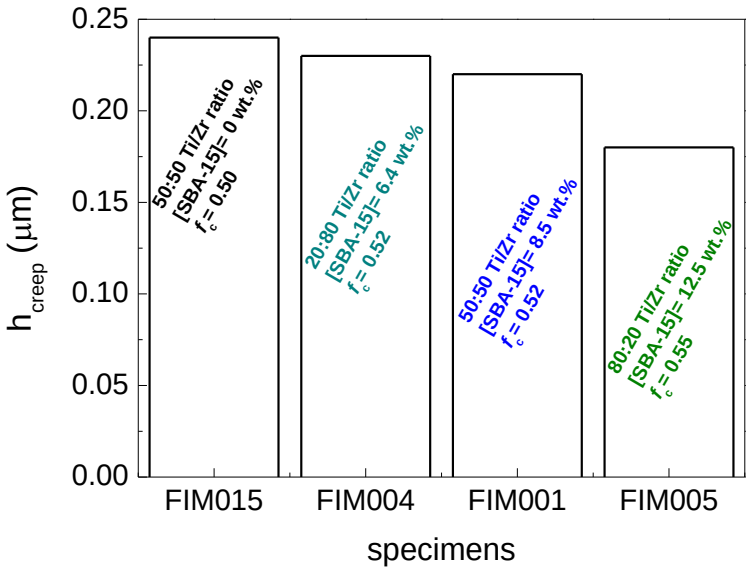

Figure 4.10: Variation of indentation creep depth for the neat FIM015 blend and those mixtures synthesized by catalysts immobilization on SBA-15 at distinct Ti:Zr molar proportion and at Al/M_t = 2500.

FIM015 blend prepared under homogeneous conditions is a rather soft material and, accordingly, its modulus and hardness values are quite small within this set. This characteristic together with its low crystallinity and the absence of SBA-15 particles are all responsible of its inferior creep resistance. Nevertheless, the FIM005 mixture, which follows FIM015 in rigidity features, showing a similar E_{it} and superior H_{it} values, is the material with the best creep performance at room temperature. This property can be ascribed to its highest crystallinity and SBA-15 contents as well as its greater average molar mass. The two former parameters provide to its macrochains higher interior constraints to slide, this slippage being even more hindered because of its highest molar mass. Chains with average lengths of two million involve the existence of a lot of entanglements that significantly hamper deformation under a constant load. Therefore, a reduction of 25 % is observed in comparison with that shown by the FIM015 blend. The FIM001 and FIM004 samples present similar crystallinity values and SBA-15 content and molar mass are gradually decreased. Consequently, creep resistance is lowered in approximately 5 and 10%, in FIM004 and FM001 blends, respectively.

4.3 Polyethylene blends prepared by *in situ* polymerization with a hafnocene and a zirconocene catalyst

4.3.1 Ethylene polymerization behavior

As in the previous section the blends were prepared using the PA method for the catalysts immobilization. It is recalled that this method consists in the contact of both catalysts with MAO before their further interaction with the SBA-15 particles. As aforementioned, the hafnocene catalyst leads to polymers with molar masses higher than those attained using the zirconocene one, and so it gives rise to the highest molar mass component of these blends. Accordingly, polyethylene blends with different compositions and molar masses are obtained by performing several polymerization runs at a fixed Al/M_t ratio and varying the Hf:Zr molar proportion between 20:80; 50:50 and 80:20.

Additional experiments to evaluate the effect of Al/M_t ratio are also performed. In this case, the Al/M_t ratio varied between 500, 1000 and 2500 at the same Ti:Zr molar proportion of 50:50. The results obtained are summarized in Table 4.5 along with some results of pristine polyethylenes and nanocomposites prepared with the two individual catalysts that are helpful to analyze the results of these blends. An additional blend, named HfM014HOM, was prepared using a mixture of the hafnocene and the zirconocene catalysts in homogeneous conditions, thus without the presence of SBA-15 particles.

Table 4.5: Polymerization conditions, activities, molar mass and dispersities for the blends obtained.

Sample	Hf (% molar)	Zr (% molar)	Al/M_t	Average activity (kg/molM_t.h)	% inorg TGA	M_w	D
ZrHOM010	-	100	2500	14030	-	187500	3.0
ZrSBA009	-	100	2500	2540	9.6	-	-
ZrSBA011[a)]	-	100	1320	1700	8.4	-	-
HfHOM021	100	-	1100	1060	-	488.300	1.6
HfHOM002	100	-	2500	1780	-	505410	1.9
HfSBA019	100	-	2500	1230	8.0	-	-
Blends							
HfM009	20	80	2500	3130	8.5	-	-
HfM008				2780	-	-	-
HfM002	50	50	2500	1380	8.1	-	-
HfM003				1630	-	-	-
HfM010	80	20	2500	930	-	495900	3.8
HfM012				960	10.5	-	-
HfM007	50	50	500	770	8.5	-	-
HfM006				670	-	-	-
HfM005	50	50	1000	1230	7.5	-	-
HfM004				1180	-	-	-
HfM014(HOM)	80	20	2500	4996	-	358000	3.5

a) Data reported in a previous study [188]

As in the previous section two polymerization tests are performed for each set of experimental conditions to check reproducibility of the polymerizations. Figure 4.11 represents the kinetic profiles of three sets of polymerization: HfM009 versus HfM008, HfM002 versus HfM0003 and HfM010 versus HfM012. We can see that for each set of experimental conditions there is a good reproducibility in the polymerization reactions in terms of kinetic profiles and also of the average activities presented in Table 4.5.

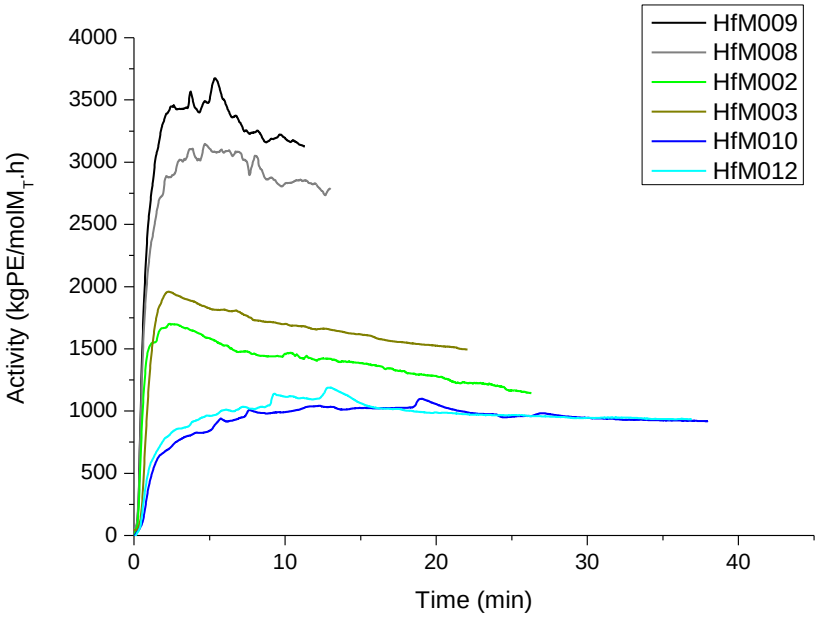

Figure 4.11: Kinetic profiles for ethylene polymerizations for three sets of experimental conditions. First set: HfM009 and HfM008. Second set: HfM002 and HfM003. Third set: HfM010 and HfM012.

Data presented in Table 4.5 shows that upon immobilization, both metallocene catalysts exhibit a decrease of the activity. This is particularly evident in the case of zirconocene. Moreover, the values of activity obtained for the blends are, in general, in the range of those achieved for the individual supported catalysts used in the synthesis of their respective nanocomposites. It is worth mentioning that, at a constant Al/M_t ratio of 2500, an increase of the amount of hafnocene in the reactor mixture results in a decrease of the activity. This fact is expected since the activity of the individual hafnocene in supported conditions is lower than that found for the zirconocene. In addition, the values of activities obtained for a constant Hf:Zr molar proportion of 50:50 indicate that increasing the Al/M_t ratio turns out in an increase of the activity, which is a common feature observed in several metallocene systems.

Figure 4.12 depicts the kinetic profile obtained during the preparation of three blends, with different Hf:Zr molar proportions, and of two nanocomposites (ZrSBA009 and HfSBA019) prepared with the individual supported catalysts.

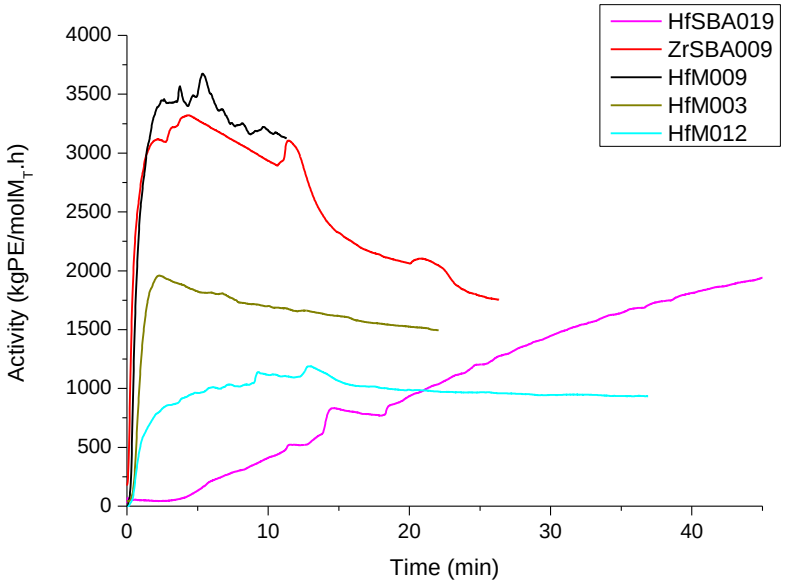

Figure 4.12: Kinetic profiles for three blends prepared with different Hf:Zr proportion and two nanocomposites obtained with the individual catalysts.

It is worthwhile to notice that the kinetic profiles of the two supported metallocenes are completely different. While zirconocene exhibits a very fast rise of activity followed by a strong decay, the hafnocene presents a build-up profile, with an induction period followed by a slow increase of activity. These different features are reflected on the profiles of the blends obtained. Therefore, several changes are observed in the kinetic profiles as zirconocene content rises in the reaction mixture (HfM012 → HfM003 → HfM009), namely: at short times the maximal activity is attained more rapidly and presents a higher value, and then, the deactivation rate increases and the profile become less stable at longer times.

Taking into account these data, the obtainment of a very low amount of PE of high molar mass may be expected at short times by the hafnocene catalyst, even when using the highest Hf:Zr molar proportion in the reactor. As far as the reaction proceeds, the proportion of this higher molar mass component is expected to increase. Consequently, the proportion of the PE produced by hafnocene and zirconocene may change along the time and be significantly different to the one expected from Hf:Zr molar proportion used in the reactor.

Data on Table 4.5 shows that the molar masses of the polyethylenes synthesized with the zirconocene and the hafnocene catalysts are within the expected range; the former leading to lower molar masses than the latter. It is seen also that, the molar masses of the blends obtained either with the homogeneous catalysts or with the co-immobilized ones are comprised between the molar masses obtained for the individual catalyst components (ZrHOM010 and HfHOM021).

Moreover, at the same Al/M_t ratio of 2500, and Hf:Zr molar proportion of 80:20, the molar mass of the blend obtained with the homogeneous catalysts is lower than the one obtained for the supported ones.

4.3.2 Characterization of the blends

4.3.2.1 Thermal behavior

4.3.2.1.1 Thermogravimetric analysis

The first characteristics to be studied in the different blends manufactured are the thermal properties. Figure 4.13 shows the thermogravimetric curves under inert and oxidant atmospheres for the blends prepared at constant Hf:Zr molar proportion and different Al/M_t ratio and also the decomposition curve for one neat polyethylene and one nanocomposite obtained with the individual hafnocene catalyst for comparative reasons.

As described in the previous section for the FI:Zr blends, in inert environment a single primary stage of decomposition is observed for all the specimens in the temperature range from 200 to 600 °C. On the other hand, four different processes are noticeable in oxidant environment.

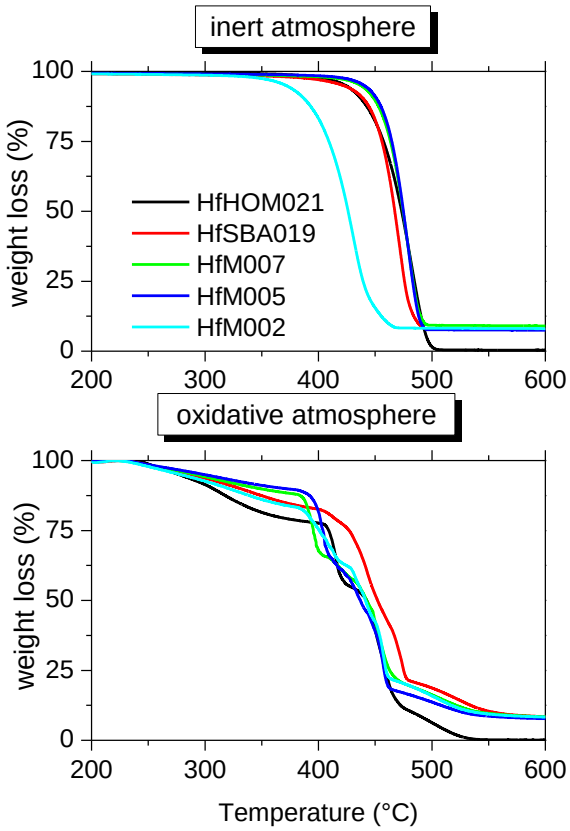

Figure 4.13: TGA curves of different blends at a constant Ti:Zr proportion of 50:50 and different Al/M_t ratios (500, 1000 and 2500) (specimens HfM007, HfM005 and HfM002, respectively) under inert (top representation) and oxidant (lower plot) conditions. For a better understanding, the HfHOM021 neat polyethylene and HfSBA019 nanocomposite both synthesized with the Hf catalyst have been also represented.

Considering the samples prepared at constant Hf:Zr molar proportion of 50:50 and increasing the Al/M_t ratio (HfM007, HfM005 and HfM002) the specimen that stands out is the HfM002, which is prepared with an Al/M_t ratio of 2500. This HfM002 sample has a much lower initial degradation temperature under inert conditions. This fact was also observed in the FI:Zr blends and could be probably associated with the larger acidity provided by the higher amount of aluminum [82].

Figure 4.14 displays the thermogravimetric curves under inert and air environments for the blends prepared at a constant Al/M_t ratio of 2500 and changing the Hf:Zr molar proportion between 20:80, 50:50 and 80:20 (HfM009, HfM002 and HfM010 samples, respectively). Again, the HfHOM021 pristine polyethylene and HfSBA019 nanocomposite prepared with the individual hafnocene are also represented for comparison reasons.

The analysis of the samples prepared at constant Al/M_t ratio of 2500 and changing the Hf:Zr molar proportion (samples HfM009, HfM002 and HfM010) shows a lower initial degradation temperature as the hafnium content increases under inert conditions. For

these samples, the $T_{10\%}$ and $T_{25\%}$ dependence is similar to the one found for the initial degradation temperature, *i.e.*, a shift to lower temperatures as hafnium amount is raised.

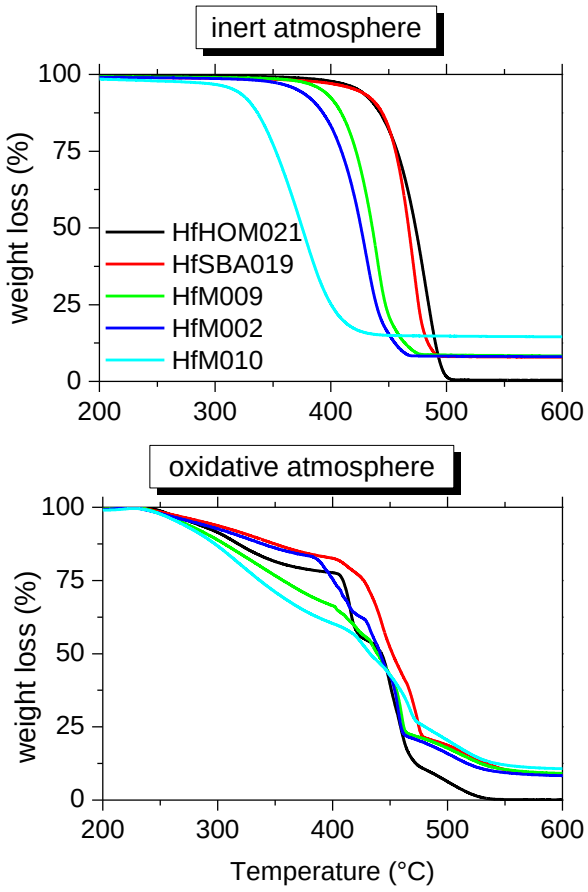

Figure 4.14: TGA curves of different blends at constant Al/M_t ratio = 2500 and different Hf:Zr molar proportion (20:80, 50:50 and 80:20) (HfM009, HfM002 and HfM010 specimens, respectively) under inert (top representation) and oxidant (lower plot) conditions. For a better understanding, the HfHOM021 neat polyethylene and HfSBA019 nanocomposite both synthesized with the Hf catalyst have been also represented.

Comparison between the HfSBA019 nanocomposite and the HfHOM021 neat polyethylene seems to indicate that there is not catalytic effect due to the presence of SBA-15 particles. Nevertheless, an evident effect is observed in the Hf:Zr blends at the largest Al/M_t ratio of 2500 that seems to increase as hafnium ratio is raised. This behavior may be also related to the SBA-15 content incorporated in the nanocomposite, since the HfM010 combines the highest Hf:Zr ratio and the highest SBA-15 content. Then, degradation process starts at lower temperatures. Similar variation was already observed by Lucas *et al.* [133] in UHMWPE/HDPE blends prepared by extrusion where those blends showed a lower thermal stability than that exhibited by the pure HDPE.

Thermogravimetric analysis also allows quantifying the SBA-15 content in the blends. Table 4.6 reports the different SBA-15 contents in the nanocomposites both under inert and oxidant atmospheres. A good reproducibility has been found for the determination of the SBA-15 incorporation independent of the atmosphere used.

Table 4.6: Average SBA-15 wt. % content and SBA-15 wt.% content calculated under each specific environment.

Sample	Average SBA-15 wt.% content	Inert atmosphere			Oxidative atmosphere		
		$T_{10\%}$	$T_{25\%}$	SBA-15 wt.% content	$T_{10\%}$	$T_{25\%}$	SBA-15 wt.% content
HfM009	8.5	405	422	8.9	295	357	8.2
HfM002	8.1	388	409	8.1	321	401	8.0
HfM010	10.5	332	352	10.6	288	337	10.4
HfM007	8.5	449	463	8.0	348	395	8.9
HfM005	7.5	452	465	7.5	370	404	7.4

4.3.2.1.2 Differential scanning calorimetry

The DSC results are summarized in Figure 4.15 and in Table 4.7. Figure 4.15 shows a single melting and crystallization peak indicating that the individual chains synthesized by these two catalysts present in the blends undergo their thermal transitions at identical temperature interval, as already observed from thermograms of the FI:Zr blends. Accordingly, the analysis of these phase transitions is not adequate for evaluating miscibility of these blends.

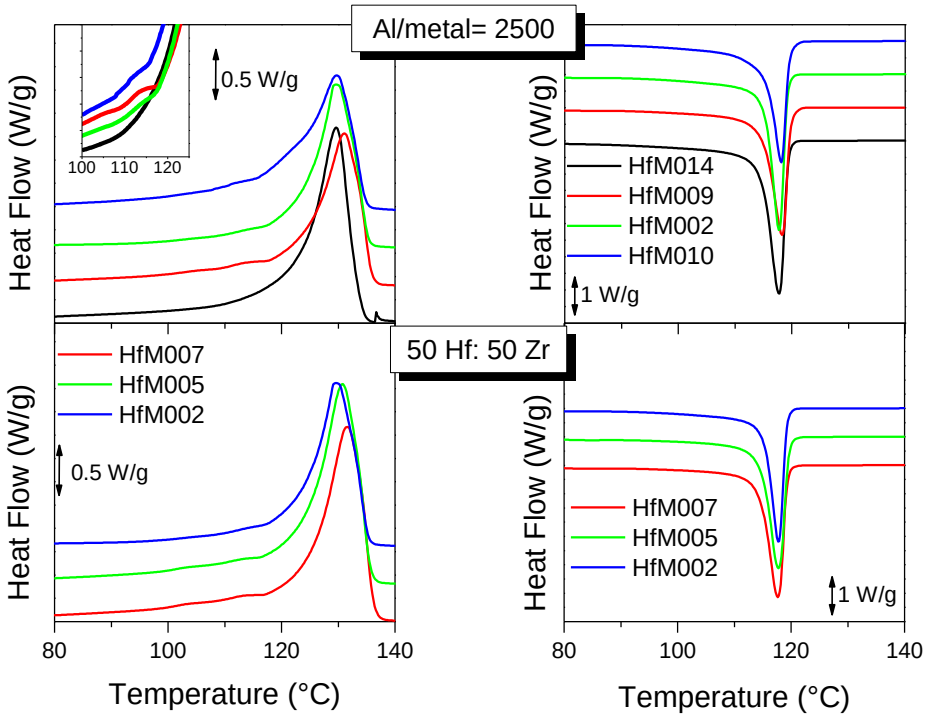

Figure 4.15: DSC curves for the first melting (left plots) and subsequent crystallization processes (right plots) of a blend without SBA-15 (HfM014) and on the top: blends at Al/M_t=2500 and different Ti:Zr molar proportion: HfM009 (20:80), HfM002 (50:50) and HfM010 (80:20). On the bottom: blends at 50:50 Ti:Zr molar proportion and distinct Al/M_t ratio: HfM007 (500), HfM005 (1000) and HfM002 (2500).

Table 4.7: DSC calorimetric data of the materials prepared.

Sample	Hf (% molar)	Zr (% molar)	Al/M_t	% inorg	M_w	D	*powder*		*film*			
							f_c	T_m (°C)	f_c	T_m (°C)	f_c	T_c (°C)
ZrHOM010	0	100	2500	0	0	-	n.d.	n.d.	0.58	129.5	0.60	118.0
HfHOM002	100	0	2500	0	505410	1.9	0.73	135.9	0.50	130.0	0.53	117.0
HfSBA019	100	-	2500	8.0	-	-	0.65	138.4	0.54	130.5	0.49	117.5
Blends												
HfM009/008	20	80	2500	8.5	-	-	0.69	136.3	0.48	131.0	0.48	118.3
HfM002/003	50	50	2500	8.1	-	-	0.73	136.6	0.45	129.5	0.50	117.7
HfM010/012	80	20	2500	10.5	495900	3.8	0.74	136.2	0.54	130.0	0.52	118.2
HfM007/006	50	50	500	8.5	-	-	0.69	137.6	0.59	131.5	0.54	117.7
HfM005/004	50	50	1000	7.5	-	-	0.70	136.8	0.58	131.0	0.54	117.8
HfM014	80	20	2500	0	358000	3.5	0.71	134.8	0.50	129.5	0.50	117.8

When comparing the melting process of blends synthesized at a constant Al/M_t ratio of 2500 that comprises samples prepared at a Hf:Zr molar proportion between 20:80, 50:50 and 80:20 (samples HfM009, HfM002 and HfM010, respectively) and the HfM014 sample prepared in homogeneous conditions no slight differences on T_m are observed but no clear trend is found for these specimens. Nevertheless, the width of the melting process in the homogenous HfM014 sample is narrower than in those nanocomposites that contain SBA-15 particles. The effect is more evident in the HfM010 blend.

If the samples prepared at a given Hf:Zr molar proportion of 50:50 and increasing Al/M_t ratio from 500, 1000 to 2500 (HfM007, HfM005 and HfM002 specimens, respectively) are now compared, then, a decrease of the melting temperature is observed as the Al/M_t increases.

Moreover, the blends that are synthesized in the presence of mesoporous SBA-15 particles present a small shoulder in the temperature interval between 100 and 125 °C, similar to the behavior shown by the other nanocomposites described in previous sections of this thesis. This endothermic peak can be associated with the polyethylene crystallites that possess small sizes because they are growing inside the SBA-15 channels and their development is then confined. HfM002 sample exhibits the less intense peak since its filler content is the lowest.

A nucleant effect could not be observed during crystallization in the different Hf:Zr blends due to the presence of SBA-15 particles. Nevertheless, for the blends prepared at a constant Al/M_t ratio of 2500 and varying the Hf:Zr molar proportion between 20:80, 50:50 and

80:20 (samples HfM009, HfM002 and HfM010, respectively) an increase in the crystallinity is detected.

4.3.2.2 Mechanical properties

Indentation measurements are performed for the analysis of the mechanical properties of these blends. The indentation elastic modulus and hardness, E_{it} and H_{it}, respectively, are presented in Table 4.8.

Table 4.8: Indentation parameters attained at 25 °C: indentation modulus (E_{it}) and hardness (H_{it}) for some pristine polyethylene and nanocomposites as well as for the reactor blends prepared under different experimental conditions.

Sample	Hf (% molar)	Zr (% molar)	Al/M_t	% inorg	M_w	D	H_{it} (MPa)	E_{it} (MPa)	f_c	T_m (°C)
ZrHOM010	0	100	2500	0	187500	3.0	53	985	0.66	129.5
ZrSBA011[a)]	0	100	500	10.9	-	-	65	950	0.63	132
HfHOM002	100	0	2500		505410	1.9	46	738	0.50	130.0
HfSBA019	100	-	2500	8.0	-	-	59	923	0.54	130.5
Blends										
HfM009/008	20	80	2500	8.5	-	-	56	847	0.48	131.0
HfM002/003	50	50	2500	8.1	-	-	59	968	0.45	129.5
HfM010/012	80	20	2500	10.5	495900	3.8	60	826	0.55	129.8
HfM007/006	50	50	500	8.5	-	-	70	1265	0.59	131.7
HfM005/004	50	50	1000	7.5	-	-	n.d.	830	0.58	130.8
HfM014 (H)	80	20	2500	-	358000	3.5	54	863	0.50	129.7

a) Data reported in a previous study [188]

Table 4.8 also lists indentation parameters for the neat polyethylenes prepared with the individual zirconocene and the hafnocene catalysts, ZrHOM010 and HfHOM002 samples, and for the nanocomposites synthesized with those individual catalysts, ZrSBA011 and HfSBA019, respectively. The pristine polyethylenes and the nanocomposite synthesized with the zirconocene present higher E_{it} and H_{it} values than the materials prepared with the hafnocene. These results are clearly understood considering that two main variables may affect the stiffness of the different materials: crystallinity and SBA-15 content. Rigidity is enlarged as both ones increase while different scenarios can appear depending on their balance.

This increase of modulus has been also observed in previous works by the introduction of MCM-41 on a HDPE matrix [82, 84]. The importance of this effect was dependent of several

factors, namely: the crystallinity of the polymer matrix, the MCM-41 content and the dispersion of the MCM-41 particles within the polymer matrix. The reinforcement effect of SBA-15 appears to be also dependent, in this study, on the nature of the catalyst used. In fact, the increase of E_{it} modulus and of H_{it} seems more important when the polyethylene matrix is obtained using a hafnocene supported catalyst rather than when the zirconocene one is used. Therefore, the introduction of about 8% wt. of SBA in samples obtained with the individual hafnocene (HfHOM002 and HfSBA019) leads to a 25% increase of modulus (from 738 to 923 MPa) in spite of showing a decrease of crystallinity. For zirconocene samples, the incorporation of SBA-15 content (10% wt.) and an almost constancy of crystallinity do not affect the mechanical properties of the samples in a similar way. It seems that the reinforcement effect of SBA-15 particles is more noticeable as softness of the matrix is more pronounced.

Despite of the fact that the crystallinity values observed for the blends are much lower than the ones found for the nanocomposites it can be said, as a general trend, that the indentation modulus are in the range of the values obtained for the nanocomposites prepared from the individual components. However, when we look to the HfM007 blend, whose crystallinity is in the range of that presented by the HfSBA019 and ZrSBZ011nanocomposites, then a significant increase of both hardness and indentation modulus, either relatively to the nanocomposites or to the other blends, is clearly seen. The superior performance of this blend (E_{it}=1265 MPa) and H_{it}=70 MPa) is well demonstrated in Figure 4.16 and Table 4.8).

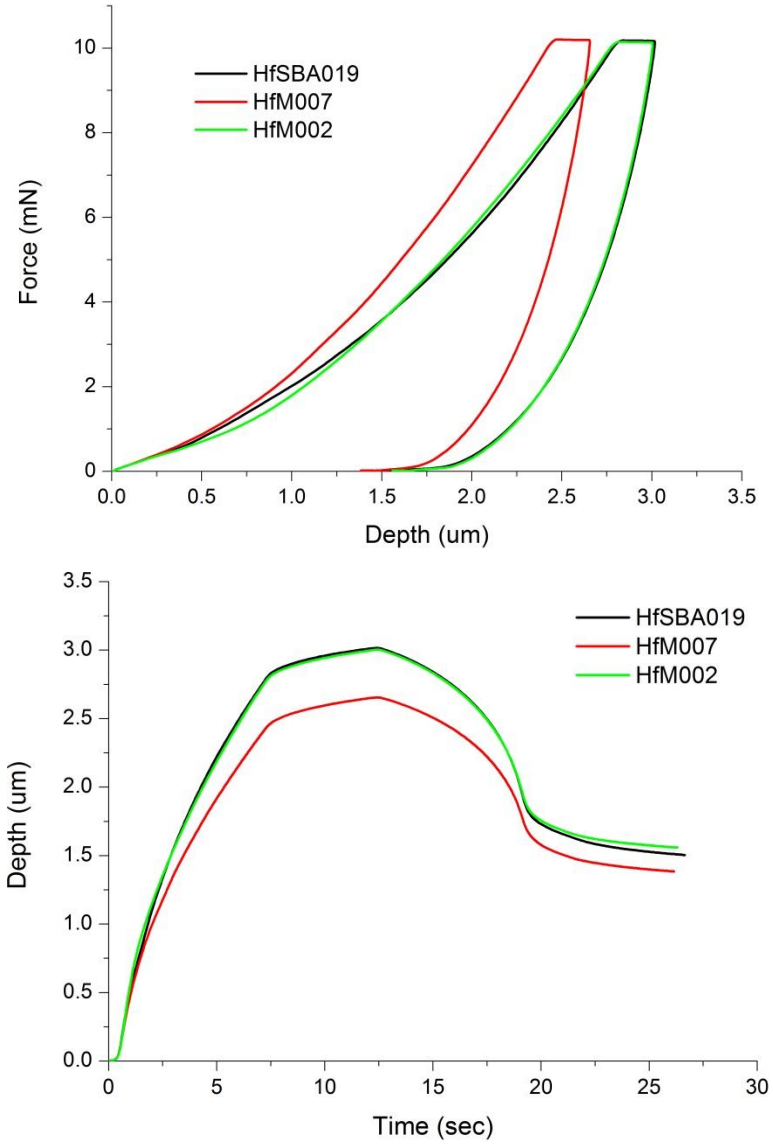

Figure 4.16: Indentation curves of load-maintenance-unload vs. depth (top) and indenter depth dependence on experimental time (bottom) for a nanocomposite and two blends.

4.4 Conclusions

Several in-reactor PE blends with different compositions have been produced by *in situ* polymerization in a single reactor. These blends are synthesized combining two different catalysts (one for each targeted molar mass) co-immobilized in SBA-15 using the preactivation approach.

In a first set of blends, named FI- based blends, the UHMWPE component was synthesized by a phenoxy-imine titanium based catalyst while the production of HDPE was carried out with the metallocene Cp_2ZrCl_2. The activities obtained during the preparation of these blends are in the range of the values achieved for the individual supported catalysts used. Moreover the kinetic profiles can be rationalized taking into account the contribution of

each one of the immobilized catalysts. The highest activity is obtained for the blend prepared at a fixed Al/M_t ratio of 2500 and with a Ti:Zr molar proportion of 50:50. For the blends prepared at a constant Ti:Zr molar proportion the activity increases with the Al/Ti ratio.

The characterization of these blends by thermogravimetric analysis under inert atmosphere, revealed that decomposition tends to start at higher temperature as FI content in the support is increased, *i.e.* as molar mass rises whereas, a shift to much lower temperatures is observed as the Al/M_t ratio is increased. This fact can be associated with the higher acidity provided by a higher amount of aluminum. Under oxidative conditions a more complex behavior is observed: the $T_{10\%}$ shows a similar dependence to that found under inert conditions but, this trend is modified at higher temperatures and, above 400 °C the thermal response of the blends is quite analogous. Moreover increasing amounts of SBA-15 in the blends seem to promote degradation.

Regarding the DSC results, a single melting and crystallization peak is observed indicating that the individual chains synthesized by these two catalysts present in the blends undergo their thermal transitions at identical temperature interval. Moreover, it is observed a displacement of the melting temperature to slightly higher values as Ti:Zr ratio varies from 20:80 to 80:20 proportion. In addition, it is noticeable the appearance of a small shoulder in the temperature interval ranging from 100 to 125 °C. This small endothermic peak was also seen for the nanocomposites characterized in the previous chapters and it is attributed to those polyethylene crystallites, either coming from the UHMWPE or from the HDPE component that are developed inside the SBA-15 channels. Concerning the crystallization, there is not a significant variation in the location of T_c for these samples, indicating that there is no nucleant effect due to the presence of SBA-15. Nevertheless a slight decrease in crystallinity is found when increasing the Al/M_t ratio. For the blends containing a higher amount in SBA-15 at constant Al/M_t ratio the phase transition temperatures do not show significant changes as well as crystallinity values for the first melting process. Nevertheless, there is a considerable difference in the degree of crystallinity developed during crystallization and the variation might be related to the increasing content in SBA-15.

The UHMWPE/HDPE blends exhibit a behavior dependent on the Ti:Zr molar proportion used during polymerization. A reduction in rigidity and hardness values as well as in the indentation modulus is observed as the amount of UHMWPE is supposed to be increased in the blend, *i.e.* as Ti:Zr molar proportion is raised. This trend is the result of a significant reinforcing effect of the addition of a minor amount of a UHMWPE component to a HDPE matrix but, of any reinforcement effect upon addition of a small amount of a HDPE component to a UHMWPE matrix.

The best mechanical performance in terms of E_{it} e H_{it} is shown respectively by the FIM004 and the FIM006 blends. However sample FIM005 shows the best creep resistance, since this sample presents the highest crystallinity and SBA-15 content as well as the greater average molar mass. In fact, chains with average lengths of two million involve the existence of a lot of entanglements that significantly hamper deformation under a constant load.

In a second set of blends the production of HDPE was carried out again by the metallocene Cp_2ZrCl_2 while the highest molar mass component was synthesized by a hafnocene (named Hf-based blends).

As for FI-based blends, the activities values obtained for the preparation of Hf-based blends are in the range of the activities achieved for the individual supported catalysts used and can be rationalized taking into account the contribution of each one of the immobilized catalysts. This way, at a constant Al/M_t ratio of 2500, an increase of the amount of hafnocene in the reactor mixture results in a decrease of the activity, which is explained by the lower activity of the supported hafnocene when compared to the supported zirconocene. Moreover, at a constant Hf:Zr molar proportion an increase of the Al/M_t ratio turns out in an increase of the activity. It is also worthwhile to notice that the kinetic profiles of the two supported metallocenes are completely different and this explains the changes observed in the kinetic profiles as the zirconocene content rises in the reaction mixture. Taking this in mind it is possible that the proportion of the PE produced by hafnocene and zirconocene may change with time and may be even significantly different of the one expected from the Hf:Zr molar proportion used in the reactor.

The thermogravimetric analysis show, as for FI-based blends, that the decomposition occurs in a single stage in inert atmosphere but is a multi-stage process in an oxidant atmosphere. In a similar way to what happens with the FI-based blends, in inert conditions a high Al/Hf ratio promotes de decomposition at lower temperature. However at constant Al/Hf ratio of 2500 and changing the Hf:Zr molar proportion, a lower initial degradation temperature is observed as the hafnium content increases. As observed for FI-based blends, a single melting and crystallization peak is seen in the DSC thermograms of the Hf-based blends, together with a small shoulder in the temperature interval between 100 and 125 °C. Comparison of the blends synthesized at a constant Al/M_t ratio of 2500, *i.e.* at varied Hf:Zr molar proportion, show no significant differences in the melting temperatures of these samples. On the other hand, when increasing the Al/M_t ratio a diminishment of the melting temperature is observed. Again, as for the previous FI-based blends, no clear nucleant effect, due to the presence of SBA-15 particles is observed during crystallization. Nevertheless, an increase in the crystallinity is detected.

When comparing the mechanical properties of the neat polyethylenes with the corresponding nanocomposite samples it appears that the increase of E_{it} modulus and of H_{it}, due to the presence of SBA-15 particles, is more important when the polyethylene matrix is obtained using a supported hafnocene rather than a supported zirconocene catalyst. Thus, the reinforcement effect of SBA-15 particles is more noticeable as the softness of the matrix is more pronounced. In what concerns the behavior of the blends it can be said that although the crystallinity values observed for the blends are lower than the ones found for the nanocomposites the indentation modulus are in the range of the values obtained for the nanocomposites prepared from the individual components. However, the HfM007 blend, whose crystallinity in the same range of that presented by the nanocomposites of each of the individual catalysts, shows a significantly enlarged indentation modulus (1265 MPa), either relatively to the nanocomposites or the other blends.

5. Preliminary ethylene polymerization studies in the presence of cellulose nanowhiskers

The growing ecological and environmental consciousness has driven efforts for the development of innovative materials for various end-use applications. There is currently a considerable interest in developing bio-based and green nanocomposites in industrial and technological areas owing to their biodegradability, biocompatibility and environmental friendliness.

With the emergence and development of these green nanocomposites, cellulose, the most ancient and important natural polymer on earth revives and attracts more attention in the form of ''nanocellulose'' to be used as novel and advanced material [202]. Cellulose is a polysaccharide with the common formula $(C_6H_{10}O_5)_n$, consisting of a linear chain of several hundreds to over thousands of linked cellobiose units. The degree of polymerization is approximately 10000 for cellulose chains in nature and 15000 for native cellulose cotton [203]. Nanocellulose is described as the products or extracts from native cellulose (found in plants, animals, and bacteria) composed of the nanoscaled structure material.

The nomenclature of nanocelluloses has not been used in a uniformly manner in the past [204]. Although all nanocellulose types are based on cellulose fibrils (see Figure 5.1) with one dimension in the nanometer range, each has a distinctive preparation method and set of properties.

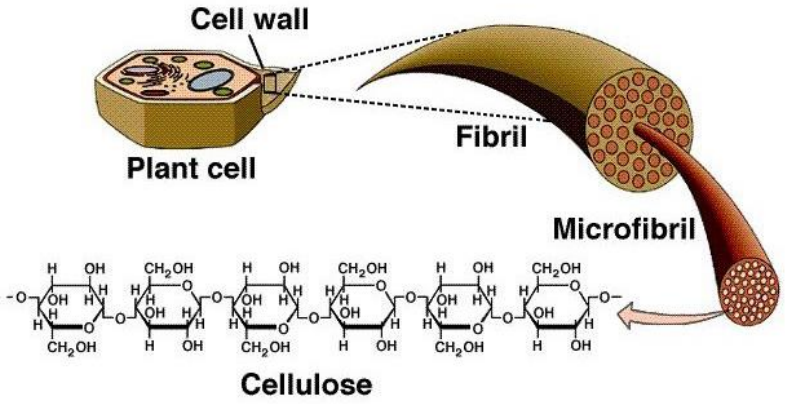

Figure 5.1: Arrangement of fibrils, microfibrils and cellulose in cell walls. Reprinted from [205]

On the basis of their dimensions, functions and preparation methods, which in turn depend mainly on the cellulosic source and on the processing conditions, nanocelluloses may be classified in three main types:

(1) Bacterial cellulose, also referred to as microbial cellulose or biocellulose;

(2) Cellulose nanofibrils, with the synonyms of nanofibrillated cellulose, microfibrillated cellulose, cellulose nanofibers;

(3) Cellulose nanocrystals, with other designations such as nanocrystalline cellulose, cellulose nanowhiskers, rod-like cellulose microcrystals. In this thesis it will be used the cellulose nanowhiskers (CNW) designation.

Bacterial cellulose is typically synthesized by aerobic bacteria (such as *Acetobacter xylinum*) in a pure form which requires no intensive processing to remove unwanted impurities or contaminants such as lignin, pectin and hemicellulose [206].

Regarding the preparation of cellulose nanofibrils, mechanically induced destructuring strategy is mainly applied, which involves high-pressure homogenization and/or grinding before and/or after chemical or enzymatic treatment.

The third type of nanocellulose, cellulose nanowhiskers, is extracted from native semi-crystalline cellulose by the removal of amorphous regions and preservation of highly-crystalline structure by a chemically induced destructuring strategy, such as acid hydrolysis (Figure 5.2). This chemical process starts with the removal of polysaccharides bound at the fibril surface and is followed by the cleavage and destruction of the more readily accessible amorphous regions to liberate rod-like crystalline cellulose sections. This separation happens due to the faster hydrolysis kinematics of amorphous regions than the crystalline parts. When the appropriate level of glucose-chain depolymerization has been reached, the acidic mixture is diluted, and the residual acids and impurities are fully removed by repeated centrifugation and extensive dialysis. The hydrolysis is followed by a mechanical process, typically sonication, which disperses the nanocrystals as a uniform stable suspension.

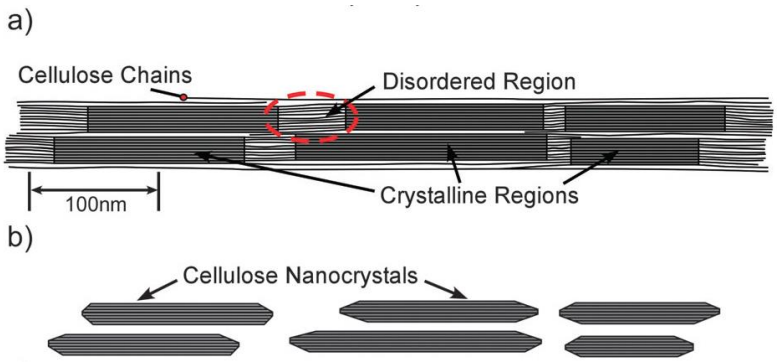

Figure 5.2: (a) idealized cellulose microfibrils showing one of the suggested configurations of the crystalline and amorphous regions, and (b) cellulose nanowhiskers after acid hydrolysis dissolved the disordered regions. Reprinted from [207]

The structure, properties and phase-separation behavior of cellulose nanowhisker suspensions are strongly dependent on the type of mineral acid used and its concentration, the hydrolysis temperature and time and the intensity of the ultrasonic irradiation [208-210]. Different strong acids have been shown to successfully degrade the amorphous regions of cellulose fibers to release crystalline cellulosic nanoparticles, such as sulfuric, hydrochloric, phosphoric, hydrobromic, nitric acids, and a mixture composed of hydrochloric and organic acids [211]. Nevertheless, the hydrolysis treatment with sulfuric acid has been extensively investigated and appears to be the most effective method. One of the main reasons for using sulfuric acid as a hydrolyzing agent is that, if nanocrystals are prepared using hydrochloric acid, their ability to disperse in solvents is limited and the

suspension is unstable [212, 213], tending to flocculate. However, during hydrolysis, sulfuric acid reacts with the surface hydroxyl groups via an esterification process allowing the grafting of anionic sulfate ester groups ($-OSO_3^-$) to approximately one tenth of the glucose units [214]. These sulfate groups are randomly distributed on the surface of the cellulosic nanoparticle stabilizing the nanowhiskers by strong electrostatic repulsion [215].

Cellulose sources are variable and their degree of crystallinity strongly influences the dimensions of the liberated crystals. Released nanowhiskers present a diameter of 5–30 nm and length of 100 nm to several micrometers (from the highly crystalline tunicate and algae celluloses) or shorter lengths of 100–500 nm (from the less crystalline plant cellulose) [208, 209, 216-222]. With microscopic observations and light scattering techniques, the morphology and dimensions of CNW can be assessed as elongated rod-like (or needle-like) nanoparticles, and each rod can therefore be considered as a rigid cellulosic crystal with no apparent defect [223]. Although similar in size to cellulose nanofibrils, CNW have very limited flexibility, as they do not contain amorphous regions.

Cellulose nanowhiskers have been used as green reinforcing agent in nanocomposites by virtue of their advantages of high Young's modulus and strength, biodegradability, biocompatibility, non-toxicity, renewability and easy chemical modification due to abundant hydroxyl groups. Although it is challenging to determine the true modulus and strength of cellulose crystals [224], theoretical calculations and numerical simulations were used to estimate the axial modulus of a cellulose crystal to be approximately 58–180 GPa [225-228]. Theoretical predictions indicate that cellulose nanowhiskers have a tensile strength in the range of 0.3–22 GPa [229, 230]. The predicted high tensile strength of cellulose is due to the extended chain conformation of crystalline cellulose, the high density of covalent bonds per cross-sectional area and the large number of inter- and intra-molecular hydrogen bonding sites. These impressive mechanical properties make cellulose crystals an ideal candidate as reinforcement with both petrochemical-based polymer and bio-based polymer matrices.

The first use of nanocellulose as reinforcement for various polymer including polypropylene, polystyrene and high density polyethylene was reported by Boldizar *et al.* [231] although the full implications of using nanocellulose as reinforcement were not apparent. Later the strong reinforcing effects of small amounts of nanocellulose were demonstrated and clarified by Favier *et al.* [218, 221]. They used nanocellulose whiskers derived from tunicate to reinforce styrene and butyl acrylate copolymer latex with nanocellulose whisker loading fractions of up to 6 vol. %. Even at such low nanocellulose loading, the nanocomposites had significantly higher mechanical properties than the neat polymer in its elastomeric state. The authors ascribed this improvement to the formation of a rigid cellulose whisker network within the nanocomposites due to percolation of the nanocellulose whiskers. The nanocellulose percolation threshold was estimated to be between 1 and 6 vol.% depending on the cellulose source [232].

Following this result, the incorporation of cellulose nanocrystals from different sources into composite materials with enhanced properties has been investigated thoroughly and summarized in several review papers [203, 233]. Like for any multiphase materials, the properties of these cellulosic nanocomposites depend on that of the two constituents,

namely whiskers and polymer matrix in addition to morphological aspects and their interfacial comportments (whiskers/matrix interactions).

Processing techniques have an important incidence on the final properties of the composites. These techniques are conditioned by both intrinsic properties of whiskers and polymer matrix (solubility, dispersibility and degradation) and the desired final properties such as geometrical shape.

In general, polymer nanocomposites can be prepared by dispersing nanofillers in the polymer matrix using a common solvent [234-236] or via melt-processing [237, 238]. Processing based on solution casting and evaporation of the solvent is straightforward but in the case of CNCs is limited to a rather small subset of polymers, which are soluble in water or highly polar solvents [239]. Water is the preferred processing medium because of the high stability of aqueous cellulose whisker dispersions and the expected high level of dispersion of the filler within the host matrix in the resulting composite film. The dispersion of hydrophilic CNWs in hydrophobic polymer matrices such as polyethylene and polypropylene *via* this process is therefore not possible.

Melt-compounding such as extrusion, commonly used to process thermoplastic polymers, is infrequently employed for the preparation of CNW reinforced polymer nanocomposites because of inherent incompatibility and thermal stability issues. Indeed, the hydrophilic nature of polysaccharides causes irreversible agglomeration upon drying and aggregation in nonpolar matrices because of the formation of additional hydrogen bonds between the nanoparticles. Moreover, sulfuric acid prepared CNWs present low thermal stability when heated at moderated temperatures, which limits their processing with methods involving heat [240]. This is ascribed to the dehydration reaction resulting from the presence of sulfate groups with negative charge on the surface of CNWs.

It is often challenging to achieve uniform dispersion of nanofiller in the polymer matrix, and to eliminate agglomerates. These issues are even more pronounced when incorporating hydrophilic fillers into hydrophobic polymers [237, 239]. Hydroxy groups present in the native cellulose and sulfate ester units introduced during hydrolysis with sulfuric acid both contribute to the hydrophilic character of the cellulose nanocrystals. Consequently, while cellulose nanowhiskers are an active polar hydrophilic material, non-polar polymer materials exhibit significant hydrophobicity [241, 242]. The weak interfacial bonding between highly polar cellulose and non-polar organophilic matrix can lead to a loss in final properties of the nanocomposites and ultimately hinders their industrial usage [243]. Different strategies have been applied to eliminate this deficiency in compatibility and interfacial bond strength, allowing the dispersion of the cellulose whiskers in an adequate (with regard to matrix) organic medium: coating whiskers surface with a surfactant [244, 245] or by chemically modifying their surface [246, 247]. The main challenge with chemical modification is to choose a reagent and reaction medium that enable modification of the nanowhisker surface without dissolving it in the reaction medium and without undesired bulk changes. The chemically modified nanoparticles can be dispersed in organic liquids of low polarity and mixed with polymer solution or eventually directly added in the polymer melt after drying. However, two conflicting effects arise from this procedure. On the one hand, it allows improving the dispersion of the modified nanoparticles in the continuous

apolar medium, which is beneficial to optimize the mechanical properties of the ensuing nanocomposite. On the other hand, it restricts the interactions between nanoparticles through hydrogen-bonding which is the basis of the outstanding mechanical properties of polysaccharide nanocrystal-based nanocomposites [248].

When introducing inorganic fillers into polymer matrixes via *in situ* polymerization, a good dispersion of the fillers, as well as a more effective interaction between the filler particles and the polymer matrix was reported [109, 117]. Taking this into consideration, in this chapter we are going to present some exploratory tests using this *in situ* alternative approach for the synthesis of polyethylene nanocomposites involving the use of cellulose nanowhiskers.

The purpose of this preliminary study is to produce well-dispersed HDPE/CNW composite materials by *in situ* polymerization and to evaluate the possibility of the use of the CNW in a double role as filler and as support to immobilize the catalyst on the CNW surface.

5.1 Ethylene polymerization behavior

Ethylene polymerization was performed using the Cp_2ZrCl_2/MAO catalytic system in toluene. Several polymerization procedures with the catalyst in homogeneous phase were tested in order to investigate the behavior of this catalytic system in the presence of the CNW and to identify the difficulties and the procedure specifications necessary for handling this material.

The key step of the composite preparation is the mixing process used to disperse CNW and polymers, as homogeneity significantly affects composite performance. In preliminary experiments, it was visible to the naked eye that addition of the cocatalyst MAO to the suspension of CNW in toluene improved dispersion. Taking this into consideration, ethylene polymerization tests with homogeneous Cp_2ZrCl_2 were performed in presence of CNW suspensions prepared with and without MAO.

In the first procedure that we tested, CNW were initially dried at 60°C under vacuum overnight. Despite these soft drying conditions, the CNW particles tend to collapse and aggregate into flakes, making the proper transfer of CNW suspension to the reactor impossible, even when the dispersion was performed in presence of MAO. Within this procedure the ethylene polymerization tests showed severe reproducibility issues mostly due to obstruction problems in the needle during the transfer of CNW suspension with the syringe (even for large diameters). So, after these initial experiments CNW were always used as received and without further drying.

In an attempt to solve the above-mentioned problem, instead of the preparation of the CNW suspension in the schlenk tube and subsequent syringe transfer, the suspension of the CNW in toluene was prepared directly in the reactor. Once again the dispersion of CNW was done both in the presence and absence of MAO. Although the variation in the observed polymerization activities is decreased compared to the previous procedure, reproducibility issues were not completely solved. Additionally, in order to work under inert conditions, the reactor must go through several vacuum/nitrogen cycles and this cause the CNW to become spread all over the reactor remaining stuck to the glass walls. Therefore, it is not

possible to guarantee that the initial CNW amount introduced in the reactor matches the final CNW content on PE matrix of the final nanocomposite.

As it is mandatory to be able to control the CNW content on the final HDPE/CNW composite material, this last procedure was abandoned and a new one developed (procedure A). It consists in, prior to CNW dispersion, passing the CNW particles through sieves with adequate mesh opening in order to separate the bigger particles that may block the syringe during transfer of CNW suspension to the reactor. A schematic representation of this procedure is presented in Figure 5.3. Once again the dispersion of CNW was done both in the presence and absence of MAO (procedure A1 & A2 respectively). The experiments performed with this modified procedure showed no reproducibility problems.

Procedure A

A1)

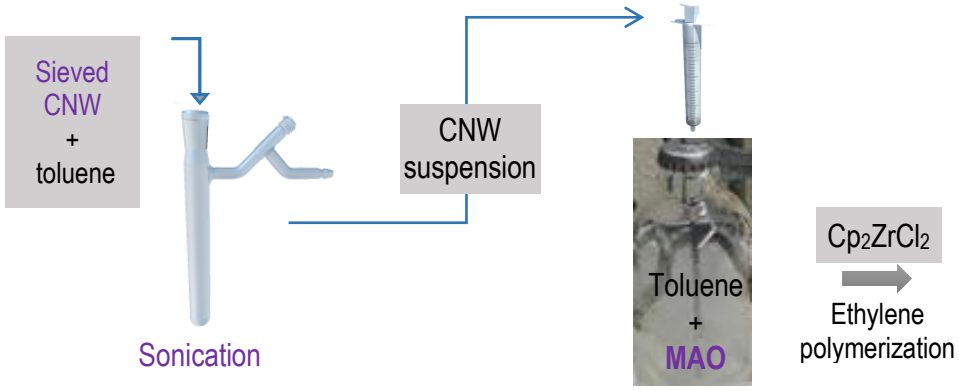

A2)

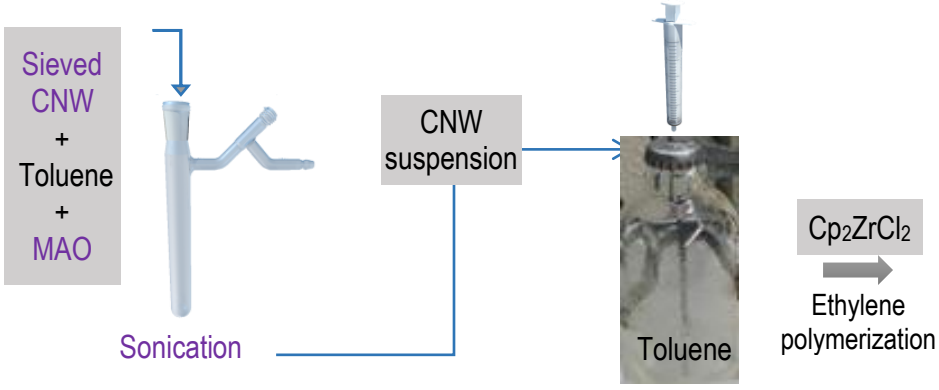

Figure 5.3: Schematic representation of the polymerization procedures A1 and A2.

The next step was the immobilization of Cp_2ZrCl_2 on the CNW particles and, to do so, different impregnation methodologies were envisaged. In the first one direct immobilization of 17 µmolZr/g CNW on the surface of the CNW was attempted, but even after 16h the catalyst was not fully immobilized.

In the second approach the surface of the CNW was modified with different amounts of MAO. The CNW modified with MAO was then put in contact with the metallocene in order to obtain the immobilized catalyst. No further addition of MAO was done before ethylene polymerization.

Procedure B)

Immobilization of Cp_2ZrCl_2 in CNW modified with MAO

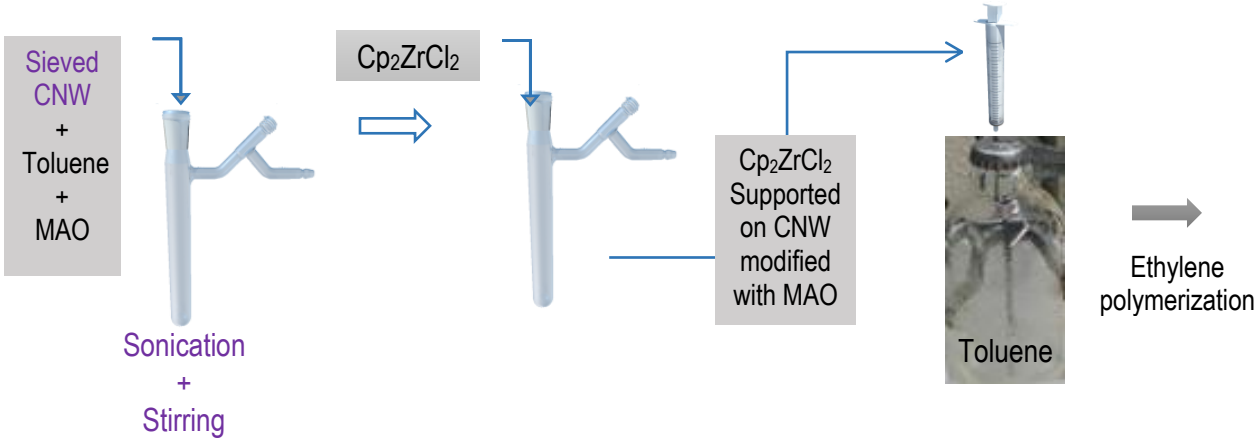

Figure 5.4: Schematic representation of the polymerization procedure where the catalyst was immobilized on the CNW modified with MAO.

Table 5.1 presents a summary of the activity values obtained with these different methods A and B. Results show that polymerization activities obtained when using the homogeneous metallocene, either in presence or absence of CNW, are similar and very high. So it seems that the CNW do not have a poisoning effect on the metallocene, despite all the hydroxyl groups in their surface. This feature is most probably linked to the protective effect of MAO, towards the deactivating role of OH groups.

Table 5.1: Activities (kgPE/molTi.h) obtained for the different polymerization conditions.

Procedure	***A1***		***A2***	***B***
	Homogenous Cp_2ZrCl_2			
Al/Zr	-	**+ CNW dispersed in toluene**	**+ CNW dispersed in toluene/MAO**	**Cp_2ZrCl_2 Supported in CNW modified with MAO**
3000	18240	-	*ZrCNW008* 16760	*ZrCNW009* 18700
1000	*ZrHOM020* 20050	20330	23600	*ZrCNW024* 3330
500	*ZrHOM007* 19090	*ZrCNW021* 20490	17500	*ZrCNW023* 2880

However, as reported for catalyst immobilization on SBA-15, a significant decrease activity is observed when using the supported system (procedure B). The exception to this behavior is the activity obtained for the Al/Zr ratio of 3000 which is similar to the one obtained with the homogenous catalyst. This could be due to the fact that the MAO was not totally fixed on the CNW surface and therefore the presence of highly active homogeneous species could account for the very high activity observed.

Table 5.2 presents the molar masses and dispersities of the materials synthesized. The polymerization of ethylene with homogeneous Cp_2ZrCl_2 either in the presence or in absence of CNW afforded similar molar masses. The highest molar masses correspond to those samples obtained with the zirconocene catalyst supported on CNW modified with MAO (samples ZrCNW023 and ZrCNW024).

Table 5.2: Molar masses and dispersities of various materials obtained in different polymerization conditions.

	Mn g/mol	**Mw g/mol**	***D***
ZrHOM007	127000	284400	2.2
ZrCNW021	100700	258700	2.6
ZrCNW023	185300	349100	1.9
ZrCNW024	161600	316000	2.0

The nanowhiskers may have different nucleation ability and may induce different crystal morphology. Figure 5.5 shows SEM pictures of the as-synthesized composite materials. With procedure B, where the metallocene is supported in CNW, the HDPE matrix seems to have a spherical morphology.

A1 (Al/Zr=3000)

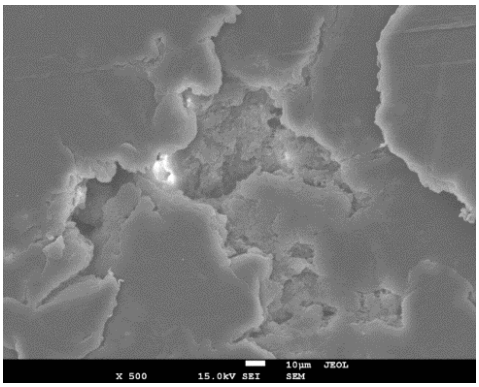

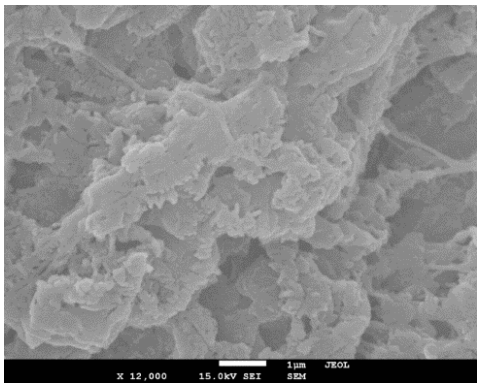

A2 (Al/Zr=500)

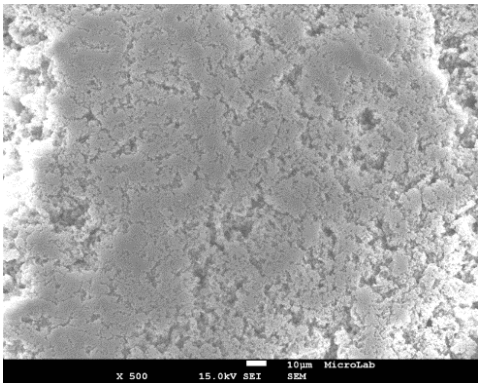

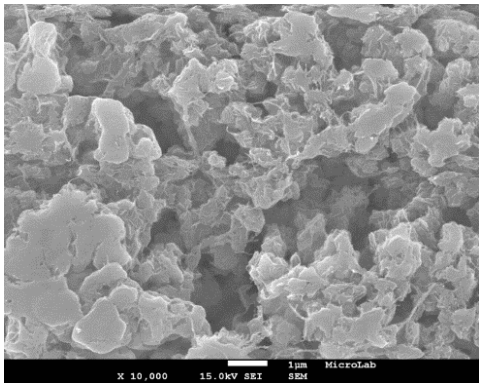

B (Al/Zr=500)

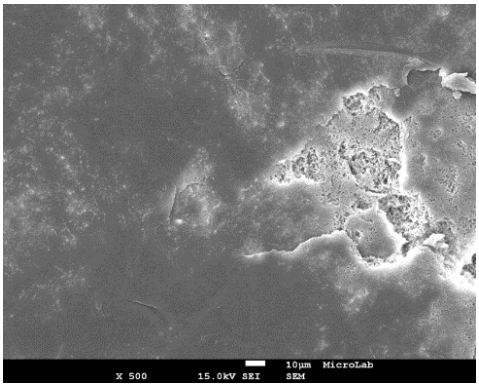

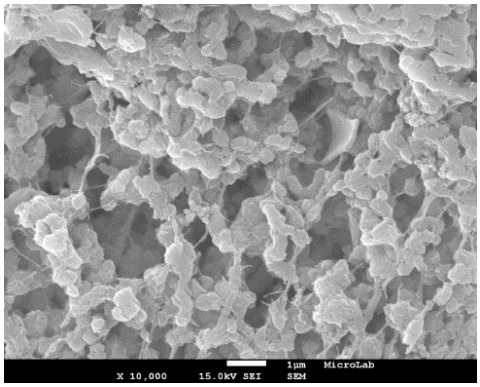

Figure 5.5: SEM pictures of three nanocomposites synthesized by the different methodologies.

5.2 Characterization of the synthesized materials

5.2.1 Thermal behavior

5.2.1.1 Thermogravimetric analysis

The analysis of thermal properties of the materials is important to determine their processing temperature range and end-use conditions. The thermal degradation behavior of some of the materials synthesized was investigated using thermogravimetric analysis, which measures weight loss as a function of temperature for a given heating rate. The degradation curves are presented in Figure 5.6.

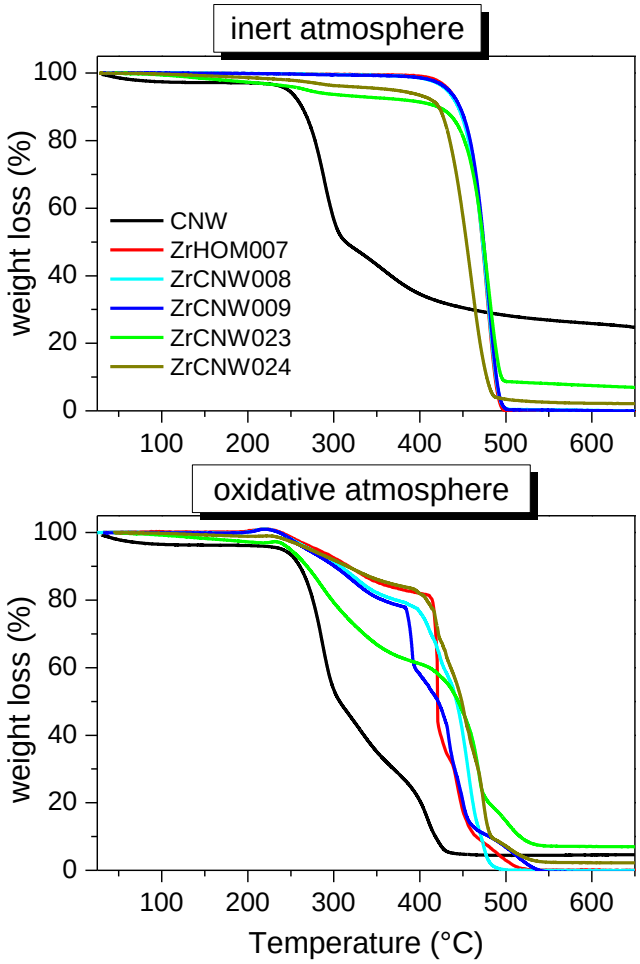

Figure 5.6: TGA curves of cellulose nanowhiskers, one neat polyethylene and several nanocomposites prepared with the CNW.

Thermal degradation of cellulose materials or the reduction in mechanical properties at elevated temperatures is one of the major issues that limit CNW applications. The onset of thermal degradation of CNWs typically occurs at ~200–300 °C, depending on heating rate,

particle type, and type of surface modification [219, 249] and provides an upper limit to the application and processing temperatures appropriate for CNW-based products.

Figure 5.6 displays for neat CNC, an initial weight loss upon heating up to 100 °C. It corresponds to the removal of moisture in the material. At higher temperatures, a gradual weight loss in the range 250–425 °C is reported. Small amounts of sulfate groups resulting from the sulfuric acid hydrolysis process induce a considerable decrease in degradation temperatures. A complex behavior was reported, in which the lower temperature degradation process may correspond to the degradation of more accessible and therefore more highly sulfated amorphous regions, whereas the higher temperature process is related to the breakdown of unsulfated crystal. The residue fraction was also found to increase upon acid hydrolysis and displayed a continuous increase upon prolonged hydrolysis time [240]. It was ascribed to the higher amount of sulfated groups acting as flame-retardants.

Nevertheless, it is noticeable in Figure 5.6 that the presence of CNW only alters the thermal stability of the nanocomposites with the highest values of CNW incorporation, samples ZrCNW023 and ZrCNW024. The TGA curves of these samples show a small mass loss step at temperatures lower than the main degradation step. This is expected since the whiskers should decompose before the HDPE.

Samir *et al.* [250] reported that there was no influence on the thermal stability of the poly(oxyethylene) matrix upon the addition of whiskers despite strong interaction found between the polymeric matrix and the whiskers. Alloin *et al.* [251] also reported that there was no effect of the processing method on the thermal degradation under an inert atmosphere. However, they did find that the extruded films had lower degradation temperatures than the cast/evaporated ones in an oxidative atmosphere.

There is a key drawback for the use of CNW as filler in nanocomposites since there is a major degradation of CNW within the polymer matrix caused by the inferior thermal stability of cellulose, which is further impaired by the 150 °C degradation temperature of the sulfate end groups left from the acid hydrolysis step during its preparation [240, 252]. In addition to particle agglomeration, the long mixing times and high temperatures employed in the melt processing often cause major CNW degradation. Figure 5.7 shows photographs of the compression-molded films obtained from unfilled HDPE and cellulose nanowhisker composites prepared at 160 °C. These films are translucent as any low thickness polymeric film with a relatively low degree of crystallinity so it can be concluded that for a ~5 wt. % of cellulose whiskers, there is no visible degradation in the films prepared.

ZrHOM010 **ZrCNW008** **ZrCNW009**

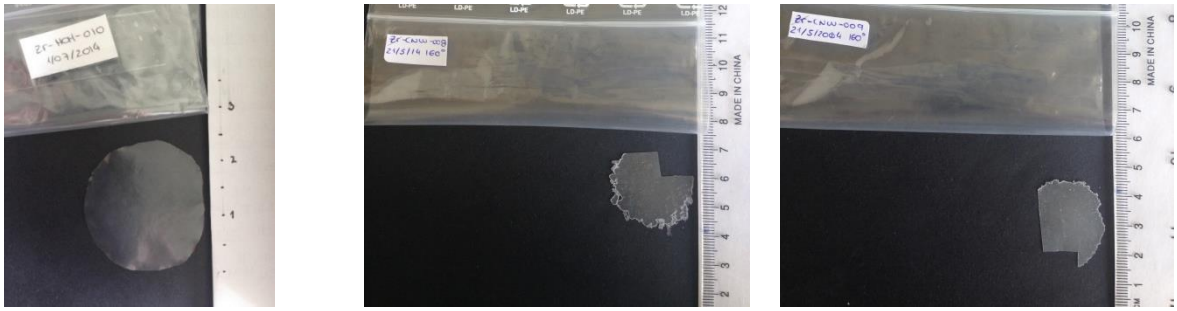

Figure 5.7 Photographs of the unfilled HDPE films and of cellulose nanowhiskers composites compression-molded films.

Unlike other nanofillers such as silica, carbon nanotubes or graphite that do not degrade under these conditions, CNWs undergo thermal degradation [240, 252-254]. This makes quantitative analysis of filler content from final ash remaining at 650°C impossible.

5.2.1.2 Differential scanning calorimetry

The thermal characterization of the neat PE and of the PE/CNW composites was also carried by DSC and the results are presented in Table 5.3 and in Figure 5.8.

Table 5.3: DSC calorimetric data of neat HDPE and nanocomposites reinforced with CNW.

Procedure	Sample	Al/Zr	% CNW	f_c^m	f_c^m NORM	T_m (°C)	f_c^C	f_c^C NORM	T_C (°C)
Homogeneous	ZrHOM007	500	-	0.56	-	130.8	0.59	-	118.5
	ZrHOM010	2500	-	0.58	-	129.5	0.60	-	118.2
With CNW									
A2	ZrCNW021	500	5	0.50	0.52	133.6	0.50	0.53	117.9
A1	ZrCNW008	3000	6	0.52	0.55	131.3	0.57	0.61	119.4
B	ZrCNW009	3000	4	0.50	0.52	131.2	0.56	0.58	119.6
B	ZrCNW024	1000	24	0.49	0.65	133.0	0.52	0.68	118.2
B	ZrCNW023	500	19	0.45	0.56	131.7	0.45	0.55	118.6

The results show that there is an increase in the melting temperature upon CNW addition, regardless of the amount of nanowhiskers introduced or the experimental conditions used to prepare the nanocomposites. So it seems that the size of the crystallites is slightly increased by the presence of the filler. Grunert and Winter also found that the melting temperature increased with increasing silylated whiskers content as a result of stronger filler–matrix interaction [217].

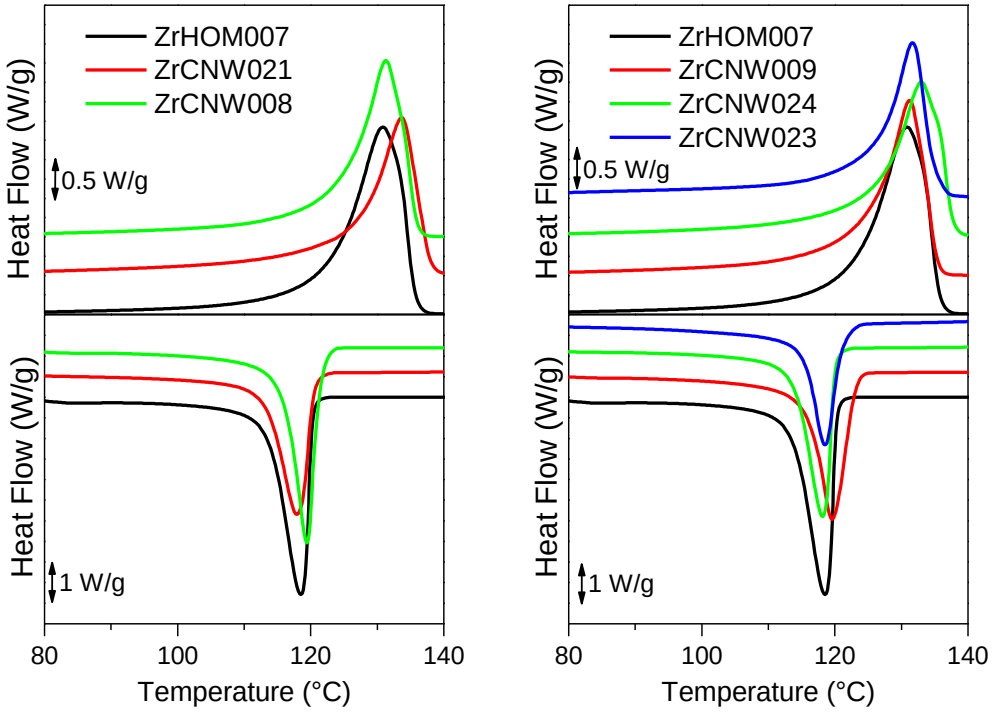

Figure 5.8: DSC curves of the first melting (upper plots) and subsequent crystallization processes (lower plots) of a neat HDPE and some nanocomposites prepared in the presence of CNW.

As it was impossible to determine the amount of CNW in the nanocomposites by TGA, the crystallinity of the HDPE matrix was corrected with the theoretical amount of CNW. The true value of the crystallinity is somewhere in the middle between the two values presented in Table 5.3, the unnormalized and the one normalized to the exact amount of HDPE. Nevertheless, as a general trend it seems that the degree of crystallinity of the HDPE matrix is not strongly affected by the presence of the CNW, except for the sample with the highest CNW content where a significant increase of crystallinity is noticed. Cellulosic fillers are often good nucleating agents for polymer crystallization. However, the extent of enhancement in crystallization depends strongly on filler dispersion and size reduction and the inherent crystallizability of the polymer. The HDPE used in this study has already a very fast crystallization rate, and hence incorporating cellulosic fillers provides no additional benefit. HDPE/CNW nanocomposites retain crystallization behavior not very different from that of neat HDPE. The same behavior was observed by Iyer *et al.* in LDPE/waste cardboard nanocomposites [255]. This behavior is also consistent with Bahar *et al.* [77] PP/CNC composites prepared by solution processing showed no change in onset crystallization temperature.

5.2.2 Mechanical properties

The mechanical properties of the neat polyethylenes and of the nanocomposites obtained were evaluated by nanoindentation.

Table 5.4: Indentation parameters attained at 25 °C: indentation modulus (E_{it}) and hardness (H_{it}) for some neat HDPE synthesized at different Al/Hf ratio and some nanocomposites prepared with CNW.

Procedure	Sample	Al/Zr	% CNW	H_{it} (MPa)	E_{it} (MPa)
Homogeneous	ZrHOM007	500	-	56	1069
	ZrHOM010	2500	-	53	985
With CNW					
A2	ZrCNW021	500	5	53	871
A1	ZrCNW008	3000	6	51	862
B	ZrCNW009	3000	4	51	791
B	ZrCNW024	1000	24	53	790
B	ZrCNW023	500	19	60	1002

Three main parameters were identified to affect the mechanical properties of such materials, viz. the morphology and dimensions of the nanoparticles, the processing method, and the microstructure of the matrix and matrix/filler interactions. The matrix structure and the resulting competition between matrix/filler and filler/filler interactions is one of the main parameters that affect the mechanical properties of these materials. Classical composite science tends to privilege the former as a condition for optimal performance. In cellulose nanowhisker-based composite materials, the opposite trend is observed. The higher the affinity between the cellulosic filler and the host matrix, the lower the mechanical performances [203].

From the results presented in Table 5.4, it seems that there is no reinforcement effect of the presence of the CNW. One factor that could help to explain this behavior is the surface modification of the CNW with MAO, since a potential drawback to surface functionalization is the possibility that the distinctive properties of the CNW may be lost upon modification. For example, mechanical properties could be compromised by surface chemical modification of the CNW as a result of disruption of the 3D crystal network, as reported for whiskers of the polysaccharide chitin [256]. Therefore, any parameter that affects the formation of the percolating nanocrystal network or interferes with it is a critical issue that changes dramatically the mechanical performances of the composite.

Another drawback of cellulosic fillers is their high moisture absorption and the resulting swelling and decrease in mechanical properties. Moisture absorbance and corresponding dimensional changes can be largely prevented if the hydrophilic filler is thoroughly encapsulated in a hydrophobic polymer matrix and there is good adhesion between both components. However, if the adhesion level between the filler and the matrix is not good enough, a diffusion pathway can pre-exist or can be created under mechanical solicitation. The existence of such a pathway is also related to the filler connection and therefore to its percolation threshold [203].

5.3 Conclusions

Increasing environmental concerns have led to developing new bio-based nanocomposites prepared with cellulose nanowhiskers and investigating the potential uses of this renewable resource for such application.

However, to broaden the range of polymeric matrices that can be used in association with cellulose nanowhiskers, homogeneous dispersion of the nanoparticles in any liquid medium, regardless the polarity, is desirable. To promote this dispersion it is necessary to lower the surface energy of the nanoparticles to fit with that of the liquid or polymer melt. In this thesis, this was achieved by coating the CNW surface with the cocatalyst MAO which allowed an improved dispersion of CNW in the polymerization reaction media. However, it seems that the hindered interactions between physically or chemically modified nanowhiskers limit the formation of a strong percolating nanoparticle network and thus the reinforcing effect.

Nevertheless, in the presence of undried cellulose nanowhiskers it was possible to performed ethylene polymerization without a significant lost in activity.

For the nanocomposites synthesized in this section no reinforcement effect could be observed due to the presence of the CNW. The properties of cellulose nanocrystal-reinforced polymer nanocomposites are mainly governed by the possibility of strong interparticle interactions through hydrogen bonding, which are exacerbated by the nanoscale effect resulting from their dimensions. The challenge consists therefore in promoting the homogeneous dispersion of the cellulosic nanoparticles and avoiding agglomeration during processing, thus requiring favorable filler/matrix interactions, and at the same time promoting filler/filler interactions to allow the beneficial formation of a percolating network of nanoparticles. These two requirements are conflicting and thus further work is still necessary.

6. General conclusions

Ultra-high molecular weight polyethylene (UHMWPE) is a material with mechanical properties well suited for particular industrial applications. However, the difficulties inherent to the melt processing of this class of polymers are the major drawback that prevents its wider application. These difficulties arise from the entanglement of the polymer chains that occur during the melt processing and being particularly severe for UHMWPE, although it may also be a concern for the melt processing of high molar mass polyethylene.

Taking this into consideration, the main objective of the present thesis were the development of strategies towards the reduction of the entanglement in this type of materials and the intimate mixing of polymer blends using polymerization *in situ*. The way to achieve these goals involved the preparation of high and ultra-high molecular weight polyethylene, the preparation of nanocomposites using SBA-15, both as support catalyst and filler, as well as the preparation polyethylene blends comprising HDPE and a higher molar mass polyethylene through co-immobilization on SBA-15 of two distinct catalysts, one for each molar mass component.

A set of neat UHMWPE was prepared using the bis[*N*-(3-*tert*-butylsalicylidene)-2,3,4,5,6-pentafluoroanilinate] titanium (IV) dichloride complex as catalyst (FI catalyst) in association with MAO. This catalyst, known to be highly active and to have a living character, gives rise to very high polymerization activities for the homogeneous system. However, the dependence of molar masses on polymerization time shows deviations from the expected living character even at low reaction times. In what concerns the influence of the variation of the Al/Ti ratio, the results have shown that this parameter does not seem to influence the molar masses of the neat polyethylenes. This behavior may be explained by the balance of the promotion of the activation and stabilization effect of the MAO on the catalytic species and the detrimental effect of the TMA present in the MAO on the same species.

Different methodologies were evaluated in order to support the catalyst on SBA-15 and, as expected, this gave rise to an important decrease of the polymerization activity. This decrease was more evident when the catalyst was immobilized after a pre-treatment of the SBA-15 with MAO (SBA-MAO method), presumably due to the formation of Si-O-Al$(Me)_2$ species. The decomposition of the final materials under oxidative conditions seems also to be influenced by the method used for the catalyst immobilization. However, no specific trend could be identified under inert environment.

The DSC thermograms obtained for the various samples prepared with the FI catalyst have shown that the crystallinity is higher when the samples are tested in the form of as-powder from the reactor than if tested in the form of films obtained by compression molding at 230 °C. This may be explained by a more disentangled state and rather chain-extended crystals with a small proportion of amorphous regions that can be developed under the polymerization conditions and the catalytic system used. The transition temperatures estimated by DSC seem rather independent of the presence of SBA-15 and of the method for supporting the FI catalyst. On the other hand, the presence of SBA-15 particles in the polymer matrix seems to decrease slightly the crystallinity and also to hinder the UHMWPE

crystallization. It should also be noticed that the pre-activation method (PA method) seems to favor the formation of polymer chains inside the channels of SBA-15

In what concerns the mechanical behavior of these composite materials it could be observed that the presence of SBA-15 gives rise to stiffer materials with higher elastic modulus, mechanical strength, toughness and creep resistance than those found in the neat polymers. The amount of support followed by molar mass variations are the main factors that trigger the deformation process.

When processing the nascent disentangled UHMWPE based materials in solid-state, by compression molding at high pressure and below its melting temperature, UHMWPE films of very high crystallinity are formed. These T120 films show an impressive improvement of mechanical parameters (around 200% in indentation modulus, E_{it}, and 100% in hardness, H_{it}) relatively to compressed molded samples above melting temperature (T230 films).

The use of the complex bis-(*n*-butylcyclopentadienyl)-dichloro-hafnium (IV) as polymerization catalyst, with different characteristics in terms of polymerization activity and polyethylene molar masses when compared with the FI catalyst, is a contribution to the comprehension of the complex process of polymerization *in situ* and an additional tool to attain the objectives of the thesis.

Contrarily to the FI catalyst, this hafnocene complex allows a direct immobilization on the surface of SBA-15 and therefore this method was also used in this case. The polymerization activity depends on immobilization methodology and on immobilization time. Under optimized conditions this catalyst shows rather high activities when compared with the homogeneous system. Moreover, a noticeable increase of polyethylene molar mass is observed when using the supported hafnocene catalyst that points out the ability of SBA-15 to reduce chain transfer reactions under these confined polymerization conditions.

The thermal decomposition behavior of the polymers prepared with this catalyst exhibits a complex pattern that depends on several factors including the working atmosphere, the immobilization procedure and the presence of SBA-15. In terms of crystallinity and transition temperatures obtained from the melting DSC curves, no specific trends could be observed. However, the effect of the Al/Hf ratio and the immobilization method is evident in particular cases. The presence of SBA-15 seems to hinder the crystallization of polyethylene and no nucleant effect could be observed. As in previous case, evidences were found for the presence of polyethylene chains inside the channels of SBA-15.

The mechanical behavior of the materials prepared with this catalyst is also similar to that of the samples obtained with the previous FI catalyst, *i.e.*, the introduction of SBA-15 into de polymeric matrix increases the stiffness of the final materials when compared with the neat polyethylenes, while keeping a good deformability at high filler contents.

The study of the single supported systems was the basis for the next step involving the immobilization in the same support of two different polymerization catalysts. Aiming the preparation of polyethylene blends containing a component with high or ultra-high molar mass polyethylene and a component with a lower molar mass (common HDPE), catalytic systems comprising a zirconocene and FI or the hafnocene catalysts were developed. This task required a considerable optimization work.

For both cases, FI blends and Hf blends, the average polymerization activities are in the range of the ones of the individual catalysts and may be rationalized in terms of the relative proportion of Ti or Hf with respect to Zr.

The thermal decomposition under inert atmosphere and constant Al/M_t ratio of the two sets of blends is somewhat different. For the FI blends the increase of the Ti:Zr proportion gives rise to an increase of the decomposition temperature whereas the opposite behavior is observed for the Hf blends. The increase of the molar mass obtained with the increase of Ti proportion is probably the reason for the trend that was observed. For both set of blends, a single melting and crystallization peak is observed in DSC thermograms indicating that the individual chains synthesized by the two catalysts present in the blends undergo their thermal transitions at identical temperature interval. Again, no nucleant effect due to the presence of SBA-15 could be observed.

Evaluation of the mechanical behavior of the FI blends has shown a reinforcing effect due to the addition of a minor amount of the UHMWPE component to the HDPE matrix, but no reinforcement effect could be seen upon addition of a small amount of the HDPE component to the UHMWPE matrix. In the case of the Hf blends this trend is not observed, which is probably related with the smaller difference between the molar masses of the two components, when compared with the FI blends.

Another interesting tendency is that the increase of E_{it} modulus and of H_{it}, due to the presence of SBA-15 particles, is more important when the polyethylene matrix is obtained using a supported hafnocene rather than a supported zirconocene catalyst. Therefore, the reinforcement effect of SBA-15 particles is more noticeable as the softness of the polymer matrix is more pronounced, *i.e.* for polymer matrixes with lower crystallinities.

After the detailed work done using SBA-15 as catalyst support, which has allowed the preparation and characterization of different nanocomposites and blends, some preliminary research work was carried out aiming to explore the preparation and study the properties of a new class of composites containing cellulose nanowhiskers (CNW).

Nanocellulose-based materials are carbon-neutral, sustainable, recyclable, and non-toxic. Thus, they have the potential to be green nanomaterials, with many useful and unexpected properties. The polymerization activity of Cp_2ZrCl_2 in the presence of cellulose nanowhiskers was explored and even with undried CNW it was possible to perform ethylene polymerization without a significant lost in activity. The immobilization of the catalyst to the CNW surface previously coated with the cocatalyst MAO was possible.

For the nanocomposites synthesized in this thesis no reinforcement effect could be observed due to the presence of the CNW. The properties of cellulose nanocrystal-reinforced polymer nanocomposites are mainly governed by the possibility of strong interparticle interactions through hydrogen bonding, which are exacerbated by the nanoscale effect resulting from their dimensions. The challenge consists therefore in promoting the homogeneous dispersion of the cellulosic nanoparticles and avoiding agglomeration during processing, thus requiring favorable filler/matrix interactions and, at the same time, promoting filler/filler interactions to allow the beneficial formation of a percolating network of nanoparticles. These two requirements are conflicting and thus further work is still necessary.

Globally, this study has shown that the synthetic approach here used, involving *in situ* polymerization combined with immobilization or co-immobilization of selected catalysts to target specific molar mass ranges on a mesoporous silica support, is an effective route to produce high performance polyethylene nanocomposites and in-reactor polyethylene blends. These materials generally show higher elastic modulus, mechanical strength, toughness and creep resistance than those found in neat polyethylene. The crystallinity and the molar masses of the polymer samples, as well as the content in SBA-15 are crucial parameters for the observed mechanical behavior.

Additionally, nascent UHMWPE based materials with a reduced number of entanglements may be obtained when using a titanium phenoxy-imine based catalyst. By further processing of these powders by compression molding, at high pressure and below its melting temperature, disentangled UHMWPE films of very high crystallinity are formed. An impressive increase of the mechanical parameters (around 300% for the indentation modulus, E_{it}, and 100% for the hardness, H_{it}) is obtained this way.

7. Experimental part

7.1 Materials and chemicals

All the chemicals for the synthesis of the SBA-15 particles, P-123 (poly(ethyleneglycol)-block-poly(propyleneglycol)-block-poly(ethyleneglycol)), hydrochloric acid (37% aq. sol.), TEOS (tetraethylorthosilicate), NaCl and ethanol, were purchased from Sigma-Aldrich and used as received.

The celluloses nanocrystals were purchased from the Process Development Center of the University of Maine (USA) and produced by the US Forest Service, Forest Products Laboratory (USA). They are produced from wood pulp using 64% sulfuric acid, which hydrolyzes the amorphous regions of the cellulose polymer, leaving the acid resistant crystals as a product.

All the experiments for the SBA-15 modification and ethylene polymerization were carried out under dry nitrogen using standard Schlenk techniques. Ethylene and nitrogen (Air Liquide) were purified through absorption columns containing molecular sieves 4A and 13X. bis [*N*-(3-*tert*-butylsalicylidene)-2,3,4,5,6-pentafluoroanilinate] titanium (IV) dichloride (FI catalyst, MCAT), bis-(*n*-butylcyclopentadienyl)-dichloro-hafnium (IV) (Hf catalyst, MCAT), bis-(cyclopentadienyl) zirconium dichloride (Zr catalyst, Sigma-aldrich) and methylaluminoxane (MAO, 7 wt.% Al in toluene solution, AkzoNobel) were used as received. Toluene (VWR Chemicals) was dried by refluxing over metallic sodium under a dry nitrogen atmosphere, using benzophenone as indicator.

7.2 Preparation and characterization of the SBA-15

The synthesis of pure SBA-15 support was carried out as follows: 13.2 g of P-123 were dissolved in 500 mL of water and kept stirring during the night, at room temperature. The temperature was raised to 40 °C and then 45 mL of hydrochloric acid (37% aq. sol.) and 30.8 g of TEOS were added. After ca. 2 h, 12.3 g of NaCl were added and the final mixture was kept under stirring at 40 °C for more 22 h. Subsequently, the compound was crystallized at 100 °C during 3 days in a polypropylene bottle. The product was recovered by centrifugation, washed with distilled water until pH 6-7 and dried overnight at 80 °C. The template was partially removed by extraction with 96% ethanol, at reflux temperature for 16h. The solid was further calcined under a flux of dry air (6L/g.h) at 550 °C for 12 h. The temperature was increase from 20 to 550 °C at 5 °C/min.

The powder XRD pattern of SBA-15 was recorded on a Panalytical X'Pert Pro diffractometer using CuKα radiation filtered by Ni and an X'Celerator detector. Nitrogen adsorption isotherm was measured at -196 °C using ASAP 2010 Micromeritics equipment. Prior to the measurement, the sample was degassed at 350 °C for 3 h. SEM images were obtained on a JEOL JSM-7001F equipment coupled with an Oxford EDX detector and TEM images were obtained on a Hitachi H8100 equipment. Samples were deposited in a Cu/polymer grid sample holder.

Prior to use, SBA-15 was dried under a flux of dry air (4L/g.h) at 300 °C for 1 h. The temperature was increased from 20 to 300 °C at 5 °C/min. Then, the support was kept at this temperature during another 1 h under a nitrogen flow (4L/g.h) and finally cooled to room temperature and stored under dry nitrogen in a Schlenk flask.

7.3 Ethylene polymerization

Polymerizations were carried out in a 250 mL dried and nitrogen-flushed bottle for pressure reactions (Wilmad LabGlass LG-3921) magnetically stirred. The reactor was filled with 50 mL of toluene, the adequate amount of the cocatalyst MAO, the catalyst and ethylene. Polymerizations took place at 20 °C and 1.1 bar of ethylene. Temperature, pressure and ethylene consumption were monitored in real time and the data stored, enabling acquisition of kinetic profiles. The polymerization run until a given amount of ethylene was consumed allowing this way the preparation of HDPE nanocomposites with a given SBA-15 content. Polymerization mixtures were then quenched by the addition of methanol acidified with 5% HCl. The polymer was collected and washed twice with methanol before drying.

Throughout the course of this work, duplicate polymerizations were carried out in order to check that reproducible activities could be obtained with various conditions. Generally activity values presented in this thesis correspond to the average of the independent experiments, only when indicated it is presented the value corresponding to each individual experiment.

7.4 Preparation of the supported catalysts

Three different methods were used for the preparation of the supported catalysts as detailed below:

7.4.1 Direct impregnation of the catalyst on SBA-15 (Method DI)

0.15 g of SBA-15 was contacted with 14×10^{-6} mol of hafnocene (in the form of a solution 1.7×10^{-3} M in toluene) for a given period of time, in a Schlenk flask under magnetic stirring, concealed from ambient light. In order to confirm that all the hafnocene was immobilized on the mesoporous solid, the catalyst suspension, obtained after the contact time between the support and the catalyst solution, was allowed to decant. Then a small volume (~2 mL) of the clear supernatant liquid was tested in polymerization conditions, with further addition of MAO (the same as used for polymerization runs). The polymerization test with this clarified solution did not exhibit any activity, confirming that no catalyst remained in the supernatant solvent [93]. The influence of the impregnation time on the polymerization activity was checked by varying this experimental parameter between 3 and 8h.

7.4.2 Pretreatment of the SBA-15 with MAO and impregnation of the catalysts on the pretreated support (Method SBA-MAO)

The SBA-15 was first treated with MAO in a Schlenk flask under nitrogen atmosphere at room temperature by addition of 1.75 mL of MAO to 1 g of support dispersed in 25 mL of toluene. After 16 h under stirring, the solid is washed three times with ca. 20 mL of dry toluene and dried at room temperature under vacuum overnight. The aluminum load on the support, determined by elemental analysis, was 2.7 mmol Al/g support. The distribution of Al from MAO in SBA-15 was assessed by Energy Dispersive X-ray spectroscopy, with a Si and an Al map.

After drying, 100 mg of this MAO treated SBA-15 solid is contacted with 1.9 μmol of the FI catalyst in toluene (orange solution) and stirred for 4 min. Complete discoloration of the toluene solution and transfer of color to the solid support was observed after this time, suggesting complete immobilization of the catalyst (Figure 7.1).

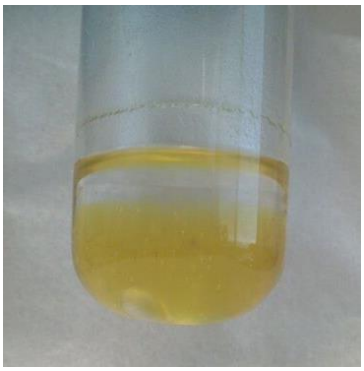

Figure 7.1: Supernatant liquid colorless of a FI catalyst solution in toluene with SBA-MAO after complete immobilization of the catalyst.

Severn *et al.* also reported a transfer of color from the toluene solution to the solid support after complete immobilization of FI catalyst [257]. In order to confirm that all the FI catalyst is immobilized on the mesoporous solid, the catalyst suspension, obtained after 4 min of contact between the support and the catalyst solution, is allowed to decant. Then a small volume (~2 mL) of the clear supernatant liquid is tested in polymerization conditions, with further addition of MAO (same as used for polymerization runs). The polymerization test with this clarified solution does not exhibit any activity, confirming that no catalyst remained in the supernatant solvent [93]. Determination of the metal content of the supported system, by elementary analysis confirmed that all the catalyst was immobilized on the SBA-15 support.

In the case of the hafnocene, after drying, 100 mg of this MAO treated SBA-15 solid is contacted with 1.9 μmol of the hafnium catalyst in toluene and stirred for 4 min. After this period of time, the catalyst suspension undergoes the clarified liquid test described before. If this test is passed successfully, a new catalyst suspension is prepared in the same conditions for use in the ethylene polymerizations.

For both catalysts, additional supported catalysts were prepared with higher impregnation times, in order to check the influence of this parameter on the polymerization activity.

7.4.3 Impregnation of MAO pre-activated catalysts on SBA-15 (Method PA)

The solution of the catalyst in toluene is pre-activated with MAO (Al/Metal = 150) by stirring for 15 min at room temperature. After this time, the equivalent of 0.85 μmol of MAO pre-activated catalyst is mixed with 100 mg of the support in toluene and stirred for 90 min. As in DI or SBA-MAO method, upon immobilization no activity of the supernatant liquid is shown in polymerization conditions, confirming that there is no catalyst remaining in homogeneous solution.

7.4.3.1 Impregnation of MAO pre-activated FI or Hf and Zr dual catalysts on SBA-15

Two individual solutions of each of the catalysts in toluene were pre-activated with MAO (Al/Metal = 150) by stirring for 15 min at room temperature. After this time, the equivalent of 0.85 μmol of MAO of each pre-activated catalyst is mixed with 100 mg of the support in toluene and stirred for 90 min. For the various blends prepared the order of addition was kept constant: first the FI or Hf catalyst and then the Zr catalyst. As for all the methods previously described, upon immobilization no activity of the supernatant liquid is shown in polymerization conditions.

7.5 Polymerization in the presence of cellulose nanowhiskers

For the polymerization in the presence of CNW three procedures were tested.

7.5.1 Procedure A

In Procedure A, 28 mL of toluene were added to 56 mg of sieved CNW and this suspension was sonicated for 1 min. Then 25 mL of this suspension was transferred for the dried and nitrogen-flushed polymerization reactor that already contains 25 mL of toluene and a given amount of MAO. After the introduction of the catalyst Cp_2ZrCl_2 the polymerization took place and was stopped as described before.

7.5.2 Procedure B

Comparing with procedure A, the only difference is that in this procedure the cocatalyst MAO is added to the suspension of CNW in toluene and not in the reactor.

7.5.3 Procedure C

In Procedure B, 30 mL of toluene were added to 60 mg of previously sieved CNW and this suspension was sonicated for 1 min and then stirred for 90 min. After that, a given amount of catalyst Cp_2ZrCl_2 is added and the suspension is stirred for an additional 15 min. Then 25

mL of this suspension was transferred for the dried and nitrogen-flushed polymerization reactor that already contain 25 mL of toluene and the polymerization took place and was stopped as described before.

7.6 Characterization of the polymers

As a general procedure, powders obtained after polymerization were processed as thick films by compression molding in a Collin P-200-P press between hot plates at 230°C for 2 min without pressure, 3 min at a pressure of 5 bar, then 2 min at 10 bar and finally cooling with cold water for 3 min at 10 bar. For the materials containing cellulose nanowhiskers, the processing procedure was the same in what concerns the pressure history but the temperature was 160 °C.

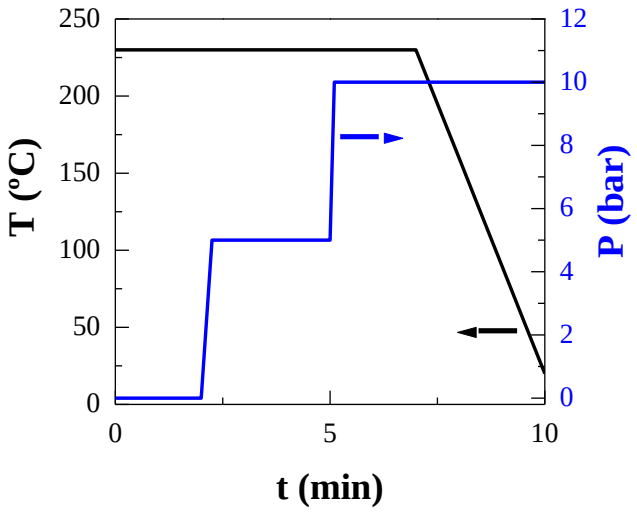

Figure 7.2: Compression molding conditions used during film preparation.

However, in the last section of Chapter 2 powders (specimens with *p* at the end of their nomenclature) obtained after polymerization were processed as films by compression molding under two different conditions: a) the previously described as general procedure. These samples are called as T230 at the end of their name; b) in a press between hot plates at 120 °C for 5 min without pressure, and then 30 min at a pressure of 2.95 kbar and finally cooling process was performed switching off the heating control in the press and maintaining the pressure. These samples are called as T120 at the end of their name.

Thermogravimetric analysis (TGA) was performed in a Q500 equipment of TA Instruments under air or nitrogen atmosphere at a heating rate of 10 °C/min.

Calorimetric analyses were carried out in a TA Instruments Q100 calorimeter connected to a cooling system and calibrated with different standards. The sample weights ranged from 3 to 5 mg. A temperature interval from -40 to 190 °C was studied at a heating rate of 10 °C/min. For the nanocomposites the sample weights are normalized for the total content in

polymer. For the determination of the crystallinity, a value of 290 J/g was used as the enthalpy of fusion of a perfectly crystalline material [258].

SEM and TEM micrographs were obtained in the equipments described above for the pure SBA-15. For the TEM analysis parallel cuts were prepared from different samples at -100 °C using a LEICA EM FC6 cryo-camera in order to attain thin sections (80 nm) of the film surface by means of the LEICA EM UC6ultramicrotome. Those cuts were picked up on cooper grids.

X-ray diffraction patterns were recorded from polymeric films in the reflection mode by using a Bruker D8 Advance diffractometer provided with a PSD Vantec detector (from Bruker, Madison, Wisconsin). CuKα radiation (λ = 0.1542 nm) was used, operating at 40 kV and 40 mA. The parallel beam optics was adjusted by a parabolic Göbel mirror with horizontal grazing incidence Soller slit of 0.12° and LiF monochromator. The equipment was calibrated with different standards. A step scanning mode was employed for the detector. The diffraction scans were collected within the range of 2θ between 1°and 43°, with a step size of 0.024° and 0.2 s per step.

The strain-stress tests were performed at two different temperatures, at 25 °C in a Instron 3366 dynamometer with a load of 100 N and at 90 °C in a Minimat 2000 dynamometer with a load of 20 N. Rate of uniaxial stretching was 1 mm/min at both temperatures. Specimens for these experiments were punched out from the polymer films. The dimensions of these strips were 10 mm long, 2 mm wide and around 0.15 mm thick. All the samples were stretched until a final strain value of 350%.

Depth Sensing Indentation, DSI, experiments were performed at room temperature with a Shimadzu tester (model DUH211S) equipped with a Berkovich type diamond indenter. In all specimens, at least 10 indentations were performed at different regions of surface. The experimental protocol consisted in: a) the application of a load of 10 mN at a loading speed of 1.46 mN/s; b) the maintenance of this constant load for 5 s, and c) the release of the load at an unloading speed equal than the one used along the loading stage. Finally, indentation depth was registered, additionally, for 5 s after reaching the minimum load (0.1 mN). Martens hardness, HMs, and indentation hardness, H_{it}, were calculated according to Oliver-Pharr method [259]. These hardness values are related to the ratio of the maximum load to the contact area under load and after releasing the indentor, respectively. Consequently, HMs is related to elastic, viscoelastic and permanent strains, whereas H_{it} only depends on viscoelastic and plastic strains.

High temperature size exclusion chromatography (HT-SEC) analyses were performed using a Viscotek system (from Malvern Instruments) equipped with three columns (Polefin 300 mm x 8 mm I. D. from Polymer Standards Service, porosity of 1,000 Å, 100,000 Å and 1,000,000 Å). 200 µL of sample solutions with concentration of 5 mg·mL^{-1} were eluted in 1,2,4-trichlorobenzene using a flow rate of 1 mL·min^{-1} at 150 °C. The mobile phase was stabilized with 2,6-di(*tert*-butyl)-4-methylphenol (200 mg·L^{-1}). Online detection was performed with a differential refractive index detector and a dual light scattering detector (LALS and RALS) for absolute molar mass measurement. The OmniSEC 5.02 software was used for calculations.

Regarding the nomenclature of the three types of UHMWPE samples studied, neat polyethylene were designated by Metal_HOM, nanocomposites with SBA-15 designated by Metal_SBA and with CNW by Metal_CNW and finally blends by Metal_M.

8. References

1. Wypych, G., *UHMWPE ultrahigh molecular weight polyethylene*, in *Handbook of Polymers*, G. Wypych, Editor 2012, Elsevier: Oxford. p. 672-676.
2. Spiegelberg, S., *Chapter 24 - Characterization of Physical, Chemical, and Mechanical Properties of UHMWPE*, in *UHMWPE Biomaterials Handbook (Second Edition)*, S.M. Kurtz, Editor 2009, Academic Press: Boston. p. 355-368.
3. Kurtz, S.M., *Chapter 1 - A Primer on UHMWPE*, in *UHMWPE Biomaterials Handbook (Second Edition)*, S.M. Kurtz, Editor 2009, Academic Press: Boston. p. 1-6.
4. Katti, K.S., *Biomaterials in total joint replacement.* Colloids and Surfaces B: Biointerfaces, 2004. **39**(3): p. 133-142.
5. Ianuzzi, A. and C. Mkandawire, *Chapter 11 - Applications of UHMWPE in Total Ankle Replacements*, in *UHMWPE Biomaterials Handbook (Second Edition)*, S.M. Kurtz, Editor 2009, Academic Press: Boston. p. 153-169.
6. Musib, M.K., *A Review of the History and Role of UHMWPE as A Component in Total Joint Replacements.* International Journal of Biological Engineering, 2011. **1**(1): p. 5.
7. Farrar, D.F. and A.A. Brain, *The microstructure of ultra-high molecular weight polyethylene used in total joint replacements.* Biomaterials, 1997. **18**(24): p. 1677-1685.
8. Kelly, J.M., *Ultra-high molecular weight polyethylene* Journal of Macromolecular Science, Part C, 2002. **42**(3): p. 355-371.
9. Fu, J., B.W. Ghali, A.J. Lozynsky, E. Oral, and O.K. Muratoglu, *Ultra high molecular weight polyethylene with improved plasticity and toughness by high temperature melting.* Polymer, 2010. **51**(12): p. 2721-2731.
10. Jauffrès, D., O. Lame, G. Vigier, and F. Doré, *Microstructural origin of physical and mechanical properties of ultra high molecular weight polyethylene processed by high velocity compaction.* Polymer, 2007. **48**(21): p. 6374-6383.
11. Hambir, S. and J.P. Jog, *Sintering of ultra high molecular weight polyethylene.* Bulletin of Materials Science, 2000. **23**(3): p. 221-226.
12. Siegmann, A., I. Raiter, M. Narkis, and P. Eyerer, *Effect of powder particle morphology on the sintering behaviour of polymers.* Journal of Materials Science, 1986. **21**(4): p. 1180-1186.
13. Kurtz, S.M., *UHMWPE Biomaterials Handbook*. Second ed, ed. S.M. Kurtz2009, Boston: Academic Press.
14. K. Nakayama, A.F., T. Okamoto, K. Yagi, A. Kaito, C. R. Choe, L. Wu, G. Zhang, L. Xiu, D. Liu, T. Masuda and A. Nakajima, *Structure and mechanical properties of ultrahigh molecular weight polyethylene deformed near melting temperature (Technical report).* Pure and Applied Chemistry, 1991. **63**(12): p. 12.
15. Smith, P. and P. Lemstra, *Ultra-high-strength polyethylene filaments by solution spinning/drawing.* Journal of Materials Science, 1980. **15**(2): p. 505-514.

16. Smith, P. and P.J. Lemstra, *Ultrahigh-strength polyethylene filaments by solution spinning/drawing, 2. Influence of solvent on the drawability.* Die Makromolekulare Chemie, 1979. **180**(12): p. 2983-2986.

17. Smith, P. and P.J. Lemstra, *Ultra-high strength polyethylene filaments by solution spinning/drawing. 3. Influence of drawing temperature.* Polymer, 1980. **21**(11): p. 1341-1343.

18. Smith, P. and P.J. Lemstra, *Tensile strength of highly oriented polyethylene.* Journal of Polymer Science: Polymer Physics Edition, 1981. **19**(6): p. 1007-1009.

19. Rastogi, S., A.B. Spoelstra, J.G.P. Goossens, and P.J. Lemstra, *Chain Mobility in Polymer Systems: on the Borderline between Solid and Melt. 1. Lamellar Doubling during Annealing of Polyethylene.* Macromolecules, 1997. **30**(25): p. 7880-7889.

20. Rastogi, S., L. Kurelec, and P.J. Lemstra, *Chain Mobility in Polymer Systems: On the Borderline between Solid and Melt. 2. Crystal Size Influence in Phase Transition and Sintering of Ultrahigh Molecular Weight Polyethylene via the Mobile Hexagonal Phase.* Macromolecules, 1998. **31**(15): p. 5022-5031.

21. Gul, R.M. and F.J. McGarry, *Processing of ultra-high molecular weight polyethylene by hot isostatic pressing, and the effect of processing parameters on its microstructure.* Polymer Engineering & Science, 2004. **44**(10): p. 1848-1857.

22. Jauffrès, D., O. Lame, G. Vigier, F. Doré, and T. Douillard, *Sintering mechanisms involved in high-velocity compaction of nascent semicrystalline polymer powders.* Acta Materialia, 2009. **57**(8): p. 2550-2559.

23. Rastogi, S., et al., *Heterogeneity in polymer melts from melting of polymer crystals.* Nature Materials, 2005. **4**(8): p. 635-641.

24. Pandey, A., Y. Champouret, and S. Rastogi, *Heterogeneity in the Distribution of Entanglement Density during Polymerization in Disentangled Ultrahigh Molecular Weight Polyethylene.* Macromolecules, 2011. **44**(12): p. 4952-4960.

25. Rastogi, S., et al., *Novel Route to Fatigue-Resistant Fully Sintered Ultrahigh Molecular Weight Polyethylene for Knee Prosthesis.* Biomacromolecules, 2005. **6**(2): p. 942-947.

26. Rastogi, S., Y. Yao, S. Ronca, J. Bos, and J. van der Eem, *Unprecedented High-Modulus High-Strength Tapes and Films of Ultrahigh Molecular Weight Polyethylene via Solvent-Free Route.* Macromolecules, 2011. **44**(14): p. 5558-5568.

27. Romano, D., E.A. Andablo-Reyes, S. Ronca, and S. Rastogi, *Effect of a cocatalyst modifier in the synthesis of ultrahigh molecular weight polyethylene having reduced number of entanglements.* Journal of Polymer Science Part A: Polymer Chemistry, 2013. **51**(7): p. 1630-1635.

28. Smith, P., H. Chanzy, and B. Rotzinger, *Drawing of virgin ultrahigh molecular weight polyethylene: An alternative route to high strength/high modulus materials.* Journal of Materials Science, 1987. **22**(2): p. 523-531.

29. Ottani, S., E. Ferracini, A. Ferrero, V. Malta, and R.S. Porter, *SAXS Investigations on Relationships between Synthesis Conditions and Solid State Drawability of High*

Molecular Weight Polyethylene Nascent Reactor Powders. Sintering and Annealing of Powders. Macromolecules, 1995. **28**(7): p. 2411-2423.

30. Sano, A., Y. Iwanami, K. Matsuura, S. Yokoyama, and T. Kanamoto, *Ultradrawing of ultrahigh molecular weight polyethylene reactor powders prepared by highly active catalyst system.* Polymer, 2001. **42**(13): p. 5859-5864.
31. Jones, R.L. and M. Armoush, *Catalysts for UHMWPE.* Macromolecular Symposia, 2009. **283–284**(1): p. 88-95.
32. McKenna, T.F. and J.B.P. Soares, *Single particle modelling for olefin polymerization on supported catalysts: A review and proposals for future developments.* Chemical Engineering Science, 2001. **56**(13): p. 3931-3949.
33. Ziegler, K., E. Holzkamp, H. Breil, and H. Martin, *Das Mülheimer Normaldruck-Polyäthylen-Verfahren.* Angewandte Chemie, 1955. **67**(19-20): p. 541-547.
34. Natta, G., *Une nouvelle classe de polymeres d'α-olefines ayant une régularité de structure exceptionnelle.* Journal of Polymer Science, 1955. **16**(82): p. 143-154.
35. Natta, G., et al., *Crystalline high polymers of α-olefins.* Journal of the American Chemical Society, 1955. **77**(6): p. 1708-1710.
36. Sinn, H. and W. Kaminsky, *Ziegler-Natta Catalysis*, in *Advances in Organometallic Chemistry*, F.G.A. Stone and W. Robert, Editors. 1980, Academic Press. p. 99-149.
37. Park, S., et al., *Non-Cp type homogeneous catalytic systems for olefin polymerization.* Journal of Organometallic Chemistry, 2004. **689**(24): p. 4263-4276.
38. Kaminsky, W., *Discovery of Methylaluminoxane as Cocatalyst for Olefin Polymerization.* Macromolecules, 2012. **45**(8): p. 3289-3297.
39. Zijlstra, H.S., M.C.A. Stuart, and S. Harder, *Structural Investigation of Methylalumoxane Using Transmission Electron Microscopy.* Macromolecules, 2015.
40. Sinn, H., *Proposals for structure and effect of methylalumoxane based on mass balances and phase separation experiments.* Macromolecular Symposia, 1995. **97**(1): p. 27-52.
41. Mason, M.R., J.M. Smith, S.G. Bott, and A.R. Barron, *Hydrolysis of tri-tert-butylaluminum: the first structural characterization of alkylalumoxanes [(R2Al)2O]n and (RAlO)n.* Journal of the American Chemical Society, 1993. **115**(12): p. 4971-4984.
42. Kaminsky, W. and H. Sinn, *Methylaluminoxane: Key Component for New Polymerization Catalysts*, in *Polyolefins: 50 years after Ziegler and Natta II*, W. Kaminsky, Editor 2013, Springer Berlin Heidelberg. p. 1-28.
43. Kaminsky, W., *Trends in Polyolefin Chemistry.* Macromolecular Chemistry and Physics, 2008. **209**(5): p. 459-466.
44. Pédeutour, J.-N., K. Radhakrishnan, H. Cramail, and A. Deffieux, *Reactivity of Metallocene Catalysts for Olefin Polymerization: Influence of Activator Nature and Structure.* Macromolecular Rapid Communications, 2001. **22**(14): p. 1095-1123.

45. Zurek, E. and T. Ziegler, *Theoretical studies of the structure and function of MAO (methylaluminoxane).* Progress in Polymer Science, 2004. **29**(2): p. 107-148.

46. Bochmann, M., *Kinetic and mechanistic aspects of metallocene polymerisation catalysts.* Journal of Organometallic Chemistry, 2004. **689**(24): p. 3982-3998.

47. Jordan, R.F., W.E. Dasher, and S.F. Echols, *Reactive cationic dicyclopentadienyl zirconium(IV) complexes.* Journal of the American Chemical Society, 1986. **108**(7): p. 1718-1719.

48. Bochmann, M. and L.M. Wilson, *Synthesis and insertion reactions of cationic alkylbis(cyclopentadienyl)titanium complexes.* Journal of the Chemical Society, Chemical Communications, 1986(21): p. 1610-1611.

49. Eilertsen, J.L., J.A. Støvneng, M. Ystenes, and E. Rytter, *Activation of Metallocenes for Olefin Polymerization As Monitored by IR Spectroscopy.* Inorganic Chemistry, 2005. **44**(13): p. 4843-4851.

50. Alt, H.G. and A. Köppl, *Effect of the Nature of Metallocene Complexes of Group IV Metals on Their Performance in Catalytic Ethylene and Propylene Polymerization.* Chemical Reviews, 2000. **100**(4): p. 1205-1222.

51. F. Albert Cotton, G.W., Carlos A. Murillo, Manfred Bochmann, *Advanced Inorganic Chemistry*. 6th edApril 1999.

52. Shaltout, R.M., J.Y. Corey, and N.P. Rath, *The X-ray crystal structures of the ansa-metallocenes, $Me_2C(C_5H_4)_2MCl_2$ (M = Ti, Zr and Hf).* Journal of Organometallic Chemistry, 1995. **503**(2): p. 205-212.

53. King, W.A., et al., *Absolute Metal–Ligand σ Bond Enthalpies in Group 4 Metallocenes. A Thermochemical, Structural, Photoelectron Spectroscopic, and ab Initio Quantum Chemical Investigation.* Journal of the American Chemical Society, 1999. **121**(2): p. 355-366.

54. Deck, P.A., C.L. Beswick, and T.J. Marks, *Highly Electrophilic Olefin Polymerization Catalysts. Quantitative Reaction Coordinates for Fluoroarylborane/Alumoxane Methide Abstraction and Ion-Pair Reorganization in Group 4 Metallocene and "Constrained Geometry" Catalysts.* Journal of the American Chemical Society, 1998. **120**(8): p. 1772-1784.

55. Chen, E.Y.-X. and T.J. Marks, *Cocatalysts for Metal-Catalyzed Olefin Polymerization: Activators, Activation Processes, and Structure–Activity Relationships.* Chemical Reviews, 2000. **100**(4): p. 1391-1434.

56. Guan, Z., P.M. Cotts, E.F. McCord, and S.J. McLain, *Chain Walking: A New Strategy to Control Polymer Topology.* Science, 1999. **283**(5410): p. 2059-2062.

57. Ittel, S.D., L.K. Johnson, and M. Brookhart, *Late-Metal Catalysts for Ethylene Homo- and Copolymerization.* Chemical Reviews, 2000. **100**(4): p. 1169-1204.

58. Younkin, T.R., et al., *Neutral, Single-Component Nickel (II) Polyolefin Catalysts That Tolerate Heteroatoms.* Science, 2000. **287**(5452): p. 460-462.

59. Na, S.J., et al., *Bimetallic nickel complexes of macrocyclic tetraiminodiphenols and their ethylene polymerization.* Journal of Organometallic Chemistry, 2006. **691**(4): p. 611-620.

60. Makio, H., N. Kashiwa, and T. Fujita, *FI Catalysts: A New Family of High Performance Catalysts for Olefin Polymerization.* Advanced Synthesis & Catalysis, 2002. **344**(5): p. 477-493.

61. Makio, H., H. Terao, A. Iwashita, and T. Fujita, *FI Catalysts for Olefin Polymerization—A Comprehensive Treatment.* Chemical Reviews, 2011. **111**(3): p. 2363-2449.

62. Matsui, S. and T. Fujita, *FI Catalysts: super active new ethylene polymerization catalysts.* Catalysis Today, 2001. **66**(1): p. 63-73.

63. Furuyama, R., et al., *New High-Performance Catalysts Developed at Mitsui Chemicals for Polyolefins and Organic Synthesis.* Catalysis Surveys from Asia, 2004. **8**(1): p. 61-71.

64. Mitani, M., et al., *FI Catalysts: new olefin polymerization catalysts for the creation of value-added polymers.* The Chemical Record, 2004. **4**(3): p. 137-158.

65. Makio, H. and T. Fujita, *Development and Application of FI Catalysts for Olefin Polymerization: Unique Catalysis and Distinctive Polymer Formation.* Accounts of Chemical Research, 2009. **42**(10): p. 1532-1544.

66. Fujita, T. and K. Kawai, *FI Catalysts for Olefin Oligomerization and Polymerization: Production of Useful Olefin-Based Materials by Unique Catalysis.* Topics in Catalysis, 2014. **57**(10-13): p. 852-877.

67. Domski, G.J., J.M. Rose, G.W. Coates, A.D. Bolig, and M. Brookhart, *Living alkene polymerization: New methods for the precision synthesis of polyolefins.* Progress in Polymer Science, 2007. **32**(1): p. 30-92.

68. Quirk, R.P. and B. Lee, *Experimental Criteria for Living Polymerizations.* Polymer International, 1992. **27**(4): p. 359-367.

69. Saito, J., et al., *Living Polymerization of Ethylene with a Titanium Complex Containing Two Phenoxy-Imine Chelate Ligands.* Angewandte Chemie International Edition, 2001. **40**(15): p. 2918-2920.

70. Makio, H. and T. Fujita, *Observation and identification of the catalytically active species of bis(phenoxy-imine) group 4 transition metal complexes for olefin polymerization using 1H NMR spectroscopy.* Macromolecular Symposia, 2004. **213**(1): p. 221-234.

71. Mitani, M., T. Nakano, and T. Fujita, *Unprecedented Living Olefin Polymerization Derived from an Attractive Interaction between a Ligand and a Growing Polymer Chain.* Chemistry – A European Journal, 2003. **9**(11): p. 2396-2403.

72. Mitani, M., et al., *Living Polymerization of Ethylene Catalyzed by Titanium Complexes Having Fluorine-Containing Phenoxy–Imine Chelate Ligands.* Journal of the American Chemical Society, 2002. **124**(13): p. 3327-3336.

73. Severn, J.R., J.C. Chadwick, R. Duchateau, and N. Friederichs, *"Bound but Not Gagged"Immobilizing Single-Site α-Olefin Polymerization Catalysts.* Chemical Reviews, 2005. **105**(11): p. 4073-4147.

74. Hlatky, G.G., *Heterogeneous Single-Site Catalysts for Olefin Polymerization.* Chemical Reviews, 2000. **100**(4): p. 1347-1376.

75. Choi, Y. and J.B.P. Soares, *Supported single-site catalysts for slurry and gas-phase olefin polymerisation.* The Canadian Journal of Chemical Engineering, 2012. **90**(3): p. 646-671.

76. Tisse, V.F., C. Boisson, F. Prades, and T.F.L. McKenna, *A systematic study of the kinetics of polymerisation of ethylene using supported metallocene catalysts.* Chemical Engineering Journal, 2010. **157**(1): p. 194-203.

77. John R. Severn, J.C.C.E., *Tailor-Made Polymers: Via Immobilization of Alpha-Olefin Polymerization Catalysts*2008: Wiley-VCH.

78. Kresge, C.T., M.E. Leonowicz, W.J. Roth, J.C. Vartuli, and J.S. Beck, *Ordered mesoporous molecular sieves synthesized by a liquid-crystal template mechanism.* Nature, 1992. **359**(6397): p. 710-712.

79. Beck, J.S., et al., *A new family of mesoporous molecular sieves prepared with liquid crystal templates.* Journal of the American Chemical Society, 1992. **114**(27): p. 10834-10843.

80. Dong, X., et al., *MCM-41 and SBA-15 supported Cp_2ZrCl_2 catalysts for the preparation of nano-polyethylene fibres via in situ ethylene extrusion polymerization.* Journal of Molecular Catalysis A: Chemical, 2005. **240**(1–2): p. 239-244.

81. Guo, C., D. Zhang, and G. Jin, *Mesoporous zeolite SBA-15 supported nickel diimine catalysts for ethylene polymerization.* Chinese Science Bulletin, 2004. **49**(3): p. 249-253.

82. Campos, J.M., J.P. Lourenço, E. Pérez, M.L. Cerrada, and M.R. Ribeiro, *Self-Reinforced Hybrid Polyethylene/MCM-41 Nanocomposites: In-Situ Polymerisation and Effect of MCM-41 Content on Rigidity.* Journal of Nanoscience and Nanotechnology, 2009. **9**(6): p. 3966-3974.

83. Campos, J.M., J.P. Lourenço, H. Cramail, and M.R. Ribeiro, *Nanostructured silica materials in olefin polymerisation: From catalytic behaviour to polymer characteristics.* Progress in Polymer Science, 2012. **37**(12): p. 1764-1804.

84. Cerrada, M.L., E. Pérez, J.P. Lourenço, J.M. Campos, and M. Rosário Ribeiro, *Hybrid HDPE/MCM-41 nanocomposites: Crystalline structure and viscoelastic behaviour.* Microporous and Mesoporous Materials, 2010. **130**(1–3): p. 215-223.

85. Kurek, A., S. Mark, M. Enders, M.O. Kristen, and R. Mülhaupt, *Mesoporous Silica Supported Multiple Single-Site Catalysts and Polyethylene Reactor Blends with Tailor-Made Trimodal and Ultra-Broad Molecular Weight Distributions.* Macromolecular Rapid Communications, 2010. **31**(15): p. 1359-1363.

86. Xu, H. and C.-Y. Guo, *Polymerization in the confinement of molecular sieves: Facile preparation of high performance polyethylene.* European Polymer Journal, 2015. **65**(0): p. 15-32.

87. Ko, Y.S., J.S. Lee, J.-H. Yim, J.-K. Jeon, and K.Y. Jung, *Influence of Nanopores of MCM-41 and SBA-15 Confining (n-BuCp)2ZrCl2 on Copolymerization of Ethylene-α-Olefin.* Journal of Nanoscience and Nanotechnology, 2010. **10**(1): p. 180-185.

88. Lee, J.S., J.-H. Yim, J.-K. Jeon, and Y.S. Ko, *Polymerization of olefins with single-site catalyst anchored on amine-functionalized surface of SBA-15.* Catalysis Today, 2012. **185**(1): p. 175-182.

89. Ronca, S., G. Forte, H. Tjaden, Y. Yao, and S. Rastogi, *Tailoring molecular structure via nanoparticles for solvent-free processing of ultra-high molecular weight polyethylene composites.* Polymer, 2012. **53**(14): p. 2897-2907.

90. Kageyama, K., J.-i. Tamazawa, and T. Aida, *Extrusion Polymerization: Catalyzed Synthesis of Crystalline Linear Polyethylene Nanofibers Within a Mesoporous Silica.* Science, 1999. **285**(5436): p. 2113-2115.

91. Dong, X., et al., *Preparation of nano-polyethylene fibers and floccules using MCM-41-supported metallocene catalytic system under atmospheric pressure.* European Polymer Journal, 2005. **41**(4): p. 797-803.

92. Ye, Z., S. Zhu, W.-J. Wang, H. Alsyouri, and Y.S. Lin, *Morphological and mechanical properties of nascent polyethylene fibers produced via ethylene extrusion polymerization with a metallocene catalyst supported on MCM-41 particles.* Journal of Polymer Science Part B: Polymer Physics, 2003. **41**(20): p. 2433-2443.

93. Campos, J.M., M.R. Ribeiro, J.P. Lourenço, and A. Fernandes, *Ethylene polymerisation with zirconocene supported in Al-modified MCM-41: Catalytic behaviour and polymer properties.* Journal of Molecular Catalysis A: Chemical, 2007. **277**(1–2): p. 93-101.

94. Xu, G.C., et al., *Nanomechanic Properties of Polymer-Based Nanocomposites with Nanosilica by Nanoindentation.* Journal of Reinforced Plastics and Composites, 2004. **23**(13): p. 1365-1372.

95. Severn, J.R. and J.C. Chadwick, *Immobilisation of homogeneous olefin polymerisation catalysts. Factors influencing activity and stability.* Dalton Transactions, 2013. **42**(25): p. 8979-8987.

96. Welborn, H.C., *Supported polymerization catalyst* 1989.

97. Takahash, T., *Process for producing ethylene copolymers*, 1991.

98. T.J. Burkhardt , M.M., W.B. Brandley *Long chain branched polymers and a process to make long chain branched polymers*, 1993.

99. Ribeiro, M.R., A. Deffieux, and M.F. Portela, *Supported Metallocene Complexes for Ethylene and Propylene Polymerizations: Preparation and Activity.* Industrial & Engineering Chemistry Research, 1997. **36**(4): p. 1224-1237.

100. Nakayama, Y., et al., *New olefin polymerization catalyst systems comprised of bis(phenoxy-imine) titanium complexes and $MgCl_2$-based activators.* Journal of Catalysis, 2003. **215**(1): p. 171-175.

101. Nakayama, Y., H. Bando, Y. Sonobe, and T. Fujita, *Olefin polymerization behavior of bis(phenoxy-imine) Zr, Ti, and V complexes with $MgCl_2$-based cocatalysts.* Journal of Molecular Catalysis A: Chemical, 2004. **213**(1): p. 141-150.

102. Nakayama, Y., J. Saito, H. Bando, and T. Fujita, *$MgCl_2/R'_nAl(OR)_{3-n}$: An Excellent Activator/Support for Transition-Metal Complexes for Olefin Polymerization.* Chemistry – A European Journal, 2006. **12**(29): p. 7546-7556.

103. Cui, K., B. Liu, C. Wang, J.-Y. Yu, and Z. Ma, *A silica-supported titanium(IV) complex bearing [O–NS] tridentate ligand and its behavior in ethylene homo- and copolymerization with 1-hexene.* Journal of Molecular Catalysis A: Chemical, 2007. **266**(1–2): p. 93-99.

104. Carlini, C., A. Ceccarini, E.G. Fernandes, A.M.R. Galletti, and G. Sbrana, *Ethylene polymerization with silica-supported bis[3,5-dinitro-N-(2,6-diisopropylphenyl) salicylaldiminate]nickel(II)/methylaluminoxane catalysts.* Journal of Polymer Science Part A: Polymer Chemistry, 2005. **43**(9): p. 1978-1984.

105. Guo, C., D. Zhang, F. Wang, and G.-X. Jin, *Nanofibers of polyethylene produced by SBA-15 supported zirconium catalyst [N-(3-tert-butylsalicylidene)-4′-allyloxylanilinato]$_2$Zr(IV)Cl_2.* Journal of Catalysis, 2005. **234**(2): p. 356-363.

106. Chen, S., et al., *Immobilization of a zirconium complex bearing bis(phenoxyketimine) ligand on MCM-41 for ethylene polymerization.* Polymer, 2005. **46**(24): p. 11093-11098.

107. Zou, H., S. Wu, and J. Shen, *Polymer/Silica Nanocomposites: Preparation, Characterization, Properties, and Applications.* Chemical Reviews, 2008. **108**(9): p. 3893-3957.

108. Kango, S., et al., *Surface modification of inorganic nanoparticles for development of organic–inorganic nanocomposites—A review.* Progress in Polymer Science, 2013. **38**(8): p. 1232-1261.

109. Amoli, B.M., S.A.A. Ramazani, and H. Izadi, *Preparation of ultrahigh-molecular-weight polyethylene/carbon nanotube nanocomposites with a Ziegler–Natta catalytic system and investigation of their thermal and mechanical properties.* Journal of Applied Polymer Science, 2012. **125**(S1): p. E453-E461.

110. Sánchez, Y., C. Albano, A. Karam, R. Perera, and E. Casas, *In situ Polymerization of Nanocomposites by TpTiCl_2(Et) System: UHMWPE Filled with Carbon Nanotubes.* Macromolecular Symposia, 2009. **282**(1): p. 185-191.

111. Dangsheng, X., *Friction and wear properties of UHMWPE composites reinforced with carbon fiber.* Materials Letters, 2005. **59**(2–3): p. 175-179.

112. Deng, M. and S.W. Shalaby, *Properties of self-reinforced ultra-high-molecular-weight polyethylene composites.* Biomaterials, 1997. **18**(9): p. 645-655.

113. Tjong, S.C., *Structural and mechanical properties of polymer nanocomposites.* Materials Science and Engineering: R: Reports, 2006. **53**(3–4): p. 73-197.

114. Dorigato, A., Y. Dzenis, and A. Pegoretti, *Filler aggregation as a reinforcement mechanism in polymer nanocomposites.* Mechanics of Materials, 2013. **61**(0): p. 79-90.

115. Zhang, M.Q., M.Z. Rong, H.B. Zhang, and K. Friedrich, *Mechanical properties of low nano-silica filled high density polyethylene composites.* Polymer Engineering & Science, 2003. **43**(2): p. 490-500.

116. Olmos, D., F. Martínez, G. González-Gaitano, and J. González-Benito, *Effect of the presence of silica nanoparticles in the coefficient of thermal expansion of LDPE.* European Polymer Journal, 2011. **47**(8): p. 1495-1502.

117. Kaminsky, W., A. Funck, and K. Wiemann, *Nanocomposites by In Situ Polymerization of Olefins with Metallocene Catalysts.* Macromolecular Symposia, 2006. **239**(1): p. 1-6.

118. Park, S. and I.S. Choi, *Production of Ultrahigh-Molecular-Weight Polyethylene/Pristine MWCNT Composites by Half-Titanocene Catalysts.* Advanced Materials, 2009. **21**(8): p. 902-905.

119. Ramazani, A., M.G. Saremi, B.N. Amoli, and H. Izadi, *Production and characterization of UHMWPE/fumed silica nanocomposites.* Polymer Composites, 2012. **33**(10): p. 1858-1864.

120. Cerrada, M.L., E. Pérez, J.P. Lourenço, A. Bento, and M.R. Ribeiro, *Decorated MCM-41/polyethylene hybrids: Crystalline details and viscoelastic behavior.* Polymer, 2013. **54**(11): p. 2611-2620.

121. Bento, A., J.P. Lourenço, A. Fernandes, M.L. Cerrada, and M. Rosário Ribeiro, *Functionalization of Mesoporous MCM-41 (Nano)particles: Preparation Methodologies, Role on Catalytic Features, and Dispersion Within Polyethylene Nanocomposites.* ChemCatChem, 2013. **5**(4): p. 966-976.

122. Han, B., J. Zhang, S. Zhang, and C. Zhang, *Study on the processability of UHMWPE filled with different size distribution calcium carbonate particles.* Polymer Composites, 2015. **36**(10): p. 1807-1812.

123. Shin, J., J.-C. Kim, and J.-H. Chang, *Characterizations of ultrahigh molecular weight polyethylene nanocomposite films with organomica.* Polymer Engineering & Science, 2011. **51**(4): p. 679-686.

124. Puértolas, J.A. and S.M. Kurtz, *Evaluation of carbon nanotubes and graphene as reinforcements for UHMWPE-based composites in arthroplastic applications: A review.* Journal of the Mechanical Behavior of Biomedical Materials, 2014. **39**: p. 129-145.

125. Park, H.-J., S.-Y. Kwak, and S. Kwak, *Wear-Resistant Ultra High Molecular Weight Polyethylene/Zirconia Composites Prepared by in situ Ziegler-Natta Polymerization.* Macromolecular Chemistry and Physics, 2005. **206**(9): p. 945-950.

126. Stürzel, M., S. Mihan, and R. Mülhaupt, *From Multisite Polymerization Catalysis to Sustainable Materials and All-Polyolefin Composites.* Chemical Reviews, 2015.

127. Tinçer, T. and M. Coşkun, *Melt blending of ultra high molecular weight and high density polyethylene: The effect of mixing rate on thermal, mechanical, and morphological properties.* Polymer Engineering & Science, 1993. **33**(19): p. 1243-1250.

128. Diop, M.F., W.R. Burghardt, and J.M. Torkelson, *Well-mixed blends of HDPE and ultrahigh molecular weight polyethylene with major improvements in impact strength achieved via solid-state shear pulverization.* Polymer, 2014. **55**(19): p. 4948-4958.

129. Zuo, J.-D., Y.-M. Zhu, S.-M. Liu, Z.-J. Jiang, and J.-Q. Zhao, *Preparation of HDPE/UHMWPE/MMWPE blends by two-step processing way and properties of blown films.* Polymer Bulletin, 2007. **58**(4): p. 711-722.

130. Suwanprateeb, J., *Binary and ternary particulated composites: UHMWPE/$CACO_3$/HDPE.* Journal of Applied Polymer Science, 2000. **75**(12): p. 1503-1513.

131. Lim, K.L.K., et al., *High-density polyethylene/ultrahigh-molecular-weight polyethylene blend. I. The processing, thermal, and mechanical properties.* Journal of Applied Polymer Science, 2005. **97**(1): p. 413-425.

132. Song, S., P. Wu, M. Ye, J. Feng, and Y. Yang, *Effect of small amount of ultra high molecular weight component on the crystallization behaviors of bimodal high density polyethylene.* Polymer, 2008. **49**(12): p. 2964-2973.

133. Lucas, A.d.A., J.D. Ambrósio, H. Otaguro, L.C. Costa, and J.A.M. Agnelli, *Abrasive wear of HDPE/UHMWPE blends.* Wear, 2011. **270**(9–10): p. 576-583.

134. Boscoletto, A.B., R. Franco, M. Scapin, and M. Tavan, *An investigation on rheological and impact behaviour of high density and ultra high molecular weight polyethylene mixtures.* European Polymer Journal, 1997. **33**(1): p. 97-105.

135. Aguilar, M., S. Martín, J.F. Vega, A. Muñoz-Escalona, and J. Martínez-Salazar, *Processability of a metallocene-catalyzed linear PE improved by blending with a small amount of UHMWPE.* Journal of Polymer Science Part B: Polymer Physics, 2005. **43**(21): p. 2963-2971.

136. Dumoun, M.M., L.A. Utracki, and J. Lara, *Rheological and mechanical behavior of the UHMWPE/MDPE mixtures.* Polymer Engineering & Science, 1984. **24**(2): p. 117-126.

137. Shen, H., et al., *Improving the integration of HDPE/UHMWPE blends by high temperature melting and subsequent shear.* Materials Letters, 2015. **138**: p. 247-250.

138. Jacobs, O., N. Mentz, A. Poeppel, and K. Schulte, *Sliding wear performance of HD-PE reinforced by continuous UHMWPE fibres.* Wear, 2000. **244**(1–2): p. 20-28.

139. Böhm, L.L., *High mileage Ziegler-catalysts: excellent tools for polyethylene production.* Macromolecular Symposia, 2001. **173**(1): p. 53-64.

140. Galli, P. and G. Vecellio, *Technology: driving force behind innovation and growth of polyolefins.* Progress in Polymer Science, 2001. **26**(8): p. 1287-1336.

141. Galli, P. and G. Vecellio, *Polyolefins: The most promising large-volume materials for the 21st century.* Journal of Polymer Science Part A: Polymer Chemistry, 2004. **42**(3): p. 396-415.

142. Alt, F.P., L.L. Böhm, H.-F. Enderle, and J. Berthold, *Bimodal polyethylene – Interplay of catalyst and process.* Macromolecular Symposia, 2001. **163**(1): p. 135-144.

143. de Souza, R.F. and O.L. Casagrande Jr, *Recent Advances in Olefin Polymerization Using Binary Catalyst Systems.* Macromolecular Rapid Communications, 2001. **22**(16): p. 1293-1301.

144. Mota, F.F., R.S. Mauler, R.F. de Souza, and J.O.L. Casagrande, *Tailoring Polyethylene Characteristics Using a Combination of Nickel α-Diimine and Zirconocene Catalysts under Reactor Blending Conditions.* Macromolecular Chemistry and Physics, 2001. **202**(7): p. 1016-1020.

145. Liu, W., et al., *Synthesis of molecular weight controllable bimodal polyethylene from fluorinated FI–Ti catalyst coupled with ZnEt2.* European Polymer Journal, 2013. **49**(7): p. 1823-1831.

146. Kukalyekar, N., L. Balzano, G.W.M. Peters, S. Rastogi, and J.C. Chadwick, *Characteristics of Bimodal Polyethylene Prepared via Co-Immobilization of Chromium and Iron Catalysts on an $MgCl_2$-Based Support.* Macromolecular Reaction Engineering, 2009. **3**(8): p. 448-454.

147. Mecking, S., *Reactor blending with early/late transition metal catalyst combinations in ethylene polymerization.* Macromolecular Rapid Communications, 1999. **20**(3): p. 139-143.

148. Kim, J.D. and J.B.P. Soares, *Copolymerization of ethylene and α-olefins with combined metallocene catalysts. II. Mathematical modeling of polymerization with single metallocene catalysts.* Journal of Polymer Science Part A: Polymer Chemistry, 2000. **38**(9): p. 1417-1426.

149. Li Pi Shan, C., J.B.P. Soares, and A. Penlidis, *HDPE/LLDPE reactor blends with bimodal microstructures—part I: mechanical properties.* Polymer, 2002. **43**(26): p. 7345-7365.

150. Shan, C.L.P., J.B.P. Soares, and A. Penlidis, *HDPE/LLDPE reactor blends with bimodal microstructures—Part II: rheological properties.* Polymer, 2003. **44**(1): p. 177-185.

151. Soares, J.B.P. and J.D. Kim, *Copolymerization of ethylene and α-olefins with combined metallocene catalysts. I. A formal criterion for molecular weight bimodality.* Journal of Polymer Science Part A: Polymer Chemistry, 2000. **38**(9): p. 1408-1416.

152. Kurek, A., R. Xalter, M. Stürzel, and R. Mülhaupt, *Silica Nanofoam (NF) Supported Single- and Dual-Site Catalysts for Ethylene Polymerization with Morphology Control and Tailored Bimodal Molar Mass Distributions.* Macromolecules, 2013. **46**(23): p. 9197-9201.

153. Kurek, A., S. Mark, M. Enders, M. Stürzel, and R. Mülhaupt, *Two-site silica supported Fe/Cr catalysts for tailoring bimodal polyethylenes with variable content of UHMWPE.* Journal of Molecular Catalysis A: Chemical, 2014. **383–384**: p. 53-57.

154. Liu, C.R.M.a.H.-T., *Polyethylene pipes*, I. Pat., Editor 2006.

155. J. Kipke, S.M., R. Karer, J. Auffermann, M. Hecker, P. de Lange and H. Schmitz, *Polyethylene composition suitable for the preparation of films and process for preparing the same*, I. Pat., Editor 2007.

156. Iwashita, A., M.C.W. Chan, H. Makio, and T. Fujita, *Attractive interactions in olefin polymerization mediated by post-metallocene catalysts with fluorine-containing ancillary ligands.* Catalysis Science & Technology, 2014. **4**(3): p. 599-610.

157. Vyboishchikov, S.F., D.G. Musaev, R.D.J. Froese, and K. Morokuma, *Density Functional Study of Ethylene Polymerization Catalyzed by a Zirconium Non-Cyclopentadienyl Complex, L2ZrCH3+. Effects of Ligands and Bulky Substituents.* Organometallics, 2001. **20**(2): p. 309-323.

158. Silveira, F., et al., *Supported metallocene on mesoporous materials.* Applied Catalysis A: General, 2007. **333**(1): p. 96-106.

159. de Fátima V. Marques, M., O.C. da Silva, A.S.L.S. Coutinho, and A. de Araujo, *Ethylene polymerization catalyzed by metallocene supported on mesoporous materials.* Polymer Bulletin, 2008. **61**(4): p. 415-423.

160. Lee, K.-S., C.-G. Oh, J.-H. Yim, and S.-K. Ihm, *Characteristics of zirconocene catalysts supported on Al-MCM-41 for ethylene polymerization.* Journal of Molecular Catalysis A: Chemical, 2000. **159**(2): p. 301-308.

161. Guo, C., D. Zhang, F. Wang, and G.-X. Jin, *Nanofibers of polyethylene produced by SBA-15 supported zirconium catalyst [N-(3-tert-butylsalicylidene)-4-allyloxylanilinato]$_2$Zr(IV)Cl2.* Journal of Catalysis, 2005. **234**(2): p. 356-363.

162. Carrero, A., R. van Grieken, and B. Paredes, *Hybrid zeolitic-mesostructured materials as supports of metallocene polymerization catalysts.* Catalysis Today, 2012. **179**(1): p. 115-122.

163. Silveira, F., M.d.C.M. Alves, F.C. Stedile, S.B. Pergher, and J.H.Z. dos Santos, *Microporous and mesoporous supports and their effect on the performance of supported metallocene catalysts.* Journal of Molecular Catalysis A: Chemical, 2010. **315**(2): p. 213-220.

164. Trong On, D., D. Desplantier-Giscard, C. Danumah, and S. Kaliaguine, *Perspectives in catalytic applications of mesostructured materials.* Applied Catalysis A: General, 2001. **222**(1–2): p. 299-357.

165. Zhao, D., Q. Huo, J. Feng, B.F. Chmelka, and G.D. Stucky, *Nonionic Triblock and Star Diblock Copolymer and Oligomeric Surfactant Syntheses of Highly Ordered, Hydrothermally Stable, Mesoporous Silica Structures.* Journal of the American Chemical Society, 1998. **120**(24): p. 6024-6036.

166. Klimova, T., et al., *Factorial design for the evaluation of the influence of synthesis parameters upon the textural and structural properties of SBA-15 ordered materials.* Microporous and Mesoporous Materials, 2006. **93**(1–3): p. 331-343.

167. Baier, M.C., M.A. Zuideveld, and S. Mecking, *Post-Metallocenes in the Industrial Production of Polyolefins.* Angewandte Chemie International Edition, 2014. **53**(37): p. 9722-9744.

168. Talebi, S., et al., *Molar Mass and Molecular Weight Distribution Determination Of UHMWPE Synthesized Using a Living Homogeneous Catalyst.* Macromolecules, 2010. **43**(6): p. 2780-2788.

169. Ivanchev, S.S., V.K. Badaev, N.I. Ivancheva, and S.Y. Khaikin, *Living Polymerization of Ethylene on the Bis[N-(3-tert-butylsalicylidene)anilinato]titanium Dichloride–Methylalumoxane Catalyst System.* Doklady Physical Chemistry, 2004. **394**(4-6): p. 46-49.

170. Ivanchev, S., V. Trunov, V. Rybakov, D. Al'bov, and D. Rogozin, *Structure and Catalytic Activity of Titanium and Zirconium Phenoxyimine Complexes.* Doklady Physical Chemistry, 2005. **404**(1-3): p. 165-168.

171. Zohuri, G., S. Damavandi, S. Ahmadjo, R. sandaroos, and M. Shamekhi, *Synthesis of high molecular weight polyethylene using FI catalyst.* Polyolefins Journal, 2014. **1**(1): p. 25-32.

172. Sandaroos, R., S. Damavandi, and A. Farhadipour, *A New Family of High-Performance Ti Catalysts for Olefin Polymerization.* Macromolecular Chemistry and Physics, 2010. **211**(21): p. 2339-2346.

173. Bryliakov, K.P., et al., *Active Intermediates in Ethylene Polymerization over Titanium Bis(phenoxyimine) Catalysts.* Organometallics, 2005. **24**(23): p. 5660-5664.

174. Panchenko, V.N., N.V. Semikolenova, I.G. Danilova, E.A. Paukshtis, and V.A. Zakharov, *IRS study of ethylene polymerization catalyst SiO_2/methylaluminoxane/zirconocene.* Journal of Molecular Catalysis A: Chemical, 1999. **142**(1): p. 27-37.

175. Sinfrônio, F.S.M., et al., *Influence of H-ZSM-5, Al-MCM-41 and acid hybrid ZSM-5/MCM-41 on polyethylene decomposition.* Journal of Thermal Analysis and Calorimetry, 2006. **85**(2): p. 391-399.

176. Díez-Pascual, A.M., M.A. Gómez-Fatou, F. Ania, and A. Flores, *Nanoindentation in polymer nanocomposites.* Progress in Materials Science, 2015. **67**(0): p. 1-94.

177. Bakshi, S.R., K. Balani, T. Laha, J. Tercero, and A. Agarwal, *The nanomechanical and nanoscratch properties of MWNT-reinforced ultrahigh-molecular-weight polyethylene coatings.* JOM, 2007. **59**(7): p. 50-53.

178. Affatato, S., et al., *Comparative study on the wear behaviour of different conventional and cross-linked polyethylenes for total hip replacement.* Tribology International, 2008. **41**(8): p. 813-822.

179. Doucet, N., O. Lame, G. Vigier, F. Dore, and R. Seguela, *Sintering kinetics of UHMWPE nascent powders by high velocity compaction: Influence of molecular weight.* European Polymer Journal, 2013. **49**(6): p. 1654-1661.

180. dos Santos, J.H.Z., et al., *Hybrid supported zirconocene and niobocene catalysts on MAO-modified silicas.* Journal of Molecular Catalysis A: Chemical, 2002. **184**(1–2): p. 167-173.

181. Guimarães, R., F.C. Stedile, and J.H.Z. dos Santos, *Ethylene polymerization with catalyst systems based on supported metallocenes with varying steric hindrance.* Journal of Molecular Catalysis A: Chemical, 2003. **206**(1–2): p. 353-362.

182. Campos, J.M.D.G., *Polimerização de etileno com zirconoceno suportado em MCM-41 modificado: estudo catalítico e propriedades dos materials obtidos*, 2009, Instituto Superior Técnico.

183. Casas, E., R. van Grieken, and J.M. Escola, *Polymerization of ethylene with $(nBuCp)_2ZrCl_2$ supported over mesoporous SBA-15 functionalized with sulfonic acid groups.* Applied Catalysis A: General, 2012. **437–438**: p. 44-52.

184. Bryliakov, K.P., E.P. Talsi, A.Z. Voskoboynikov, S.J. Lancaster, and M. Bochmann, *Formation and Structures of Hafnocene Complexes in MAO- and $AlBui_3/CPh_3[B(C_6F_5)_4]$-Activated Systems.* Organometallics, 2008. **27**(23): p. 6333-6342.

185. Busico, V., R. Cipullo, R. Pellecchia, G. Talarico, and A. Razavi, *Hafnocenes and MAO: Beware of Trimethylaluminum!* Macromolecules, 2009. **42**(6): p. 1789-1791.

186. Zimnoch Dos Santos, J.H., et al., *Effects of ethylene polymerization conditions on the activity of SiO2-supported zirconocene and on polymer properties.* Journal of Polymer Science Part A: Polymer Chemistry, 1999. **37**(13): p. 1987-1996.

187. Bunn, C.W., *The crystal structure of long-chain normal paraffin hydrocarbons. The "shape" of the <CH2 group.* Transactions of the Faraday Society, 1939. **35**(0): p. 482-491.

188. Carlos, A.S., *Polietilenos de ultra elevado peso molecular (UHMWPE) para aplicações biomédicas*, 2014, Instituto Superior Técnico.

189. Grau, P., H. Meinhard, and S. Mosch, *Nanoindentation Experiments on Glass and Polymers at Different Loading Rates and the Power Law Analysis.* MRS Online Proceedings Library, 1998. **522**: p. null-null.

190. Briscoe, B.J., L. Fiori, and E. Pelillo, *Nano-indentation of polymeric surfaces.* Journal of Physics D: Applied Physics, 1998. **31**(19): p. 2395.

191. Cifuentes, S.C., E. Frutos, R. Benavente, J.L. González-Carrasco, and V. Lorenzo, *Strain rate effect on semi-crystalline PLLA mechanical properties measured by instrumented indentation tests.* European Polymer Journal, 2014. **59**: p. 239-246.

192. Seguela, R. and F. Rietsch, *Double yield point in polyethylene under tensile loading.* Journal of Materials Science Letters, 1990. **9**(1): p. 46-47.

193. Brooks, N.W., R.A. Duckett, and I.M. Ward, *Investigation into double yield points in polyethylene.* Polymer, 1992. **33**(9): p. 1872-1880.

194. Murakami, S., M. Yamakawa, M. Tsuji, and S. Kohjiya, *Structure development in the uniaxial-drawing process of poly(ethylene naphthalate).* Polymer, 1996. **37**(17): p. 3945-3951.

195. Wu, C.L., M.Q. Zhang, M.Z. Rong, and K. Friedrich, *Tensile performance improvement of low nanoparticles filled-polypropylene composites.* Composites Science and Technology, 2002. **62**(10–11): p. 1327-1340.

196. Bikiaris, D.N., A. Vassiliou, E. Pavlidou, and G.P. Karayannidis, *Compatibilisation effect of PP-g-MA copolymer on iPP/SiO2 nanocomposites prepared by melt mixing.* European Polymer Journal, 2005. **41**(9): p. 1965-1978.

197. Marcilla, A., A. Gómez-Siurana, S. Menargues, R. Ruiz-Femenia, and J.C. García-Quesada, *Oxidative degradation of EVA copolymers in the presence of MCM-41.* Journal of Analytical and Applied Pyrolysis, 2006. **76**(1–2): p. 138-143.

198. Campos, J.M., J.P. Lourenço, E. Pérez, M.L. Cerrada, and M.R. Ribeiro, *Self-Reinforced Hybrid Polyethylene/MCM-41 Nanocomposites: In-Situ Polymerisation and Effect of MCM-41 Content on Rigidity.* Journal of Nanoscience and Nanotechnology, 2009. **9**(6): p. 3966-3974.

199. Aguado, J., D.P. Serrano, M.D. Romero, and J.M. Escola, *Catalytic conversion of polyethylene into fuels over mesoporous MCM-41.* Chemical Communications, 1996(6): p. 725-726.

200. Chaianansutcharit, S., et al., *Catalytic degradation of polyolefins over hexagonal mesoporous silica: Effect of aluminum addition.* Journal of Analytical and Applied Pyrolysis, 2007. **80**(2): p. 360-368.

201. Collins, M.N., E. Dalton, B. Schaller, J.J. Leahy, and C. Birkinshaw, *Crystal morphology of strained ultra high molecular weight polyethylenes.* Polymer Testing, 2012. **31**(5): p. 629-637.

202. Baillie, C., *Eco-Composites.* Composites Science and Technology, 2003. **63**(9): p. 1223-1224.

203. Azizi Samir, M.A.S., F. Alloin, and A. Dufresne, *Review of Recent Research into Cellulosic Whiskers, Their Properties and Their Application in Nanocomposite Field.* Biomacromolecules, 2005. **6**(2): p. 612-626.

204. Klemm, D., et al., *Nanocelluloses: A New Family of Nature-Based Materials.* Angewandte Chemie International Edition, 2011. **50**(24): p. 5438-5466.

205. Mounika, M. and K. Ravindra, *Characterization of Nanocomposites Reinforced with Cellulose Whiskers: A Review.* Materials Today: Proceedings, 2015. **2**(4–5): p. 3610-3618.

206. Lin, S.-P., et al., *Biosynthesis, production and applications of bacterial cellulose.* Cellulose, 2013. **20**(5): p. 2191-2219.

207. Moon, R.J., A. Martini, J. Nairn, J. Simonsen, and J. Youngblood, *Cellulose nanomaterials review: structure, properties and nanocomposites.* Chemical Society Reviews, 2011. **40**(7): p. 3941-3994.

208. Beck-Candanedo, S., M. Roman, and D.G. Gray, *Effect of Reaction Conditions on the Properties and Behavior of Wood Cellulose Nanocrystal Suspensions.* Biomacromolecules, 2005. **6**(2): p. 1048-1054.

209. Dong, X.M., T. Kimura, J.-F. Revol, and D.G. Gray, *Effects of Ionic Strength on the Isotropic–Chiral Nematic Phase Transition of Suspensions of Cellulose Crystallites.* Langmuir, 1996. **12**(8): p. 2076-2082.

210. Bondeson, D., A. Mathew, and K. Oksman, *Optimization of the isolation of nanocrystals from microcrystalline cellulose by acid hydrolysis.* Cellulose, 2006. **13**(2): p. 171-180.

211. Habibi, Y., L.A. Lucia, and O.J. Rojas, *Cellulose Nanocrystals: Chemistry, Self-Assembly, and Applications.* Chemical Reviews, 2010. **110**(6): p. 3479-3500.

212. Araki, J., M. Wada, S. Kuga, and T. Okano, *Influence of surface charge on viscosity behavior of cellulose microcrystal suspension.* Journal of Wood Science, 1999. **45**(3): p. 258-261.

213. Araki, J., M. Wada, S. Kuga, and T. Okano, *Birefringent Glassy Phase of a Cellulose Microcrystal Suspension.* Langmuir, 2000. **16**(6): p. 2413-2415.

214. Edgar, C. and D. Gray, *Smooth model cellulose I surfaces from nanocrystal suspensions.* Cellulose, 2003. **10**(4): p. 299-306.

215. Revol, J.-F., et al., *Chiral nematic suspensions of cellulose crystallites; phase separation and magnetic field orientation.* Liquid Crystals, 1994. **16**(1): p. 127-134.

216. Tokoh, C., K. Takabe, M. Fujita, and H. Saiki, *Cellulose Synthesized by Acetobacter Xylinum in the Presence of Acetyl Glucomannan.* Cellulose, 1998. **5**(4): p. 249-261.

217. Grunert, M. and W. Winter, *Nanocomposites of Cellulose Acetate Butyrate Reinforced with Cellulose Nanocrystals.* Journal of Polymers and the Environment, 2002. **10**(1-2): p. 27-30.

218. Favier, V., H. Chanzy, and J.Y. Cavaille, *Polymer Nanocomposites Reinforced by Cellulose Whiskers.* Macromolecules, 1995. **28**(18): p. 6365-6367.

219. Petersson, L., I. Kvien, and K. Oksman, *Structure and thermal properties of poly(lactic acid)/cellulose whiskers nanocomposite materials.* Composites Science and Technology, 2007. **67**(11–12): p. 2535-2544.

220. Terech, P., L. Chazeau, and J.Y. Cavaille, *A Small-Angle Scattering Study of Cellulose Whiskers in Aqueous Suspensions.* Macromolecules, 1999. **32**(6): p. 1872-1875.

221. Favier, V., et al., *Nanocomposite materials from latex and cellulose whiskers.* Polymers for Advanced Technologies, 1995. **6**(5): p. 351-355.

222. Elazzouzi-Hafraoui, S., et al., *The Shape and Size Distribution of Crystalline Nanoparticles Prepared by Acid Hydrolysis of Native Cellulose.* Biomacromolecules, 2008. **9**(1): p. 57-65.

223. Lin, N., J. Huang, and A. Dufresne, *Preparation, properties and applications of polysaccharide nanocrystals in advanced functional nanomaterials: a review.* Nanoscale, 2012. **4**(11): p. 3274-3294.

224. Eichhorn, S.J., et al., *Review: current international research into cellulose nanofibres and nanocomposites.* Journal of Materials Science, 2010. **45**(1): p. 1-33.

225. Eichhorn, S.J. and G.R. Davies, *Modelling the crystalline deformation of native and regenerated cellulose.* Cellulose, 2006. **13**(3): p. 291-307.

226. Tanaka, F. and T. Iwata, *Estimation of the Elastic Modulus of Cellulose Crystal by Molecular Mechanics Simulation.* Cellulose, 2006. **13**(5): p. 509-517.

227. Tashiro, K. and M. Kobayashi, *Theoretical evaluation of three-dimensional elastic constants of native and regenerated celluloses: role of hydrogen bonds.* Polymer, 1991. **32**(8): p. 1516-1526.

228. Lyons, W.J., *Theoretical Value of the Dynamic Stretch Modulus of Cellulose.* Journal of Applied Physics, 1959. **30**(5): p. 796-797.

229. de Boer, J.H., *The influence of van der Waals' forces and primary bonds on binding energy, strength and orientation, with special reference to some artificial resins.* Transactions of the Faraday Society, 1936. **32**(0): p. 10-37.

230. Lee, K.-Y., Y. Aitomäki, L.A. Berglund, K. Oksman, and A. Bismarck, *On the use of nanocellulose as reinforcement in polymer matrix composites.* Composites Science and Technology, 2014. **105**: p. 15-27.

231. Boldizar, A., C. Klason, J. Kubát, P. Näslund, and P. Sáha, *Prehydrolyzed Cellulose as Reinforcing Filler for Thermoplastics.* International Journal of Polymeric Materials and Polymeric Biomaterials, 1987. **11**(4): p. 229-262.

232. Siqueira, G., J. Bras, and A. Dufresne, *Cellulosic Bionanocomposites: A Review of Preparation, Properties and Applications.* Polymers, 2010. **2**(4): p. 728.

233. Lin, N. and A. Dufresne, *Nanocellulose in biomedicine: Current status and future prospect.* European Polymer Journal, 2014. **59**: p. 302-325.

234. Anglès, M.N. and A. Dufresne, *Plasticized Starch/Tunicin Whiskers Nanocomposites. 1. Structural Analysis.* Macromolecules, 2000. **33**(22): p. 8344-8353.

235. Azizi Samir, M.A.S., F. Alloin, W. Gorecki, J.-Y. Sanchez, and A. Dufresne, *Nanocomposite Polymer Electrolytes Based on Poly(oxyethylene) and Cellulose Nanocrystals.* The Journal of Physical Chemistry B, 2004. **108**(30): p. 10845-10852.

236. Kvien, I., J. Sugiyama, M. Votrubec, and K. Oksman, *Characterization of starch based nanocomposites.* Journal of Materials Science, 2007. **42**(19): p. 8163-8171.

237. Ben Azouz, K., E.C. Ramires, W. Van den Fonteyne, N. El Kissi, and A. Dufresne, *Simple Method for the Melt Extrusion of a Cellulose Nanocrystal Reinforced Hydrophobic Polymer.* ACS Macro Letters, 2012. **1**(1): p. 236-240.

238. Kumar, S., M. Hofmann, B. Steinmann, E.J. Foster, and C. Weder, *Reinforcement of Stereolithographic Resins for Rapid Prototyping with Cellulose Nanocrystals.* ACS Applied Materials & Interfaces, 2012. **4**(10): p. 5399-5407.

239. Capadona, J.R., et al., *A versatile approach for the processing of polymer nanocomposites with self-assembled nanofibre templates.* Nature Nanotechnology, 2007. **2**(12): p. 765-769.

240. Roman, M. and W.T. Winter, *Effect of Sulfate Groups from Sulfuric Acid Hydrolysis on the Thermal Degradation Behavior of Bacterial Cellulose.* Biomacromolecules, 2004. **5**(5): p. 1671-1677.

241. Jawaid, M. and H.P.S. Abdul Khalil, *Cellulosic/synthetic fibre reinforced polymer hybrid composites: A review.* Carbohydrate Polymers, 2011. **86**(1): p. 1-18.

242. John, M.J. and S. Thomas, *Biofibres and biocomposites.* Carbohydrate Polymers, 2008. **71**(3): p. 343-364.

243. Dittenber, D.B. and H.V.S. GangaRao, *Critical review of recent publications on use of natural composites in infrastructure.* Composites Part A: Applied Science and Manufacturing, 2012. **43**(8): p. 1419-1429.

244. Heux, L., G. Chauve, and C. Bonini, *Nonflocculating and Chiral-Nematic Self-ordering of Cellulose Microcrystals Suspensions in Nonpolar Solvents.* Langmuir, 2000. **16**(21): p. 8210-8212.

245. Kvien, I., B.S. Tanem, and K. Oksman, *Characterization of Cellulose Whiskers and Their Nanocomposites by Atomic Force and Electron Microscopy.* Biomacromolecules, 2005. **6**(6): p. 3160-3165.

246. Araki, J., M. Wada, and S. Kuga, *Steric Stabilization of a Cellulose Microcrystal Suspension by Poly(ethylene glycol) Grafting.* Langmuir, 2001. **17**(1): p. 21-27.

247. Goussé, C., H. Chanzy, G. Excoffier, L. Soubeyrand, and E. Fleury, *Stable suspensions of partially silylated cellulose whiskers dispersed in organic solvents.* Polymer, 2002. **43**(9): p. 2645-2651.

248. Dufresne, A., *Comparing the Mechanical Properties of High Performances Polymer Nanocomposites from Biological Sources.* Journal of Nanoscience and Nanotechnology, 2006. **6**(2): p. 322-330.

249. Fukuzumi, H., T. Saito, T. Iwata, Y. Kumamoto, and A. Isogai, *Transparent and High Gas Barrier Films of Cellulose Nanofibers Prepared by TEMPO-Mediated Oxidation.* Biomacromolecules, 2009. **10**(1): p. 162-165.

250. Azizi Samir, M.A.S., F. Alloin, J.-Y. Sanchez, and A. Dufresne, *Cellulose nanocrystals reinforced poly(oxyethylene).* Polymer, 2004. **45**(12): p. 4149-4157.

251. Alloin, F., A. D'Aprea, A. Dufresne, N. Kissi, and F. Bossard, *Poly(oxyethylene) and ramie whiskers based nanocomposites: influence of processing: extrusion and casting/evaporation.* Cellulose, 2011. **18**(4): p. 957-973.

252. Wang, N., E. Ding, and R. Cheng, *Thermal degradation behaviors of spherical cellulose nanocrystals with sulfate groups.* Polymer, 2007. **48**(12): p. 3486-3493.

253. Masuda, J.i. and J.M. Torkelson, *Dispersion and Major Property Enhancements in Polymer/Multiwall Carbon Nanotube Nanocomposites via Solid-State Shear Pulverization Followed by Melt Mixing.* Macromolecules, 2008. **41**(16): p. 5974-5977.

254. Wakabayashi, K., P.J. Brunner, J.i. Masuda, S.A. Hewlett, and J.M. Torkelson, *Polypropylene-graphite nanocomposites made by solid-state shear pulverization:*

Effects of significantly exfoliated, unmodified graphite content on physical, mechanical and electrical properties. Polymer, 2010. **51**(23): p. 5525-5531.

255. Iyer, K.A., A.M. Flores, and J.M. Torkelson, *Comparison of polyolefin biocomposites prepared with waste cardboard, microcrystalline cellulose, and cellulose nanocrystals via solid-state shear pulverization.* Polymer, 2015. **75**: p. 78-87.

256. Gopalan Nair, K., A. Dufresne, A. Gandini, and M.N. Belgacem, *Crab Shell Chitin Whiskers Reinforced Natural Rubber Nanocomposites. 3. Effect of Chemical Modification of Chitin Whiskers.* Biomacromolecules, 2003. **4**(6): p. 1835-1842.

257. Severn, J.R. and J.C. Chadwick, *Activation of Titanium-Based Single-Site Catalysts for Ethylene Polymerization Using Supports of Type $MgCl_2/AlR_n(OEt)_{3-n}$.* Macromolecular Chemistry and Physics, 2004. **205**(15): p. 1987-1994.

258. Quinn, F.A. and L. Mandelkern, *Thermodynamics of Crystallization in High Polymers: Poly-(ethylene)1.* Journal of the American Chemical Society, 1958. **80**(13): p. 3178-3182.

259. Oliver, W.C. and G.M. Pharr, *An improved technique for determining hardness and elastic modulus using load and displacement sensing indentation experiments.* Journal of Materials Research, 1992. **7**(06): p. 1564-1583.